17 March 2006 | $10

Science

Detection Technologies

AAAS

Genetic Engineering that is Right on Target!

The TargeTron™ Gene Knockout System is a revolutionary method for rapid and specific disruption of genes in prokaryotic organisms. Utility of the technology has been demonstrated for prokaryotic genetic engineering, systems biology and functional genomics approaches.

The method exploits the retrohoming ability of group II introns and utilizes a simple PCR step to "re-target" the TargeTron group II intron for specific insertion into the host genome. Gene knockout using the TargeTron system has been validated in a broad range of bacterial strains such as *Escherichia coli, Staphylococcus aureus, Lactococcus lactis, Clostridium perfringens, Shigella flexneri* and *Salmonella typhimurium.*

- Targeted and permanent gene disruption
- Simple, streamlined protocol; Knockouts in 3 days or less
- Minimal screening to isolate mutants.
- No cell conjugation or specific host factor requirements
- >90% successful targeted insertion

Product	Description	Unit
TA0100	TargeTron™ Gene Knockout System	3EA 10EA

For additional details and product availability, please visit www.sigma-aldrich.com/s1target

There's a new kit on the block.

Introducing StrataClone™ PCR Cloning Kits: A new, more affordable choice in Topoisomerase I technology

Our StrataClone™ PCR Cloning Kit* saves you time and money with topoisomerase-based PCR cloning priced lower than the competition. The simple, three step process, >95% efficiency guarantee, and affordable pricing make StrataClone™ PCR Cloning Kits your kit of choice for topoisomerase-based PCR cloning.

- **High-performance PCR cloning at a more affordable price**
- **Clone both long and short PCR amplicons with the same kit**
- **High efficiency results in >95% clones with insert**

Need More Information? Give Us A Call:

Stratagene USA and Canada
Order: (800) 424-5444 x3
Technical Services: (800) 894-1304 x2

Stratagene Europe
Order: 00800-7000-7000
Technical Services: 00800-7400-7400

Stratagene Japan K.K.
Order: 03-5159-2060
Technical Services: 03-5159-2070

Ask Us About These Great Products:

StrataClone™ PCR Cloning Kit	**20 reactions**	**240205**
	10 reactions	**240206**

StrataClone™ is a trademark of Stratagene in the United States.
* Patent pending.

STRATAGENE®

www.stratagene.com

GE Healthcare

Why do 100,000 scientists trust GE Healthcare for all their protein purification needs?

Here's Ä clue.

To 100,000 scientists worldwide, the name ÄKTA™ has always meant outstanding protein purification, and now it's brought to you by GE Healthcare. With the ability to purify virtually 100% of all biomolecules, the ÄKTAdesign™ platform can handle the toughest of challenges. Whatever the scale, from laboratory, to process development and manufacturing, there's an ÄKTAdesign system to meet every need. All systems in the ÄKTAdesign family work with the intelligent UNICORN™ software, which makes it easy to control every stage of your purification processes. Accurate, reproducible results just take a little pure imagination.

Visit www.amershambiosciences.com/aktadesign

imagination at work

YYePG Proudly Presents,Thx for Support

GE15-05

Volume 311, Issue 5767

COVER

Direct analysis of plant tissue by ambient mass spectrometry. Charged microdroplets of water are sprayed onto the surface of a flower, and the released ions are vacuumed into a nearby mass spectrometer. This methodology is applicable to large biomolecules and small organics in complex natural matrices, including biological fluids and animal tissue. See page 1565.
Photo: Z. Ouyang and T. A. Blake

DEPARTMENTS

EDITORIAL

SPECIAL SECTION

Detection Technologies

INTRODUCTION

REVIEWS

>> Reports pp. 1592, 1595, and 1600

For related online content in STKE, see page 1515 or go to www.sciencemag.org/sciext/detection/

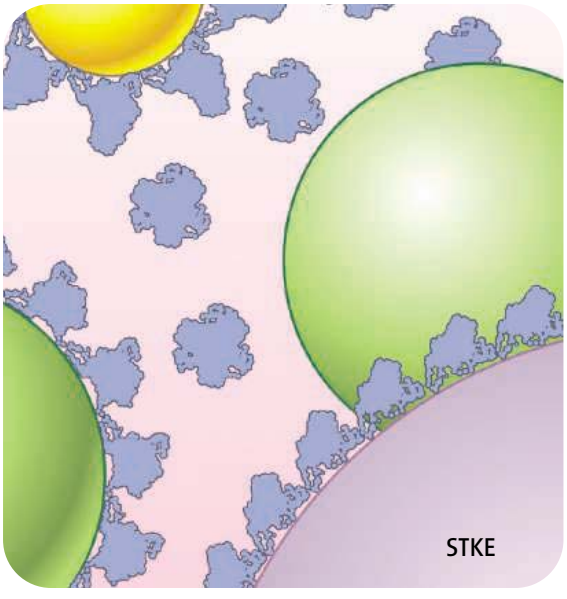

NEWS OF THE WEEK

NEWS FOCUS

CONTENTS continued >>

Systems Biology — RNAi and Gene Expression Analysis

GeneGlobe — the world's largest database of matching siRNAs and RT-PCR assays

New

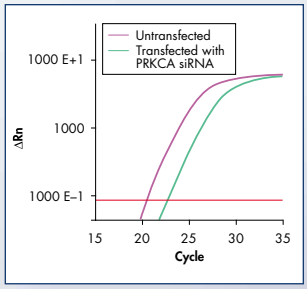

Reliable quantification after knockdown

Visit www.qiagen.com/GeneGlobe

Enter the world of reliable gene silencing and gene expression analysis!

Genomewide solutions from QIAGEN include potent, specific siRNAs and matching, ready-to-use, validated primer sets for SYBR® Green based real-time RT-PCR assays. Benefits include:

- Easy online access to RNAi and gene expression solutions at GeneGlobe
- siRNAs and RT-PCR assays for the entire human, mouse, and rat genomes
- RT-PCR assays for arabidopsis, drosophila, dog, and chicken

For matched siRNAs and real-time RT-PCR assays you can rely on, go to www.qiagen.com/GeneGlobe !

QIAGEN

Science

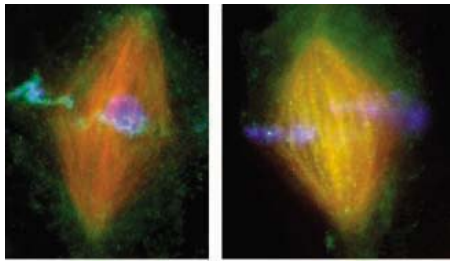

SCIENCE EXPRESS

www.sciencexpress.org

ATMOSPHERIC SCIENCE

Deconvolution of the Factors Contributing to the Increase in Global Hurricane Intensity
C. D. Hoyos, P. A. Agudelo, P. J. Webster, J. A. Curry
Higher sea surface temperature was the only statistically significant controlling variable related to the upward trend in global hurricane strength since 1970.
10.1126/science.1123560

VIROLOGY

Structure and Receptor Specificity of the Hemagglutinin from an H5N1 Influenza Virus
J. Stevens et al.
A surface protein on the "bird flu" virus binds avian cells and with a few mutations could allow more avid attachment to human cells, facilitating infection.
10.1126/science.1124513

CELL SIGNALING

A Mitotic Lamin B Matrix Induced by RanGTP Required for Spindle Assembly
M.-Y. Tsai et al.
Lamin B, a structural protein of the interphase nucleus, also coordinates assembly of the mitotic spindle.
10.1126/science.1122771

NEUROSCIENCE

SV2 Is the Protein Receptor for Botulinum Neurotoxin A
M. Dong et al.
One of the toxins from botulinum enters neurons by hitching a ride on proteins that are exposed when synaptic vesicles release neurotransmitters and are then recycled.
10.1126/science.1123654

LETTERS

BOOKS *ET AL.*

POLICY FORUM

PERSPECTIVES

TECHNICAL COMMENT ABSTRACTS

ECOLOGY

BREVIA

ECOLOGY

RESEARCH ARTICLE

VIROLOGY

REPORTS

MATERIALS SCIENCE

CONTENTS continued >>

ISI Web of Knowledge℠

Take the next step

Where ideas turn into knowledge.

The search for new knowledge is an ongoing challenge …
but the search for the best research resources need not be.

ISI Web of Knowledge assures your access to the critical information you require. Whether the ideas you seek are across the globe, have their roots in the past, or can be found in today's newest discoveries, *ISI Web of Knowledge* delivers all the research data and tools you need to reach your goals.

Navigate freely. Explore confidently. Search successfully.

with *ISI Web of Knowledge*

Come see us at ACS in booth numbers 402 and 404

THOMSON™

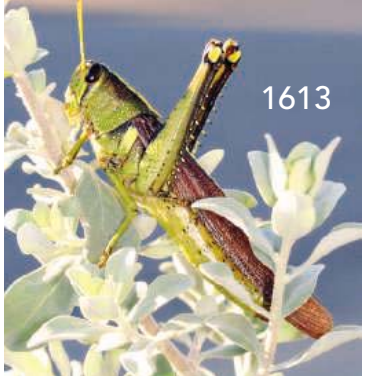

REPORTS *CONTINUED...*

AAAS
ADVANCING SCIENCE, SERVING SOCIETY

SCIENCE (ISSN 0036-8075) is published weekly on Friday, except the last week in December, by the American Association for the Advancement of Science, 1200 New York Avenue, NW, Washington, DC 20005. Periodicals Mail postage (publication No. 484460) paid at Washington, DC, and additional mailing offices. Domestic individual membership and subscription (51 issues): $139 ($74 allocated to subscription). Domestic institutional subscription (51 issues): $650; Foreign postage extra: Mexico, Caribbean (surface mail) $55; other countries (air assist delivery) $85. First class, airmail, student, and emeritus rates on request. Canadian rates with GST available upon request, GST #1254 88122. Publications Mail Agreement Number 1069624. **Printed in the U.S.A.**

Change of address: Allow 4 weeks, giving old and new addresses and 8-digit account number. **Postmaster:** Send change of address to *Science*, P.O. Box 1811, Danbury, CT 06813–1811. **Single-copy sales:** $10.00 per issue prepaid includes surface postage; bulk rates on request. *Science* is indexed in the *Reader's Guide to Periodical Literature* and in several specialized indexes.

CONTENTS continued **>>**

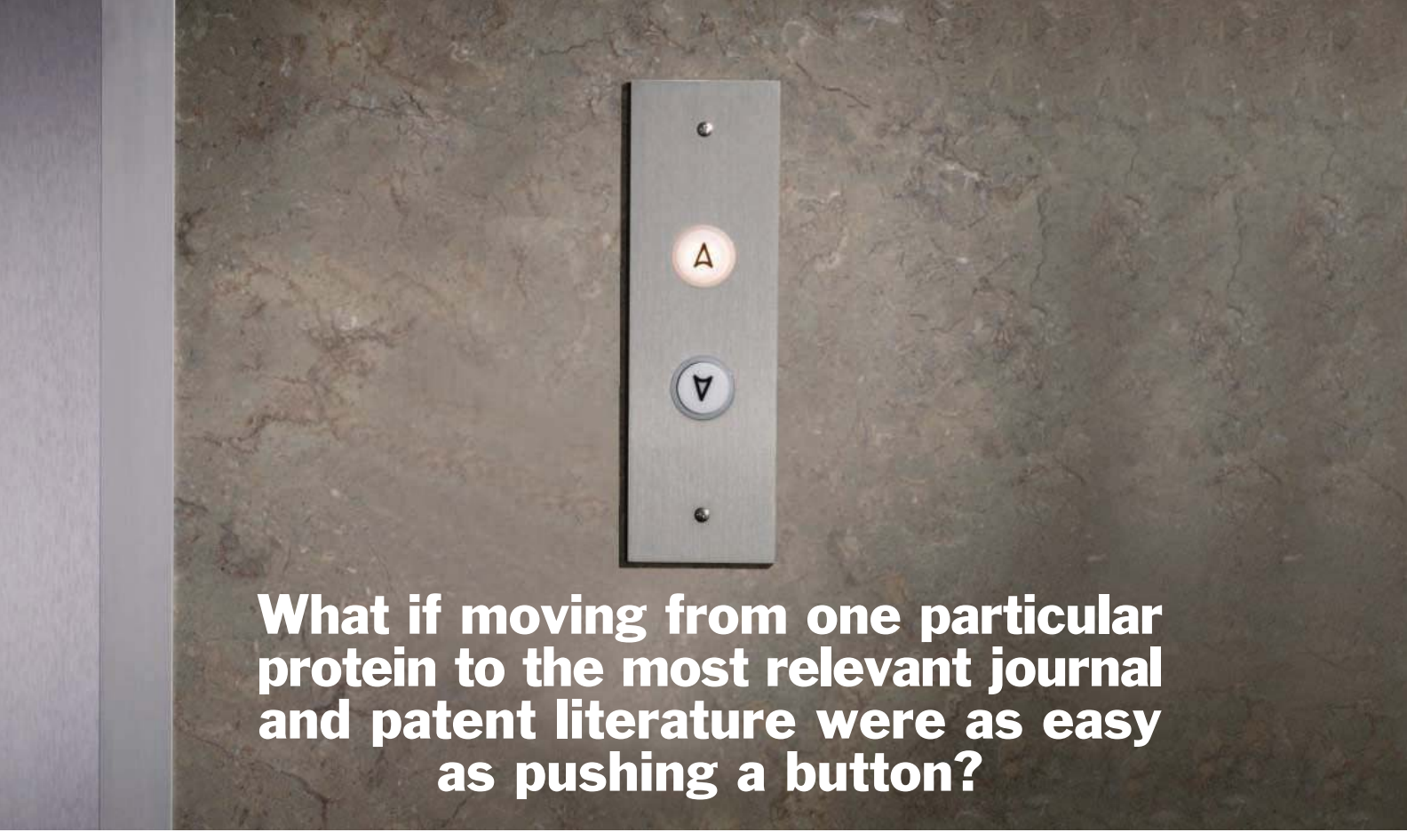

What if moving from one particular protein to the most relevant journal and patent literature were as easy as pushing a button?

It is.

Not only does SciFinder provide access to more proteins and nucleic acids than any publicly available source, but they're a single click away from their referencing patents and original research.

Coverage includes everything from the U.S. National Library of Medicine's (NLM) MEDLINE® and much more. In fact, SciFinder is the only single source of patents and journals worldwide.

Once you've found relevant literature, you can use SciFinder's powerful refinement tools to focus on a specific research area, for example: biological studies such as target organisms or diseases; expression microarrays; or analytical studies such as immunoassays, fluorescence, or PCR analysis. From each reference, you can link to the electronic full text of the original paper or patent, plus use citation tools to track how the research has evolved and been applied.

Visualization tools help you understand results at a glance. You can categorize topics and substances, identify relationships between areas of study, and see areas that haven't been explored at all.

Comprehensive, intuitive, seamless—SciFinder directs you. It's part of the process. To find out more, call us at 1-800-753-4227 (North America) or 1-614-447-3700 (worldwide) or visit www.cas.org/SCIFINDER.

SciFinder®

Part of the process.℠

Keeping the luster on biological baubles.

SCIENCE'S **SAGE KE**

www.sageke.org SCIENCE OF AGING KNOWLEDGE ENVIRONMENT

NEWS FOCUS: Buffing Up the Family Jewels
M. Beckman
Obliterating a protein that fosters testosterone production keeps testicles young.

CLASSIC PAPER: The Neuroendocrinology of Stress and Aging—The Glucocorticoid Cascade Hypothesis
R. M. Sapolsky, L. C. Krey, B. S. McEwen
Termination of adrenocortical stress hormone secretion is impaired in aged male rats; *Endocr. Rev.* **7**, 284 (1986).

Tips for telephone interviews.

SCIENCE **CAREERS**

www.sciencecareers.org CAREER RESOURCES FOR SCIENTISTS

US: Tooling Up—Telephone Interviews
D. Jensen
Our columnist passes on his six most important tips for a successful telephone interview.

US: Making the Most Out of Life
I. Levine
Christina Fong deftly balances her roles as public economist, teacher, and spouse.

EUROPE: Mediating Science and Society
A. Forde
A scientist finds tangible rewards working at the interface of science and society.

MISCINET: Training Minorities in Environmental Science
E. Francisco
A program at Arkansas State University encourages minorities to enter careers in environmental science.

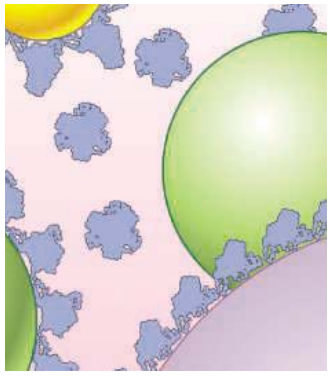

SPECIAL ONLINE CONTENT

Detection Technologies

SCIENCE'S **STKE**

www.stke.org SIGNAL TRANSDUCTION KNOWLEDGE ENVIRONMENT

EDITORIAL GUIDE: Focus Issue—Measurement on a Small Scale
N. R. Gough
Advances in technology allow exploration of cell signaling at the level of individual molecules.

PERSPECTIVE: Multiple Routes for Glutamate Receptor Trafficking—Surface Diffusion and Membrane Traffic Cooperate to Bring Receptors to Synapses
L. Cognet, L. Groc, B. Lounis, D. Choquet
Multiple techniques provide insight into receptor delivery mechanisms in neurons.

PERSPECTIVE: Detecting Cryptic Epitopes Created by Nanoparticles
I. Lynch, K. A. Dawson, S. Linse
Understanding how nanoparticles affect cell signaling is crucial to their application in medicine and research.

SCIENCE**NOW**

www.sciencenow.org DAILY NEWS COVERAGE

Red Planet's Newest Visitor
NASA's Mars Reconnaissance Orbiter gets into position.

Buyer Beware: Conservation Can Backfire
Economic model shows that purchasing land sometimes threatens biodiversity.

The Best Defense Is Gene Nonsense
Mutation in immunity gene helps people ward off maladies of modern life.


"I choose Scopus because I can easily navigate through all the information in my field without losing my purpose."
Scopus has been really useful in completing my doctoral thesis. It's amazing how much information you can get and how easily you can navigate to what's hot. If you want to be confident in your results, use Scopus.
I do!
Come to Elsevier Booth #1009 at ACS Atlanta 2006 for a demo.
Zaida Chinchilla-Rodríguez
Senior Researcher
University of Granada, Spain
www.scopus.com
YYePG Proudly Presents,Thx for Support
SCOPUS™
Find out.

EDITED BY STELLA HURTLEY AND PHIL SZUROMI

Starting Statues Sooner

When Dutch sailors arrived on Easter Island in 1722, they encountered a famished population of Polynesians living on a denuded landscape marked by giant stone statues. It has been generally assumed that colonists arrived on the island between about 400 and 1000 A.D.; only later, around 1200 A.D., did they erect the statues and cleared the once-abundant forests. **Hunt and Lipo** (p. 1603) present radiocarbon dates from a recent excavation on Easter Island and analyze previous dates from other sites. Their dates and analysis imply that colonization occurred near the time of statue construction. If so, then irreversible deforestation may have started immediately after the Polynesians arrived.

Mobility for Artificial Muscles

Electrically powered motor or actuators can serve as artificial muscles in robots or prosthetic limbs, but significant "down times" will likely occur if their power needs are met by rechargeable batteries. **Ebron *et al***. (p. 1580; see the Perspective by **Madden**) demonstrate two alternative approaches that use fuel cells. In one approach, a catalyst containing carbon nanotubes acts as muscle, fuel cell electrode, and supercapacitor electrode in a hydrogen-fueled system. In the other approach that can be fueled by hydrogen, methanol, or formic acid, a shape-memory alloy is used; this artificial muscle achieves actuator stroke and power density comparable to that of natural skeletal muscle and generates stresses that are one hundred times greater.

Sporadic Spokes

Dark radial streaks or spokes in Saturn's main B-ring were first seen with the Voyager space probes, and later by the Hubble Space Telescope. In 1998, they faded from view from the Earth as Saturn's rings became oriented edge on. Contrary to expectations, the spokes remained absent even when the Cassini spacecraft flew close to the rings in 2004 but then reappeared faintly in September 2005. These latter findings suggested that the spokes are intermittent features whose presence depends on the rings' angle to the Sun. **Mitchell *et al*.** (p. 1587) use Cassini data to model the formation of spokes as charged dust particles are lifted into the plasma above the ring plane by electrostatic forces. They find a sharp switch in the spokes' visibility, such that they disappear abruptly when the rings are open to the Sun, and also predict when the spokes are likely to appear clearly.

Deflection Detection

A promising approach for highly sensitive detection of biomolecules makes use of microfabricated cantilevers decorated with receptors or other molecules that would bind a molecule of interest. Binding creates a surface stress that deflects the cantilever. However, this deflection is small (on the order of tens of nanometers), and the methods used to date (optical, capacitive, and piezoelectric) have various limitations. **Shekhawat *et al*.** (p. 1592, published online 2 February) show that they can build a field-effect transistor into the cantilever that responds to surface stresses. Detected deflection changes of ~5 nanometers can be followed and allows detection of biotin and antibodies.

Construction in Tight Spaces

Forming high-aspect-ratio metal or semiconducting wires can be difficult because the main fabrication technique, chemical vapor deposition (CVD), does not work well when filling long narrow channels. **Sazio *et al*.** (p. 1583) have developed a modified CVD process that allows for the integration of functional materials within an optical waveguide, which can tolerate a much higher pressure CVD process. Specifically, metals and semiconductors with lateral dimensions down to a few nanometers are formed within microstructured optical fibers.

The Ringdown Cycle

The use of spectroscopy for chemical analysis often requires tradeoffs between bandwidth (how much of the spectral range is being recorded), resolution, and data acquisition speed. For example, in cavity-ringdown spectroscopy (CRDS), adsorption by molecules depletes light that is bouncing back and forth in an optical cavity, and the light adsorption curve can provide extremely high detection limits. However, the range of frequencies that can be followed is limited. **Thorpe *et al*.** (p. 1595) created a broadband version of CRDS by coupling an optical frequency comb to a high-finesse optical cavity whose mirror position could be finely adjusted, and followed the simultaneous decay of numerous ringdown modes. They obtained spectral data across a 100-nanometer wavelength range in the visible and near-infrared for species such as water and ammonia.

Observing Proteins One by One

Detection of single messenger RNA (mRNA) molecules has led to exciting insights into gene expression in live cells. **Yu *et al*.** (p. 1600) have developed a method to image single protein molecules in living *Escherichia coli* cells. They expressed a membrane-targeted version of yellow fluorescent protein (YFP) and, under repressed conditions, detected individual membrane-localized YFP molecules as they were being synthesized. The protein molecules were expressed in bursts, and each burst originated

Continued on page 1519

This Week in Science presents Editor's Choice for Support

SPECIAL INTRODUCTORY OFFER
See our website for details.

NEW ENGLAND BIOLABS

Competent Cells from New England Biolabs

SUPERIOR COMPETENT *E.COLI* STRAINS FOR CLONING AND PROTEIN EXPRESSION

For many years staff scientists at New England Biolabs have been using their own line of optimized chemically competent *E.coli* cells for cloning and protein expression. These strains have made all the difference to a highly demanding research and production program. Now when you are looking for a versatile cloning strain, rapid colony growth, or tight control of protein expression, you can benefit from the superior performance and high quality of these strains.

- **NEB Turbo Competent *E.coli*** **C2984H**
  Ligate, transform, plate and pick colonies in one day
- **NEB 5-alpha Competent *E.coli*** **C2991H**
  Versatile cloning strain
- **T7 Express Competent *E.coli*** **C2566H**
  High efficiency transformation and protein expression
- **T7 Express *I*^{q} Competent *E.coli*** **C2833H**
  Tight control of protein expression
- **dam^{-}/dcm^{-} Competent *E.coli*** **C2925H**
  Grow plasmids free of dam and dcm methylation

Advantages:

- Ready to transform – packaged in single-use transformation tubes (20 x 0.05 ml)
- Free of animal products
- 5 minute transformation protocols
- Supplied with outgrowth media and control DNA

	NEB Turbo	NEB 5-alpha	T7 Express	T7 Express *I*^{q}	dam^{-}/dcm^{-}
Transformation Efficiency (cfu/µg)	>10^{9}	1-3 x 10^{9}	2-6 x 10^{8}	2-6 x 10^{8}	>2 x 10^{6}
Strain	K12	K12	B	B	K12
T1 Phage Resistant	✓	✓	✓	✓	✓
Blue/White Screening	✓	✓	–	–	–
lac *I*^{q}	✓	✓	–	✓	–
Colonies Visible after 8 hours	✓	–	–	–	–
Endonuclease I Deficient	✓	✓	✓	✓	✓
Protease Deficient	–	–	✓	✓	–
Restriction Deficient	✓	✓	✓	✓	✓
M13 Phage Capable (F^{+})	✓	✓	–	✓	–
RecA Deficient	–	✓	–	–	–

Chemically Competent *E.coli* Strain Characteristics

For more information and international distribution network, please visit www.neb.com

- **New England Biolabs Inc.** 240 County Road, Ipswich, MA 01938 USA 1-800-NEB-LABS Tel. (978) 927-5054 Fax (978) 921-1350 info@neb.com
- **Canada** Tel. (800) 387-1095 info@ca.neb.com
- **Germany** Tel. 0800/246-5227 info@de.neb.com
- **UK** Tel. (0800) 318486 info@uk.neb.com
- **China** Tel. 010-82378266 beijing@neb-china.com

NEW ENGLAND BioLabs® Inc.
the leader in enzyme technology

Continued from page 1517

from a stochastically transcribed mRNA molecule. The technique may make it possible to study the dynamics of the many proteins present in low numbers per cell.

A Catalog of Avian Flu

Large-scale sequence analysis of avian flu isolates based on 4339 virus genes from many wild birds confirms long-known facts of flu biology, such as the variability of hemagglutinin and neuraminidase sequences, the frequency of reassortment, and the restricted compatibility of internal virion subunits. **Obenauer *et al.*** (p. 1576, published online 26 January; see the Perspective by **Krug**) have developed the means to characterize these viruses by a technique they term "proteotyping" and use the method to identify specific combinations of genes and gene products that travel together. They also identified a previously overlooked motif that appears to correlate closely with virulence, at least in strains of avian origin.

Higher Brain Functions in Primary Visual Cortex

According to the classical textbook view, the early stages of visual cortex operate as a hard-wired, feature-detecting system and are little affected by nonvisual features of external stimuli. However, **Shuler and Bear** (p. 1606) show that neurons in primary visual cortex (area V1) have very different response patterns during presentation of the same stimuli at early and late stages of visual discrimination training. They found an association of responses of area V1 neurons with the timing of a reward. Animals were trained to receive water after a certain number of licks, on a tube, after stimulation of one eye. Reward time was different for both eyes, and neurons in the primary visual cortex predicted the time of the reward in trained, but not in naïve, animals.

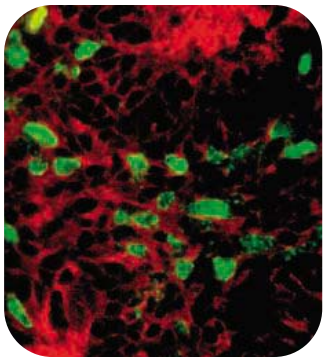

CREDIT: LIEN *ET AL.*

Managing the Neural Production Line

Neural progenitors in the developing brain interact with neighboring cells through αE-catenin–containing adherens junctions. **Lien *et al.*** (p. 1609; see the Perspective by **DiCicco-Bloom**) found that conditional knock-out of the *αE-catenin* gene during embryonic brain development resulted in mice whose brains at birth contained twice as many cells as normal. It seems that the area of cell surface occupied by adherens junctions defines the density of cells and regulates cellular proliferation such that enough, but not too many, brain cells are produced.

Eye of Lizard

The parietal eye of lizards responds to light and dark but does not form images. **Su *et al.*** (p. 1617) show that blue light and green light, working through opsins unlike those in visual eyes, send antagonistic signals to a key cyclic guanosine monophosphate (cGMP) phosphodiesterase. Subsequent alterations in cGMP concentrations modulate channel openings to depolarize or hyperpolarize the parietal photoreceptor cells. Comparison of the opsins and signaling molecules involved suggests an evolutionary trajectory by which the parietal eye diverged from the visual eyes.

Promising Therapy for Progeria?

Progerias are a group of rare genetic disorders characterized by the onset in children of symptoms typically seen in aging individuals, such as osteoporosis, vascular disease, and hair loss. Several progeroid disorders are caused by mutations that alter the function of prelamin A, a protein that helps maintain the structural integrity of the cell nucleus. Cells from patients with progeria display dramatic changes in nuclear architecture because prelamin A remains aberrantly attached to the nuclear membrane by virtue of a farnesyl lipid modification. In a mouse model of progeria, **Fong *et al.*** (p. 1621, published online 16 February; see the 17 February news story by **Travis**) now show that a drug that inhibits protein farnesylation (farnesyltransferase inhibitor, or FTI) and that is already in clinical development for potential anticancer activity can ameliorate symptoms of the disease. FTI-treated mice had greater grip strength were less likely to develop rib fractures and, in a short-term study, appeared to live slightly longer than untreated mice.

R&D Systems reagents for Obesity & Diabetes Research

R&D Systems offers many tools for the study of endocrinology and related fields including appetite, obesity, metabolism, and their associated diseases. We offer high-quality assay kits, antibodies, and proteins to study endocrinology-related cytokines, growth factors, peptide hormones, steroid hormones, their receptors, as well as reagents to study eicosanoids.

- Adiponectin
- AgRP
- BDNF
- CNTF
- Cortisol
- DPPIV
- FGF-19
- Glucagon
- Glut 1-5
- Growth Hormone
- IGF
- IL-11
- Insulin
- Leptin
- Orexin A, B
- OSM
- RAGE
- Resistin
- & more!

For research use only. Not for use in diagnostic procedures.

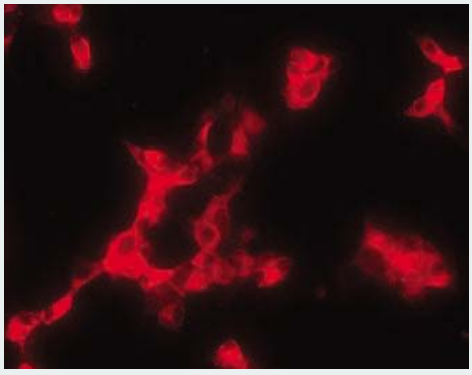

FIGURE 1 Detection of Proinsulin in mouse beta-TC6 cells using R&D Systems mouse anti-Proinsulin monoclonal antibody (Catalog # MAB1336). Cells were stained using Rhodamine Red-conjugated anti-Mouse IgG secondary antibody.

For a complete listing of endocrinology-related products visit our website at www.RnDSystems.com/go/endocrinology

Cancer Development Endocrinology Immunology Neuroscience Proteases Stem Cells

www.RnDSystems.com

U.S. & Canada | **R&D Systems, Inc.** | Tel: (800) 343-7475 | info@RnDSystems.com
Europe | **R&D Systems Europe Ltd.** | Tel: +44 (0)1235 529449 | info@RnDSystems.co.uk
Germany | **R&D Systems GmbH** | Tel: 0800 909 4455 | infogmbh@RnDSystems.co.uk
France | **R&D Systems Europe** | Tel: 0800 90 72 49 | info@RnDSystems.co.uk

R&D SYSTEMS

Quality | Selection | Performance | Results

Jeffrey D. Sachs is director of the Earth Institute at Columbia University in New York. His research concerns economic development and disease control.

Peter J. Hotez is professor and chair of the Department of Microbiology, Immunology, and Tropical Medicine at George Washington University and the Sabin Vaccine Institute in Washington, DC. His research includes the development of vaccines to treat neglected tropical diseases.

Fighting Tropical Diseases

THE GLOBAL FIGHT AGAINST EXTREME POVERTY REQUIRES A SOLID PARTNERSHIP BETWEEN physical scientists, social scientists, civil society, and policy-makers. For too long, extreme poverty has been viewed mainly or exclusively through the lens of economics and politics. Yet the root causes of extreme poverty involve science-based challenges requiring expertise in disciplines including disease ecology, medicine, public health, climatology, agronomy, and soil science. A new effort to control several of the major killer infectious diseases in Africa (www.earth.columbia.edu/malaria-ntd) illustrates the promise of a science-based policy approach to the fight against poverty, hunger, and disease.

The United Nations (UN) Millennium Development Goals—the world's shared objectives for fighting extreme poverty—put a major focus on AIDS, tuberculosis, malaria, and "other diseases" not explicitly mentioned. These include several neglected tropical diseases that impose a combined disease burden rivaling that of the "big three": AIDS, tuberculosis, and malaria. These neglected tropical diseases share a high prevalence in rural and poor urban regions of low-income countries, an ability to promote poverty, and disabling and stigmatizing characteristics. Moreover, efforts to control these diseases have been underappreciated, achieving successes not widely known in the policy community.

A policy effort initiated this year by the UN Millennium Project and the Earth Institute at Columbia University will link a scaling-up of the fight against malaria with expanded efforts against several parasitic and bacterial infections, including leishmaniasis, trypanosomiasis, hookworm, lymphatic filariasis, onchocerciasis, schistosomiasis, leprosy, Buruli ulcer, and trachoma. At a January 2006 meeting at the Karolinska Institute in Stockholm, specialists in malaria control, the neglected tropical diseases, and economic development compared evidence and planned a joint campaign for comprehensive disease control. The initial effort will focus on 10 countries (Ethiopia, Ghana, Kenya, Malawi, Mali, Nigeria, Rwanda, Senegal, Tanzania, and Uganda) that have pledged to have comprehensive scale-up plans to fight malaria as well as the neglected tropical diseases ready by the end of April 2006 and to seek funding from the Global Fund to Fight AIDS, Tuberculosis, and Malaria; the World Bank; and other sources.

There are several motivations for this new effort. First, recent analyses indicate that the disease burden imposed by neglected tropical diseases has been underestimated; they not only cause approximately 530,000 deaths annually but also cause much more long-term disability, disfigurement, and suffering. These diseases rival AIDS, tuberculosis, and malaria, resulting in a loss of up to 57 million disability-adjusted life years annually. Epidemiologic studies suggest extensive geographic overlap among these diseases and with AIDS, tuberculosis, and malaria, resulting in polyparasitism, especially among the poor. Second, chronic parasitic infections may increase an individual's risk of acquiring a "big three" disease or worsen its progression. These observations strengthen the rationale for incorporating treatments for parasitic diseases into control programs for the big three.

It is possible to design an easy-to-use "rapid-impact" package for simultaneously treating seven neglected tropical diseases— ascariasis, hookworm, trichuriasis, lymphatic filariasis, onchocerciasis, schistosomiasis, and trachoma—for less than $1 per person per year plus free donations of four of the five impact-package drugs (azithromycin, albendazole, ivermectin, and mebendazole) by Pfizer, GSK, Merck, and Johnson & Johnson, respectively. In addition, praziquantel is available from various generic manufacturers at low cost. Scaling the rapid-impact package for all of Africa would require an estimated $200 million per year in addition to approximately $3 billion per year for malaria control. By integrating the control of neglected tropical diseases with malaria control, this pro-poor package could reduce the disease burden by as much as would the control of any of the big three diseases.

This scale-up will require novel and careful coordination between national program managers for malaria and their counterparts who deal with neglected tropical diseases, with attention to the complexities of compliance, drug interactions, drug resistance, monitoring, and sustainability. However, if successful, a coordinated assault on these tropical infections could become one of the best buys in all of public health. This integration should be incorporated into the next round of funding proposals for the Global Fund to Fight AIDS, Tuberculosis, and Malaria and be considered by other global health initiatives.

– Jeffrey D. Sachs and Peter J. Hotez

10.1126/science.1126851

Faster Publication

OF YOUR HIGH-IMPACT RESEARCH

Manuscript submission to acceptance: 5 weeks

Manuscript submission to published on the web: 8 weeks

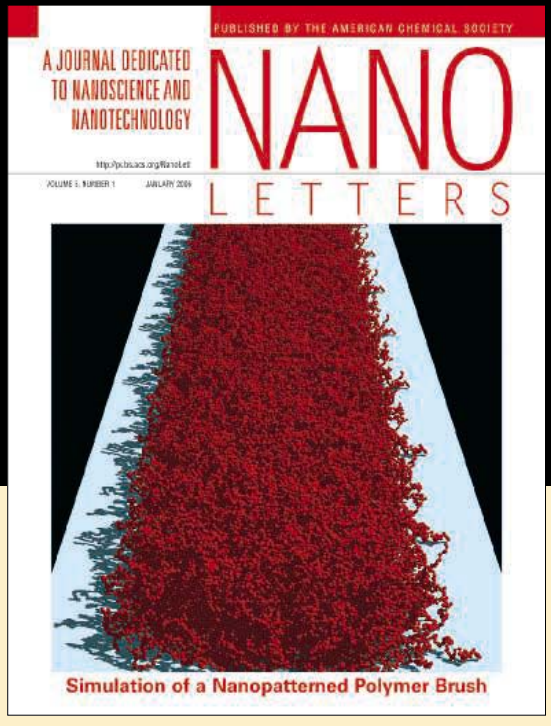

ISI impact factor 8.449

Co-Editor
A. Paul Alivisatos
University of California, Berkeley

Co-Editor
Charles M. Lieber
Harvard University

Nano Letters **offers authors extremely rapid time to publication — one of the fastest in the industry — with manuscript submission to acceptance in 5 weeks and manuscript submission to published on the web in 8 weeks.**

In addition, the journal received an impressive ISI impact factor of 8.449, ranking #5 out of 125 journals in the category of multidisciplinary chemistry and #4 out of 177 journals in materials science.*

For rapid communication of nanoscale research, ***Nano Letters*** **is the leading forum.**

As reported in the 2004 ISI® Journal Citation Reports®

2006 Subscription Information
Volume: 6, 12 Issues
Print Edition ISSN: 1530-6984; Web Edition ISSN: 1530-6992
Institutional Subscription Rate: $1,356; (Outside North America: $1,436)
For more information, call Member & Subscriber Services:
1-888-338-0012 in U.S. and Canada, or (614) 447-3674 outside North America

To submit your manuscript, register for RSS feeds or e-mail Alerts, and view lists of most-accessed articles and a free sample issue, go to http://pubs.acs.org/NanoLett

ACS PUBLICATIONS
HIGH QUALITY. HIGH IMPACT.

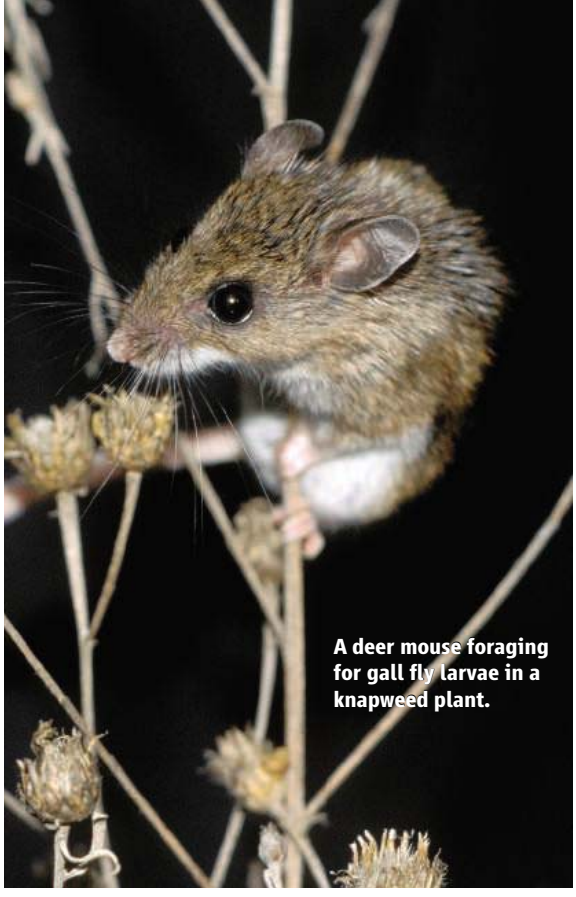

A deer mouse foraging for gall fly larvae in a knapweed plant.

HIGHLIGHTS OF THE RECENT LITERATURE

ECOLOGY

The Best Laid Plans

The invasive weed *Centaurea maculosa* (spotted knapweed) has become widespread in North America. Gall flies (*Urophora* spp.) have been introduced in an attempt at biological control of the plant. The gall flies lay their eggs in the flower heads, where the larvae induce the formation of galls in which they overwinter. The presence of the galls ultimately results in the plants producing fewer seeds. Although the flies have successfully dispersed throughout populations of the invasive weed, they have not proved to be effective control agents, and the weed continues to spread, particularly in areas disturbed by human activity.

Pearson and Callaway have discovered that therein lies a deeper threat. The fly grubs have proved to be an attractive food source for *Peromyscus* (deer) mice and bolster mouse populations during otherwise lean winter months. This genus of mice are reservoir hosts for the human pathogenic hantavirus, Sin Nombre, and, worryingly, the authors found that the abundance of hantavirus-seropositive mice is elevated in zones of high abundance of weed and flies. Deer mice also act as reservoir hosts for Lyme disease and potentially for plague and other zoonotic pathogens. — CA

Ecol. Lett. 10.1111/j.1461-0248.2006.00896.x (2006).

CELL BIOLOGY

Hide and SECIS

Insertion of the 21st amino acid, selenocysteine, into selenoproteins occurs at what is usually a translation stop codon, UGA. This creates something of a dilemma in eukaryotic cells, because mRNAs carrying a premature stop codon are normally subject to nonsense-mediated decay (NMD). NMD is a process that destroys the mRNA and prevents the cell from synthesizing potentially dangerous truncated proteins. Indeed, when selenoprotein synthesis is limiting, selenoprotein mRNAs can be degraded by NMD.

In eukaryotes, recoding of the UGA stop codon is achieved through a secondary structure, the SECIS element, in the 3′ untranslated region of the selenoprotein mRNA. This element binds a complex of the SECIS binding protein (SBP2) and the elongation factor EFsec. De Jesus *et al.* investigated the subcellular location of these two proteins. Both proteins possess functional nuclear localization and nuclear export signals, and SBP2 is capable of shuttling between the cytoplasm and the nucleus. SBP2 and EFsec co-localize, suggesting that SBP2 may contribute to nuclear retention of EFsec. Furthermore, the level of the SBP2 protein correlates with the level of selenoprotein mRNAs, suggesting that it might stabilize these mRNAs. Thus, the prompt nuclear deposition of the two proteins on the SECIS element may play a role in protecting the selenoprotein mRNA from the unwanted attentions of the NMD machinery. — GR

Mol. Cell. Biol. **26**, 1795 (2006).

CLIMATE SCIENCE

Penultimate Monsoons

Analysis of stalagmites has provided remarkably detailed records of precipitation patterns and particularly of changes in monsoonal rainfall. Some stalagmites have been used to chronicle variations of the Asian monsoon for most of the past 160,000 years, revealing close connections between these variations and regional climate behavior in distant locations. The data also help to deepen understanding of how climate dynamics have operated in the past.

Cheng *et al.* add to this body of knowledge with a record of oxygen isotopes from three stalagmites in Hulu Cave, China, characterizing most of the interval between 128,000 and 178,000 years ago. Most of the penultimate deglaciation period—during which atmospheric CO_2 concentration rose and much of the accompanying rise in atmospheric methane took place—occurred during a time of weak Asian monsoons, when the high northern latitudes likely were cold. Thus, the penultimate deglaciation seems to have been a two-phase process driven by orbital forcing in both hemispheres. — HJS

Geology **34**, 217 (2006).

CHEMISTRY

Pulled but not Distorted

Single-molecule force spectroscopy can be used to examine the potential energy landscape of displacement reactions. Such analysis assumes that the reaction mechanism remains the same when the dissociation step is assisted by mechanical force. Kersey *et al*. explored this question by attaching substituted pyridines to a substrate and an atomic force microscope tip, and then bridging the tip and substrate using a molecule with square-planar Pd centers that could bind each pyridine. They then measured force-extension curves for various loading rates that captured bond rupture events in which dimethyl-sulfoxide (DMSO) solvent displaced the pyridine ligands from Pd. The thermal rates extrapolated from the data corresponded well with rates measured by nuclear magnetic resonance for the analogous displacement reaction in free solution. Thus, the same bimolecular mechanism appears to operate in both the thermal and nonequilibrium applied

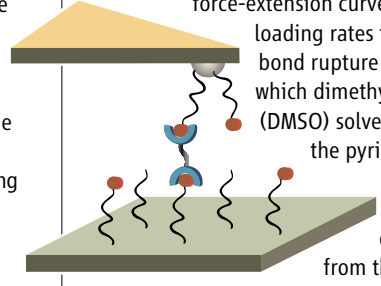

Schematic of Pd-pyridine linkages, poised to pull apart.

Continued on page 1525

SCIENCE & ENGINEERING

VISUALIZATION CHALLENGE

CALL FOR ENTRIES

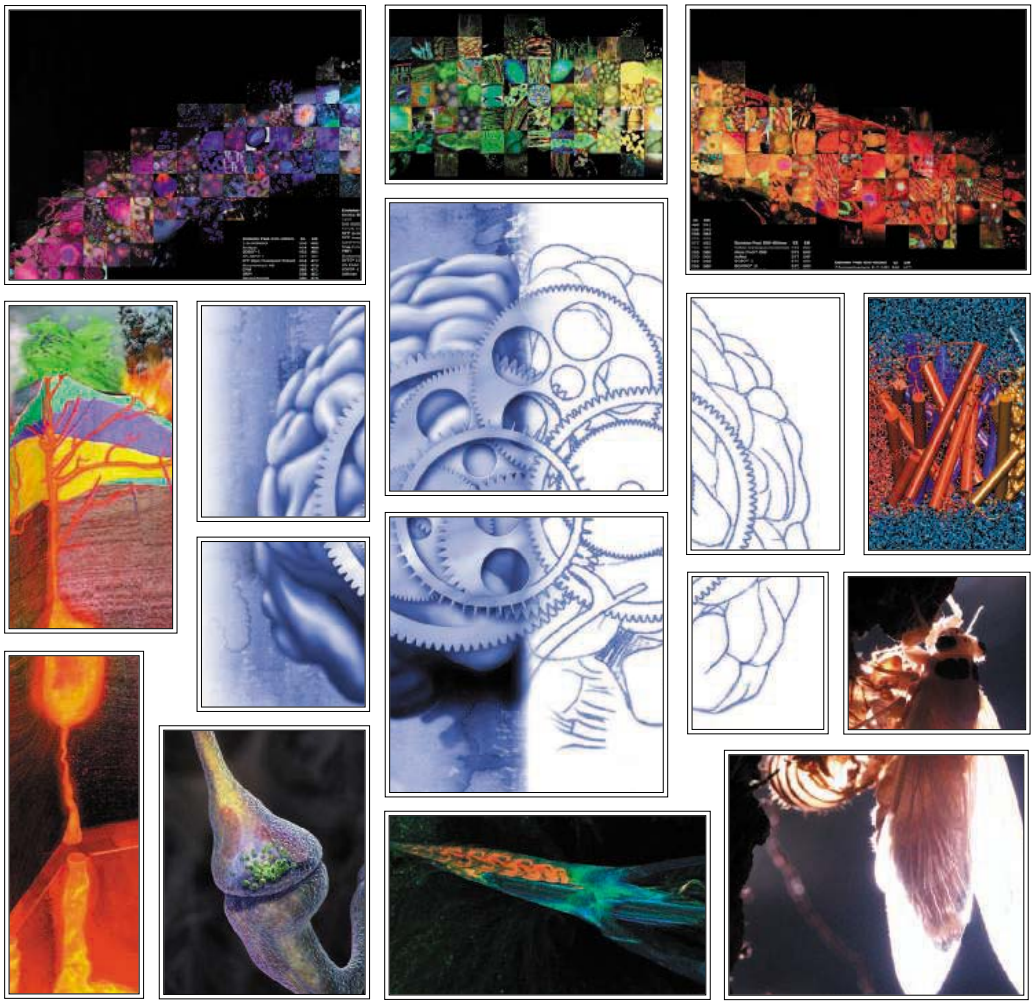

SCIENCE AND ENGINEERING'S MOST POWERFUL STATEMENTS ARE NOT MADE FROM WORDS ALONE

When the left brain collaborates with the right brain, science emerges with art to enhance communication and understanding of research results—illustrating concepts, depicting phenomena and drawing conclusions.

The National Science Foundation (NSF) and the journal *Science*, published by the American Association for the Advancement of Science, invite you to participate in the fourth annual Science and Engineering Visualization Challenge. The competition recognizes scientists, engineers, visualization specialists and artists for producing or commissioning innovative work in visual communication.

ENTRY DEADLINE: MAY 31, 2006

Award categories: Photographs, Illustrations, Interactive Media, Non-Interactive Media and Informational Graphics. Winners in each category will be published in the Sept. 22, 2006 issue of *Science* and *Science* Online, and will be displayed on the NSF Web site.

Complete Entry Information: www.nsf.gov/news/special-reports/scivis/index AND www.sciencemag.org/prizes/

Continued from page 1523

stress regimes, with the observed stress-induced acceleration (approximately a 10-fold rate increase for a 50-piconewton force) arising from a lower-energy transition state for Pd-pyridine bond scission and Pd-DMSO bond formation. — PDS

J. Am. Chem. Soc. 10.1021/ja058516b (2006).

PHYSICS

Black Hole Encryption

What happens to the quantum information ingested by a black hole? In 1997, Thorne and Hawking argued that information swallowed by a black hole is forever hidden, despite the fact that these dense objects do emit a peculiar kind of radiation and eventually evaporate. Preskill countered that for quantum mechanics to remain valid, the theory mandates that the information has to be released from the evaporating black hole in some fashion. Although Hawking conceded in 2004, the disagreement between Preskill and Thorne still stands.

Smolin and Oppenheim now find that one of the main assertions made about black holes may be flawed. It is often assumed that as the black hole evaporates, all of the information gets stored in the remnant until the very end, at which point the information is either released or else disappears forever. Instead, Smolin and Oppenheim suggest that the information is distributed among the quanta that escape during evaporation, but is encrypted and thus effectively locked away.

The catch is that it can only be accessed with the help of the quanta released when the black hole disappears, in much the same way as a cryptographic key unlocks a coded message. The result offers a link between general relativity and quantum cryptography. — DV

Phys. Rev. Lett. **96**, 081302 (2006).

IMMUNOLOGY

Dendritic Cells Diversify

Dendritic cells act as pivotal coordinators of the immune response, inducing T cells to develop specific effector functions, such as the killing of tumor cells.

Chan *et al*. present evidence that at least one new lineage of dendritic cells may, in fact, be tasked with an even broader remit than previously thought. After stimulation through innate immune receptors, a subpopulation of cells could be induced to display major features of conventional dendritic cells. However, before arriving at this point, they first transited through a phenotype more akin to that of a natural killer (NK) cell, including being able to produce interferon gamma (IFN-γ) and to kill NK-sensitive target cells. These interferon-producing killer dendritic cells (IKDCs) displayed similar properties in vivo, and after activation were seen to migrate to lymph nodes to carry out their antigen-presenting functions. Taieb *et al*. also observed that IKDCs were a principal source of IFN-γ and also used expression of the pro-apoptotic ligand TRAIL to kill malignant cells and reduce the tumor burden in a mouse melanoma model. Both studies raise questions about the relationships between the cellular components that sense, regulate, and execute tumor immunity. — SJS

Nat. Med. **12**, 207; 214 (2006).

ECOLOGY

Plant Wars

In plant ecology, it is commonly observed that some plant species will facilitate the establishment or persistence of other species. Weir and Vivanco have uncovered the biochemical basis of such facilitation in North American grasslands invaded by *Centaurea maculosa* (spotted knapweed). The invading species produces a phytotoxin, catechin, which induces oxidative stress in many native plants and often thereby eliminates them entirely from the local ecological community. A few native species, such as *Gaillardia grandiflora*, are able to resist knapweed invasion, and several of these species, including *Lupinus sericeus*, facilitate the resistance of native grasses to the invader. *Lupinus* secretes oxalate from its root tissues in response to catechin exposure. By blocking reactive oxygen species, oxalate affords protection to neighboring vulnerable plants against the toxic effects of catechin. These results suggest strategies for controlling a serious invader and also provide insight into the multiplicity of facilitation mechanisms involved as plant communities develop. — AMS

***Gaillardia* growing among *Centaurea maculosa* plants.**

CREDIT: BRIAN SMALE, SEATTLE

Plant Ecol. 10.1007/s11258-005-0193-8 (2006).

www.sciencemag.org

Science

1200 New York Avenue, NW
Washington, DC 20005
Editorial: 202-326-6550, FAX 202-289-7562
News: 202-326-6500, FAX 202-371-9227

Bateman House, 82-88 Hills Road
Cambridge, UK CB2 1LQ
+44 (0) 1223 326500, FAX +44 (0) 1223 326501

Subscription Services For change of address, missing issues, new orders and renewals, and payment questions: 800-731-4939 or 202-326-6417, FAX 202-842-1065. Mailing addresses: AAAS, P.O. Box 1811, Danbury, CT 06813 or AAAS Member Services, 1200 New York Avenue, NW, Washington, DC 20005

Institutional Site Licences please call 202-326-6755 for any questions or information

Reprints: Author Inquiries 800-635-7181
Commercial Inquiries 803-359-4578
Corrections 202-326-6501

Permissions 202-326-7074, FAX 202-682-0816

Member Benefits Bookstore: AAAS/BarnesandNoble.com bookstore www.aaas.org/bn; Car purchase discount: Subaru VIP Program 202-326-6417; Credit Card: MBNA 800-847-7378; Car Rentals: Hertz 800-654-2200 CDP#343457, Dollar 800-800-4000 #AA1115; AAAS Travels: Betchart Expeditions 800-252-4910; Life Insurance: Seabury & Smith 800-424-9883; Other Benefits: AAAS Member Services 202-326-6417 or www.aaasmember.org.

science_editors@aaas.org	(for general editorial queries)
science_letters@aaas.org	(for queries about letters)
science_reviews@aaas.org	(for returning manuscript reviews)
science_bookrevs@aaas.org	(for book review queries)

Published by the American Association for the Advancement of Science (AAAS), *Science* serves its readers as a forum for the presentation and discussion of important issues related to the advancement of science, including the presentation of minority or conflicting points of view, rather than by publishing only material on which a consensus has been reached. Accordingly, all articles published in *Science*—including editorials, news and comment, and book reviews—are signed and reflect the individual views of the authors and not official points of view adopted by the AAAS or the institutions with which the authors are affiliated.

AAAS was founded in 1848 and incorporated in 1874. Its mission is to advance science and innovation throughout the world for the benefit of all people. The goals of the association are to: foster communication among scientists, engineers and the public; enhance international cooperation in science and its applications; promote the responsible conduct and use of science and technology; foster education in science and technology for everyone; enhance the science and technology workforce and infrastructure; increase public understanding and appreciation of science and technology; and strengthen support for the science and technology enterprise.

Information for Contributors

See pages 102 and 103 of the 6 January 2006 issue or access www.sciencemag.org/feature/contribinfo/home.shtml

Want to see the forest through the trees in the world of science & technology policy and budget issues?

Join the nation's top S&T experts at the AAAS Forum on Science & Technology Policy. 20–21 April 2006 • Washington DC Washington Court Hotel

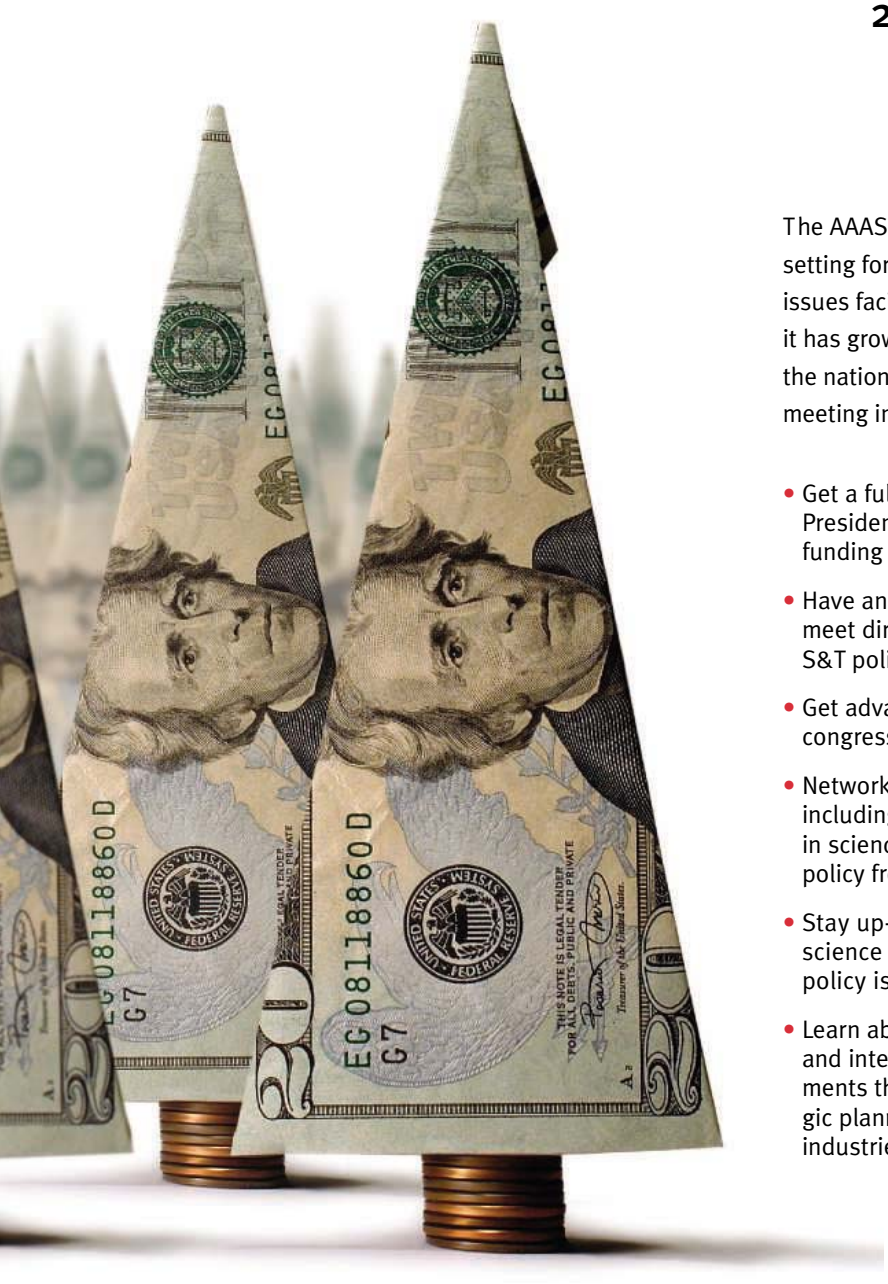

The AAAS Forum on Science and Technology Policy provides a setting for discussion and debate about budget and other policy issues facing the science and technology community. Since 1976, it has grown into an annual institution that draws over 500 of the nation's premier S&T experts. The Forum is the major public meeting in the U.S. on science and technology policy issues.

- Get a full analysis of the President's federal R&D funding proposals.
- Have an opportunity to meet directly with key S&T policymakers.
- Get advance warning of congressional developments.
- Network with colleagues, including top decisionmakers in science and technology policy from all sectors.
- Stay up-to-date on important science and technology policy issues.
- Learn about broader national and international developments that will affect strategic planning in universities, industries, and government.
- Registrants will receive, at the Forum, *AAAS Report XXXI: Research and Development, FY 2007,* a comprehensive analysis of the proposals for the FY 2007 budget, prepared by AAAS and a group of its affiliated scientific, engineering, and higher education associations.
- Registrants will also receive *Congressional Action on R&D in the FY 2007 Budget* later in the fall.

For more complete details on the program, hotel registration and on-line registration, please visit the website: **www.aaas.org/forum**.

www.aaas.org/forum

AAAS
ADVANCING SCIENCE, SERVING SOCIETY

WEB LOG

Bones, Genes, And Brains

A study suggesting that social stress leaves "molecular scars" on the brain and research exposing cultural diversity in gorillas are just two of the subjects that have snared the interest of anthropologist John Hawks of the University of Wisconsin, Madison. His wide-ranging blog excavates novel ideas and noteworthy discoveries in evolution, genetics, and human paleontology. Hawks promises to deliver three to five essays per week. Gems he's come across include a recent *New York Times* piece about the Soviet Union's unsuccessful efforts in the 1920s to prove our simian ancestry by crossbreeding chimps with humans. Readers intrigued by the tiny Flores hominid uncovered in Indonesia 2 years ago will find a section devoted to the controversial remains. >> johnhawks.net/weblog

DATABASE

Caught in a Bind

How tightly a potential drug attaches to its target determines how well the compound will work and what dose patients will need. Researchers can nab binding affinities for about 14,000 compounds at BindingDB from Mike Gilson of the University of Maryland Biotechnology Institute in Rockville and colleagues. Gleaned from the literature, the data indicate the strength of attraction between the compounds and key proteins, such as the caspase proteins that control cellular suicide. You can also upload files of molecules not in the database to compare them to inhibitors of a particular enzyme. >> www.bindingdb.org

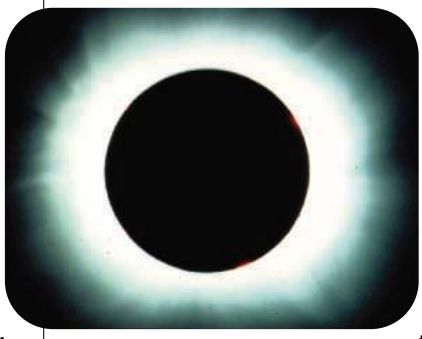

WEBCAST

<< Sun Block

Sky watchers keen to see the upcoming total solar eclipse won't be left out of the dark even if they can't get to a vantage point in South America, Africa, or western Asia. On 29 March, the Exploratorium in San Francisco will webcast the event live from Side, Turkey. On hand at the city's Roman amphitheater will be four telescopes to track the moon's progress and two scientists to explain happenings such as the appearance of the corona (above). This wispy outer layer of the solar atmosphere stands out during totality, when the moon's disk obscures the sun. The festivities start at 5 a.m. U.S. Eastern Time. Totality will begin around 5:54 a.m. and will last a mere 3 minutes and 41 seconds. >> www.exploratorium.edu/eclipse

EXHIBIT

Poor Richard's Web Site

Which early American politician could claim significant discoveries in meteorology, physics, and navigation? Benjamin Franklin (1706–1790) notched these achievements in his spare time, when he wasn't earning a fortune in the printing business or helping invent a country. This biographical site from the Benjamin Franklin Tercentenary, a Philadelphia nonprofit organization set up to honor the Founding Father's 300th birthday this year, offers several pages on Franklin's scientific work. It goes beyond the famous kite-flying experiment that demonstrated lightning was a form of electricity. For instance, Franklin's shipboard notes on everything from sea temperatures to whale feeding habits inspired an improved chart of the Gulf Stream. The Frankliniana section includes samples of his scientific gear, such as this early battery made from water-filled jars (above). >> www.benfranklin300.org/exhibition/_html/0_0/index.htm

IMAGES

Brighter Lights, Bigger Cities

This new map of Earth's nighttime illumination will make light bulb manufacturers glow and astronomers cringe. Released last month, the chart* from the National Geophysical Data Center (NGDC) in Boulder, Colorado, is a composite of satellite images snapped in 2003. Site visitors can download and compare images from as far back as 1992. Although changes in illumination often are hard to detect with the unaided eye, computer analysis shows that the United States and India continue to brighten, says Chris Elvidge of NGDC. However, areas of the former Soviet Union, such as Moldova and Ukraine, have been growing darker. You can peruse processed versions of the maps that highlight brightness differences at this site† from a graduate student in Aachen, Germany. >> *www.ngdc.noaa.gov/dmsp/download.html †www.blue-marble.de/night.php

CREDITS (TOP TO BOTTOM): EXPLORATORIUM; PETER HARHOLDT/AMERICAN PHILOSOPHICAL SOCIETY; NGDC

Send site suggestions to >> netwatch@aaas.org **Archive:** www.sciencemag.org/netwatch

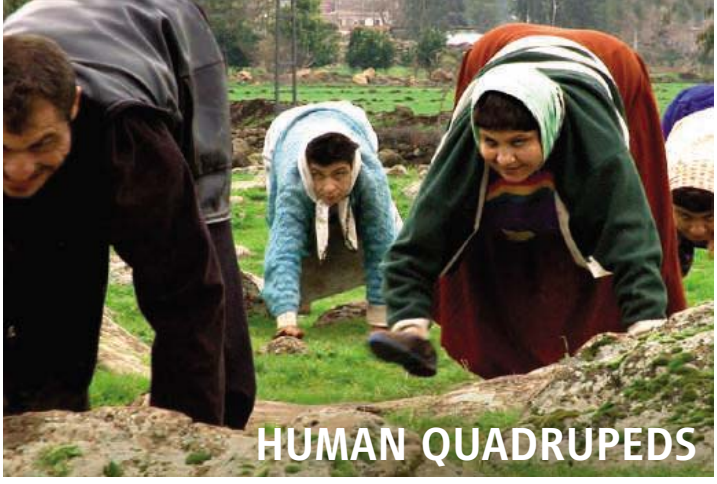

HUMAN QUADRUPEDS

It sounds like something from an old-style circus: Four sisters and a brother who have walked on all fours since childhood. But it's gotten some scientists excited that the siblings could provide a clue to our evolutionary past. And the BBC is jumping in with a special, airing 17 March, on "the first human quadrupeds the modern world has ever seen."

The five are now young adults in a family of 19 living in a village in southern Turkey. Scientists from the nearby University of Cukurova began studying them in 2004. Physiologist Uner Tan found that they are mentally retarded, with very limited vocabularies, and brain scans revealed atrophy in the cerebellum, the brain's motor area. A German-Turkish team published a DNA study online in the *Journal of Medical Genetics* in December 2005 that maps the quadrupedal trait to a particular locus on chromosome 17.

In a paper in the March *International Journal of Neuroscience*, Tan postulates that the syndrome represents "a backward stage in human evolution" and may cast light on how speech and bipedality coevolved. Because the siblings walk on the palms of their hands, rather than on their knuckles, like apes, Tan hypothesizes that our hominid ancestors were palm-walkers.

Researchers at the London School of Economics (LSE), who have also examined the family, have come up with a less dramatic interpretation. Evolutionary psychologist Nicholas Humphrey and colleague John Skoyles believe the condition is the result of a highly unlikely combination: cerebellar atrophy (which alone would not prevent bipedalism) and the whole family's unusual penchant for "bear walking"—using hands and feet instead of the usual knee crawl—in infancy. The LSE team brought in a physiotherapist, who was quickly able to teach the hand-walkers to walk upright. Nonetheless, Humphrey says the phenomenon could indeed supply "a model for how our ancestors might have walked."

Anthropologist Owen Lovejoy of Kent State University in Ohio throws cold water even on this idea, saying "people have been debating ancestral palm-walking for more than 100 years, but its emergence with this type of cerebellar dysfunction in modern humans does nothing to advance the argument."

CRYSTAL PATTERN

Researchers at the University of Wisconsin, Madison, have devised a way to grow human embryonic stem (ES) cells on liquid crystals. The crystal is covered with a thin film of Matrigel, a culture medium. As the cells grow, they reorganize the Matrigel, changing the crystal's response to polarized light. Because differentiating cells exert more tension on the surface on which they are cultured than do undifferentiated ES cells, chemical engineer Sean Palecek and his colleagues hope to develop a tool that can identify differentiating cells while they are still alive. Currently, scientists use antibodies to identify cells, which usually requires killing them.

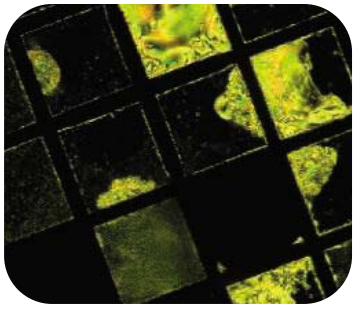

A Crustacean Yeti

What do you get when you cross a gorilla with a lobster? Probably something that looks like the 15-centimeter-long hairy crustacean found near deep-sea vents in the southern Pacific last year. Officially known as *Kiwa hirsuta*, but dubbed the "Yeti crab," the creature is described in the current issue of *Zoosystema* by its discoverers, a team led by marine biologist Michel Segonzac of the French Research Institute for Exploitation of the Sea in Paris. The animal's unusual appearance and DNA qualify it as the first new family of decapods—10-legged crustaceans that include lobsters and crabs—in a century. The lobster lacks eyes, so its "hairs"—actually extensions of its exoskeleton—may be used for sensing. "This is an amazing find," says Richard Lutz, a marine biologist at Rutgers University in New Brunswick, New Jersey. "What I would most like to know about this beast is how ancient its lineage is."

JUPITER'S RED SPOT #2

The world has long been familiar with Jupiter's "Great Red Spot," a swirling storm twice as wide as Earth that's lasted for at least 300 years. Now it may have a rival. In 2000, scientists spotted a large, white-colored oval on Jupiter, the product of three smaller storms merging. But it took amateur astronomer Christopher Go of the Philippines to notice that the spot, dubbed Oval BA, morphed from white to grayish-brown in December. Since late February, it has taken on the rusty red hue of its larger sibling.

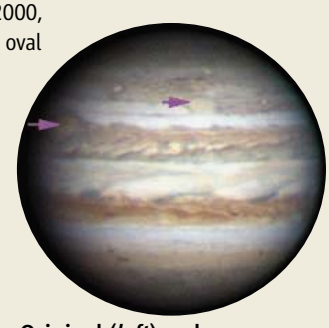

Original (*left*) and new (*right*) spots.

Scientists aren't sure of the reasons for the change, says astronomer Glenn Orton of the Jet Propulsion Lab in Pasadena, California. He and others hypothesize that particularly violent storms propel material from under Jupiter's clouds higher into the atmosphere, where the sun's radiation then sparks a chemical reaction to turn the material red. Other jovian white spots have temporarily turned red in the past; astronomers are curious to see if this one lasts.

CREDITS (TOP TO BOTTOM): BBC; MICHEL SEGONZAC/IFREMER; CHRISTOPHER GO; UNIVERSITY OF WISCONSIN, MADISON

A trace of dark matter? 1535

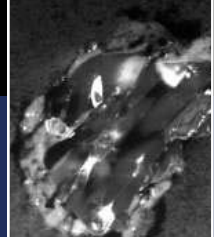

Grains of stardust 1536

NUCLEAR PHYSICS

Researchers Raise New Doubts About 'Bubble Fusion' Reports

Bubble fusion is again generating heat, but not the kind Rusi Taleyarkhan was hoping for. Last week, Purdue University in West Lafayette, Indiana, announced that it was launching a review into allegations that Taleyarkhan—a nuclear engineer at Purdue and the field's chief proponent—had obstructed the work of Purdue colleagues by removing shared equipment, declining to share raw data, and trying to stop them from publishing results that countered his own published work.

The allegations, which Purdue University Provost Sally Mason calls "extremely serious," were first made public in last week's print and online issues of *Nature*. The review also follows a meeting in Taleyarkhan's lab, attended by other researchers trying to replicate his work, at which Taleyarkhan attempted to demonstrate bubble fusion in action. Several participants say the attempt was a dismal failure. And, adding more heat to the debate, a new analysis of data in Taleyarkhan's latest publication casts doubt on the source of a purported signature of fusion.

In an interview with *Science*, Taleyarkhan says he was blindsided by the charges. "It came as a major shock to me when I first heard about it on Tuesday [7 March]," Taleyarkhan says. The following day, Taleyarkhan met with the university administration and agreed to the review. "We decided we as a university need to provide a point-by-point response," Taleyarkhan says.

Evidence that fusion occurs at the heart of collapsing bubbles has been controversial from the beginning. Fusion, the process that powers the sun, normally takes place under intense pressures and temperatures needed to cause atomic nuclei to smash together with enough force to combine, giving off intense energy in the process. On Earth, fusion researchers have tried to replicate the process with the help of intense lasers and magnetic fields. But 4 years ago, Taleyarkhan, then at Oak Ridge National Laboratory in Tennessee, and colleagues published a paper in *Science* claiming that the pressure and heat at the center of collapsing bubbles in an organic solvent had also produced the telltale signature of fusion (*Science*, 8 March 2002, pp. 1808 and 1868). The work held out enormous hope, because if it could be scaled up, it promised near-limitless energy.

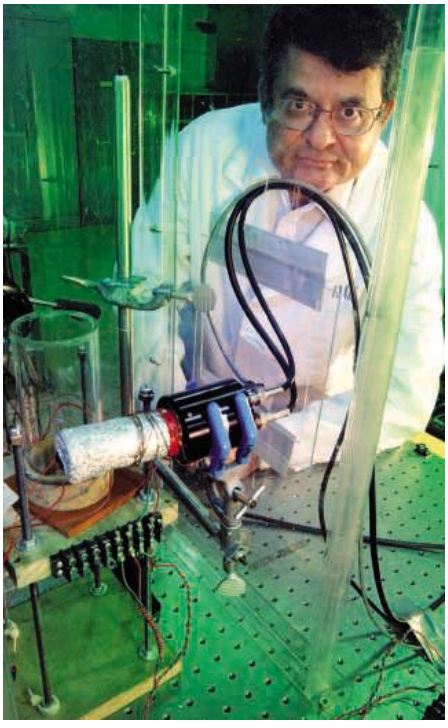

Embattled. Fusion researcher Rusi Taleyarkhan says inquiries will support his lab's evidence of nuclear reactions in hot collapsing bubbles.

In their experiments, Taleyarkhan and his colleagues started with a small cylinder of acetone, a common organic solvent, in which all the hydrogen atoms had been replaced by deuterium, a sister isotope with an additional neutron. The researchers bombarded the cylinder with intense ultrasound and zapped the deuterated acetone with a pulse of neutrons or, in the group's most recent experiment, alpha particles. The combination caused bubbles to form, swell, and then collapse, producing a tiny flash of light, a phenomenon known as sonoluminescence. According to the authors, it also fused pairs of deuterium atoms, creating either tritium and a proton or helium-3 and an extra neutron, which were counted by the group's detectors.

The work drew fire from other researchers who either could not reproduce the results or challenged it on theoretical grounds. Since the original *Science* paper, Taleyarkhan and colleagues have published two other papers in *Physical Review E* and *Physical Review Letters* (*PRL*)—both prestigious peer-reviewed journals—offering further evidence of bubble fusion. But the effect has yet to be confirmed by researchers who have not been affiliated with Taleyarkhan at one time.

It hasn't been for lack of effort. Last year, the U.S. Defense Advanced Research Projects Agency (DARPA) supported efforts by Seth Putterman, a chemist at the University of California, Los Angeles (UCLA), to replicate Taleyarkhan's results. Taleyarkhan and sonoluminescence expert Kenneth Suslick of the University of Illinois, Urbana-Champaign, also received funding. With independent confirmation still lacking, on 1 March, DARPA convened a contractors' meeting in Taleyarkhan's lab at Purdue in hopes that they could all see tabletop fusion in action. But Putterman and others at the meeting say it didn't go well. "The trip from the point of view of reproducing his experiment was a waste of time," Putterman says.

For starters, the acoustic device that generates the bubbles wasn't working well, says meeting attendee Felipe Gaitan, chief scientist at Impulse Devices, a company in Grass Valley, California, working to commercialize bubble fusion. Instead of creating a largely clear solution with a few bubbles that would concentrate the acoustic energy, the acetone was clouded with bubbles. "We expected he wouldn't see any [results]," Gaitan says. But Taleyarkhan claimed the experiment was producing fusion.

Rather than measuring fusion's excess neutrons with a standard device called a scintillation detector, however, Taleyarkhan measured them with plastic neutron traps. The devices are common among nuclear engineers but not among researchers, because they can't measure the precise energy level of recorded neutrons—an important clue to their source. Taleyarkhan says that, unlike scintillation detectors, plastic traps need not be calibrated, and they show irrefutable evidence of the presence of neutrons. But Putterman notes that because plastic traps take hours to process, the group had no time for control experiments needed to interpret the results. "It was very frustrating," Gaitan adds.

At the meeting, Putterman also presented calculations made by his graduate student Brian Naranjo that questioned the conclusions of Taleyarkhan's most recent paper, published in January. The calculations suggested that the energy levels of the neutrons Taleyarkhan reported are not what the Purdue group should have seen if deuterium atoms were in fact fusing. Instead, Naranjo said, the results are a far better match for what the scintillation detector ▶

CREDIT: LYNN FREENY/U.S. DEPARTMENT OF ENERGY FILE PHOTO

would have registered in the presence of californium-252, a radioisotope commonly used in nuclear laboratories.

Putterman says Taleyarkhan told him he does have californium-252 in his lab but keeps it enclosed in a shielded vault. Robert Block, a nuclear engineer at Rensselaer Polytechnic Institute in Troy, New York, and a co-author with Taleyarkhan, argues that cosmic rays and other background neutrons in the experiment could have made its readings resemble the expected signature of californium. But Putterman counters that when Naranjo calculated how the detectors would register radioactive cesium and cobalt that are used to calibrate the device, the result was a near-perfect match to the calibration data Taleyarkhan published in his paper. Still, Taleyarkhan says, it's hard for him to assess Naranjo's work until it has been published in a peer-reviewed journal. (Naranjo says he has submitted the work to *PRL*.) "We are trying to address the issues brought up by UCLA," Taleyarkhan says. And that will be done through publications. "That's how we believe science should be conducted," he adds.

Nevertheless, it now appears that DARPA is preparing to pull the plug on the effort to replicate Taleyarkhan's results. When a DARPA representative at the 1 March meeting suggested that the "successful" experiment be crated up and shipped to UCLA for independent verification, Putterman says, Taleyarkhan balked, saying he was too busy with teaching and research commitments. Because Putterman's lab has been unable to independently verify the results, the agency says the program won't proceed. "If that had been successful, DARPA would have considered moving into a second phase that would have focused on whether the results can be scaled up," DARPA spokesperson Jan Walker said in a statement on Friday.

Despite the latest round of controversy, Putterman and other sonoluminescence researchers all say the idea of bubble fusion remains worth exploring. Unlike the discredited notion of cold fusion in which deuterium atoms supposedly fuse in a hunk of palladium metal, collapsing bubbles are calculated to produce temperatures in the millions of degrees, possibly high enough in that tiny volume to allow atoms to fuse.

For now, however, the immediate hurdle for Taleyarkhan will be convincing Purdue officials that the effect and his methods are sound. In guidelines issued late last week, Purdue officials said their review would be conducted by three senior Purdue professors and overseen by Peter Dunn, Purdue's associate vice president for research. An initial fact-finding phase will be completed by 1 June. Mason said the results of the review will be made public. Taleyarkhan says he is confident he will be vindicated: "We stand by whatever data we have presented," he says.

–ROBERT F. SERVICE

CHEMISTRY

Columbia Lab Retracts Key Catalysis Papers

For synthetic chemists working to craft new molecules, a carbon atom surrounded by hydrogens can be as hard to handle as a greased pig. Undaunted, in recent years researchers have scrambled to devise schemes for plucking select hydrogens off carbon and replacing them with other atoms that offer an easier handhold. A pioneer of this subfield, known as C-H activation, Columbia University chemist Dalibor Sames has developed a wealth of advances along with his group members. But some of the lab's results are now in doubt.

Last week, the *Journal of the American Chemical Society* (*JACS*), a leading chemistry journal, printed corrections for three papers from the Sames lab. Two of the papers on C-H activation catalysts were fully retracted, and part of a third was withdrawn. In each case, the retractions say that the work was disavowed after Sames group members could not reproduce the results following the departure of Bengü Sezen, a former Sames group graduate student, who was the lead author of the two retracted papers and a co-author of the third. *JACS* Editor Peter Stang says the corrections came at the request of the Sames group. Sames did not reply to repeated phone and e-mail messages from *Science*.

Susan Brown, Columbia's director of public affairs, says the university has launched a review of the case, but that she cannot comment on its scope or timing. "It's our policy not to comment on reviews while they are ongoing, so the integrity of the process can be maintained," Brown says.

In an e-mail exchange, Sezen, who is now a Ph.D. candidate in the group of University of Heidelberg molecular biologist Elmar Schiebel, according to the group's Web site, says the retractions came as a surprise. "Professor Dalibor Sames or anyone else from Columbia University did not contact me regarding the retractions," she says. For the two retracted papers, Sezen named two other Sames group members who she says repeated her work while she was out of town. For the third paper, Sezen says her contribution was "limited to an intellectual one." But Kamil Godula, one of the Sames group members Sezen cited, says in an e-mail that the reactions worked only when Sezen was in town. The other Sames group member Sezen mentioned did not return messages from *Science*.

Justin Du Bois, a synthetic chemist at Stanford University in California, calls the retractions "a bit of a blow" to the subfield of C-H activation: "These were definitely important papers," he says. Sezen has at least [illegible] publications on C-H activation with Sames in addition to those corrected in *JACS*. Benjamin Lane, a former Sames group member now working as a chemist with the pharmaceutical company Biogen in Cambridge, Massachusetts, says some of Sezen's work has been replicated and has been used by chemists in the pharmaceutical industry. Says Lane, "She has done some good things and made an impact on the field."

–ROBERT F. SERVICE

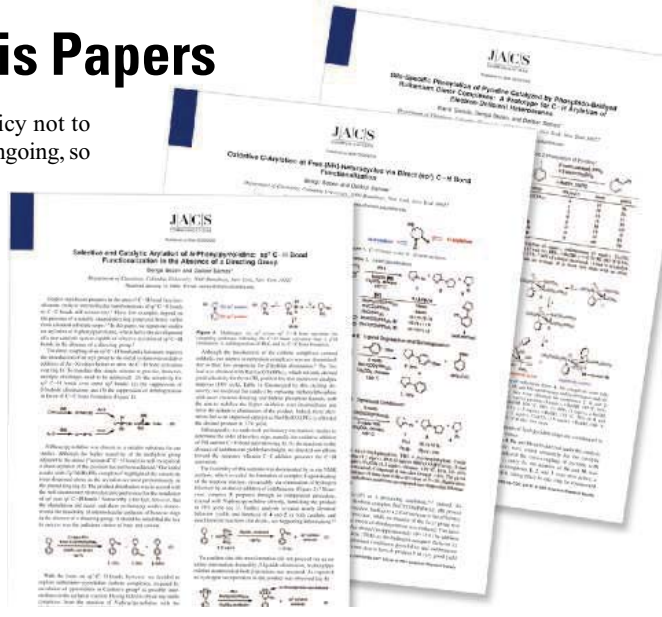

Deactivated. Researchers withdrew two synthetic-chemistry papers and part of a third after failing to reproduce the results.

You could be next

Yes, it *can* happen to you:
If you're making inroads in neurobiology research and you've received your M.D. or Ph.D. within the last 10 years, the Eppendorf & *Science* Prize for Neurobiology has been created for YOU!

$25,000 Prize

This annual research prize recognizes accomplishments in neurobiology research based on methods of molecular and cell biology. The winner and finalists are selected by a committee of independent scientists, chaired by the Editor-in-Chief of *Science*. Past winners include post-doctoral scholars and assistant professors.

If you're selected as next year's winner, you will receive $25,000, have your work published in the prestigious journal *Science* and be invited to visit Eppendorf in Hamburg, Germany.

What are you waiting for? Enter your research for consideration!

Deadline for entries:
June 15, 2006

For more information:
www.eppendorf.com/prize
www.eppendorfscienceprize.org

"This is one of the premier awards for young neuroscientists. Receiving the Prize was a true honor."

Michael D. Ehlers, M.D., Ph.D.
Associate Professor and
Wakeman Scholar
Investigator, HHMI
2003 Winner

eppendorf & Science PRIZE FOR NEUROBIOLOGY

YYePG Proudly Presents,Thx for Support

COSMOLOGY

Magnet Experiment Appears to Drain Life From Stars

It's an unassuming experiment: to see how a magnetic field affects polarized laser light. And the rotation the researchers saw was tiny, a mere 100,000th of a degree. If the result is true, however, the implications are huge. According to researchers in Italy who conducted the experiment, this slight twist in the beam—the result of disappearing photons—suggests the existence of a small, never-before-seen neutral particle, which, if made in stars, would siphon off all their energy.

Even theorists who find that scenario far-fetched are struggling to explain the disappearance of the photons. "I'm skeptical of the particle interpretation," says theoretical physicist Georg Raffelt of the Max Planck Institute for Physics in Munich, Germany. "But there are no other obvious explanations."

Standard physics predicts a very small rotation in a beam's polarization in a magnetic field due to ordinary particles popping in and out of the vacuum. But when researchers at the PVLAS experiment at Legnaro National Laboratory of Italy's National Institute for Nuclear Physics turned on their 5-tesla magnet in 2000, they immediately saw a rotation 10,000 times larger than expected, says PVLAS member Giovanni Cantatore of the University of Trieste. The rotation is caused by the loss of a small number of photons whose electric fields line up with the magnetic field. This selective disappearance is what physicists would see if the missing photons were converting into neutral particles about 1 billionth of the mass of electrons.

"If you believe the signal is real, then the interpretation is a new particle," says theoretical physicist Andreas Ringwald of DESY, Germany's particle physics center near Hamburg. But Ringwald thinks most physicists believe the rotation comes from some subtle artifact of the instruments. The PVLAS team has spent 5 years looking for such systematic effects: They have rotated and reduced the magnetic field, added air to their vacuum system, and changed the frequency of the laser. "All this time we have tried to make the signal go away," Cantatore says. It hasn't. The PVLAS team doesn't claim to have discovered a new particle. "It is important to be careful," Cantatore says. A paper in *Physical Review Letters* is due this month.

"These are very serious, very competent people," says Pierre Sikivie of the University of Florida, Gainesville, who also looks for novel particles with magnetic fields. Still, he has a "wait-and-see attitude," because the implications would be "revolutionary."

The PVLAS particle, if it exists, has the makings of an axion, a hypothetical particle that some cosmologists propose is the invisible missing dark matter that makes up a large chunk of the mass of the universe. However, the particle suggested by the PVLAS experiment is not what the theorists ordered. It couples so strongly to photons that the axion-search experiments currently scattered around the globe should have seen loads of them coming from the sun (*Science*, 15 April 2005, p. 339). Such a stream of invisible particles out into space would drain a star of its energy in a few thousand years. But we know stars, including our sun, last for billions of years. Raffelt says the PVLAS particle would need "crazy properties" to match astrophysical constraints, but there is no fundamental reason they can't behave that way.

The PVLAS collaboration plans to settle the question with an experiment involving two magnets separated by a wall. On one side, part of a laser beam would be converted into a flux of PVLAS particles, which would fly straight through the wall. On the other side, the second magnet would reconvert some of the particles back into photons, at a rate of one every 2 seconds, Cantatore predicts. Ringwald is proposing a similar experiment at DESY, and CERN, the European particle physics lab near Geneva, Switzerland, is also considering one.

Although most physicists doubt the reality of this particle, they are curious to see what comes of it. "People want to give the idea a fair hearing," Sikivie says. "If it turns out to be true, it will be a theoretical challenge to explain, but also an opportunity."

–MICHAEL SCHIRBER

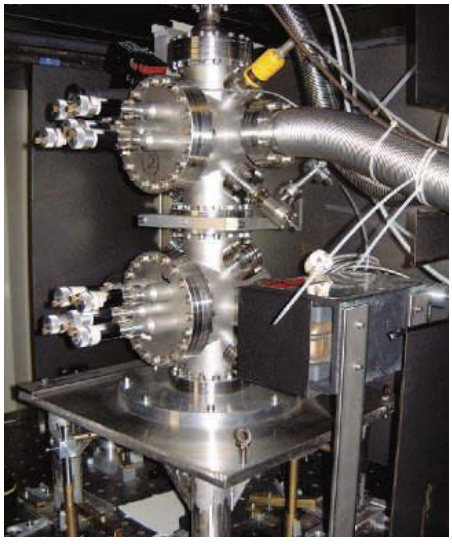

CREDIT: THE PVLAS COLLABORATION

A twist in the tale. By rotating a laser beam with magnets, this experiment may have found never-before-seen particles.

Turtles Imperiled, Biologists Say

Despite a letter of protest signed by more than 100 scientists, a regional fisheries council has moved to open a protected area of the U.S. Pacific coast to drift gillnet fishing, a practice that kills many marine species. Since 2001, this type of fishing has been seasonally banned along most of the Oregon and California coast to protect critically endangered leatherback turtles. But the Pacific Fishery Management Council says that regulations on fishing vessels, including closing all fishing if two turtles are caught during the leatherback annual migration, are sufficient to protect the species while increasing commercial access to fishing grounds during their most productive season.

Conservation scientists fear that the turtles will be pushed even closer to the brink of extinction. "There is not a lot of leeway with this species," says David Ehrenfeld, a biologist at Rutgers University in New Brunswick, New Jersey, who signed the protest letter. In April, the council also will consider whether to allow longline fishing, which often catches turtles and other marine species as well. Both decisions must be approved by the National Marine Fisheries Service, which is expected to make a decision on the proposal by the end of July.

–JENNIFER CUTRARO

UK Biobank Taking Deposits

This week, U.K. officials launched what may be the largest-ever population study. The goal of the project, dubbed UK Biobank, is to track 500,000 adult volunteers for up to 30 years seeking to link their genes, lifestyle, and common diseases.

Proposed in 1999, the $106 million effort has been criticized for its size and for the possibility of turning up spurious associations between genes and disease. Principal investigator Rory Collins of the University of Oxford says these are "misconceptions" and that the study's large size will make false associations unlikely. But organizers now emphasize that UK Biobank is a broad medical study and that biological markers such as blood protein levels may yield as much information as genes.

Manchester citizens aged 40 to 69 are receiving invitations to join in a 3000-subject pilot project; national enrollment begins later this year and will continue for 5 years. The study is funded by government agencies and the Wellcome Trust charity.

–JOCELYN KAISER

PLANETARY SCIENCE

Minerals Point to a Hot Origin for Icy Comets

HOUSTON, TEXAS—Scientists analyzing the first samples returned from a comet announced startling news this week. They are finding not the unprocessed "stardust" thought to have glommed together in the frigid fringes of the early solar system, but bits of rock forged in white-hot heat. The discovery may mean that the disk of dust and gas from which all planetary bodies formed was far more violently mixed than previously thought.

At the Lunar and Planetary Science Conference here, leaders of the 150-strong Stardust science team told how team members on four continents have been slicing, dicing, and analyzing 10-micrometer particles collected by the Stardust spacecraft. It swept by comet Wild 2 two years ago and returned its samples to Earth on 15 January. Working first on the larger particles snared in the Stardust collectors, analysts are finding mineral crystals such as forsterite, pyroxene, anorthosite, spinel, and titanium nitride. These "are all minerals that formed at moderately high to extremely high temperatures," Stardust principal investigator Donald Brownlee of the University of Washington, Seattle, later told a press conference at NASA's nearby Johnson Space Center.

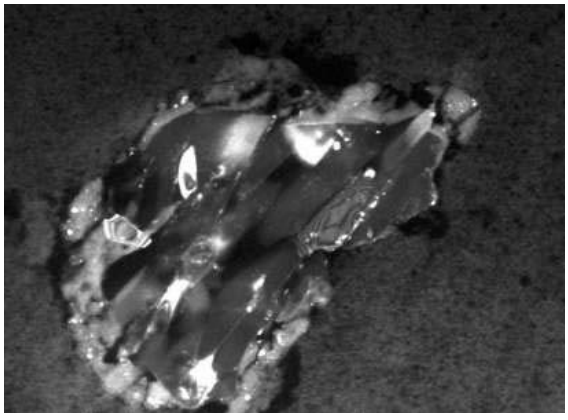

A hot one. This 2-micrometer bit of comet Wild 2—a magnesium-rich olivine called forsterite—formed at a high temperature, perhaps near the young sun.

"These are hot minerals from the coldest place in the solar system," the comet-forming region beyond Neptune.

The minerals must have formed at 1400 K or hotter, Brownlee said, especially a couple of particles resembling the so-called calcium-aluminum inclusions (CAIs) known from meteorites. In contrast, the dust the analysts expected to find in comets would be submicrometer in size and lacking in any crystalline structure. That's the form they would have taken as they condensed from vapor in deep space after being blown off other stars.

Brownlee offered two possible solutions to the hot-and-cold conundrum. The crystals "could have come from the innermost region of the [still-forming] solar system," he said. Astrophysicist Frank Shu of National Tsing Hua University in Taiwan has advanced that idea to explain CAIs and once-molten droplets called chondrules that dominate the most common type of meteorite coming from the asteroid belt (*Science*, 20 June 1997, p. 1789). Shu argues that the young, violently active sun would have blasted nearby solids to their melting points and magnetically flung them—including CAI and chondrule particles—out over the disk as far as the comet-forming region. Alternatively, says Brownlee, the Stardust minerals may have crystallized from melts near other stars and reached the forming solar system by some unspecified means.

"If this were astronomy, we'd stop there," Brownlee told his colleagues. Astronomers have nothing to go on but the electromagnetic spectrum, which would yield no further information in this case. "But we have samples; that will solve this mystery." The key will be isotopes, he said. The mix of isotopes in solar system material is wildly different from that of other stars, he noted, as evidenced in rare bits of interstellar material long known from meteorites. "We'll know in weeks or months," says Brownlee.

–RICHARD A. KERR

U.S. REGULATORY POLICY

Courts Ruled No Forum for Data-Quality Fights

A federal appeals court ruled last week that the public can't sue federal agencies over their compliance with a controversial law on the quality of scientific data. The decision is a victory for environmentalists and government watchdog groups, which have accused industry of using the so-called Data Quality Act (DQA) to delay new regulations.

The 2000 act, which requires federal agencies to set standards to ensure the quality of information they disseminate, allows critics to petition agencies that they believe have not met the standards. Many such petitions have been filed, largely by industry groups challenging reports on topics such as the effects of toxic chemicals. But petitioners have no recourse if rebuffed.

In May 2003, the Salt Institute and the U.S. Chamber of Commerce filed a DQA petition to obtain unpublished data from DASH-Sodium, a study funded partly by the National Heart, Lung, and Blood Institute (NHLBI) (*Science*, 30 May 2003, p. 1350). The study found that eating less salt lowered participants' blood pressure, and NHLBI has cited these findings in recommending that all Americans lower their salt intake. But DASH researchers had failed to break down the data for subgroups (such as white men under age 45 without hypertension), argued the industry group, which demanded that NHLBI release these data for independent analysis. After NHLBI rejected the request, the groups sued the Department of Health and Human Services (HHS), NHLBI's parent agency.

In November 2004, a Virginia federal district court turned down the suit, a decision upheld on 6 March by the U.S. Court of Appeals for the 4th Circuit in Alexandria, Virginia. The panel of three judges found that the DQA "does not create any legal right to information or its correctness," and for that reason, the plaintiffs lacked legal "standing" to pursue their case.

The decision is "very broad" and will likely stand because it's from "a very conservative panel," says University of Maryland law professor Rena Steinzor of the Center for Progressive Reform. But proponents of the law say they aren't giving up. "I'm deeply disappointed. I feel that Congress intended that the Data Quality Act should be enforced," says Richard Hanneman, president of the Salt Institute.

NHLBI has been providing a limited data set to qualified researchers since January 2004. But the Salt Institute has not requested the data because "there's no assurance" its request would be granted, Hanneman says. Jim Tozzi of the industry-funded Center for Regulatory Effectiveness, who helped craft the legislation, is thinking about suing HHS over its position that marijuana has no accepted medical benefit. "A dozen people with diseases" might have a better shot at convincing a court they have standing, says Tozzi.

Meanwhile, the Chamber of Commerce is pondering whether to push for legislation that would open up any DQA decision to legal challenge. Steinzor predicts that such an effort will mobilize opponents of the act to maintain the status quo.

–JOCELYN KAISER

CREDIT: NASA/JPL-CALTECH/UNIVERSITY OF WASHINGTON

U.S. DEPARTMENT OF ENERGY

Can Energy Research Learn to Dance to a Livelier Tune?

Turning basic research into commercial technology has never been easy. But it's especially hard in the energy sector, where problems such as cutting greenhouse gas emissions and finding less-polluting energy sources resist easy solutions despite laboratory breakthroughs by the country's best minds.

Last week, Congress took the first steps toward addressing that problem, as legislators embraced the concept of creating a small, nimble agency within the mammoth Department of Energy (DOE). The Senate Committee on Energy and Natural Resources voted out a bill (S. 2197) that would authorize an Advanced Research Projects Agency–Energy (ARPA-E) modeled on DARPA, the 48-year-old agency within the Pentagon. The next day, a House panel devoted a 2-hour hearing to the concept, proposed last fall in a National Academies report on U.S. technical competitiveness (*Science*, 21 October 2005, p. 423).

"A small, agile, DARPA-like organization could improve DOE's pursuit of R&D much as DARPA did for the Department of Defense," wrote the academies panel in a report described at the House hearing by Nobelist Steven Chu, director of DOE's Lawrence Berkeley National Laboratory in California. ARPA-E's "transformational" research, the panel said, "could lead to new ways of fueling the nation and its economy, as opposed to incremental research on ideas that have already been developed." Chu, like others, said fixing a depleted basic science base was the top priority for energy research, but that ARPA-E could help "bridge the gap between basic energy research and development/industrial innovation."

Like DARPA, ARPA-E would employ a small staff of program managers who would leave industry and academia for short stints with the government. The agency should have the freedom to start and stop programs quickly and—again like DARPA—be attuned to the spectrum of research from basic discovery through prototypes, before handing it over to the private sector for commercialization.

Melanie Kenderdine of the Gas Technology Institute in Washington, D.C., says the staff could bridge the sort of communication gaps between vehicle research and fuels work that she witnessed as a senior DOE official during the Clinton Administration. Although Dan Arvizu, director of DOE's National Renewable Energy Laboratory in Golden, Colorado, fears that a new agency could grow unwieldy, he likes DARPA's focus on the "entire spectrum" of research. That philosophy, he says, could bolster agency initiatives on ethanol and photovoltaics by focusing on basic scientific questions in addition to technological improvements.

Even so, experts warned legislators that simply recreating DARPA wouldn't work. The military is a different breed of cat than the energy sector, says former DARPA Director Frank Fernandez. The government would do a better job fostering new technologies by using taxes or mandates on existing energy sources, says House Science Committee Chair Sherwood Boehlert (R–NY), who calls himself an "open-minded skeptic."

CREDIT: ROY KALTSCMIDT/BERKELEY LAB

Risky business. Nobelist Steven Chu backs a new agency that would fund "out-of-the-box," high-payoff energy research.

Even supporters are wary of any new agency that might drain resources from President George W. Bush's request for a 14% increase in the 2007 budget of DOE's Office of Science. The Senate bill, which has 65 co-sponsors in a body of 100, would authorize a $250-million-a-year operation. But Senator Pete Domenici (R–NM), who chairs the Senate panel that controls DOE and who introduced the bill, hasn't endorsed a specific funding level.

When President Dwight D. Eisenhower created DARPA's forerunner after the Soviet Union launched Sputnik, he had to overcome the objections of military leaders. To succeed, ARPA-E's supporters will have to convince the Bush Administration that it won't "distract" from DOE's other initiatives, as Energy Secretary Samuel Bodman told a Senate panel earlier this month. But they are on their way to capturing another key element of DARPA's longevity—the support of Congress.

YYePG Proudly Presents,Thx for [illegible]

–ELI KINTISCH

Stem Cells by the Sea

Four institutions in southern California are joining forces to pool resources and position themselves better to get grants from the new California Institute for Regenerative Medicine (CIRM). The four neighbors on Torrey Pines Mesa—the University of California, San Diego (UCSD), the Burnham Institute for Medical Research, the Salk Institute for Biological Studies, and the Scripps Research Institute—plan to form an entity called the San Diego Consortium for Regenerative Medicine. The consortium envisions a central facility on the UCSD campus. As part of the agreement, the four institutions will seek grants from CIRM only as part of the consortium.

Meanwhile, CIRM is waiting for the resolution of litigation charging that it lacks adequate government oversight. A judge's decision is expected by the end of the month, but appeals are likely to delay bond sales for the $3 billion initiative by another year.

–CONSTANCE HOLDEN

Argonne Slapped for Safety Flaws

Argonne National Laboratory Director Robert Rosner is hoping that a sharp letter by the Department of Energy (DOE) criticizing the Illinois lab's safety practices won't hurt an upcoming bid by the University of Chicago to retain management of the 2900-employee lab.

Rosner, who joined the lab last year, is part of a new management team; bids to run the 60-year-old lab are expected next month. But last week, in a preliminary notice of violation, DOE announced that inspections last year turned up lapses in radiation dose monitoring, safety training, air sampling, and other practices—and that the lab would be fined $550,000.

Due to a legal loophole, the University of Chicago won't have to pay the fines. But the offenses "certainly won't help" the university's bid to retain the management contract, says Al Teich, head of science policy at AAAS (which publishes *Science*). No injuries were sustained nor research projects damaged as a result of the safety violations.

"We are committed to making safety as outstanding as the science at Argonne," says a university spokesperson. In January, Rosner stopped experiments on radioactive materials at the Alpha-Gamma Hot Cell Facility, a shielded lab for work on radiation emergencies, one of several "corrective actions" that DOE said the lab has already taken.

–ELI KINTISCH

RUSSIAN SCIENCE

Moscow Plans Tighter Control of Science Academy's Research Money

MOSCOW—The Russian Academy of Sciences (RAS) is facing a tough new challenge from the government, according to its leaders. Members say they were shocked earlier this month to learn that the Ministry of Finance is proposing changes that could give bureaucrats more authority over science funding decisions and radically alter research management.

One of the proposed changes would take away the academy's independent control over the distribution of public science funds now in its purview, sources say. The academy would no longer be funded as a line item in the national budget; instead, the government would allocate funds to the Ministry of Education and Science, which would redistribute money to various programs, including to RAS. Academicians fear this would give bureaucratic and political considerations too much weight in decisions.

Losing independence? Russian Academy of Sciences President Yuri Osipov has urged the finance minister to drop proposed changes.

In addition, the Finance Ministry has proposed that an institute's private earnings should go to the state rather than to the institute that earned them. Currently, 40% of RAS's revenue comes from independent sources such as grants and contracts for commercial, defense, and consulting work. Both finance proposals are circulating in the ministries but have not been approved by the cabinet or the Duma.

RAS Vice President Alexandr Nekipelov, among others, sees these moves as an attack on the academy's independence. Says Nekipelov: "These amendments will lead to financial collapse of the whole structure of the academy." In an "epic" struggle more than a year ago, says Nekipelov, the government tried to take control of academy resources (*Science*, 24 September 2004, p. 1889). "But we managed to assert that important organizations like the academy, Moscow University, and others … would preserve the right to be in charge of the funds at their disposal." Now, Nekipelov says, "these amendments have come up all of a sudden," renewing the struggle. The proposal to transfer outside earnings to the state is "absurd," he argues, because it could drive academic institutions out of "innovative R&D activities" that could foster new industries. RAS President Yuri Osipov has written to the finance minister urging that the proposals be dropped.

The Ministry of Education and Science seems to think RAS officials are being alarmist, however. Innovation policy department chief Alexandr Khlunov says his ministry argued that the proposed budget changes "must not affect the ability of research institutions to do research." As a result, Khlunov said, the changes will be flexible, but he declined to give specifics. "It doesn't make any difference" who provides funds," he says: Managers should manage, and "scientists should do research."

The proposed changes may not affect the other big provider of basic research money, the Russian Foundation for Basic Research. Director Vladimir Lapshin says it is too early to say what will happen: "There are many amendments at the moment … and too much confusion." He suggests that a government review of science funding could be useful if it leads to more competitive peer-reviewed science, which is already increasing "every year." But he is adamant on one point: "It takes too long" from the moment the budget is approved to when researchers get their money; something must be done to speed this up.

–ANDREY ALLAKHVERDOV AND VLADIMIR POKROVSKY

Andrey Allakhverdov and Vladimir Pokrovsky are writers in Moscow.

PARTICLE PHYSICS

Linear Collider Partners Woo Newly Opened India

NEW DELHI—With the wheels of Air Force One barely off the tarmac following U.S. President George W. Bush's visit, which ended India's 3 decades as a nuclear pariah state, a delegation of U.S. and European physicists arrived here last week to discuss India's involvement in the International Linear Collider. ILC is a multibillion-dollar particle accelerator that researchers hope will study the exotic species of particles that existed just after the big bang. "We all hope that India will become a key partner in this global collaboration," says Pier Oddone, director of the Fermi National Accelerator Laboratory near Chicago, Illinois. According to some, India could even host the machine.

Sanctions have been imposed on India since 1974 because of its clandestine nuclear weapons program and its refusal to sign the Nuclear Nonproliferation Treaty. But under the U.S.-Indian deal agreed upon earlier this month, India would be able to trade in civilian nuclear technology with other countries in exchange for opening up a majority of its nuclear facilities to international inspection.

Despite their exclusion from U.S. research programs, Indian researchers have made names for themselves in high-energy physics. India has observer status at CERN, the European particle physics lab near Geneva, Switzerland, and has contributed precision equipment worth more than $20 million to the construction of CERN's Large Hadron Collider.

With a price tag that could reach $8 billion, ILC will be a global project. India is being considered for a position as an "equal partner," says Barry Barish, director of ILC's Global Design Effort: "Early participation in ILC will enable India to integrate their program in the development stages with the world program and bring back new expertise, rather than just contributing some technology to a large external project."

"India is seriously considering to join the project," says nuclear physicist Valangiman Subramanian Ramamurthy, secretary of India's Department of Science and Technology. Some think India could play an even greater part, with its combination of skilled scientists and engineers and low labor costs. According to Carlo Pagani, a member of the visiting delegation from Italy's National Institute for Nuclear Physics in Milan: "It just might be advantageous for the world to house the project in India or China."

–PALLAVA BAGLA

CREDIT: YURI KADOBNOV/AFP/GETTY IMAGES

INFECTIOUS DISEASES

Report Concludes Polio Drugs Are Needed—After Disease Is Eradicated

As efforts to wipe out polio intensify in the handful of countries where the disease still occurs naturally, public health experts are thinking about what comes next. In a report released last week, a seven-person committee appointed by the National Research Council in Washington, D.C., argued for developing an antipoliovirus drug in the event of a posteradication outbreak. But whereas everyone on the panel endorsed that advice in principle, not all felt it was achievable.

Antivirals might seem unnecessary for a disease that will be declared eradicated. But since efforts to stamp out polio began in 1988, public health officials knew that their success might create a difficult dilemma: The very oral polio vaccine used to prevent the disease can spur fresh outbreaks, because it contains live but weakened versions of the three types of poliovirus. Vaccinated individuals, particularly immune-deficient ones, shed the virus and can transmit it to the unvaccinated. That poses a problem, because several years after the disease is declared eliminated, countries may stop vaccinating their residents. "What are we going to do then, when vaccine virus is still circulating around?" asks Samuel Katz, an infectious-disease specialist at Duke University in Durham, North Carolina, who was the committee chair. "If we get outbreaks again and go in with oral vaccine and control them, you're perpetuating the dilemma."

The report, requested by the World Health Organization (WHO) in Geneva, Switzerland, and the U.S. Centers for Disease Control and Prevention in Atlanta, Georgia, calls for developing a safe, orally administered antiviral that prevents and treats polio. But some panelists question the prescription. "I started to wonder, 'Is this going to be realistic?' " says committee member Neal Nathanson, associate dean for global health programs at the University of Pennsylvania School of Medicine in Philadelphia. Among other things, he wonders how easy it would be to persuade thousands of healthy people to take an antiviral drug for a disease they may not get. Although vaccine-driven outbreaks are real—last year, both Indonesia and Madagascar suffered outbreaks of paralytic polio caused by vaccine-derived viruses—Nathanson notes that they have been "more or less self-limited."

Moreover, developing a new drug can take years, and WHO anticipates that transmission of polio will end in about a year. James Hogle, a Harvard University structural biologist, adds that it's unclear who would fund such drug development, because a polio antiviral is unlikely to rake in anything approaching a profit. "It's rather late in the game to do this," he says.

But with the endgame in sight, Bruce Aylward, WHO's coordinator of the global eradication initiative, worries that "you're going to have an increasingly vulnerable world to polio." Antivirals haven't been pushed until now, says Aylward, because WHO only recently became confident that it could stamp out the disease. **–JENNIFER COUZIN**

SCIENTIFIC COMMUNITY

Bias Claim Stirs Up Ghost of Dolly

A hearing into a scientist's claim that he was the target of harassment and racial discrimination has put under a microscope the lab where Dolly the sheep was cloned. It also has prompted the man widely recognized as Dolly's creator, Ian Wilmut, to give detailed evidence on who deserves credit for the successful experiment—and precisely how much. In testimony, Wilmut gave himself less than a third of the credit.

The investigation arises from a suit brought by molecular biologist Prim Singh. He charges that Wilmut, then a researcher at the Roslin Institute in Midlothian, U.K., bullied him and stole his ideas. Seeking $1.74 million, he claims that Roslin passed him over for promotions because of his race and forced him to quit after he lodged a complaint against Wilmut in 2003. Wilmut and Roslin have denied the charges. (A previous discrimination claim that Singh filed was dismissed last year.) Singh did not work on the Dolly project, but testimony in his case provides an inside view of the team that pulled off one of the world's most famous biology experiments.

An employment tribunal in Edinburgh began hearing testimony from Singh and other witnesses in November 2005, but it was testimony last week from Wilmut himself that caught wider attention. Singh's lawyers questioned Wilmut about the famous paper describing Dolly, published in *Nature* in 1997. Wilmut, who is now at the University of Edinburgh, was lead author and has received most of the public credit. But in court he said that he had neither developed the key technology nor conducted the experiments that led to Dolly's birth. When Singh's lawyer asked him if the statement "I did not create Dolly" was true, Wilmut answered "Yes." He said he played a coordinating role in the project but that his colleague Keith Campbell, now at the University of Nottingham, deserved "66%" of the credit for the breakthrough.

Murky origins. A discrimination hearing has reignited old resentments among the team that cloned Dolly the sheep.

CREDIT: REUTERS

Other members of the team offered independent views to journalists covering the case. Bill Ritchie, a technician at Roslin, says he and Karen Mycock, another technician, did the nuclear transfer procedures. But neither is listed as an author on the paper. Alan Colman, now CEO of ES Cell International in Singapore, who was working at Roslin's sister institute PPL Therapeutics at the time of the Dolly experiments, says that authorship questions on the paper were controversial from the start. He says Ritchie and Mycock made important contributions to the project, but adds that Wilmut did not take an undue share of the credit. "Ian conceived the program, worked on it for many years, and hired the right people to get it done," he says.

Roslin itself, meanwhile, is planning a complete makeover and change of location. After a positive scientific review last fall, says director Harry Griffin, Roslin has been approved to join a new outfit in 2009 called the Edinburgh Bioscience Research Centre at the University of Edinburgh School of Veterinary Studies. The U.K. government is pledging $60 million to the merger, which will also bring in experts in prion diseases from the nearby Institute for Animal Health. Griffin says its leaders aim to raise another $52 million for a research facility employing 500 scientists. He would not comment on the Singh case.

–GRETCHEN VOGEL AND ELIOT MARSHALL

With reporting by John Bohannon.

Flush with new discoveries, NASA's space and earth scientists now must figure out how to get by on $3 billion less than they expected—without triggering a civil war

A Space Race To the Bottom Line

CREDIT: K. BUCKHEIT/*SCIENCE* (ILLUSTRATION); IMAGES: NASA; JUPITER IMAGES; GETTY IMAGES

SPACE SCIENCE IS GETTING PLENTY OF headlines these days. A new spacecraft is on its way to Pluto, one just arrived at Mars, and another may have spotted water on Saturn's moon Enceladus. But last week, two dozen senior researchers met in a windowless Washington, D.C., conference room to try to avert what some fear could turn into a civil war among earth and space science disciplines scrambling for science's decreasing share of the space agency's budget.

The go-go years of the past decade came to a crashing halt last month, when NASA's 2007 budget request pulled more than $3 billion out of the long-term science plan (*Science*, 10 February, p. 762). NASA has since canceled two missions close to launch, deferred a handful for a year or two, and effectively killed a half-dozen others slated for orbit in the next decade. To cope with the rapidly unfolding crisis, members of the National Academies' Space Studies Board assigned themselves the task of building a united front among notoriously fractious disciplines to make the best use of scarce dollars. They don't have much time. "Everyone recognizes that we are in this together—and we have to solve it together," says board member Daniel Baker, a space physicist at the University of Colorado, Boulder.

The unprecedented effort to find an acceptable alternative to NASA's 2007 budget request before legislators act on the bill this summer has the blessing both of the agency and Congress. Space agency chief Mike Griffin says he is willing to consider the results (see sidebar, p. 1542). And congressional staffers are cheering them on. "I hope you folks will have the answer to the problem—because we don't," Richard Obermann, a minority staffer with the House Science Committee, told the board on 6 March. Adds David Goldston, the committee's chief of staff, "Whatever pattern is set this year, it will be the pattern for the foreseeable future."

Out of business?

Griffin and other Administration officials dismiss the idea that a $5.3 billion request for research in 2007 represents a crisis for the field. "There is still a very large overall science budget, just not as large as had been hoped," says Griffin. "NASA's science budget is almost as large as the entire [budget for the] National Science Foundation. I'm unable to see the level of damage here that those who are concerned about it seem to see." Indeed, the proposed 1% boost

in NASA science over current levels beats out the average 0.5% cut borne by nondefense discretionary programs across all federal agencies.

Scientists, congressional staffers, and NASA science staff say this statement is true but misleading. Two years ago, the agency planned to boost its science budget by $1.5 billion by 2009. As recently as last year, the increase was still $1 billion by 2010. Based on such optimistic figures, NASA in recent years began funding work on an ambitious array of projects, most to meet scientific goals set by the National Academies in its various decadal plans.

But those projects are costing far more than planned. The most dramatic example is the James Webb Space Telescope (JWST), whose price tag is now $4.5 billion—$1 billion above the planned cost. A host of other projects are in the same boat. Costs for the Stratospheric Observatory for Infrared Astronomy (SOFIA) have ballooned from $400 million to $650 million, and several projects considered by the academies to be mid-size efforts now have grown to the size of flagship missions. “The problem is an enormous growth in the cost of doing programs; the numbers don’t add up,” says Thomas Young, a former aerospace executive and board member.

To cope with the budget crunch combined with rising costs, NASA officials are taking drastic steps to curtail costs and limit new starts—mostly by deferring missions, canceling troubled projects, and reducing the amount of money scientists spend to analyze research data. As a result, the number of new science missions launched will decline from a dozen this year to one in 2010. In the meantime, aging spacecraft will begin winking off. “This looks like we’re going out of business,” Baker says.

Mission	Purpose	Status
SOFIA (Stratospheric Observatory for Infrared Astronomy)	Infrared observing aboard aircraft	On hold
NuSTAR (Nuclear Spectroscopic Telescope Array)	Image high-energy x-ray radiation	Canceled
Hydros	Study Earth’s soil moisture	Canceled
Terrestrial Planet Finder	Image Earth-sized extrasolar planets	Deferred indefinitely
Global Precipitation Measurement Mission	Conduct first comprehensive precipitation measurements	Deferred
Dawn	Visit two large asteroids	Canceled/Under review
JDEM (Joint Dark Energy Mission)	Look for evidence of dark energy	To be competed
Orbiting Carbon Observatory	Carbon measurements	Delayed 1 year
Landsat Data Continuity Mission	Remote sensing	Delayed 2 years
Mars Sample Return	Martian geology	Delayed indefinitely
Space Interferometry Mission	Search for Earth-like planets	Delayed 3 years
WISE (Wide-Field Infrared Explorer)	All-sky survey	Delayed 1 year

Defer and delay

For some disciplines, that is no exaggeration. “The last mission we have in earth sciences is in 2012,” frets board member Berrien Moore, co-chair of another academies’ panel writing that discipline’s first decadal plan. “After that, we’d better be going to Mars!”

Congress forced NASA 2 years ago to reverse planned cuts in several earth science missions. But in recent weeks, the agency has canceled the Deep Space Climate Observatory (*Science*, 6 January, p. 26) and Hydros, a $170 million effort to study soil moisture. NASA officials say that Hydros was a backup to two other missions now in the works, and so it never was a confirmed project—a point disputed by some researchers. The agency also will delay the Global Precipitation Mission by 30 months and slow a precursor mission for a national environmental satellite system by 18 months.

For solar physics, the top-ranked mission in a 2003 decadal study by the academies—a magnetosphere mission—now will not be launched until 2013. Two other high-ranked missions—two separate constellations of small satellites to examine the interaction between the ionosphere and the thermosphere and understand how energy moves in Earth’s magnetotail—are on indefinite hold.

Rising costs and flat budgets also will force NASA to compete several new astrophysics flights. Constellation X—a group of four orbiting telescopes that will image the x-ray universe—will face off against the Laser Interferometer Space Antenna, designed to detect gravitational waves, and a Joint Dark Energy Mission with the Energy Department. The winner will get a green light to start work in earnest in 2009 or 2010 for a launch later in the next decade. The other two will have to wait their turn.

NASA also has stopped early work on the Terrestrial Planet Finder, a spacecraft that researchers had hoped to orbit in the next decade in search of Earth-sized planets. The Space Interferometry Mission, another planet-hunting mission, won’t be orbited until 2015 or 2016, and its cost has grown to $4 billion.

Stanford University astrophysicist Roger Blandford also fears for the future of the Explorer program, NASA’s attempt to launch smaller missions run by principal investigators. The agency earlier this month canceled the Nuclear Spectroscopic Telescope Array, which was to open up the high-energy x-ray sky, and postponed the next solicitation for an Explorer from 2007 to 2008—delaying the launch of the next mission to 2014 at the earliest.

Planetary scientists are perhaps most bitter about the 2007 budget request. Their program, complains Reta Beebe, a board member and an astronomer at New Mexico State University in Las Cruces, “has unfortunately become the source of funds supporting other NASA programs.” She and others note that of the $3.1 billion taken out of the 5-year budget projections for science, nearly all came from planetary missions. NASA recently canceled the Dawn mission to the asteroids Vesta and Ceres, rejected pleas to begin a large mission to Jupiter’s moon Europa, and cut the astrobiology budget by a whopping 50%. (On 10 March, Griffin agreed to review the decision on Dawn.) The agency also abandoned plans to launch a Mars sample return by 2016.

“The proposed budget transforms an existing, vibrant program into a stagnant holding pattern,” says Beebe. “The damage is immediate and increasingly irreversible. … We are reenacting the events of the 1970s,” she says, when a series of exciting missions was followed by a 15-year drought.

Yet even that grim prediction doesn’t match the crisis in the space life and microgravity sciences field, which had $1 billion for both ground- and space-based research as recently as 2004. With the advent of the exploration initiative, that figure has plummeted to near zero. Donald Ingber, a Harvard University biologist and board member, insists that such cuts will make long-term human space flight impossible, given

Bumpy Ride for Data-Driven NASA Chief

"Show me the data" proclaims the framed sign over Michael Griffin's desk. It is a warning to visitors to his ninth-floor office at NASA headquarters in downtown Washington, D.C., that the 56-year-old aerospace engineer and applied physicist brooks little idle chatter, speculation, or wheeling and dealing. "I don't try to be blunt," says Griffin, nearing his first anniversary as head of the $16.6 billion U.S. space agency. "I just tell the truth."

Griffin's two predecessors, Daniel Goldin and Sean O'Keefe, were known for being mercurial, visionary, and political—anything but plainspoken. And Griffin's no-nonsense approach to fixing what ails the U.S. space program—from a crippled space shuttle program and a half-completed international space station to an overmortgaged science portfolio—has earned him a large reservoir of good will in the White House and on Capitol Hill.

But that pool is drying up (*Science*, 10 March, p. 1359). President George W. Bush wants NASA to focus on building a new rocket to take humans back to the moon. Lawmakers are pressing to keep space shuttle jobs and contracts intact as long as possible. NASA's international partners worry that the agency still might back out of finishing the space station, leaving them and their hardware in the lurch. And scientists need continued big annual budget increases to build the many ambitious missions planned for the next decade (see main text, p. 1540).

To keep these disparate groups happy, Griffin last fall asked the White House to give NASA a whopping 8.8% increase in 2007. He warned the Office of Management and Budget (OMB) that a lesser boost would force him to halt the growth in science. When Bush decided to ask Congress for a 3.2% increase, Griffin kept to his word—prompting an angry reaction from scientists and their allies on Capitol Hill.

Under fire, Griffin's refreshing forthrightness can come across as political insensitivity. He dismisses the community's outcry as "a hysterical reaction, a reaction out of all proportion to the damage being done." But those words are likely to antagonize rather than assuage science advocates. Griffin is famous for responding rapidly to e-mails; he carries his Blackberry everywhere. Yet he's uncomfortable with the face-to-face socializing and back scratching that his predecessors practiced so adroitly. "You have to form relationships, not just send an e-mail," says one who has worked closely with him. Although Griffin responds rapidly, adds another, "his impatience often shows."

Griffin's style befits his career as a project engineer, industry manager, and lab department head. He also spent a difficult few years at NASA headquarters overseeing the agency's doomed lunar and Mars exploration program, an idea that George H. W. Bush proposed but Congress ultimately ignored.

This time around, he knows he will need help from all quarters. "I need the scientific community to worry about more than just what happens to science," Griffin says. To win them over, however, he may want to serve up a slice of tact and empathy along with the data.

What follows is an edited transcript of a 7 March interview with *Science*'s Andrew Lawler.

Q: You told Congress in 2003 as a private citizen that NASA needed $20 billion to do everything on its plate. What's changed?
What's changed is that I am an agency head. Every agency head would like to have more money. The average [nondefense discretionary program] took a half-percent decrease in the 2007 budget—so we got 3.7% above average. I think that is extraordinary. My response is to say thank you. Is it as much as we would like to have? Of course not.

Q: How much would you like to have?
I'm not going to answer that question.

Q: In a November letter to OMB, you asked for 8.8%.
There are months of work that go into preparing a budget with all kinds of trades, and that was a missive from a snapshot in time.

Q: Has your promise last year not to take "one thin dime" out of science come back to haunt you?
No. I found we could not complete the station and the shuttle and make any kind of progress in replacing the shuttle with the CEV [Crew Exploration Vehicle] and the CLV [Crew Launch Vehicle] without restricting the growth of science. We just ran out of money.

Q: Why should science take the fall?
Your readers should understand that everybody in NASA paid the piper. I cannot accept an argument that manned space flight operations got everything they wanted when they in fact took a huge whack.

Q: But isn't it the science aboard the station that is taking the whack?
I chose to assemble now and utilize later.

Q: Why is there no post-2010 plan to do science on the station?
I inherited what I inherited. Clearly, the [National Academies'] report [on space station science] is very specific and unequivocal in its position that we don't have a good space station utilization plan. But we have several years now to develop one, and we will.

We still have an extraordinarily healthy science program. Some missions have been delayed, some things of a doubtful nature have been canceled, and a couple of things are on the chopping block because the promised technical performance has not come true.

Q: Is there any prospect of ending the shuttle program before 2010, thereby freeing up money for exploration and science?
We're flying out the shuttle program in an orderly and disciplined way and using it to finish the space station. We have been working on it for 20 years, and we have multiple international commitments. Other things we would like to do—including exploration and science—are going to have to sacrifice for the next few years to allow that to come true.

unknowns about radiation hazards and the impact of microgravity on human health. "This will set the manned program back by decades," he warns.

Civil war or solidarity?

Short of an abrupt cancellation of the shuttle and station programs, there are few prospects for a dramatic change in science's fortunes. Indeed, this year's overall increase of 3.2% for NASA may look good in a few years, board members fear. And even if the shuttle is retired in 2010 once the space station is complete, the space agency's budget documents note that the dividends will go into the exploration program rather than science.

"We're not going to be able to execute the decadal [studies] as they exist," concludes Lennard Fisk, board chair and a geophysicist at the University of Michigan, Ann Arbor. A 1% increase in NASA's science budget, he says, translates into "a major retrenchment." And scientists say they would rather make the hard choices than leave them to NASA managers. If they don't, Blandford warns, "choices that should be scientific and technical will be left to the political process."

After hours of discussion, board members broadly agreed to protect research funds for the university community and for smaller missions. That decision puts larger efforts in each discipline on the chopping block. Moore suggested that to find earth science savings, the $430 million Landsat mission slated for launch by 2010 could be reviewed, and astronomers privately and

Q: Is that why NASA canceled NuSTAR and the asteroid mission Dawn—and soon maybe the flying observatory SOFIA [Stratospheric Observatory for Infrared Astronomy]?
Dawn was canceled because it was overrun by 20%. That's a matter of project discipline. Dawn's cancellation has nothing to do with [the NASA] budget. SOFIA is so far overrun on cost and schedule that only if we can convince ourselves that it is past its technical problems—well, the question is, can its people get to the finish? I insist on imposing discipline on our projects.

Q: But why are the shuttle and station exempt from this rule?
Or the James Webb [Space Telescope]? Our highest priority missions will be completed. And other things in science are suffering to pay for James Webb. So what's your point?

Q: Why should projects like Webb be exempt, if the smaller ones often are being managed more innovatively than large projects?
Our science program is structured to pay appropriate and ample respect to National Academy priorities. Now at present, in the astrophysics line, James Webb is the highest priority. Fifteen minutes after I arrived at NASA, I learned there was a billion-and-a-half shortfall in James Webb. My choice is either to continue to respect the academy's priority and find the money from lower priorities, or I could disrespect the academy's priorities and cancel James Webb. That is a bind. My choice will generally be to respect academy priorities. If the academy revisits the issue of whether a single flagship mission is worthy of the sacrifice of numerous lesser, possibly more innovative, more timely missions, that would be a judgment for the scientific community to make. I'm listening. But I do not view that as a judgment that a NASA administrator ought to make.

Q: NASA's credibility as a nonpartisan purveyor of science was damaged in the flap over recent complaints by agency scientist Jim Hansen. What are you doing to change that?
Even Jim Hansen has not said that anyone has interfered with his publication of his technical conclusions. Jim said he was inappropriately denied an interview he should have been able to conduct. And I think he was right. And the person who denied him that interview is no longer here. I can only assure you, as the head of NASA, that no one here wants or will tolerate any restriction on the prerogatives of technical people to publish their conclusions to their community and have them be debated on their merits in their communities.

Q: What do you say to those scientists who are angry at the 2007 request?
We have a space program that requires some sacrifices. I'm sorry they have to happen, but they do.

–ANDREW LAWLER

CREDIT: LUKE FRAZZA/AFP/GETTY IMAGES

cautiously suggest that deferring JWST by a few years could rescue smaller astrophysics missions in the near term. The largest planetary mission now scheduled is the Mars Science Laboratory, slated for a 2009 launch; among solar physicists, the big-ticket item is the Solar Dynamics Observatory due for orbit in 2008.

But some researchers already are parrying the attack on larger programs. William Smith, president of the Association of Universities for Research in Astronomy, warned in a 6 March letter to the House Science Committee that NASA's great observatories provide $70 million annually for research analysis. Canceling flagship missions "would simply shift the imbalance, not eliminate it," he says. Attempts to defer, descope, or kill JWST or the Mars Science Lab also would provoke major battles in each discipline and in Congress.

Even if NASA likes what the space board proposes, the fight is sure to move quickly to Capitol Hill, where projects with the most political muscle could triumph despite the academies' priorities. Still, researchers say they have to try. "Dividing a growing pie is not all that difficult," says George Paulikas, board vice chair and a retired aerospace executive who is heading up the academies' effort.

But the alternative to consensus is too awful to contemplate, he adds. Can independent-minded scientists agree on a plan that spreads the pain around? "Stay tuned until April," he says.

–ANDREW LAWLER

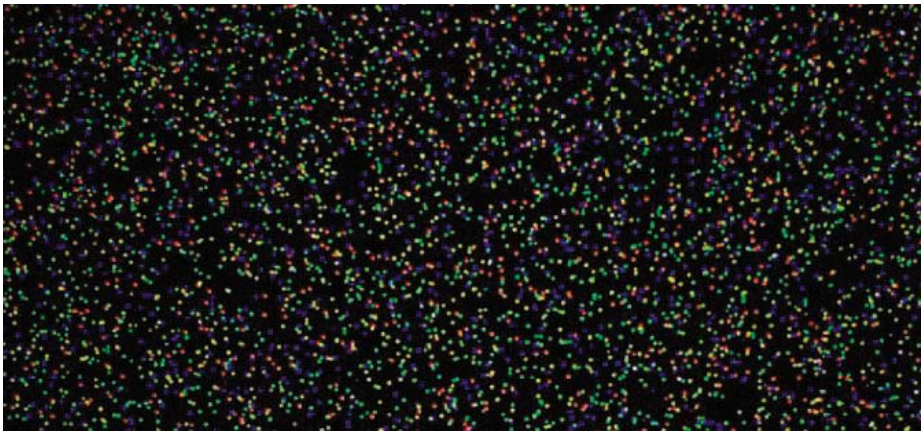

Charting islands. Glowing dots on a glass slide mark cloned DNA being sequenced.

GENE SEQUENCING

The Race for the $1000 Genome

Fast, cheap genetic analyses will soon become a reality, and the consequences—good and bad—will affect everybody

MARCO ISLAND, FLORIDA—Computers aren't the only things getting better and cheaper every time you turn around. Genome-sequencing prices are in free fall, too. The initial draft of the first human genome sequence, finished just 5 years ago, cost an estimated $300 million. (The final draft and all the technology that made it possible came in near $3 billion.) Last month, genome scientists completed a draft of the genome sequence of the second nonhuman primate—the rhesus macaque—for $22 million. And by the end of the year, at least one company expects to turn out a full mammalian genome sequence for about $100,000, a 3000-fold cost reduction in just 6 years.

It's not likely to stop there. Researchers are closing in on a new generation of technology that they hope will slash the cost of a genome sequence to $1000. "Advances in this field are happening fast," says Kevin McKernan, co–chief scientist at Agencourt Bioscience in Beverly, Massachusetts. "And they are coming more quickly than I think anyone was anticipating." Jeffrey Schloss, who heads the sequencing-technologies grant program at the National Human Genome Research Institute (NHGRI) in Bethesda, Maryland, agrees. "People are roundly encouraged and nervous," Schloss says—encouraged because their own technologies are working, and nervous because their competitors' are too.

A host of these novel sequencing technologies were on display last month at a meeting here.* Although no one at the meeting claimed to have cracked the $1000 genome sequence yet, researchers are getting more confident that it's a real possibility. "From what I've listened to the last few days, there is no physical principle that says we shouldn't be able to do a $1000 genome," says Harvard University sequencing pioneer George Church.

Even today, the declining cost of genome sequencing is triggering a flowering of basic research, looking at broad-ranging topics such as how the activation of genes is regulated and understanding genetic links to cancer. And as prices continue to drop, sequencing will revolutionize both the way biologists hunt for disease genes and the way medical professionals diagnose and treat diseases. In fact, some researchers say cheap sequencing technology could finally usher in personalized medicine in a major way. "The promise of cheap sequencing is in the understanding of disease and biology, such as cancer, where the genome changes over time," says Dennis Gilbert, chief scientist of Applied Biosystems, the leading gene-sequencing-technology company based in Foster City, California. "It will enable different kinds of science to be done." Of course, as with other forms of high technology, that promise brings new risks as well. Researchers expect cheap sequencing to raise concerns about the proliferation of bioterrorism agents as well as patient privacy.

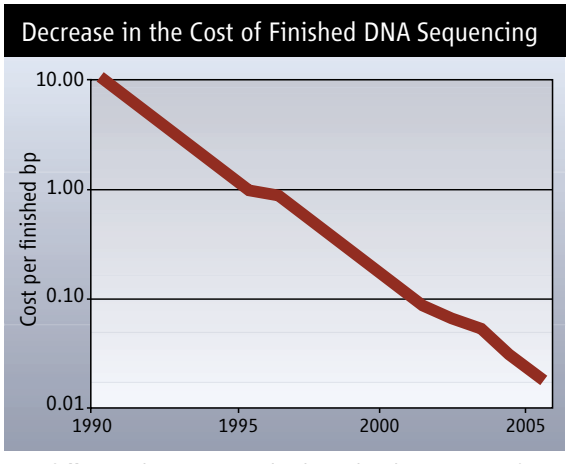

Free fall. As with computer technology, the plunging cost of DNA sequencing has opened new applications in science and medicine.

The race is on

The first group to produce a technology capable of sequencing a human genome sequence for $1000 will get instant gratification, as well as potential future profits: In September 2003, the J. Craig Venter Science Foundation promised $500,000 for the achievement. That challenge has since been picked up by the Santa Monica, California–based X Prize Foundation, which is expected to up the ante to between $5 million and $20 million. But the competition really began in earnest in 2004, when the National Institutes of Health launched a $70 million grant program to support researchers working to sequence a complete mammal-sized genome initially for $100,000 and ultimately for $1000. That program has had an "amazing" effect on the field, encouraging researchers to pursue a wide variety of new ideas, says Church. That boost in turn has led to a miniexplosion of start-up companies, each pursuing its own angle on the technology (see table, p. 1546).

All are racing to improve or replace a technology first developed by Fred Sanger of the U.K. Medical Research Council in the mid-1970s that is the basis of today's sequencing machines. The technique involves making multiple copies of the DNA to be sequenced, chopping it up into small pieces, and using those pieces as templates to synthesize short strands of DNA that will be exact complements of stretches of the original sequence. The synthesis essentially mimics the cell's processes for copying DNA.

The technology relies on the use of modified versions of the four bases that make up DNA, each of which is tagged with a different fluorescent marker. A short DNA snippet called a primer initiates the synthesis at a specific point on the template DNA, and the altered bases—which are vastly outnumbered by normal bases in the mix of reagents used to perform the synthesis—stop the process when one of them is tacked onto the end of the growing DNA strand. The result is a soup of newly synthesized DNA fragments, each of which started at the same point but ends at a different base along the chain.

Today's sequencers separate these fragments by passing the soup through tiny capillaries containing a gel; the shorter the fragment, the faster it moves through the gel. The process, known as capillary electrophoresis, is so effective that

CREDITS (TOP TO BOTTOM): OMEAD OSTADAN/SOLEXA; ADAPTED FROM GRAPH PROVIDED BY JEFFREY SCHLOSS/NHGRI

* Advances in Genome Biology and Technology Conference, Marco Island, Florida, 8–11 February 2006.

each fragment that emerges from the capillary is just one base longer than the one that preceded it. As each fragment emerges, it is hit by a laser, which causes the altered base at the fragment's tip to fluoresce. A computer records the identity of these bases and the sequence in which they appear. Eventually, the process generates billions of stretches of sequence that are fed into pattern-recognition software running on a supercomputer, which picks out overlaps and stitches the pieces together into a complete genome sequence.

A long list of refinements in capillary electrophoresis systems, coupled with increased automation and software improvements, has driven down the costs of sequencing 13-fold since these machines were introduced in the 1990s. Most of the new technologies aim to miniaturize, multiplex, and automate the process even further. They fall into three main camps. The first, called sequencing by synthesis, tracks bases as they are added to a growing DNA strand. Second is a group of techniques that sequence single DNA molecules. Finally, nanopore-sequencing technologies coax DNA to wriggle through a tiny pore and read the bases either electronically or optically as they go by.

Sequencing-by-synthesis strategies have a head start. Indeed, one company, 454 Life Sciences Corp. in Branford, Connecticut, already has a commercial instrument; it sold 20 of them last year. The company's technique, called pyrosequencing, first chops a genome into stretches 300 to 500 base pairs long, unzips the double strands, discards one strand, and links the other to compounds tethered to a plastic bead—each bead gets just one strand. These snippets are then copied by the polymerase chain reaction (PCR) until the copies cover each bead. The beads are separated on a plate containing as many as 1.6 million wells and dosed with a series of sequencing reagents and nucleotides. Every time a nucleotide is tacked onto a growing DNA chain, the reaction triggers the release of a compound called pyrophosphate, which in turn prompts a firefly enzyme called luciferase in the well to give off a flash of light. By correlating the recorded flashes from each cell with the nucleotides present at the time, a computer tracks the systematic sequence growth of hundreds of thousands of DNA snippets simultaneously.

In August 2005, 454 Life Sciences researchers reported that they had sequenced the nearly 600,000-base genome of a bacterium known as *Mycoplasma genitalium* with an accuracy of 99.4%, as well as the larger 2.1-megabase genome of *Streptococcus pneumoniae* (*Science*, 5 August 2005, p. 862). At the Florida meeting, Michael Egholm, 454's vice president for molecular biology, reported that they had since sequenced four different microbial genomes, each with greater than 99.99% accuracy. "In a 6-month period, we have dramatically improved the data quality," Egholm says. Higher accuracy is critical because two genomes being compared, such as those of normal cells and cancer cells, could differ in only one part per million.

David Bentley, chief scientist for Solexa in Little Chesterford, U.K., also reported heady progress. Like 454's approach, Solexa's turns separate snippets into roughly 1000 exact copies. Instead of attaching individual DNA strands to a separate bead, Solexa researchers fix each strand to a different spot on a glass slide, much as they do in standard microarrays. They then duplicate those strands, creating myriad tiny DNA islands. Finally, in a step akin to Sanger sequencing, they use nucleotides with four different colors and standard microarray optics to simultaneously track the growth of strands complementary to those attached to the slide. Bentley reported that his team had sequenced a 162-kilobase stretch of human DNA and compared it to the standard reference sequence worked out by the Human Genome Project. Their sequencing turned out to be more than 99.99% accurate and spotted all 162 common mutation sites known as single-nucleotide polymorphisms known to exist in that stretch of DNA.

Church has developed a slightly different sequencing approach, part of which Harvard has licensed to Agencourt. In this approach, called sequencing by ligation, researchers start with a short snippet of DNA bound to a bead or a surface. They then add a short stretch of DNA called an anchor primer that binds a known starter sequence on the DNA snippet. Additional nine-base primers, known as query primers, are then added to the mix. These primers come in each possible sequence combination, and each has a labeled A, G, T, or C at just one position. If a short query primer with a correct complementary sequence binds to the DNA, an enzyme called ligase stitches it to the anchor primer to hold it to the surface, and the other primers, which bind less tightly, are washed off. The mix is then hit with a blast of laser light to reveal the color of fluorescence that gives away the identity of the newly bound base. Finally, the query and anchor primers are stripped away, and another anchor primer is added as the first step to identifying the next base in the template strand. Agencourt's McKernan said their version of the technology could currently sequence some 200 million bases a day and may reach 3 billion a day by August.

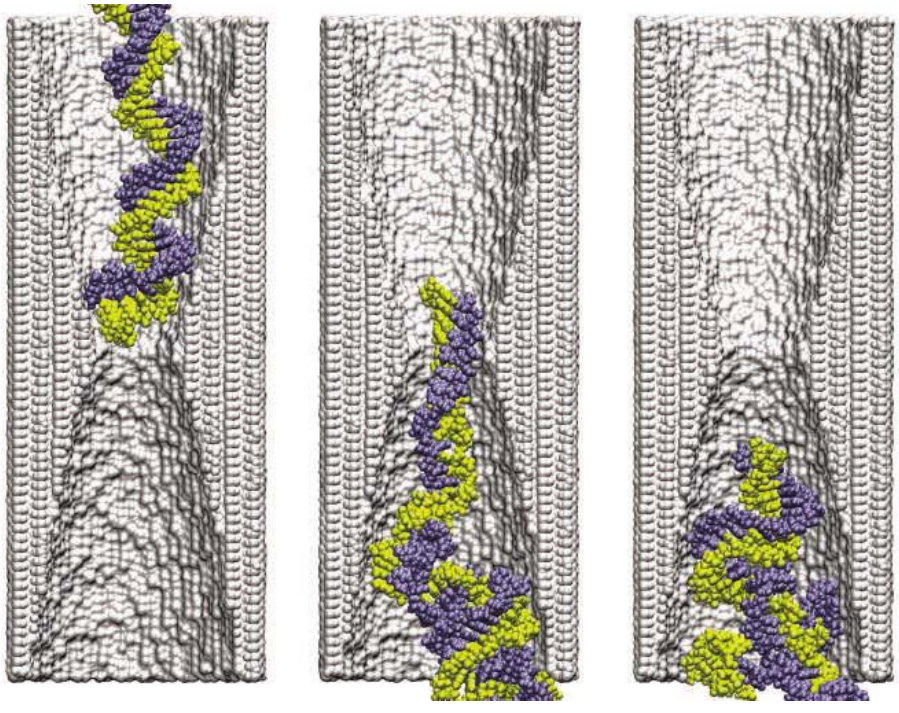

Pore fit. In this computer simulation, DNA wriggles through a 1.5-nanometer pore in silicon. Such devices hold the promise of sequencing DNA electronically.

CREDIT: IMAGE COURTESY OF ALEKSEI AKSIMENTIEV, KLAUS SCHULTEN, AND GREGORY TIMP/UNIVERSITY OF ILLINOIS, URBANA-CHAMPAIGN

Slow start, strong finish?

Despite these advances, sequencing by synthesis has its drawbacks. One is that the techniques read relatively short DNA snippets—usually several hundred base pairs in length or less, compared with the 1000 or so in current capillary systems. That can make it hard to reassemble all the pieces into a continuous genome sequence. Another drawback is that they rely on PCR, which is expensive and can introduce copying errors. Greater experience with the new sequencing technologies may improve matters. 454's Egholm, for example, says his team has developed a prototype version of their technology that increases read lengths from 100 base pairs to 400. Several groups are developing ways to sequence a single copy of a long DNA strand, thereby achieving longer reads and avoiding PCR.

One approach being pursued by VisiGen Biotechnologies in Houston, Texas, anchors a polymerase—the enzyme that tacks new

nucleotides to a growing DNA chain—onto a surface and feeds it a template strand. As the polymerase then adds fluorescently labeled bases to a complementary strand, an advanced optical system detects the tiny flashes from the single molecule, allowing a continuous sequence to be read. A variation of this approach by LI-COR Biosciences in Lincoln, Nebraska, anchors single-stranded DNA and polymerase molecules to an electrode, and then uses an electric field to drive nucleotides linked to fluorescent nanoparticles in solution toward the polymerase. In the instant between the time when the polymerase latches onto the nucleotide and the time when it cuts it off the nanoparticle, the researchers reverse the electric field, driving away nucleotide-nanoparticle pairs not bound to the DNA. Then they snap a picture to see the color of the fluorescent particles still bound to the polymerase. Once the nucleotide is cut free, the nanoparticle drifts away, and the process is repeated to identify the next base. At the meeting LI-COR's John Williams predicted that this technique could produce read lengths of up to 20,000 bases.

But another technology altogether may hold the most revolutionary potential, Church says. Called nanopore sequencing, this family of techniques aims to sequence DNA strands as they thread their way through tiny synthetic or natural pores, each just 1.5 nanometers or so across. Numerous groups are pursuing nanopore synthesis techniques, but researchers acknowledge that they have far to go. "We're still learning about the science of nanopores," Schloss says.

No group has yet reported using such a setup to sequence DNA one base at a time. But in a series of papers beginning in 1996, researchers led by John Kasianowicz and Daniel Branton at the National Institute of Standards and Technology in Gaithersburg, Maryland, reported that they could use protein-based pores embedded in a lipid membrane first to detect snippets of DNA and then to differentiate snippets with all A's from those made up of C's. But because proteins and lipids are fragile, other groups have begun making their pores out of silicon and other electronic materials in hopes of developing a more robust technology that can also integrate transistors and other electronic devices. In most versions of nanopore technology, researchers use tiny transistors to control a current passing across the pore. As the four different DNA bases go through, they perturb that electric signal in different ways, causing the voltage to spike upward or drop in a way that identifies the nucleotide passing through.

At the meeting, for example, chemist Gregory Timp of the University of Illinois, Urbana-Champaign, reported that his team has generated electrical readings of DNA moving through nanopores. Unfortunately, the DNA wriggled back and forth so much that the researchers had trouble teasing out the sequence of bases in the chain. But Timp says he and his colleagues are finishing a second-generation device that uses electric fields to keep the movement of the DNA under control. If it works, the technology promises to read long stretches of DNA without the need for expensive optical detectors.

Searching for Cheaper Genome Sequencers

Company	Format	Read Length (bases)	Expected Throughput Mb (million bases)/day
454 Life Sciences	Parallel bead array	100	96
Agencourt Bioscience	Sequencing by ligation	50	200
Applied Biosystems	Capillary electrophoresis	1000	3–4
LI-COR Biosciences	Electronic microchip	20,000	14,000
Microchip Biotechnologies	Parallel bead array	850–1000	7
Network Biosystems	Biochip	800+	5
NimbleGen Systems	Map and survey microarray	30	100
Solexa	Parallel microchip	35	500
VisiGen Biotechnologies	Single-molecule array	NA	1000

Generation next. Companies racing for the $1000 genome sequence strive simultaneously for low cost, high accuracy, the ability to read long stretches of DNA, and high throughput.

"We have to worry now"

No matter which technology or technologies make it to market, the scientific consequences of lower sequencing costs are bound to be enormous. "I think it's going to have a profound impact on biology," says Yale University molecular biologist Michael Snyder.

Some early progress is already on display. At the Florida meeting, for example, 454's Egholm reported that he and his colleagues used their technology to identify as many as four genetic variants of HIV in single blood samples, in contrast to today's technology, which identifies just the dominant strain. The technique, Egholm says, could eventually help doctors see the rise of drug-resistant HIV strains in patients at the earliest stages. In another study, the group analyzed the sequence of non–small cell lung cancer cells and identified the specific mutations that give rise to drug resistance.

In similar studies, Thomas Albert and colleagues at NimbleGen Systems, a biotechnology firm in Madison, Wisconsin, used their version of sequencing-by-synthesis technology to identify the mutations in *Helicobacter pylori*—the microbe responsible for ulcers—that cause resistance to a drug known as metronidazole, as well as the mutations in the tuberculosis-causing bacterium that trigger resistance to a new TB drug. The power of such studies is "unbelievable," Snyder says, because they hold out the hope of enabling doctors to tailor medicines to battle diseases most effectively. Some personalized-treatment strategies are already in use: Herceptin, for example, is targeted to patients with a specific genetic form of breast cancer. But cheap sequencing should make them far more widespread, Church says.

Basic researchers are looking at the early benefits of cheap sequencing as well. At the meeting, for example, Snyder talked about his team's use of gene chips to map the sites where transcription factors—proteins that control when genes are turned on—bind to the genome. The technology is effective, but gene chips are expensive. So Snyder is turning to cheap sequencing technology to rapidly sequence the millions of DNA fragments needed to identify transcription factors. Church says he is also using cheap sequencing techniques to propel his group's synthetic-biology efforts to create an extensive tool kit of microbial "parts" that can be mixed and matched to enable microbes to perform new functions.

Like most new technologies, ultracheap sequencing casts shadows as well. For starters, Church says, it's hard to imagine what privacy will mean once anyone with a sample of your DNA can determine who you are, your heritage, and what diseases you're likely to inherit. Celebrities and politicians may soon face a world hungry to scrutinize their genes. Among ordinary people, many analysts worry that insurers and employers will use genetic information to screen out those at high risk for disease. Finally, the same sequencing technology that could potentially help create beneficial new microbes, such as ones tailored to turn out large amounts of hydrogen gas to power fuel cells, could also make it easier to create new bioterrorist pathogens.

"We have to worry about these issues now, because we will be sequencing with very high throughput in 10 years," Timp says. Schloss notes that NHGRI has long supported research on ethical, legal, and social concerns. However, he adds, "it's very hard to do it in the abstract." With technology advancing at a rapid clip, neither the benefits nor the concerns of ultracheap sequencing are likely to remain abstract for long.

–ROBERT F. SERVICE

Barely beating. Patient privacy laws could shut down a heart study led by Minnesota epidemiologist Russell Luepker.

CREDIT: UNIVERSITY OF MINNESOTA

PATIENT PRIVACY

Rule to Protect Records May Doom Long-Term Heart Study

Researchers are still grappling with how to conduct medical studies while complying with federal and state laws to keep patient data private

For 25 years, heart disease researchers have tapped the medical records of more than 40,000 Minnesotans for findings on everything from sex differences in heart attack survival to the role of cholesterol-lowering drugs in saving lives. But the well may be drying up: State and federal privacy laws could make it impossible for epidemiologists at the University of Minnesota, Twin Cities, to continue to collect the hospital data they need.

The problem stems from a federal privacy rule that took effect 3 years ago and that affects biomedical researchers around the country. The rule "still is slowing down or substantially discouraging researchers from certain studies," says Susan Ehringhaus, associate general counsel for regulatory affairs of the Association of American Medical Colleges (AAMC). Prominent on that list is the Minnesota Heart Survey, which periodically reviews patient records from hospitals around Minneapolis to analyze factors in heart disease and stroke survival such as ethnicity, procedures, and medications. "They're leaders on this," says epidemiologist Steven Shea of Columbia University. "We would lose a very important, very high-quality lens on what's going on over time."

In 1996, Congress passed the Health Insurance Portability and Accountability Act (HIPAA) to make it easier for people to retain or switch their health insurance coverage. In April 2003, the Department of Health and Human Services (HHS) began to implement one provision, called the Privacy Rule, that gives patients access to their medical records and restricts how health care providers use them (*Science*, 9 July 2004, p. 168). One key change from existing practices requires researchers outside the provider organization to obtain written consent from each patient in order to use the patient's records or, if that is impractical, to get a waiver from their institutional review board (IRB). Researchers can also receive a data set stripped of identifying information. The onus is on health care providers, who can be fined or jailed for violating the rules.

A National Institutes of Health (NIH) spokesperson says most researchers have received waivers and managed to continue their studies. But the law continues to lead to delays, say some researchers, and a review of HIPAA in the February 2006 *Annual Review of Medicine* suggests that the higher costs—the government has estimated $600 million over 10 years—is causing researchers to revise or scrap some studies out of concern the work will become prohibitively expensive.

The Minnesota Heart Survey is one example of a study that has been hit particularly hard by the double whammy of federal and state laws. Investigators need identifiers such as Social Security number and birth date to match the medical data with death records, says principal investigator Russell Luepker. Although hospitals once allowed his team to view patient files, he paid a research foundation affiliated with the hospitals to collect the data after Minnesota implemented a new privacy rule in 1997. Last summer, however, the foundation folded, and Luepker hasn't found a replacement.

Luepker can't simply get an IRB waiver to HIPAA because Minnesota's privacy law requires each patient to give consent. The hospitals ask patients to sign a general consent for use of their records, but it's not easy to get written consent from a sick person admitted to a hospital for a heart attack or stroke, notes Luepker. Not everyone returns mailed consent forms, he adds, and some hospitals are even reluctant to send them.

So Luepker has been talking to lawyers from each of the 22 hospitals to work out a way to obtain the identifiers even for patients who haven't signed a form. If that approach fails, Luepker says he won't apply for a renewal of two large NIH grants that expire in June. "I'm quite frankly very worried," Luepker says about a situation first reported by *The Minneapolis Star Tribune*. "For us it's quite bad. This long-running study may stop running, and we're vain enough to think it's produced some very good information." Luepker says a related telephone population survey will continue.

Other studies face new limitations as institutions interpret their responsibilities under HIPAA. For example, at the University of Michigan, Ann Arbor, researchers who once recruited subjects for a survey of acute coronary disease care by telephone had to get their written permission first. In a 23 May 2005 paper in the *Archives of Internal Medicine*, Kim Eagle and others reported that consent rates dropped from 96% to 34% when they switched from phone calls to mail. Subjects also tended to be older, healthier, and married. Roberta Ness of the University of Pittsburgh in Pennsylvania says she must now rely on patients' doctors to recruit prospective patients for preeclampsia and cancer studies.

Studies that pool data from many centers are also feeling the impact of HIPAA. An Alzheimer's disease consortium's database of clinical data on patients that's used to develop better diagnostics and treatments has been delayed while contributing researchers obtain

> "This long-running study may stop running, and **we're vain enough to think it's produced some very good information.**"
>
> —Russell Luepker, University of Minnesota

IRB waivers to record the ages of subjects over 90, says one investigator who asked not to be named. An international trial of a drug for brain injury was hamstrung by the refusal of many U.S. hospitals to divulge ages, the exact time of injury, and other data on patients screened for the trial, reported a Dutch team in the February 2006 issue of *Intensive Care Medicine*.

Efforts to ease the load on researchers have so far been unsuccessful. For example, in 2004 a panel that advises the HHS Office for Human

Research Protections recommended nine changes, including eliminating a requirement that hospitals account for each use of a patient's data for research; shortening the list of identifiers; and allowing patients in a study approved under the federal Common Rule, which protects human subjects, to authorize use of their data for future, unspecified research. "There is still a need to bring some sense to these regulations," says former panelist attorney Mark Barnes of Ropes & Gray in New York City. AAMC has gone further, urging that any research already approved under the Common Rule should be exempt. The HHS Office of Civil Rights says its staff "continues to listen to the concerns of the research community" and is working with researchers "to enable important research to move forward."

Meanwhile, researchers are doing their best to get by. The University of Michigan's IRB, for example, eventually allowed Eagle's team to send prospective patients a letter saying their records could be part of the survey unless they mailed back a postcard to opt out. Only 5% have objected, says Eagle, and many "are delighted that we're doing the study." New York University's Douglas Morse, who's had trouble finding patients for an oral cancer study in Puerto Rico through pathology labs, says that life under HIPAA is like coexisting with an infected toe. "You might be able to get around, … but the result might not be everything you hoped for."

–JOCELYN KAISER

RESEARCH FUNDING

China Bets Big on Big Science

For a few lucky research fields, a new government road map for science is like winning the lottery

BEIJING—He Fuchu, a major general in the People's Liberation Army, is combat ready. "Advanced countries compete fiercely to control the high ground in protein research," says He, using military jargon to describe his primary objective as director of the Beijing Protein Research Center. Now He, a vice president of the Chinese Academy of Military Medical Sciences, is about to get a substantial war chest to fund his center's research in proteomics, a big winner in China's new 15-year plan for science and technology (S&T).

The long-awaited S&T plan, a set of marching orders handed down to scientists last month, may set the tone of science in China for years to come. It specifies 16 major engineering projects, including design of large aircraft, moon exploration, and drug development. Four major basic research programs are highlighted: protein science, topics in quantum physics, nanotechnology, and developmental and reproductive science. Although not stated in the plan, R&D spending by all sources, industry included, will rise from 236 billion yuan ($30 billion) in 2005 to 900 billion yuan ($113 billion) in 2020, Chinese officials announced last month. Basic research is slated to climb from 6% of R&D expenditure in 2004 to as much as 15% in 15 years.

With government coffers flush, Chinese scientists had hoped the new plan would give a bigger boost for basic research. However, "basic science is still not playing a central role in the government's mind," asserts Shing-Tung Yau, a mathematician at Harvard University. As in the past, scientific activity will be yoked tightly to economic development. "New scientific knowledge and inventions need to be industrialized and transformed," says Lu Yongxiang, president of the Chinese Academy of Sciences (CAS). A buzzword permeating the document and on the lips of science officials is "innovation": the key, the plan states, to reducing China's reliance on imported technology and intellectual property. Industry is expected to shoulder a heavier load than it currently does. For encouragement, the plan offers companies tax incentives to spend more on R&D.

Although the details have not been filled in, the plan has been hailed as a noble attempt to reshape a landscape of patchy scientific talent into a cohesive community churning out innovations, rivaling the West. The plan is "an important platform for China to transform from the largest developing country to a world powerhouse," says Duan Yibing, a science policy expert at the CAS's Institute of Policy and Management.

Others are hesitant to jump on the bandwagon. They worry that a heavy emphasis on applied science and megaprojects will stifle creativity. "The most innovative ideas come from very few creative scientists at rare moments, whereas planning of large-scale projects requires the consensus of many scientists," says Yi Rao, a neurobiologist at Northwestern University in Evanston, Illinois, and deputy director for academic affairs of China's National Institute of Biological Sciences (NIBS). "It is unrealistic to expect very innovative science projects to come out of planning."

Muffled criticism

Drafting the S&T plan was not straightforward. Twenty working groups involving 2000 scientists and officials wrangled over the document for close to 3 years, revising it a dozen times at a cost of $10 million. The buck stopped with Prime Minister Wen Jiabao, who chaired a ministerial committee over the working groups. Since becoming China's prime minister in March 2003, Wen has made a "scientific approach to development" a theme of his administration, backed by steady increases in R&D funding. "I believe that Prime Minister Wen had the best intentions when he decided to increase funding and, at the same time, required scientists and engineers to come up with visionary plans on how to use the funds," says Rao.

A Few of China's Billion-Dollar Babies

Major science programs	Engineering programs
Protein science	Next-generation broadband
Quantum research	Large-scale oil and gas exploitation
Nanotechnology	Transgenic plant breeding
Development and reproductive biology	Drug development
	Manned moon exploration

Raising the Ante

	R&D spending (All sources, $ billions)	Percent of GDP	Central government R&D appropriation ($ billions)	Central government R&D appropriation (% of overall)
2004	$24.60	1.23%	$8.70	35%
2010	$45.00	2.00%	$18.00	40%
2020	$113.00	2.50%	NA	NA

SOURCE: CHINA'S STATE COUNCIL

Ready for liftoff. A large share of China's R&D spending will be funneled to a few favored projects.

It quickly became clear that Wen hoped to replicate the success of China's first S&T plan, a 1956 blueprint that led to the creation of scores of CAS institutes, produced the nation's first atom and hydrogen bombs, and sent up its first satellite. Although the government never spelled out "two bombs and one satellite" as a goal, people associate these triumphs with the 1956 document, and Wen was determined to rekindle past glory by embracing large projects.

Deliberations slowed, however, when some scientists openly questioned the new plan's emphasis on big programs. In the fall of 2004, as the working groups were putting the finishing touches on the plan, *Nature* published a compilation of essays, some sharply critical of elements of the plan and of the Ministry of Science and Technology (MOST), the lead agency for crafting and implementing it.

In one essay, three prominent Chinese scientists—Rao; Bai Lu, a neuroscientist at the U.S. National Institutes of Health; and CAS biophysicist Chen-Lu Tsou—asserted that MOST's spending lacks transparency and gives bureaucrats too much power over scientists. The authors recommended stripping MOST of its budgetary authority and bolstering mechanisms for awarding peer-reviewed grants. In a second essay, Mu-ming Poo, a biologist at the University of California, Berkeley, and director of CAS's Institute of Neurosciences of the Shanghai Institutes for Biological Sciences, blasted waste and poor accountability, which he said are inevitable in big science projects. Chinese media devoured the broadsides.

MOST complained to the General Administration of Press and Publication. The oversight body squelched the debate, banning distribution of *Nature*'s China supplement and warning Chinese editors not to play into the hands of foreign forces. "What's most difficult for me to understand was their assertion that we were in cahoots with foreign publications," says Liu Dun, editor-in-chief of *Science and Culture Review*, a small journal ordered to scrap plans to publish debates on China's S&T structural reform. Discussions of the S&T planning process were purged from Chinese media, and several critics were bounced from working groups.

After more than a year's delay, the S&T plan emerged—with big science front and center.

Supersized

The four basic science programs deemed most strategic are areas in which China has already invested considerable sums. Each megaprogram is expected to receive about $1 billion over the next 15 years, says a researcher close to government planners. "There are surely more chances for innovation" in hot areas such as nanotechnology, says Xie Sishen, chief scientist at the National Center for Nanoscience and Technology (NCNST). The center was created in late 2003 by merging CAS's nanoscience center and research groups at Beijing University and Qinghua University. The move, some say, anticipated the high profile awarded by the new S&T plan.

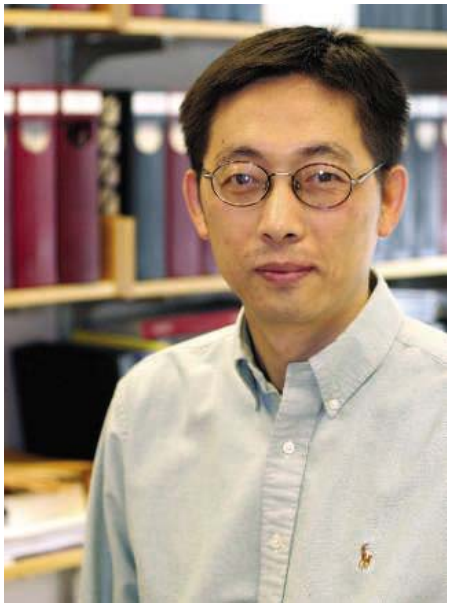

Dissenting voices. Megaprojects are not fertile ground for innovations, argues Yi Rao (*top*). Yigong Shi (*bottom*) worries that too few scientists will control the purse strings.

The plan places NCNST and the Beijing Protein Research Center in the driver's seats of the megaprojects in their respective fields. That disturbs some observers. "I am resolutely against the system of one chief scientist" controlling tens of millions of dollars of research funds, says Yigong Shi, a molecular biologist at Princeton University. In August 2004, Shi and 10 other members of the Society of Chinese Bioscientists in America—a group of Chinese biologists working in the United States—wrote an open letter to Wen expressing concern about the big biology projects in the draft S&T plan. They claimed that such projects would fail to achieve their goals and would strangle competition.

Features of the other two basic science megaprograms may make them more appealing to small teams. Scientists who helped shape the program on developmental and reproductive biology say they intend to establish a merit-based system to distribute funds. The program "probably will stimulate the interaction among genetics, developmental biology, and evolution, which is a very promising direction," says Zhang Ya-ping, director of CAS's Kunming Institute of Zoology.

Some critics worry that money will be wasted and that expensive new instruments will languish because there are too few skilled scientists to use them. "The number of basic-science scholars is far from satisfactory," Yau says, despite government programs to entice talented expatriates and foreigners to work in China.

Others see a strategic flaw: Enshrining narrow priorities in a 15-year plan could make it hard to change course in the future, warns Yau. "It is very bad to commit money [over a long term] to directions that are considered to be important now," Yau says, noting that the plan ignores "many important areas"—including his own, mathematics. Indeed, some predict an exodus from disciplines not in vogue. "Scientists may shift their research focus to favored areas in the plan. If they don't, they can hardly get funding," says Deng Xingwang, an agricultural biotechnologist and director of NIBS. Even the country's bastion of basic research funding, the National Natural Science Foundation of China, seems to toe the line. Although its budget is slated to increase by $50 million to between $400 million and $500 million this year, sources say, its 2006 handbook stresses "an integration of the national strategic need and the independent development of science."

Another worry is that big programs may be impervious to adequate oversight. Because almost everybody in a field in China will be involved in a big science project, nobody can objectively evaluate it, as Rao and his colleagues pointed out in their essay. Some have suggested bringing in expats to conduct reviews. "The government should establish a more open mechanism so that overseas Chinese scientists can take part," says Shi.

Duan says the critics will be proved wrong. "By catering to the national need, basic research will enjoy an opportunity for development by leaps and bounds," he says. "There is still much room for the free exploration driven by curiosity." Others see the plan as a multibillion-dollar gamble.

–HAO XIN AND GONG YIDONG

Gong Yidong writes for *China Features* in Beijing.

CREDITS (TOP TO BOTTOM): ELIZABETH J. RAO; DENISE APPLEWHITE/PRINCETON UNIVERSITY

EDITED BY KELLI WHITLOCK BURTON

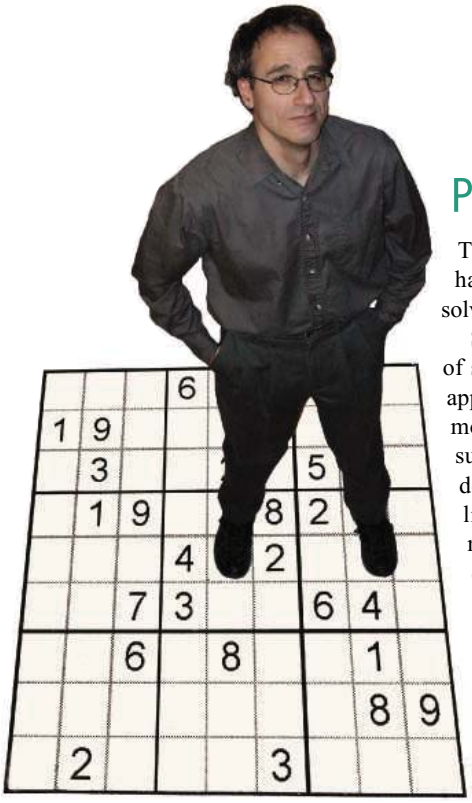

Problem Solver

GAME OVER. Puzzle fans, avert your eyes: Theoretical physicist Veit Elser of Cornell University has developed a computer program that efficiently solves the popular game Sudoku.

Sudoku requires puzzlers to fill a nine-by-nine grid of squares with the digits 1 through 9, with no digit appearing more than once in each column and row or more than once in any of nine smaller three-by-three subgrids. Elser, 48, used an algorithm he helped develop to decipher x-ray diffraction data because, like the data analysis, Sudoku requires solving a mathematical problem while satisfying two different constraints. "I had an 'Aha! moment' that finally I had a vehicle to explain what this algorithm does," Elser says. That vehicle is Sudoku, a game Elser himself once found particularly vexing.

The average Sudoku player probably won't use the algorithm, says Frazer Jarvis, a mathematician at the University of Sheffield, U.K., and a member of the team that last year calculated there are 6,670,903,752,021,072,936,960 possible Sudoku grids. But, Jarvis says, "there are applications for the mathematical side of the problem where we would like to be able to solve puzzles extremely quickly."

On Campus >>

FIRST FOREIGNER. Neurophysiologist Fraser Wilson has become the first non-Chinese principal investigator to receive a research grant from the National Natural Science Foundation of China.

Wilson, 52, joined the Kunming Institute of Zoology (KIZ) last year from the University of Arizona, Tucson, where he was an assistant professor. He says he was impressed by the institute's nonhuman primate facilities, which are essential for his work on how the brain processes and stores visual information. The 3-year grant is for $187,000.

Wilson will be working with longtime collaborator Ma Yuanye. "KIZ has certain [research] facilities that would be difficult to obtain in the States and Europe," Wilson says, including an outdoor enclosure in which monkeys can roam freely. "We are making good progress in both conventional neurophysiology, as well as in more novel experiments in freely moving monkeys."

MOVERS

HELP WANTED. The Global Fund to Fight AIDS, Tuberculosis and Malaria is looking for a new leader. Richard Feachem, a global health expert, said this month that he will not seek a second term as executive director.

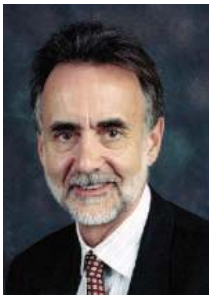

Feachem helped the Geneva-based fund grow from just an idea to a $9 billion enterprise with activities in 130 countries. But his tenure has not been without controversy. An internal investigation into procurement and personnel policies did not find any evidence of misconduct, but it apparently increased tension between Feachem and the fund's 25-member Board of Directors. Feachem announced his departure after the board said it would consider other applications for the post, but he agreed to stay until a successor is named. His term ends in July.

Feachem excelled at communicating the importance of the fund's mission, says Bernard Rivers of Aidspan in New York City, a self-styled watchdog of the fund. But Rivers thinks what's needed now is "a brilliant bureaucrat." Feachem plans to return to dual appointments at the University of California campuses in Berkeley and San Francisco.

WINDY REUNION. The University of Chicago (UC) has welcomed back a longtime faculty member as its next president. Robert J. Zimmer, a former chair of the mathematics department who also oversaw the university's management of Argonne National Laboratory, will take office on 1 July. He replaces Don Michael Randal, who is leaving to head the Andrew W. Mellon Foundation.

Zimmer, 58, was on the UC faculty for 25 years before leaving in 2002 to become provost of Brown University. The university's management contract for Argonne expires 30 September, and officials say Zimmer's expertise should come in handy. "The risk of losing the contract is greater than zero, but we hope not much more than zero," says James Crown, chair of the UC Board of Trustees.

The first mathematician to serve as UC president, Zimmer holds a Ph.D. from Harvard University.

AWARDS

FORWARD THINKERS. Two cancer researchers in the U.S. will split this year's $1 million Dan David Prize for scientific achievements that benefit society. John Mendelsohn, president of the University of Texas M. D. Anderson Cancer Center, was honored for his studies of antibody-mediated cancer therapy. The work led to the development of ErbituxT, a drug that prevents the growth of several types of cancers. Joseph Schlessinger, a professor and chair of the department of pharmacology at Yale University School of Medicine, was recognized for research on how information is passed between the cell surface and the cell, work that led to the discovery of anticancer drugs. The Dan David Prize is named after a Romanian native who made his fortune in the photography business.

Got a tip for this page? E-mail people@aaas.org

Is this the bird?
1555

Nuclear earthmoving
1556

LETTERS

edited by Etta Kavanagh

1918 influenza.

Vaccine Against Spanish Flu

IT WOULD APPEAR THAT THE RECENT RE-CREATION OF THE Spanish flu ("Characterization of the reconstructed 1918 Spanish influenza pandemic virus," T. M. Tumpey *et al.*, Research Articles, 7 Oct. 2005, p. 77) could become a case of curiosity killing the cat. Saving the world from a disaster similar to the 1918 epidemic is a noble aim, but the dangers posed by this flu getting out of hand must have crossed the minds of those engaged in the race to re-create the flu (the papers on the characterization and re-creation of the virus were required by the U.S. National Science Advisory Board for Biosecurity to state that the work is important for public health and was conducted safely). Scientists must consider the consequences of this work. Biosecurity experts seem inclined to believe that the risk that the re-created strain might escape is so high, it is almost a certainty (*1*). Containment cannot be fail proof; neither can shipment in the mail (as now allowed by CDC and stated to be "very, very safe") (*2*). Regeneration is possible in any well-equipped molecular biology laboratory. Indeed, the Canadians wishing to work with this flu find it less complicated to make it themselves by following the published procedure than to get permission to import it from the United States (*2*).

The spread of the Spanish flu virus appears more likely and to pose more dire consequences than those conceived for the avian flu virus. Now that the virus has been re-created and has yielded important new information about its virulence factors and high replication efficiency, it may be prudent to use this same information to create a vaccine, given that containment can never be certain.

JENS C. JENSENIUS

Department of Medical Microbiology and Immunology, University of Aarhus, Aarhus DK8000, Denmark.

References

1. J. K. Taubenberger *et al.*, *Nature* **437**, 889 (2005).
2. A. von Bubnoff, *Nature* **438**, 134 (2005).

Response

WE SHARE JENSENIUS'S BELIEF THAT THE RE-creation of the 1918 influenza pandemic virus has yielded important new information about what made this virus so virulent. There is still much to learn about this lethal virus that killed an estimated 50 million people. The recently published findings reveal essential information to speed our preparation for—and potentially thwart—the next influenza pandemic.

These new studies provide an immediate impact by helping scientists focus on detecting changes in the evolving H5N1 virus that might make widespread transmission among humans more likely. The findings may lead to identification of new targets for drugs and vaccines to treat and prevent influenza, now and in the future.

Although some have been concerned about the re-creation of this historical killer, descendents of the 1918 pandemic virus circulate widely and most people in the world have some immunity. Any risk to the public of accidental release of the 1918 virus is remote. All work was conducted with stringent biosafety and biosecurity precautions designed to protect workers and the public from possible exposure to this virus. CDC has no plans to send the virus outside of CDC. Any requests we do receive will be carefully considered on a case-by-case basis, taking into account scientific merit, biocontainment concerns, and any additional standards deemed appropriate for this particular virus.

Understandably, some have questioned whether the findings should have been reported publicly. We are confident about the necessity of this work and the obvious benefits that will continue to be obtained by a robust and responsible research agenda aimed at developing the means to detect, prevent, and treat patients from threats like the 1918 influenza virus. By publishing the results and making them widely available to the scientific community, we encourage additional research at a time when we desperately need to engage the scientific community and accelerate the development of diagnostic assays, treatments, and vaccines to improve our ability to prevent or control pandemic influenza.

TERRENCE M. TUMPEY,[1] CHRISTOPHER F. BASLER,[2] PATRICIA V. AGUILAR,[2] HUI ZENG,[1] ALICIA SOLORZANO,[2] DAVID E. SWAYNE,[3] NANCY J. COX,[1] JACQUELINE M. KATZ,[1] JEFFERY K. TAUBENBERGER,[4] PETER PALESE,[2] ADOLFO GARCIA-SASTRE[2]

[1]Influenza Branch, Division of Viral and Rickettsial Diseases, National Center for Infectious Diseases, Centers for Disease Control and Prevention, 1600 Clifton Road, NE, Atlanta, GA 30333, USA. [2]Department of Microbiology, Mount Sinai School of Medicine, New York, NY 10029, USA. [3]Southeast Poultry Research Laboratory, Agricultural Research Laboratory, U.S. Department of Agriculture, 934 College Station Road, Athens, GA 30605, USA. [4]Department of Molecular Pathology, Armed Forces Institute of Pathology, Rockville, MD 20850, USA.

Williams-Beuren Syndrome

THE ARTICLE BY YUDHIJIT BHATTACHARJEE "FRIENDly faces and unusual minds" (4 Nov. 2005, p. 802) was informative and well written. However, as the parent of a 16-year-old who has Williams-Beuren syndrome (WS) and as a former member of the national Williams Syndrome Association Board of Directors, I must object to the author's description of WS as an "illness." People with WS are not ill. People with cancer or heart disease may have an illness. People with WS have a broad constellation of physical and mental characteristics that are explained, in part, by a small deletion on a single chromosome (in part because not all individuals with WS have the deletion, adding to the mystery). People with WS live and learn differently from most of us who do not have WS, but they are not ill.

JAMES J. MENEGAZZI

Emergency Medicine, University of Pittsburgh, 230 McKee Place, Suite 400, Pittsburgh, PA 15213, USA.

Impacts on marine sources
1557

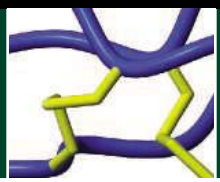

Tough circles
1563

Smaller, Hungrier Mice

IN THEIR BREVIA "INCREASE IN ACTIVITY DURING calorie restriction requires Sirt1" (9 Dec. 2005, p. 1641), D. Chen *et al.* report that elevation in physical activity in response to 40% food restriction is absent in mice lacking the longevity protein Sirt 1, in spite of their motor performances being preserved or even increased as assessed by the treadmill and rotarod tests. Since Sirt1 is the closest mammalian homolog of Sir 2.1, which is necessary for life-span extension by calorie restriction (CR) in lower organisms (*1*), this intriguing phenotype provides the first evidence that sirtuins may have conserved roles in mediating physiological effects of food restriction (including perhaps extended longevity) also in mammals.

To make the point that the behavioral response to restricted feeding, rather than the metabolic consequences of the dietary regimen per se, is modified by lack of Sirt1, the authors provide evidence for "equal food intake" (grams of chow/day) in the two strains fed ad libitum (AL) and for comparable plasma levels of glucose, triglycerides, and IGF-1 in both AL and CR conditions. The authors also claim that body weights were reduced in wildtype (WT) and knockout (KO) mice and that "inability [of KO mice] to respond to calorie restriction was also not due to them experiencing a lower degree of food restriction."

However, in the figure legend and the Supporting Online Material, the body weight reduction is from 37.8 ± 3.8 g (AL) to 19.9 ± 1.9 g (CR) in wild-type animals and from 18.3 ± 2.7 g (AL) to 15.4 ± 1.4 g (CR) in KO mice. It is not indicated whether body weights in the two strains fed AL diverged so dramatically during the 9-month treatment or were different since the beginning.

In fact, Sirt1 KO mice are smaller than their littermates (*2*). Independent of the effect of the mutation, smaller mice are expected to have lower energy requirements, especially if (in CR) they have less spontaneous activity. In this perspective, the data on food intake are rather surprising, because mutant mice eat almost as much as double-sized WT mice, and their food intake is much higher when normalized for body weight. Moreover, either loss of weight in food-restricted KO mice is very limited, or they don't gain enough weight during AL feeding.

Although it is not clear why smaller mutant mice eat ad libitum as much as much bigger wild-type animals (maybe they are hypermetabolic?), 40% food restriction may still leave the smaller strain with enough energy support to prevent at least some aspects of the CR response, including the "hungry" hyperactive behavior. IGF-1 function may be altered in Sirt1 KO mice (as also suggested by their reduced size) (*3*), and its plasma level may not be a reliable marker of negative energy balance.

GIOVAMBATTISTA PANI, SALVATORE FUSCO, TOMMASO GALEOTTI

Institute of General Pathology, Catholic University Medical School, Rome 00168, Italy.

References

1. L. Bordone, L. Guarente, *Nat. Rev. Mol. Cell Biol.* **6**, 298 (2005).
2. M. W. McBurney, *Mol. Cell. Biol.* **23**, 38 (2003).
3. M. E. Lemieux, *Mech Ageing Dev.* **126**, 1097 (2005).

Response

WE SHOWED THAT CALORIE RESTRICTION (CR) promoted a large increase in physical activity

in wild-type but not in Sirt1 knockout (KO) mice, demonstrating the first example in which a mammalian sirtuin is required for any phenotype induced by this dietary regimen. Pani *et al.* suggest that our KO mice might not have been as calorie restricted and energy limited as the wildtype (WT) mice. However, both wild-type and KO mice showed comparable physiological changes in response to CR, namely similar reductions in blood glucose, triglycerides, and IGF-1. As we stated, "body weights were also reduced by calorie restriction" in both strains, but as Pani *et al.* correctly point out, the KO mice did not lose as high a percentage of their body weight on the regimen.

Food intake for both wild-type and KO mice was restricted to 60% of their ad libitum food-consumption levels, which turned out to be very similar despite the smaller size of the KO mice. The KO mice showed less weight loss on the CR diet most likely because they were smaller and leaner than wild type, even though they ate comparable levels of food ad libitum. Previous studies establish the precedent that leaner mice can exhibit less weight loss on a CR diet (*1*). However, we concluded then and now that the KO mice were as calorie restricted as the wild type, first, because they were food-restricted to the same degree of their ad libitum levels as wild type and second, because they underwent similar changes in the physiological parameters mentioned above.

Although a comprehensive study of the Sirt1 KO mice is clearly important, we believe that the data in our Brevia do indicate important defects in the ability of the Sirt1 KO mice to respond normally to CR.

DANICA CHEN,[1] ANDREW STEELE,[2] SUSAN LINDQUIST,[2] LEONARD GUARENTE[1]

[1]Department of Biology, Massachusetts Institute of Technology, Cambridge, MA 02139, USA. [2]Whitehead Institute for Biomedical Research, Nine Cambridge Center, Cambridge, MA 02142, USA.

Reference

1. J. G. Vander Tuig, D. R. Romsos, G. A. Leveille, *Int. J. Obes.* **4** (no. 1), 79 (1980).

Letters to the Editor

Letters (~300 words) discuss material published in *Science* in the previous 6 months or issues of general interest. They can be submitted through the Web (www.submit2science.org) or by regular mail (1200 New York Ave., NW, Washington, DC 20005, USA). Letters are not acknowledged upon receipt, nor are authors generally consulted before publication. Whether published in full or in part, letters are subject to editing for clarity and space.

Sea Urchins as Crystallographers

IN THEIR PERSPECTIVE "CHOOSING THE CRYSTALlization path less traveled" (12 Aug. 2005, p. 1027), S. Weiner *et al.* emphasize the significance of a disordered amorphous precursor phase in a biological strategy for making "beautifully sculpted carbonate minerals." Size and sculpted shape are only part of the problem because most organisms form minerals that also have a precisely oriented crystallography (*1*–*3*). Thus, the finished product may be a large *c*-axis–oriented single crystal derived from an amorphous precursor within an organic compartment, as in sea urchin plates, or small *c*-axis–oriented crystals derived from epitactic growth on an ordered amelogenin microribbon, as in dental enamel (*4*). Yet the more fundamental problem remains unsolved: What orients the "small crystal seed," the "nucleation substrate," or the long axes of the microribbons? In 1972 (*1*), I wrote, "The single most important feature of almost all mineralized tissues … is not so much the shape or even the mineralogy of the inorganic phase but rather its crystallography. The crystallographic preferred orientation, the ordered arrangement of crystallographic axes, is of paramount concern." This precise orienta-

tion remains the big mystery of biomineralization. Organisms know how to do it; we do not yet know how they know.

KENNETH M. TOWE

Senior Scientist Emeritus, Department of Paleobiology, Smithsonian Institution, 230 West Adams Street, Tennille, GA 31089, USA.

References

1. K. M. Towe, *Biomineralization Res. Rep.* **4**, 1 (1972).
2. H. A. Lowenstam, S. Weiner, *On Biomineralization* (Oxford Univ. Press, Oxford, 1989).
3. K. M. Towe, W. U. Berthold, D. E. Appleman, *J. Foraminiferal Res.* **7**, 58 (1977).
4. C. Du *et al.*, *Science* **307**, 1450 (2005).

Response

TOWE'S LETTER HIGHLIGHTS AN IMPORTANT aspect of biological crystal formation, namely control over crystal orientation. Progress on this issue has been made over the last few decades using both proteins and designed nucleation substrates (*1*–*4*). Progress has also been made on polymorph selection by proteins extracted from the organic matrix of mollusk shells, which involves nucleation (*5*, *6*), although more remains to be learned. The Perspective, however, highlighted another unusual feature of biomineralization—the role of an amorphous precursor phase. Eventually these different aspects will need to be integrated, and perhaps the conclusion at this stage should be that the road less traveled is still long.

STEPHEN WEINER AND LIA ADDADI

Department of Structural Biology, Weizmann Institute of Science, Rehovot 76100, Israel.

References

1. L. Addadi, S. Weiner, *Proc. Natl. Acad. Sci. U.S.A.* **82**, 4110 (1985).
2. J. Aizenberg, A. J. Black, G. M. Whitesides, *Nature* **397**, 4500 (1999).
3. A. Berman *et al.*, *Science* **269**, 515 (1995).
4. S. Mann *et al.*, *Science* **261**, 1286 (1993).
5. A. M. Belcher *et al.*, *Nature* **381**, 56 (1996).
6. G. Falini, S. Albeck, S. Weiner, L. Addadi, *Science* **271**, 67 (1996).

TECHNICAL COMMENT ABSTRACTS

Comment on "Ivory-billed Woodpecker (*Campephilus principalis*) Persists in Continental North America"

David A. Sibley, Louis R. Bevier, Michael A. Patten, Chris S. Elphick

We reanalyzed the video presented as confirmation that an ivory-billed woodpecker (*Campephilus principalis*) persists in Arkansas (Fitzpatrick *et al*., Reports, 3 June 2005, p. 1460). None of the features described as diagnostic of the ivory-billed woodpecker eliminate a normal pileated woodpecker (*Dryocopus pileatus*). Although we support efforts to find and protect ivory-billed woodpeckers, the video evidence does not demonstrate that the species persists in the United States.

Full text at www.sciencemag.org/cgi/content/full/311/5767/1555a

Response to Comment on "Ivory-billed Woodpecker (*Campephilus principalis*) Persists in Continental North America"

John W. Fitzpatrick, Martjan Lammertink, M. David Luneau Jr., Tim W. Gallagher, Kenneth V. Rosenberg

Claims that the bird in the Luneau video is a normal pileated woodpecker are based on misrepresentations of a pileated's underwing pattern, interpretation of video artifacts as plumage pattern, and inaccurate models of takeoff and flight behavior. These claims are contradicted by experimental data and fail to explain evidence in the Luneau video of white dorsal plumage, distinctive flight behavior, and a perched woodpecker with white upper parts.

Full text at www.sciencemag.org/cgi/content/full/311/5767/1555b

APPLIED PHYSICS

Dr. Strangelove Moves Mountains

Hugh Gusterson

Sometimes we look back at the idées fixes of earlier scientists and ask, "What were they thinking?" In *Proving Grounds*, Scott Kirsch explores a spectacular example: Project Plowshare, the obsessive quest by physicist Edward Teller and a group of true believers at the Lawrence Livermore National Laboratory to use nuclear weapons to excavate harbors, canals, and mines. "We will change the earth's surface to suit us," proclaimed Teller.

Proving Grounds
Project Plowshare and the Unrealized Dream of Nuclear Earthmoving

by Scott Kirsch

Rutgers University Press, New Brunswick, NJ, 2005. 272 pp. $39.95. ISBN 0-8135-3666-9.

Despite mounting evidence of environmental harm from the aboveground nuclear tests of the 1950s, Teller and his team planned to use five nuclear weapons to create a harbor at Cape Thompson, Alaska. Although the harbor would have been unconnected by rail or road to inland Alaska and iced in nine months of the year, Livermore's "geographical engineers" had secured the support of the Atomic Energy Commission (AEC) and Alaska politicians. They only gave up in 1962, after four years of planning for "Project Chariot," because of increasingly vocal opposition from the local Inupiat people and an outspoken group of Alaskan ecologists who were concerned that radiation would concentrate in lichen and, thence, in the caribou eaten by the Inupiat. Worried that the AEC was misrepresenting research it had contracted him to do, one of these ecologists, Les Viereck, wrote "it is the duty of every scientist to protect his data and to be sure that it is interpreted correctly. A scientist's allegiance is first to truth and personal integrity." He was promptly fired by the University of Alaska.

Teller's group withdrew from Alaska to the Nevada Test Site, where, in 1962, they conducted the 100-kiloton Sedan shot. Sedan displaced 12 million tons of dirt and left a crater a quarter of a mile wide. Teller's promises of a new generation of "clean bombs" notwithstanding, the Sedan device showered northern Nevada and Utah with radioactive iodine-131, which moved via grass into cow's milk and thus into human thyroids. The next test shot, Sulky, was supposed to make a crater but instead left a mound. Then, in 1965, came the 4-kiloton Palanquin shot, which was supposed to create a mound but instead left a crater. (Clearly geographical engineering with nuclear weapons was a rather imprecise art.) Despite promises that the Palanquin shot had been engineered to contain fallout, it spewed a radioactive cloud that drifted to Canada, thus placing the United States in violation of the Limited Test Ban Treaty. The Johnson Administration decided it would be prudent to keep news of the test to itself until the radiation had dissipated.

Plowshare's first test. Although engineers correctly predicted the volume of the crater created by the Sedan shot, they greatly underestimated the resulting dust cloud and radioactive fallout.

These shots at the Nevada Test Site were intended to pave the way for grander projects: the excavation of a 20-mile canal to join the Tennessee and Tombigbee Rivers in Mississippi, highway construction in Southern California, the blasting of a harbor in Western Australia, and the construction of a new Trans-Isthmian canal in Panama or Colombia. The last, Livermore's scientists calculated, would require between 250 and 310 nuclear explosions and the relocation of 30,000 to 40,000 people. John Gofman, a dissident scientist at Livermore, called it "biological insanity." One by one, the projects were abandoned as Livermore failed to develop the clean bombs Teller had promised and as a global environmental movement gathered strength. 1962, the year the Alaska harbor was canceled, was, after all, the year Rachel Carson published *Silent Spring* (*1*). A trickle of funding for Project Plowshare continued until 1974, but the program was effectively dead by the end of the 1960s.

Kirsch, a young geography professor at the University of North Carolina, sees Plowshare as a utopian effort to exercise "human control over nuclear technology as over nature itself." It was intended "to provide a positive story of the bomb at the precise moment when fears of nuclear war, and of the increasingly tangible effects of radioactive fallout, had become palpable in calls for nuclear testing bans." Kirsch is interested in the contending visions of geography exhibited by Teller and his environmentalist antagonists. He sees Teller's team of geographical engineers as a "failed technocracy" unable to deal with human geography and stymied by a rival system of scientific expertise—ecology—that mined the Plowshare tests for data about contamination.

Kirsch has done substantial research in the archives of the Lawrence Livermore National Laboratory and the Department of Energy (which inherited the records of the AEC). He integrates what he found there with secondary sources, such as Dan O'Neill's vivid narrative of Project Chariot (*2*), that have already told parts of the story in more detail. Kirsch's contributions are to provide a narrative of Plowshare in its entirety and to use new archival material to convey a richer sense of what the nuclear bureaucracy was up to. Until he tips his hand in the last few pages, he tells the story with dry restraint and care, adding a light dusting of theory from critical geography.

Proving Grounds is a timely book. The Pentagon has been seeking to persuade us, contrary to the opinion of most civilian experts, that a new Robust Nuclear Earth Penetrator could be used against buried targets in "rogue states" without contaminating the environment, and the United States is debating whether it was misled into war in Iraq. At such a moment, Kirsch's understated descriptions of the weapons bureaucracy repeatedly distorting and concealing data about the public health hazards of nuclear explosions will give many readers an eerie sense that, the more things change, the more they remain the same.

References

1. R. Carson, *Silent Spring* (Houghton Mifflin, Boston, 1962).
2. D. T. O'Neill, *The Firecracker Boys* (St. Martin's, New York, 1984).

The reviewer is at the Department of Anthropology and the Program in Science, Technology, and Society, Massachusetts Institute of Technology, Cambridge, MA 02139, USA. E-mail: guster@mit.edu

10.1126/science.1124932

CREDIT: NASA

ECOLOGY

Globalization, Roving Bandits, and Marine Resources

Marine resource exploitation can deplete stocks faster than regulatory agencies can respond. Institutions with broad authority and a global perspective are needed to create a system with incentives for conservation.

F. Berkes,[1*] T. P. Hughes,[2] R. S. Steneck,[3] J. A. Wilson,[4] D. R. Bellwood,[2] B. Crona,[5,6] C. Folke,[5,6] L. H. Gunderson,[7] H. M. Leslie,[8] J. Norberg,[6] M. Nyström,[5,6] P. Olsson,[5] H. Österblom,[6] M. Scheffer,[9] B. Worm[10]

Overfishing is increasingly threatening the world's marine ecosystems (*1, 2*). The search for the social causes of this crisis has often focused on inappropriate approaches to governance and lack of incentives for conservation (*3*, *4*). Little attention, however, has been paid to the critical impact of sequential exploitation: the spatially expanding depletion of harvested species (*5*). The economist Mancur Olson (*6*) argued that local governance creates a vested interest in the maintenance of local resources, whereas the ability of mobile agents—roving bandits in Olson's terminology—to move on to other, unprotected resources severs local feedback and the incentive to build conserving institutions. Distant water fleets and mobile traders can operate like roving bandits (*7*), because global markets often fail to generate the self-interest that arises from attachment to place.

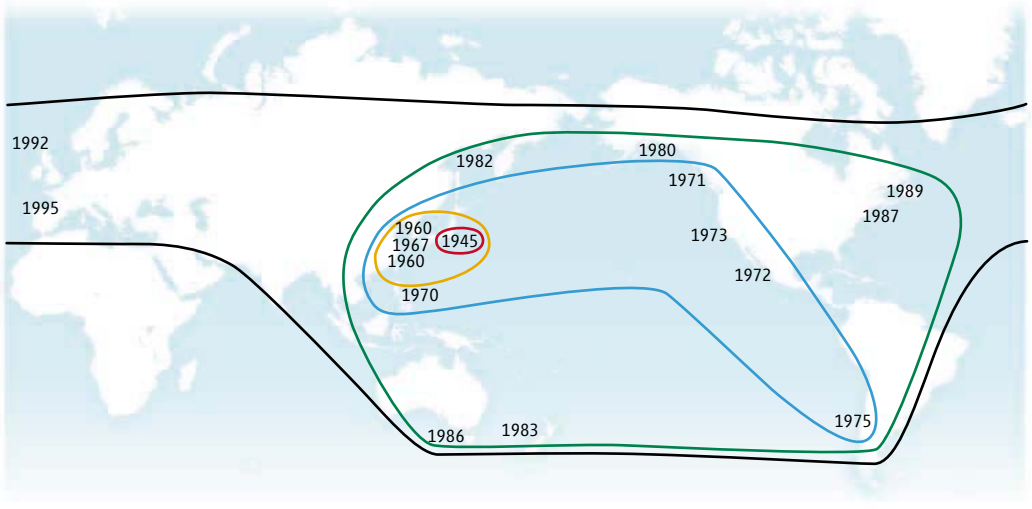

Sequential exploitation of a marine resource. Initiation year by location of major commercial fishery for sea urchins.

The effect of roving bandits can be explained by "tragedy of the commons," whereby a freely accessible (or open-access) resource is competitively depleted. Harvesters have no incentive to conserve; whatever they do not take will be harvested by others. Developing the institutions to deal with commons issues is problematic and slow (*8*). Roving banditry is different from most commons dilemmas in that a new dynamic has arisen in the globalized world: New markets can develop so rapidly that the speed of resource exploitation often overwhelms the ability of local institutions to respond.

Until recently, exploitation of marine resources was commonly constrained by the inaccessibility of remote and offshore locations. Consequently, early examples of global markets in fisheries (e.g., Newfoundland Grand Banks in the 1500s) were characterized by slow growth and relatively inefficient harvest technology. They were typically based on species that were plentiful, readily caught, and easily transported without refrigeration (e.g., dried, salted, or rendered for oil). Many of these constraints have evaporated with globalization. The trade-induced increases in demand for fisheries resources have resulted in an increasingly serious ecological and management problem.

Ecological Implications

Sequential depletions of species that are major conduits for the flow of energy and materials in marine food webs pose the greatest ecological risks. For example, historic exploitation of sea otters for their pelts in Alaska's remote Aleutian Islands had profound ecological consequences, because this keystone predator controls the abundance of sea urchins that graze on kelp. Depletion of sea otters caused massive deforestation of kelp beds by plagues of sea urchins for over a century, before active reintroductions of sea otters provided this control (*9*).

There is a rich history of roving bandits targeting ecologically important large predators such as the cod that historically dominated North Atlantic coastal ecosystems. By the middle of the last century, fishing technology had developed to the point where cod spawning aggregations in the Gulf of Maine could be removed wholesale. Within two decades, local stocks had been depleted, contributing to the rise of invertebrate species such as lobsters, crabs, and sea urchins that had formerly been prey to cod and other apex predators (*10*).

Highly altered ecosystems can often stimulate new fisheries, which typically target lower trophic levels (*1*). In Maine, the green sea urchin (*Strongylocentrotus droebachiensis*) proliferated after the loss of its fish predators in the mid-1980s (*9*), itself in turn becoming a fishery for sushi markets. Spurred by demand from the Japanese market, an unregulated harvest began in 1987. The state of Maine was unprepared to deal with the explosive growth of the fishery, and stocks were rapidly depleted.

To put the Maine sea urchin fishery in historical context, we show the spatial expansion of harvests (see figure, this page) and the sequential depletion of stocks (see graph, page 1558) by waves of exploitation around the globe. Commercial sea urchin harvest began largely for export to Japanese markets, after Japan's own resources declined. The Chilean fishery, for example, supplied relatively small domestic

[1]Natural Resources Institute, University of Manitoba, Winnipeg, Manitoba R3T 2N2, Canada. [2]Australian Research Council Centre of Excellence for Coral Reef Studies, School of Marine Biology, James Cook University, Townsville, QLD 4811, Australia. [3]School of Marine Sciences, University of Maine, Walpole, ME 04573, USA. [4]School of Marine Sciences, University of Maine, Orono, ME 04469, USA. [5]Centre for Transdisciplinary Environmental Research, [6]Department of Systems Ecology, Stockholm University, 106 91 Stockholm, Sweden. [7]Department of Environmental Studies, Emory University, Atlanta, GA 30322, USA. [8]Department of Ecology and Evolutionary Biology, Princeton University, Princeton, NJ 08544, USA. [9]Aquatic Ecology and Water Quality Management Group, Department of Environmental Sciences, Wageningen University, 6700 DD Wageningen, The Netherlands. [10]Biology Department, Dalhousie University, Halifax, Nova Scotia B3H 4J1, Canada.

*Author for correspondence. E-mail: berkes@cc.umanitoba.ca

Sea Otters Provide Ecosystem Support

markets until 1975, when it rapidly expanded into an export fishery (*11*). Spatial expansion masked regional depletions, a common characteristic of sequential exploitation (*2*, *5*). Global harvest peaked in about 1990 with the expansion of the fishery to new regions, but declined after that because there were no frontiers left to exploit.

The resulting simplification of food webs and loss of biodiversity are eroding the resilience of marine ecosystems and increasing their vulnerability to environmental change (*12*, *13*). For example, fishing pressure on many coral reefs has increased dramatically with the emergence of export markets for restaurant and aquarium trades, highly mobile boom-and-bust fisheries based on rapid air transport to growing luxury markets. Depletion of herbivorous fishes has contributed to algal blooms on reefs, because algae released from their consumers out-compete corals for space. Consequently, overfished reefs are less resilient to recurrent disturbances, such as hurricanes, and more vulnerable to coral bleaching and mortality caused by global warming (*14*).

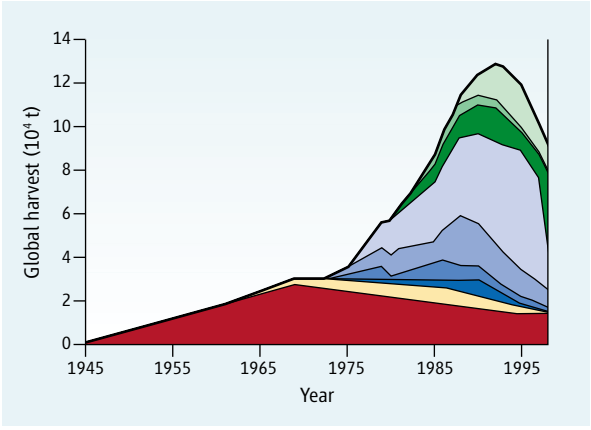

Global sea urchin harvests over time. Color coded by region, in chronological ascending order: Japan; Korea; Washington and Oregon; Baja, Mexico; California; Chile; NE Pacific (Alaska and British Columbia); Russia; NW Atlantic (Maine, Nova Scotia, New Brunswick). All data are from (*11*).

Management Implications

There have been few effective responses to this kind of exploitation, because the emergence of specialized export markets for hitherto unexploited stocks is almost always a surprise to managers. In the case of small or highly localized stocks, the resource may vanish even before the problem is noted. In the case of more widely distributed, relatively abundant species, serial depletions of local stocks may be masked by spatial shifts in exploitation (see figure, p. 1557, and graph, this page).

Existing marine protected areas (MPAs) and no-take areas (NTAs) are often too small and too far apart to sustain processes within the broader seascape, and monitoring and enforcement are often inadequate. Even the Great Barrier Reef Marine Park, the largest MPA in the world (33% of which is zoned as NTA) is too small to maintain stocks of marine mammals, turtles, and sharks that migrate across its boundaries. In any case, areas outside NTAs and MPAs also need protection.

At the international scale, CITES (U.N. Convention on International Trade in Endangered Species) bans or controls trade only in species placed on appendix I or II of CITES, respectively. The meetings to vote on proposals to place species in the appendices take place every 2 years, a blunt and ineffective instrument indeed to protect stocks that may be scooped up within months. Even identifying species at risk is a gigantic task. Other than CITES, there are no restraints on trade or even effective reporting mechanisms.

Addressing the ecological impacts of globalization means finding ways to match the growth in demand for local marine products, with the development of institutions to regulate harvesting (*15*). Appropriate restraining institutions must be in place before the resource is at risk. Solutions depend ultimately on changed behavior at the local level, but the problem must be addressed at multiple scales. Global, regional, and national bodies need to monitor trade and resource trends and find ways to disseminate information that stimulates problem-solving consistent with local practices. They need to enable local authorities to learn from the experience of others around the world. Most important, they have to encourage local governance and assist in the development of resource rights that align individual self-interest with the long-term health of the resource.

Checks can be established through harvesting permits, certification, and controls over delivery of products to markets to dampen the rate of increase in demand. Technological changes make detection in global transport of a product possible. Monitoring of foreign direct investments (*7*), increased transparency of vessel flag history, and identification of vessel owners and roving buyers will improve the ability to track potential problems. Costs of regulation must be balanced against the costs of potential losses due to inaction (*16*). For example, Maine's precautionary fisheries laws (adopted in response to the urchin debacle) recognize the need to deliberately seek to slow down the development of new marine products.

Common property theory predicts that the establishment of property rights (*8*) and/or comanagement regimes (*17*) counters the tragedy of the commons. Individual or community property rights over resources can internalize costs and benefits to create incentives for local protection and monitoring. Property rights approaches have proved to be particularly effective with stationary resources such as sea urchins and abalone (*3*, *4*). For migratory marine resources, however, the challenge is to establish governance mechanisms that operate at national and international scales (*18*, *19*). If major markets and targeted species are known, the next exploitation wave may be foreseeable from analyses such as the one here and from patterns of depletion and recovery of key species groups (*20*).

Crucially important here are multilevel governance institutions operating at diverse levels, from local to international (*21*). No single approach can solve problems emerging from globalization and sequential exploitation. But the various approaches used together can slow down the roving bandit effects, and can replace destructive incentives with a resource rights framework that mobilizes environmental stewardship, i.e., one that builds the self-interested, conserving feedback that comes from attachment to place.

References and Notes

1. J. B. C. Jackson *et al.*, *Science* **293**, 629 (2001).
2. R. A. Myers, B. Worm, *Nature* **423**, 280 (2003).
3. R. Hilborn, J. M. Orensanz, A. M. Parma, *Philos. Trans. R. Soc. London Ser. B* **360**, 47 (2005).
4. J. C. Castilla, O. Defeo, *Science* **309**, 1324 (2005).
5. M. Huitric, *Ecol. Soc.* **10**(1), 21 (2005); (www.ecologyandsociety.org).
6. M. Olson, *Power and Prosperity* (Basic Books, New York, 2000).
7. Organization for Economic Cooperation and Development (OECD), *Fish Piracy: Combating Illegal, Unreported and Unregulated Fishing* (OECD Publications, Paris, 2004).
8. T. Dietz, E. Ostrom, P. C. Stern, *Science* **302**, 1907 (2003).
9. R. S. Steneck *et al.*, *Environ. Conserv.* **29**, 436 (2002).
10. R. S. Steneck, E. Sala, in *Large Carnivores and the Conservation of Biodiversity*, J. Ray, K. Redford, R. Steneck, and J. Berger, Eds. (Island Press, Washington, DC, 2005), pp. 110–137.
11. N. L. Andrew *et al.*, *Oceanogr. Mar. Biol. Annu. Rev.* **40**, 343 (2002).
12. T. P. Hughes *et al.*, *Trends. Ecol. Evol.* **20**, 380 (2005).
13. D. R. Bellwood, T. P. Hughes, C. Folke, M. Nystrom, *Nature* **429**, 827 (2004).
14. T. P. Hughes *et al.*, *Science* **301**, 929 (2003).
15. O. Young, *The Institutional Dimensions of Environmental Change* (MIT Press, Cambridge, MA, 2002).
16. R. Costanza *et al.*, *Ecol. Econ.* **31**, 171 (1999).
17. D. C. Wilson, J. Raakjaer Nielsen, P. Degnbol, Eds., *The Fisheries Co-Management Experience* (Kluwer, Dordrecht, Netherlands, 2003).
18. F. Berkes, in *Indigenous Use and Management of Marine Resources,* N. Kishigami, J. M. Savelle, Eds. (National Museum of Ethnology, Osaka, 2005), pp. 13–31.
19. J. Wilson, *Ecol. Soc.* **11**(1), 9 (2006); (www.ecologyandsociety.org).
20. R. A. Myers, B. Worm, *Philos. Trans. R. Soc. London Ser. B* **360**, 13 (2005).
21. C. Folke *et al. Annu. Rev. Environ. Resour.* **30**, 441 (2005).

22. We thank James Cook University and the Beijer International Institute for Ecological Economics for co-hosting workshops on Resilience of Marine Ecosystems in Sweden and Australia that led to this article.

10.1126/science.1122804

MATERIALS SCIENCE

Artificial Muscle Begins to Breathe

John D. Madden

In robots, the power source is usually distant from the actual moving parts, which can be inefficient. One solution is to provide power locally, as in real muscles, by incorporating fuel cell technology directly into artificial muscles.

Electrically driven motors and actuators have a major disadvantage when used in autonomous systems—they rely on batteries. The results presented on page 1580 of this issue by Ebron and colleagues (*1*) offer a unique solution to this problem by creating artificial muscle actuators that breathe. The invention should lead to powerful devices that truly keep on going by consuming energy-rich fuels and oxygen.

This work also suggests a new, highly distributed machine architecture that mimics nature in a number of ways: The muscle consumes oxygen and fuel that can be transported via a circulation system; the muscle itself supports the chemical reaction that leads to mechanical work; electrochemical circuits can act as nerves, controlling actuation; some energy is stored locally in the muscle itself; and, like natural muscle, the materials studied by Ebron *et al.* contract linearly. The approach is not without challenges, but it could transform the way complex mechanical systems are built.

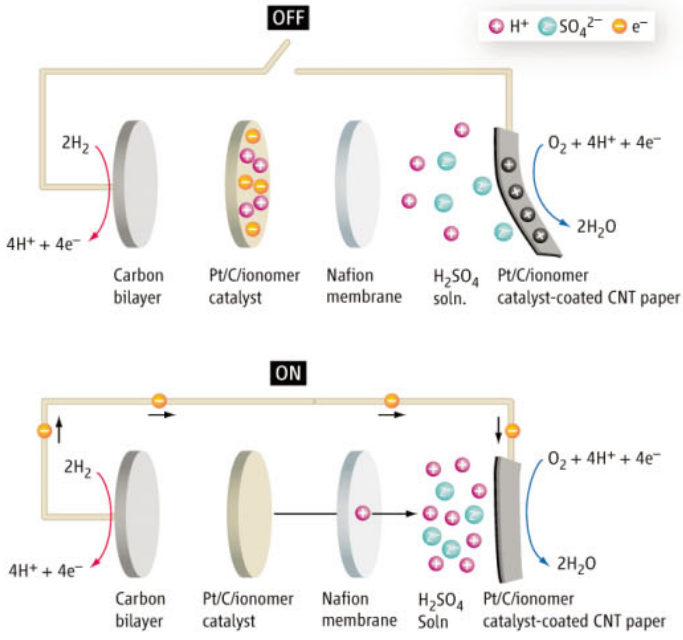

Fuel cell muscle. (Top) Oxygen dissolved in water transfers charge (assisted by the platinum catalyst) to paper made of carbon nanotubes (CNT). The nanotube film (black) expands as a result of the charging (*3*), causing it to bend as it expands relative to the platinum/carbon/ionomer layer (dark gray). **(Bottom)** The bending is reversed by closing the circuit to a hydrogen electrode, which neutralizes the charge. The counter electrode is a carbon bilayer-platinum catalyst-Nafion membrane electrode assembly shown in "exploded view."

The new breathing actuator is a fuel cell. Why is this of interest? The energy per unit mass of hydrogen and methanol, like that of sugars, fats, and gasoline, is approximately two orders of magnitude higher than that of batteries. This difference in energy has limited the performance of battery-driven electric vehicles and devices. For example, ASIMO, Honda's humanoid robot, strolls along for 45 min on battery power, while we can walk for much longer without refueling. Hydrogen and hydrocarbons are incredibly energy-dense not only because of their high chemical potential energy, but also because they are light elements and they react with oxygen, which is freely available. Fuel cells provide an emerging solution to the power needs of electrically driven autonomous devices, especially where combustion engines are impractical, as in many robots, active medical devices, small pumps, valves, toys, and micro- and nanodevices.

What is particularly intriguing in the work of Ebron *et al*. is that the actuators themselves are the fuel cell electrodes, converting chemical potential into work. The authors convert two actuator technologies into fuel cells by coating them with catalyst. In the first case, the dimensional changes induced in sheets of single-walled carbon nanotubes (SWNTs) when they are charged are put to use. The charge is generated by the fuel cell at open circuit (see the first figure). In the second system, nickel-titanium shape-memory alloys (SMAs) produce large-dimensional changes when they undergo a thermally induced phase transition. Often Joule heating is used, but in this case, heat produced by the fuel cell leads to actuation (see the second figure). In both cases these materials are used as linear actuators, like natural muscle. No separate fuel cell is required, so mass and complexity are reduced.

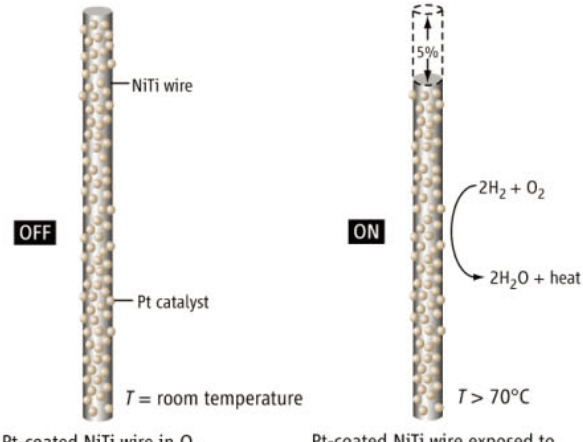

Tensile actuator. (Left) Nickel titanium shape memory alloys can also be used as actuators. The NiTi wire is coated with platinum catalyst. **(Right)** When dissolved hydrogen and oxygen react on the platinum coating to produce water, the resulting heat induces a phase change in the NiTi leading to contraction and force generation (*2*). Both actuator reactions are reversible.

The new challenge is to create a circulation system that replaces the wires that usually drive these actuators. As in our own circulation and respiration systems, pressures (or diffusion gradients) need to be generated and waste gases (water and CO_2) exchanged. Can such a circulation system deliver the power effectively? A copper wire carries about 1 MW m^{-2} at the low voltages used for these actuators. Hydrogen at 1 atm will produce the same power per unit area at a flow speed of 10 cm s^{-1}. In methanol, flow speeds can be less than 0.1 mm s^{-1}. These relatively modest flows suggest that direct fuel delivery can provide an effective alternative to electrical energy transmission in machines.

How can fuel-powered actuators be controlled? Low-energy nerve impulses activate natural muscle; the authors show that an analogous "twitch" can be induced in SWNT actuators by briefly discharging their fuel cells. In this approach there is no need for special valves or pumps, and control signals can be small. The approach may not work for all situations but is a promising beginning.

The idea of having artificial muscles that "breathe" is an exciting one, but what are the near-term prospects of the approach using the actuators chosen? SMAs produce an unmatched combina-

CREDIT: P. HUEY/SCIENCE

Published by AAAS

tion of work density and power density, far exceeding that of combustion engines (*2*). However, SMA actuators are driven by heat and are limited to the Carnot efficiency—several percent at best. As a result, when Joule heating is used to actuate them, huge currents are needed, especially where high power is demanded. The slow response and energy density of batteries result in low power and short duration of operation. The use of the SMAs as part of a fuel cell means that the actuators can operate for longer periods and at higher power. The circulation system might be used to rapidly cool the SMAs, enabling fast cycling. Although the fuel cell approach overcomes a number of obstacles that have limited the breadth of application of these actuators, some remain, including the moderate cycle life of SMAs. These actuators won't propel our cars just yet, but they could operate the windows and door locks in fuel cell vehicles, or could serve as replaceable artificial muscles in lifelike robots.

Similar benefits are offered by SWNTs, whose work densities are potentially even higher than those of SMAs. Increases in elastic modulus and tensile strength of SWNT fibers are needed to achieve this potential, along with effective methods of amplifying their strains (similar to the challenge faced by piezoceramics). SWNTs and SMAs are not the only actuator technologies that can be converted to fuel cells. A number of other emerging artificial-muscle technologies that rely on charge transfer will benefit from this approach (*2*). The demonstration by Ebron *et al*. changes the perception of what is possible, and may even initiate the design of new materials optimized for breathing.

Are there other ways in which nature can be mimicked to advantage? Often there is exquisite control within a single muscle, allowing selective activation of subsets of muscle fibers to optimize force and stiffness, which is critical for activities such as catching and throwing a ball. Fine control over individual actuators and the use of a large number of distributed actuators will go a long way toward creating highly dexterous robots that, in the words of the authors, can "freely prance around." An exciting challenge is the development of fabrication methods that can create such systems.

References

1. V. H. Ebron *et al*., *Science* **311**, 1580 (2006).
2. J. D. Madden *et al*., *IEEE J. Ocean. Eng.* **29**, 706 (2004).
3. R. Baughman *et al*., *Science* **284**, 1340 (1999).

10.1126/science.1123995

NEUROSCIENCE

Neuron, Know Thy Neighbor

Once thought only to contribute to cell adhesion as a structural link between a cell's cytoskeleton and its surface, the protein α-catenin now appears to be a key regulator of cytoskeletal dynamics and cell proliferation.

Emanuel DiCicco-Bloom

Our most sophisticated thoughts and feelings depend critically on the cellular composition and functional organization of the cerebral cortex. Indeed, changes in the numbers of neurons, their positions within the tissue, and their interconnections via synapses may underlie a variety of human brain disorders, from autism and bipolar depression to mental retardation and epilepsy (*1*). On page 1609 of this issue, Lien *et al*. (*2*) identify an unexpected role for a cell-to-cell adhesion apparatus, specifically the protein α-catenin, in regulating early vertebrate brain development. Selectively abolishing αE-catenin (the form expressed in epithelia) in the developing nervous system of the mouse produces marked tissue hyperplasia and dysplasia, resulting in an enlarged brain (macrocephaly) that functions abnormally. This suggests that proper cell adhesion is important for the orderly formation of neurons.

Enhanced online at www.sciencemag.org/cgi/content/full/311/5767/1560

Like other developing epithelia, the proliferative ventricular zone lining the central canal of the neural tube (the structure that develops into the vertebrate brain and spinal cord) consists of polarized neural precursor cells that are connected by junctional complexes (see the figure). These junctions are further associated with intracellular bands of actin bundles, a major structural component of the cell's cytoskeletal infrastructure. Cell division by these interconnected neural precursors in the ventricular zone is followed by a delamination process in which newly formed precursors presumably detach from neighboring cells and migrate radially toward distal regions of the developing cerebral cortex. αE-Catenin may be a molecular switch in this process, promoting precursor transition from a stable to migratory state (*2*–*4*). Generally, neural precursor cell division in the ventricular zone is asymmetric, producing one precursor that remains in the ventricular zone to continue proliferating, and another that migrates away along the extended processes of radial glial cells (*1*, *5*). Sometimes, the migrating cell will divide again in the overlying region, the subventricular zone. There, it undergoes symmetric division to produce two neural precursors. Alternatively, it migrates to the cortical plate and differentiates into a mature neuron.

In addition to these spatial domains, neurogenesis is temporally regulated (*1*). The type and localization of a mature neuron depends critically on when its cell division cycle ends, such that early "born" cells localize to inner layers of cortex, and later born cells populate outer layers. Recent time-lapse studies demonstrate that neuronal precursors exhibit region-specific patterns of asymmetric and symmetric cell division in the ventricular and subventricular zones, respectively, and complex patterns of migration (*5*). This process is supported on a highly organized and structured neuroepithelial population of neural precursors, and the studies suggest that neuroepithelia are differently structured in these distinct developmental domains.

By selectively deleting αE-catenin expression in the developing mouse brain, Lien *et al*. disrupted the apical junctional complexes that maintain the neuroepithelial sheet of the developing cerebral cortex. The result was an enlarged and disorganized brain, thus implicating αE-catenin in the control of cell proliferation and migration. Apical junctional complexes are composed of a transmembrane protein called cadherin, which forms homophilic bonds between the surfaces of neighboring cells; β-catenin, which binds cadherin's cytoplasmic domain; and α-catenin, which binds β-catenin and interacts with actin filaments to promote bundle formations that stabilize the cell (see the figure). Loss of αE-catenin from day 12.5 of embryonic development onward enhanced cell proliferation and decreased cell death, leading to a 40% increase in brain cell number on day 13.5 and a twofold increase by birth, 6 days later. Brain tissue was entirely disorganized with features of tumor pathology, including ectopic neurons in proliferative zones, and dividing cells in the differentiating cortical plate. Similar cell disorganization with aberrant migration following loss of cell adhesion has been observed in some cancers.

Although there were effects on cell division and cell death, fewer effects on overall differentiation were observed. Analysis of gene expression revealed surprisingly few changes in the deletion mutant mice. The most

The author is in the Department of Neuroscience and Cell Biology/Pediatrics (Neurology), University of Medicine and Dentistry of New Jersey–Robert Wood Johnson Medical School, Piscataway, NJ 08854, USA. E-mail: diciccem@umdnj.edu

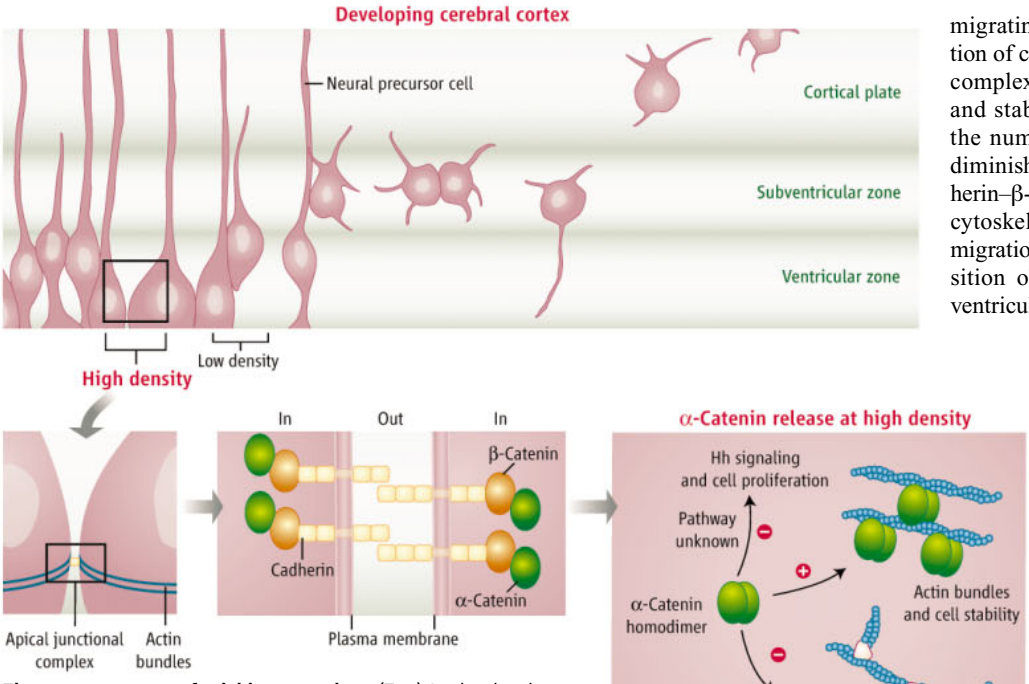

The consequences of sticking together. (Top) In the developing mammalian cerebral cortex, polarized neural precursors constitute a neuroepithelial layer in the ventricular zone. These precursors undergo asymmetric and symmetric cell divisions in the ventricular and subventricular zones, respectively. Following division, some prescursors migrate to the cortical plate where they differentiate into mature neurons or glial cells. **(Bottom)** In the ventricular zone, neural precursors are joined by apical junctional complexes, and intracellular bands of actin stabilize them into a neuroepithelial sheet (left). The apical junctional complex that links neighboring precursor cells consists of cadherin at the cell surface and α- and β-catenin in the cytoplasm (middle). At high apical junctional complex density, α-catenin is released from β-catenin, and forms homodimers that inhibit Hedgehog (Hh) signaling and cell proliferation, and promote actin bundle formation and cell stability. In contrast, by blocking Arp2/3 binding to actin, α-catenin homodimers reduce actin chain branching and cell motility decreases (right).

revealing difference was the expression of components of a cell signaling pathway regulated by Hedgehog, a protein that controls growth and patterning during development in various animals including mammals. The absence of αE-catenin increased expression of GLI1 and FGF15, targets of Hedgehog signaling, and of smoothened, a Hedgehog receptor component. In a stunning test of Hedgehog's involvement in cortical hyperplasia, treatment of pregnant mice lacking αE-catenin with cyclopamine, an inhibitor of smoothened, at day 12.5 of embryonic development, prevented increased proliferation and decreased cell death in the brains of developing mice. The result was the normalization of brain cell number. In contrast, the abnormal appearance of brain tissue with aberrant cell migration remained, functionally distinguishing these phenomena. The authors propose a new mechanism by which apical junctional complexes regulate cortical cell population size through αE-catenin. As cell numbers increase over the course of neurogenesis, so will cell density and adherens contacts. Because αE-catenin negatively regulates Hedgehog signaling (and thus, tissue growth), increasing the number of cortical neurons will lead to progressive reductions in cell proliferation. The locus of αE-catenin effects, whether cytoplasmic or nuclear, remains to be defined.

Traditionally, apical junctional complexes were considered static epithelial structures, formed and stabilized by interactions between cadherin, β-catenin, α-catenin, and actin. However, recent studies challenge this idea. Biochemical and live-cell imaging (*3*, *4*, *6*) suggest that α-catenin serves as a molecular switch: As a monomer, α-catenin is bound to β-catenin and does not bind actin efficiently, allowing for a dynamic cytoskeleton. However, when α-catenin abundance increases—for example, through increased apical junctional complex formation—α-catenin is released from β-catenin and forms dimers that bind avidly to actin, thereby promoting actin bundle formation and stability. Moreover, the α-catenin homodimer competes with a protein called Arp2/3 to bind actin, and this competition reduces Arp2/3-actin interaction (see the figure). This is important because Arp2/3 induces branching of actin fibers, such as that observed in the motile leading edge of migrating-cell lamellipodia. Thus, the formation of cell-cell adhesions via apical junctional complexes promotes α-catenin dimerization and stabilizes actin bundles. Conversely, as the number of apical junctional complexes diminishes, α-catenin monomers bind the cadherin–β-catenin complex, freeing up local actin cytoskeleton to dynamically mediate cell migration. These events may underlie the transition observed in asymmetrically dividing ventricular zone neural precursors, as one sibling migrates to distant locales in the developing cerebral cortex. The brains of αE-catenin–deficient mice exhibit loss of proteins that form the apical junctional complex and disorganized cell-migration patterns, consistent with a loss of intercellular adhesion.

Other cell signaling pathways are likely also affected by disruption of the apical junctional complex (*7*). The ventricular zone contains many mitogenic signaling molecules whose effects on neural precursor proliferation require cellular organization. These molecules include soluble ligands (such as fibroblast growth factors, Wnts, insulin-like growth factor 1, and bone morphogenetic proteins), extracellular matrix proteins (proteoglycans), and membrane-bound proteins (ephrins, Eph receptors and neural cell adhesion molecules) (*1*, *8*). Moreover, emerging evidence suggests that signals from differentiating neurons in the cortical plate may act on ventricular zone precursors to regulate the timing and rate of proliferation (*5*). Such input is lost with tissue dysplasia. Furthermore, proteins of the apical junctional complex could interact with plasma membrane receptor signaling complexes or proteins that lie downstream in the signaling cascades. Indeed, in mouse kerotinocytes lacking α-catenin, mitogenic signaling by insulin-like growth factor 1 was markedly increased (*9*). Thus, a host of differences in the control of local cell proliferation could result from changing the structure of intercellular adhesions.

Based on the macrocephaly and cortical disorganization of the brain, could α-catenin and related adhesive junctions serve as loci for brain disease? Although it is premature to conclude that the brain is enlarged in autism, increased brain size (5 to 10%) and accelerated growth rate during early childhood have been documented (*10*–*12*). The underlying cause of this change is unclear. From the limited neuropathology available, the cerebral cortex of autistic individuals exhibits a number of developmental abnormalities, including aberrant neuronal migration and positioning (*13*) and abnormal axonal connections. Changes in the apical junctional complex could well lead to increased cell production that is not counterbalanced by enhanced cell death, altering brain

cell composition and number. It is possible that minor changes in the expression or timing of apical junctional complex function may also contribute to developmental abnormalities underlying the pathogenesis of conditions such as autism.

References and Notes

1. E. DiCicco-Bloom, M. Sondell, in *Kaplan & Sadock's Comprehensive Textbook of Psychiatry*, B. J. Sadock, V. A. Sadock, Eds. (Lippincott, Williams, and Wilkins, Philadelphia, ed. 8, 2005), pp. 33–49.
2. W.-H. Lien, O. Klezovitch, T. E. Fernandez, J. Delrow, V. Vasioukhin, *Science* **311**, 1609 (2006).
3. F. Drees, S. Pokutta, S. Yamada, W. J. Nelson, W. I. Weis, *Cell* **123**, 903 (2005).
4. S. Yamada, S. Pokutta, F. Drees, W. I. Weis, W. J. Nelson, *Cell* **123**, 889 (2005).
5. S. C. Noctor *et al.*, *Nat. Neurosci.* **7**, 136 (2004).
6. J. Gates, M. Peifer, *Cell* **123**, 769 (2005).
7. U. Cavallaro, G. Christofori, *Nat. Rev. Cancer* **4**, 118 (2004)
8. K. L. Ferguson, R. S. Slack, *Trends Neurosci.* **26**, 283 (2003).
9. V. Vasioukhin, C. Bauer, L. Degenstein, B. Wise, E. Fuchs, *Cell* **104**, 605 (2001).
10. E. Courchesne *et al.*, *Neurology* **57**, 245 (2001).
11. B. F. Sparks *et al.*, *Neurology* **59**, 184 (2002).
12. H. C. Hazlett *et al.*, *Arch. Gen. Psychiatry* **62**, 1366 (2005).
13. S. J. Palmen, H. van Engeland, P. R. Hof, C. Schmitz, *Brain* **127**, 2572 (2004).

14. E.D-B. acknowledges grant support from the National Institutes of Health and the National Alliance for Autism Research.

10.1126/science.1126397

VIROLOGY

Clues to the Virulence of H5N1 Viruses in Humans

Why is H5N1 avian influenza so virulent? Genomic analysis of various isolates suggests that, in addition to two known surface proteins, a third previously unnoticed sequence in a small viral protein may contribute to virulence.

Robert M. Krug

H5N1 strains of avian influenza A virus have already caused the deaths of more than 90 people since the outbreak of infection in Southeast Asia in 1997, corresponding to a death rate of ~50% for known infections. These viruses, which have now spread from Asia to Europe and Africa, are strong candidates for causing the next flu pandemic if they acquire the ability for efficient human-to-human transmission. A major research goal has been to identify the molecular basis of the virulence of H5N1 viruses in humans (*1*, *2*). Several virus-encoded proteins will likely contribute to virulence in humans, because previous studies have shown that the virulence of influenza A virus of different organisms is caused by multiple genes (*2*). The study by Obenauer *et al*. (*3*) on page 1576 of this issue, presents evidence suggesting that the virulence of H5N1 viruses may be caused at least in part by the function of a previously unnoticed amino acid sequence motif in the virus-encoded nonstructural protein called NS1 (see the figure).

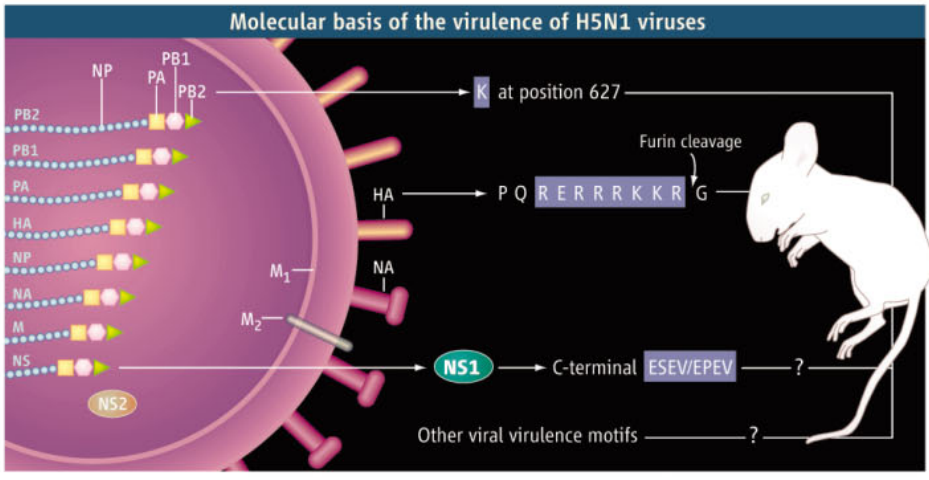

Variation locations. Strains of the H5N1 influenza A virus that are virulent in mammals, including mice and humans, have alterations in the sequences of any of three viral proteins hemagglutinin (HA), the viral polymerase protein PB2, and the nonstructural protein NS1. Influenza A virus has 8 genomic RNA strands and 10 proteins, as shown.

The NS1 protein is synthesized in infected cells but not incorporated into virus particles. Rather, this small, multifunctional protein participates in both protein-RNA and protein-protein interactions during infection. Its amino-terminal RNA-binding domain binds to double-stranded RNA (dsRNA) with low affinity (*4*), but the significance of this activity during viral infection is controversial (*5*, *6*). The NS1 protein also binds and inhibits the function of two cellular proteins that are required for the modification of the 3′ ends of cellular messenger RNAs (mRNAs) (*6*). Consequently, the production of a key component of the host antiviral response, interferon-β mRNA, is substantially reduced, although not eliminated (*7*). The NS1 sequences that participate in binding to either these two cellular proteins or dsRNA are not part of the putative new virulence determinant in NS1.

Ten other proteins are encoded by influenza A virus, whose genome consists of eight single-stranded RNAs (*8*). Three proteins (PB1, PB2, and PA) comprise the polymerase that is associated with each of the viral genomic RNAs in the virus particle. The polymerase copies these genomic RNAs into viral mRNAs and also catalyzes the replication of the genomic RNAs in infected cells. Investigators have identified the amino acid sequences of the PB1, PB2, and PA proteins that function in specific steps of virus-specific RNA synthesis or in mediating interactions between the three proteins (*2*). The amino acid at position 627 in PB2, which has been implicated in human virulence of H5N1 viruses, does not participate in these known functions. H5N1 viruses that are virulent in mice encode lysine at this position in PB2, whereas H5N1 viruses that are not virulent in mice, as well as other avian influenza A virus strains, encode glutamic acid at this position (*9*). It is thought that this change from glutamic acid to lysine represents an adaptation of H5N1 viruses for efficient replication in mammalian cells (*10*).

Another virulence determinant for the H5N1 virus in mammals has previously been identified in the hemagglutinin, the major surface protein of the virus (*8*). Hemagglutinin, which binds to sialic acid–containing receptors on host cells, is the protein against which neutralizing antibodies are produced. Because the H5 type of hemagglutinin in avian influenza A viruses has not been found in previously circulating human influenza A virus strains, humans are potentially susceptible to infection by these viruses. Cleavage of hemagglutinin into two disulfide-linked sub-

The author is at the Institute for Cellular and Molecular Biology, University of Texas at Austin, Austin, TX 78712, USA. E-mail: rkrug@mail.utexas.edu

CREDIT: P. HUEY/*SCIENCE*

units is a prerequisite for initiating infection (*8*). H5N1 viruses that are highly pathogenic in mice contain a stretch of basic residues adjacent to the hemagglutinin cleavage site, enabling these hemagglutinins to be cleaved by ubiquitous intracellular proteases, including furin. Recombinant H5N1 viruses lacking these basic amino acids are no longer virulent in mice (*9*), demonstrating that the presence of these amino acids, and the consequent cleavage by intracellular proteases, are required for the virulence of these viruses.

To further understand the molecular basis of virulence, Obenauer *et al*. first sequenced the genes of a large number of H5N1 viruses isolated from wild birds and poultry, providing an invaluable resource for many investigators. This analysis revealed not only the expected variability in the sequences of the two major surface proteins of the virus, hemagglutinin and neuraminidase, but also variability in the sequence of the NS1 protein. Despite variability in the latter, it was noted that the carboxyl terminus of the NS1 proteins of the vast majority of avian H5N1 viruses contains a sequence motif, Glu-Ser-Glu-Val (ESEV). These residues are predicted to mediate binding to proteins bearing a region called a PDZ domain. The multitude of human proteins that contain a PDZ domain function in diverse cellular signaling pathways including those that regulate protein traffic within the cell and those that maintain cell morphology and organization. Another PDZ-binding sequence, Glu-Pro-Glu-Val (EPEV), was identified at the carboxyl terminus of the NS1 proteins of all the virulent H5N1 viruses isolated from humans. In contrast, the carboxyl terminus of the NS1 proteins of low-virulence human influenza A usually contains a different sequence, Arg-Ser-Lys-Val (RSKV), which is not a PDZ-binding motif. Further, Obenauer *et al.* verified that the carboxyl-terminal ESEV and EPEV sequences indeed bind to PDZ domains. Consequently, the presence of a functional carboxyl-terminal PDZ-binding domain in the NS1 protein of H5N1 viruses correlates with human virulence. This supports the authors' hypothesis that the carboxyl-terminal domain of the NS1 proteins of avian H5N1 viruses acts as a virulence factor by binding cellular PDZ-containing proteins and disrupting their participation in important cellular processes.

This is an intriguing hypothesis that, however, needs to be evaluated in animal experiments with H5N1 viruses that have been altered to express a NS1 protein lacking the carboxyl-terminal ESEV/EPEV sequence. Such experiments are critical because it has already been established that this carboxyl-terminal sequence is not required for the virulence of previously isolated H5N1 viruses in ferrets (*11*). An analysis of the virulence of H5N1 viruses isolated in 2004 identified the human isolate A/Vietnam/1203/04 as the most pathogenic isolate. The NS1 protein encoded by this virus is truncated and consequently lacks the suspect carboxyl-terminal ESEV/ EPEV motif. Future experiments will establish whether eliminating the carboxyl-terminal ESEV/EPEV sequence of the NS1 protein of other H5N1 viruses has any effect on their virulence in animal models. In addition, the search for other molecular determinants of the virulence of H5N1 viruses in humans will undoubtedly continue.

References

1. T. Horimoto, Y. Kawaoka, *Nat. Rev. Microbiol.* **3**, 591 (2005).
2. D. L. Noah, R. M. Krug, in *Advances in Virus Research*, K. Maramorsch, A. J. Shatkin, Eds. (Elsevier, Amsterdam, 2005), vol. 65, pp. 121–145.
3. J. C. Obenauer *et al*., *Science* **311**, 1576 (2006); published onlne 26 January 2006 (10.1126/science.1121586).
4. C. Y. Chien *et al.*, *Biochemistry* **43**, 1950 (2004).
5. A. Garcia-Sastre, *Virology* **279**, 375 (2001).
6. R. M. Krug, W. Yuan, D. L. Noah, A. G. Latham, *Virology* **309**, 181 (2003).
7. D. L. Noah, K. Y. Twu, R. M. Krug, *Virology* **307**, 386 (2003).
8. R. A. Lamb, R. M. Krug, in *Fields Virology*, D. M. Knipe, P. M. Howley, Eds. (Lippincott, Williams, and Wilkins, Philadephia, 2001), vol. 1, pp. 1487–1531.
9. M. Hatta, P. Gao, P. Halfmann, Y. Kawaoka, *Science* **293**, 1840 (2001).
10. K. Shinya *et al.*, *Virology* **320**, 258 (2004).
11. E. A. Govorkova *et al.*, *J. Virol.* **79**, 2191 (2005).

10.1126/science.1125998

CHEMISTRY

Seamless Proteins Tie Up Their Loose Ends

Natural circular proteins found in bacteria, plants, and mammals show antimicrobial activity and exceptional stability, making them ideal templates for engineering better drugs. But just how they close into loops remains a mystery.

David J. Craik

In the early 1970s, tribeswomen in the Congo were reported to drink a medicinal tea made from a local plant to induce labor and facilitate childbirth (*1*). Twenty-five years later, it was discovered that the active ingredient, robust enough to withstand boiling and ingestion, is a small protein with a circular shape (*2*). It turns out that the protein, kalata B1, was not a one-off example. Many other naturally occurring circular and stable proteins have since been found in bacteria, plants, and animals from Africa, South America, Australia, and Europe (*3*). What makes them so interesting? The exceptional stability and wide range of activities of these circular proteins, from insecticidal and antimicrobial to thwarting cellular infection by HIV (*4*), may guide the development of more effective and stable drugs.

The discovery of proteins bearing two ends that are linked together, producing a circular topology (*2*), is a new and mysterious twist in protein synthesis. Most proteins are synthesized as linear chains of amino acids in which the amino terminus of one residue is linked to the carboxyl terminus of the next. Whether assembled in the cell by nature's ribosomal machinery that translates a genomic blueprint, or by the synthetic methodology of peptide chemists, a newly formed chain folds into a complex three-dimensional shape that determines the protein's function. Circular proteins have no beginning or end, and deciphering their mode of construction presents some interesting challenges. So far, we know very little about how cyclization occurs. Circular proteins appear to derive from larger precursor proteins (see the figure), but we have little knowledge of the enzymes or other processes that cleave the mature peptide from its precursor and facilitate formation of a cyclic backbone.

The diversity of sequence of the nearly 100 circular proteins known to date across species suggests that cyclization has evolved independently in vastly different organisms as a way of tidying up the loose ends of conventional proteins. Microorganisms appear to have seized upon the advantages of cyclizing peptides long ago, as has the pharmaceutical industry. For example, in the course of making the cyclic peptide cyclosporin for their own defense, fungi have provided humankind with a drug that has now revolutionized transplant therapy because of its potent immunosuppressive activity. But cyclosporin and other previously known cyclic peptides are typically small rings of fewer than a dozen amino acids and are produced not by direct gene translation but by multidomain enzymes called peptide synthetases. The excite-

The author is at the Institute for Molecular Bioscience, University of Queensland, Brisbane, Queensland 4072, Australia. E-mail: d.craik@imb.uq.edu.au

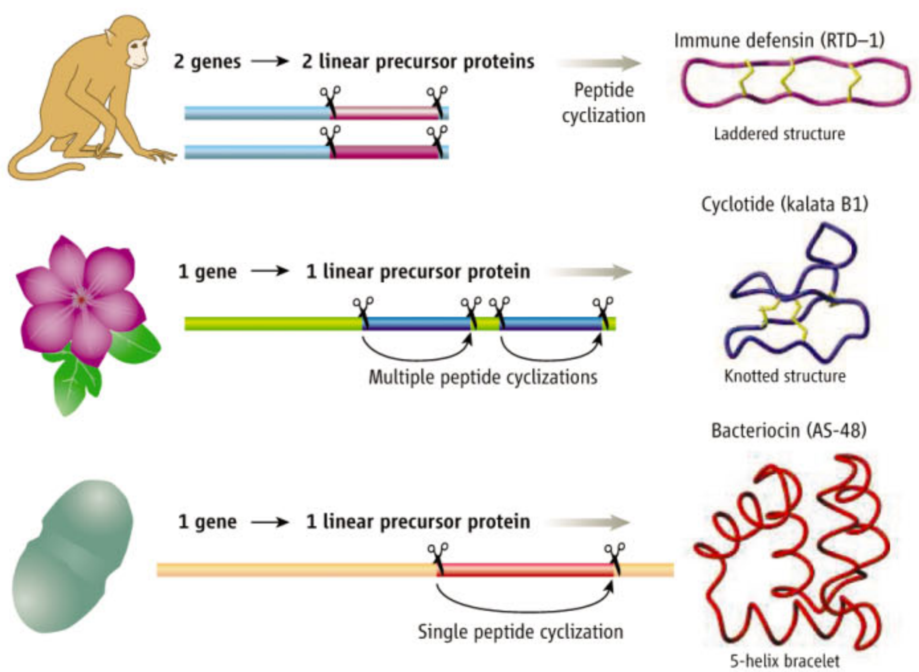

Diced, spliced, and coming full circle. Gene-encoded circular proteins are produced as fragments of linear precursor proteins that are excised and spliced head-to-tail. In the case of rhesus θ-defensin–1 (RTD-1) (**top**), two genes each code for half of the 18–amino acid mature peptide and a double head-to-tail ligation produces the circular peptide. In the case of the plant cyclotides (**middle**), a cystine knot embedded in the circular backbone provides extra stabilization. (**Bottom**) The circular backbone of the bacterial protein AS-48 folds up to form a bracelet of five helices. Images of structures are adapted from (*3*).

ment associated with the new generation of circular proteins discovered in the last decade, and ranging in size from 14 (*5*) to 78 (*6*) amino acids, is that they are true gene products and hence can be manipulated using the tools of molecular biology. For example, genes from circular proteins that have insecticidal properties (*7*) could be transferred to crop plants to provide built-in protection against herbivorous pests, and thereby reduce the need for chemical spraying.

What are the advantages of a circular form? For one, the free ends of conventional proteins are routinely targeted by exopeptidases—enzymes whose function is to nip away at proteins to digest them. Joining the ends thus removes a major degradation pathway. Also, the ends of linear proteins are often flexible or ill-defined, in contrast to their highly structured interior. This flexibility is bad from an entropic perspective when proteins bind to their molecular receptors, leading to reduced binding affinity and biological activity. Thus, in principle, both the stability and the activity of proteins can be improved by tying up their loose ends. What is particularly impressive about circular proteins is their indestructible nature. Most proteins denature irreversibly upon heating, as exemplified by the familiar transformation when an egg is cooked. But circular proteins can be subjected to boiling, extremes of pH, and proteolytic enzymes yet still retain their structure and function—a tough crowd.

Some of the secrets to their stability have been revealed in the details of their structures. Structural determination of kalata B1 by nuclear magnetic resonance spectroscopy (*2*) revealed two surprises: Not only does it have a seamless circular backbone, but it also has a knotted arrangement of disulfide bonds that contribute to its exceptional stability (see the figure). The name "cyclotide" was coined for this family of plant proteins, which is now estimated to comprise thousands of members (*8*). The exceptional stability of the cyclotide framework suggests the possibility of using it as a template in drug design (*9*). The aim here would be to "graft" bioactive peptide sequences into the cyclotide framework. Chemical methods for the synthesis of cyclotides have been developed, so the approach is feasible. The main challenge in such studies is to ensure that the foreign peptide sequence can be grafted into the framework in such a way that it retains its biological activity

The genes for bacterial and plant circular proteins encode linear precursor proteins from which the mature peptides are excised and cyclized (see the figure). The first cyclic peptide discovered in mammals, an antibacterial called rhesus θ-defensin–1 found in macaques, is in fact a product of not one but two genes, each coding for short peptides that are subsequently linked in a double head-to-tail ligation (*10*). Rhesus θ-defensin–1 is expressed in white blood cells of the macaque monkey and is part of its innate immune system. Like the cyclotides, it contains three cross-bracing disulfide bonds, but they are in a "laddered" arrangement rather than knotted.

Why would organisms go to the trouble of producing cyclic peptides, and in different conformations? Again, stability and enhanced activity appear to be the answer, as cyclic rhesus θ-defensin–1 is more potent and stable than a synthetic acyclic counterpart that is active in vitro but is essentially inactive at physiological salt concentrations. The remarkable range of conformations into which the circular proteins are folded—from a ladder, to a knot, to a helix bundle—highlights the fact that circular proteins, just like conventional proteins, need to adopt diverse shapes specific to their functions.

In contrast to bacteria, plants, and some of our primate cousins, humans do not make cyclic peptides. A sequence similar to rhesus θ-defensin–1 was recently discovered in the human genome, but the gene is silenced by a premature stop codon (*11*). Not put off by this genetic impediment, Lehrer and colleagues (*11*) chemically synthesized retrocyclin, a putative defensin-like molecule, and found it to be a potent anti-HIV agent. The same group then analyzed DNA from a range of primates and showed that the stop codon emerged in the human lineage about 7 million to 10 million years ago (*12*). It is an ironic twist of fate that our evolutionary forebears acquired a mutation whose nonappearance would have left us with built-in protection against HIV.

The discovery of naturally occurring circular proteins has offered inspiration to protein engineers, as demonstrated by recent successes in the artificial cyclization of conotoxins, marine venom peptides of approximately 12 to 30 amino acids (*13*). Cyclization of a prototypic conotoxin improved its resistance to proteolytic degradation, which opens the door to enhanced applications of this class of molecules in medicine. The biggest challenge in the field of circular proteins is deciphering just how their ends are stitched together from their linear precursors: What enzymes are involved? Do cleavage and cyclization occur simultaneously? Are auxiliary proteins involved? These unanswered questions will certainly continue to drive the field forward.

References

1. L. Gran, *Acta Pharmacol. Toxicol.* **33**, 400 (1973).
2. O. Saether *et al.*, *Biochemistry* **34**, 4147 (1995).
3. M. Trabi, D. J. Craik, *Trends Biochem. Sci.* **27**, 132 (2002).
4. K. R. Gustafson, T. C. McKee, H. R. Bokesch, *Curr. Protein Pept. Sci.* **5**, 331 (2004).
5. S. Luckett *et al.*, *J. Mol. Biol*. **290**, 525 (1999).
6. R. Eisenbrandt *et al*, *J. Biol. Chem*. **274**, 22548 (1999).
7. C. Jennings *et al.*, *Proc. Natl. Acad. Sci. U.S.A.* **98**, 10614 (2001).
8. S. M. Simonsen *et al.*, *Plant Cell* **17**, 3176 (2005).
9. D. J. Craik *et al.*, *Curr. Opin. Drug Discov. Devel.* **9**, 251 (2006).
10. Y.-Q. Tang *et al.*, *Science* **286**, 498 (1999).
11. A. M. Cole *et al.*, *Proc. Natl. Acad. Sci. U.S.A.* **99**, 1813 (2002).
12. A. M. Cole *et al.*, *Curr. Protein Pept. Sci.* **5**, 373 (2004).
13. R. J. Clark *et al.*, *Proc. Natl. Acad. Sci. U.S.A.* **102**, 13767 (2005).

10.1126/science.1125248

CREDIT: P. HUEY/*SCIENCE*

INTRODUCTION

Chemical Detectives

LIKE THE DETECTIVE IN A MURDER MYSTERY TRYING TO RECONSTRUCT EVENTS FROM A thicket of useful and extraneous information, the analytical chemist often seeks to determine the composition of only a tiny fraction of a complex sample. Classically, the approach has been to perform an initial step of separation into purer components before proceeding to quantification. However, many problems, especially in biology and in earth and atmospheric sciences, benefit from approaches that can minimize sample preparation and skip straight to analysis. In this special issue, we focus on advances in this mode of direct detection.

Mass spectrometry can inherently deal with complex samples because it integrates separation and detection; it is the means of delivering the sample to the vacuum chamber for ionization that often limits applications. Cooks *et al*. (p. 1566) review recent methods that allow molecules to be skimmed straight off the surface of samples in the open air for mass analysis.

In a similar vein, Wightman (p. 1570) reviews the applications of electrodes whose micrometer dimensions facilitate high-resolution probing of cellular environments with minimal perturbation of the surrounding system. Through electrochemical detection, the concentration gradients that regulate physiological processes can be tracked in real time, even in live animals.

Three Reports highlight further technological advances to improve detection. A promising approach for detecting biomolecules is to decorate microcantilevers with receptors or antibodies and then observe stress-induced changes in cantilever position. Shekhawat *et al*. (p. 1592) show that a field-effect transistor embedded in the end of the cantilever can provide sufficient sensitivity and is unaffected by the analyte solution. Yu *et al.* (p. 1600) have developed a method to observe single protein molecules as they are synthesized in live *Escherichia coli* cells. Low-level expression of yellow fluorescent protein gives bursts of protein molecules from single mRNA transcripts. For spectroscopic detection of more diffuse species, such as atmospheric contaminants, a tradeoff is often made between the spectral width of the probe (for versatility) and the detection resolution (for specificity). Thorpe *et al*. (p. 1595) have created a broadband version of cavity ringdown spectroscopy that allows rapid high-resolution detection across a 100-nm wavelength range.

In related online features, the Signal Transduction Knowledge Environment (STKE) features two Perspectives. Cognet *et al.* describe how the movement of surface receptors can be monitored by means of electrophysiological and optical methods. These approaches have allowed the real-time measurement of glutamate receptor surface trafficking in live neurons. Lynch *et al.* describe how the adsorption of proteins onto nanoparticles may produce aberrant signaling due to conformational changes in the adsorbed proteins.

All great detective stories must come to an end. For scientists, though, these technological advances open the door to an ever-broadening vista of the complexities underlying the natural world.

–NANCY GOUGH, PHIL SZUROMI, JAKE YESTON

Detection Technologies

CONTENTS

Reviews

See also related Reports pages 1592, 1595, and 1600; STKE material on page 1515 or at www.sciencemag.org/sciext/detection

CREDIT: ZHENG OUYANG AND THOMAS A. BLAKE

REVIEW

Ambient Mass Spectrometry

R. Graham Cooks,[1]* Zheng Ouyang,[1] Zoltan Takats,[1,2] Justin M. Wiseman[1]

A recent innovation in mass spectrometry is the ability to record mass spectra on ordinary samples, in their native environment, without sample preparation or preseparation by creating ions outside the instrument. In desorption electrospray ionization (DESI), the principal method described here, electrically charged droplets are directed at the ambient object of interest; they release ions from the surface, which are then vacuumed through the air into a conventional mass spectrometer. Extremely rapid analysis is coupled with high sensitivity and high chemical specificity. These characteristics are advantageously applied to high-throughput metabolomics, explosives detection, natural products discovery, and biological tissue imaging, among other applications. Future possible uses of DESI for in vivo clinical analysis and its adaptation to portable mass spectrometers are described.

The application of mass spectrometry (MS) to the identification of chemical compounds in a mixture, including determining the structural composition of large biomolecules, depends on much more than the resolving power of the analyzer used for discriminating mass/charge (*m*/*z*) ratios. Often, the main limitation is getting the sample of interest into the vacuum environment of the spectrometer in the form of ions suitable for mass analysis. This problem was solved, for the case of samples in the solution phase, with the introduction of electrospray ionization (ESI) (*1*). ESI is a method where the solution is nebulized to create a fine spray of droplets under conditions in which solvent evaporation occurs as the droplets traverse the atmospheric interface, hence introducing molecular ions into the analyzer.

A critical development for the analysis of condensed-phase samples was that of the desorption/ionization (DI) methods, where molecules embedded in a substrate and introduced into the vacuum system are rapidly desorbed and ionized using energetic charged particles or laser beams. High-energy sputtering methods such as SIMS (secondary ion MS) (*2*) can be used to produce intact molecular ions. Larger molecules such as proteins are also amenable to DI methods if they are embedded in a frozen solvent (typically ice) or in an ultraviolet (UV)-absorbing matrix that can be rapidly volatilized with a laser pulse, as in MALDI (matrix-assisted laser desorption/ionization) (*3*). Although vacuum conditions are a simple choice for creating and maintaining ions, this environment is not absolutely necessary. Ions can in fact be generated in air; an atmospheric pressure version of the MALDI experiment (*4*) was an important progenitor of ambient MS experiments, even though it did not have unimpeded access to the sample nor the lack of sample preparation that characterize more recent methods.

Recently, a new family of techniques has emerged that allows ions to be created under ambient conditions and then collected and analyzed by MS. In the desorption electrospray ionization (DESI) method (*5*), a fine spray of charged droplets hits the surface of interest, from which it picks up small organic molecules and large biomolecules, ionizes them, and delivers them—as desolvated ions—into the mass spectrometer. DESI can be considered an atmospheric pressure version of SIMS, being especially close to versions that use C_{60} projectiles (*6*) or massive water clusters as primary impacting particles (*7*). In the DART (direct analysis in real time) method, an electrical potential is applied to a gas with a high ionization potential (typically nitrogen or helium) to form a plasma of excited-state atoms and ions, and these desorb low–molecular weight molecules from the surface of a sample (*8*). Other closely related methods have also been introduced. Desorption atmospheric pressure chemical ionization (DAPCI) (*9*), a variant of DESI that uses gas-phase projectile ions generated by an atmospheric pressure corona discharge in the vapor of toluene or another compound, produces ions by a heterogeneous (gaseous ion/adsorbed analyte) charge-transfer mechanism. Electrospray-assisted laser desorption/ionization (ELDI) (*10*) uses a laser for the desorption of neutral molecules from an ambient surface and uses charged droplets produced by electrospray for post-desorption ionization of the ablated neutral molecules. In atmospheric solids analysis probe (ASAP) (*11*), another variant on atmospheric-pressure DI methods for solids analysis, a heated gas jet is directed onto the sample surface, and desorbed species are ionized by corona discharge in the gas phase.

Here we focus on the DESI method, on which there is the most literature, while noting cases in which the applications of the other methods yield comparable results. The ambient ionization methods retain the signature advantages of MS—speed, chemical specificity, low detection limits, and, via the MS/MS experiment, applicability to complex mixtures. However, these characteristics are now implemented in a direct experiment that requires no sample preparation. Applications to high-importance samples—such as traces of explosives on luggage, drug metabolites in urine, lipids in intact tissue, and active ingredients in

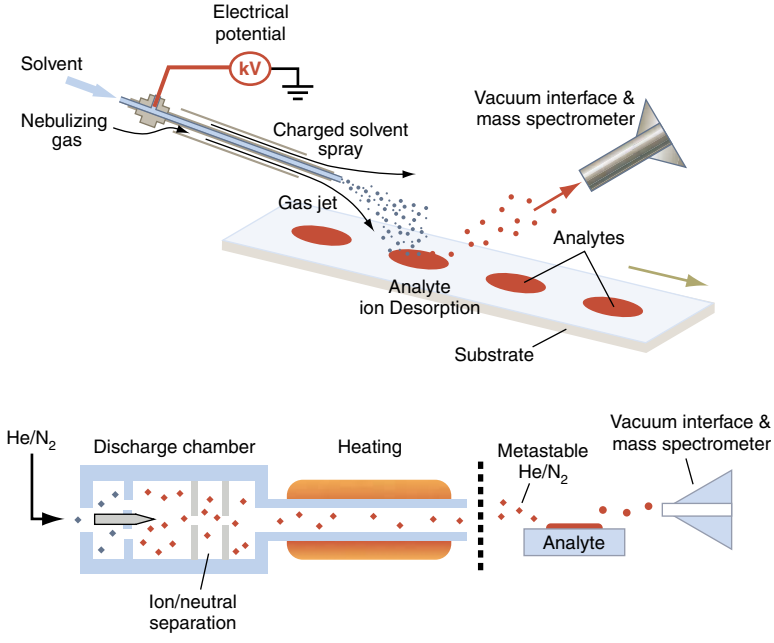

Fig. 1. DESI (upper) and DART (lower) analyses for ambient high-throughput mass spectrometric analysis of unprepared samples (skin, bricks, urine spots, clothing, tissue, etc.).

[1]Purdue University, Department of Chemistry, West Lafayette, IN 47907, USA. [2]Institute of Structural Chemistry, Chemical Research Centre of the Hungarian Academy of Sciences, Pusztaszeri ut 59-67, Budapest, Hungary.

*To whom correspondence should be addressed. E-mail: cooks@purdue.edu

pharmaceutical tablets—have quickly followed the introduction of the methodology.

Implementation

The essential aspects and the simple instrumentation of the DESI experiment are illustrated in Fig. 1. The condensed phase–to–gaseous ion transfer that is a feature of DI methods is achieved by using charged droplets (for larger molecules) or primary ions (for smaller molecules), either of which is produced by ESI (*1*). The sample of interest is in the solid phase—not in the solution phase as it is in ESI—and, in contrast to the established DI methods like SIMS and MALDI, the sample is not under vacuum. Figure 1 also summarizes the DART experiment, which differs because it uses a gas rather than a solvent to generate the energetic agents that desorb and ionize the analyte molecules.

DESI applies to both large and small molecules. The charged microdroplets used as projectiles in DESI pick up proteins and other large biomolecules from the surface, ionize them, and transport them to the mass spectrometer. This process gives the mass spectra of proteins in the solid phase, which typically closely resemble the ESI spectra of protein solutions. In addition, gas-phase solvent ions in the spray protonate or otherwise react with analyte molecules on the surface, generating ions from compounds that have low desorption energies, including volatile and semivolatile compounds (e.g., aromatic hydrocarbons and pesticides), low-polarity molecules of smaller size (e.g., terpenes and lipids), low–molecular weight polar compounds (e.g., amino acids and drug molecules), and certain inorganic ions (e.g., perchlorate). In MS, free gas-phase analyte ions are characterized by their *m/z* ratio and sometimes, in more detail, by recording their dissociation products (MS/MS spectra) and their ion-molecule reactivity. Similar to other atmospheric ionization methods (*1*, *4*, *10*, *11*), DESI causes minimum fragmentation; that is, it is a soft ionization technique that produces low-energy, intact molecular ions. This feature is associated with fast collisional cooling of nascent ions at atmospheric pressure and ambient temperature.

Analytical Performance and Characteristics

The type of ions observed in DESI, DART, and other ambient MS methods depends on the nature of the sample, substrate, and reagent. For example, the explosive RDX (hexahydrotrinitro-1,3,5-triazine) is observed as the chloride adduct $[RDX + Cl]^-$ when electrosprayed with a dilute HCl solution, but is observed as the protonated molecule $[RDX + H]^+$ when sprayed with pure water. The ionized molecules observed in the mass spectrum are conveniently mass-selected and individually examined by recording their dissociation products in the form of MS/MS spectra. Figure 2 illustrates the DESI mass spectrum of a dry urine spot on paper (2 μL of urine), showing the complex nature of this mixture. Even minor components can be identified by recording their MS/MS spectra; for example, the isolation of the ion with *m/z* = 214 and the measurement of its product spectrum allows its identification as aspartyl-4-phosphate. Experiments of the type illustrated in Fig. 2 can be performed at a rate of one per second. There is no preparation of the biological fluid other than its deposition on the surface.

Not only is DESI a very rapid method, but it is well suited to trace analysis. Luggage screening in airports is a task where very high sensitivity must be combined with high chemical specificity (low false positives, low false negatives), while maintaining immunity to matrix effects and achieving very high throughput rates. Success has been achieved in laboratory experiments with several classes of explosives and their compositions (Fig. 3) (*12*). Under artificial conditions, detection limits into the femtomole (fmol) range have been observed for some of these compounds (Fig. 3). Analogous data have been reported for DART, including cocaine detection on banknotes (*8*). Limit of detection (LOD) values in the low fmol range have been reported for proteins by using DESI (*13*) and ELDI (*10*).

DESI operating characteristics can be chosen to favor the ionization of small or large molecules. Small molecules are often seen well in the positive ion mode by using a spray voltage of 5 kV, a tip-to-sample distance of 5 mm, and an incident angle of 40° to the surface normal. Oligosaccharides and proteins require smaller tip-to-sample distances and steeper impact angles. These conditions are associated with the need to have droplets hit this type of sample to cause ionization ("droplet pick-up" mechanism). Both small and macromolecule analytes were examined from a variety of surfaces including paper, plastics, and glass surfaces, with no significant differences in the spectra. Polymer analyses included determinations of molecular weights of industrial polymers such as polyethylene glycol (*14*), as well as those of proteins and oligosaccharides (*13*).

Complex processes are involved in producing gas-phase ions from condensed-phase samples through impact of charged aqueous droplets, gas-phase ions, or metastable atoms. It is well known that molecules at surfaces under vacuum can be simultaneously desorbed and ionized by charge transfer (electron, proton, or other ion) using primary ions with low translational energies. This low-energy heterogeneous process known as chemical sputtering (*15*) occurs in the ambient DI methods also, even though projectile ion energies are so low that reaction exothermicity must be the source of the desorption endothermicity. The involvement of liquid droplets in DESI introduces an additional and fundamentally different mechanism of ion formation. The charged droplets pick up molecules as they splash off the surface, and the secondary droplets produce gaseous ions by well-known ESI mechanisms of direct ion emission (ion evaporation model) or complete evaporation of the neutral solvent molecules (charge residue model) (*16*). Because the secondary droplets contain the analyte and move through the normal ESI atmospheric interface,

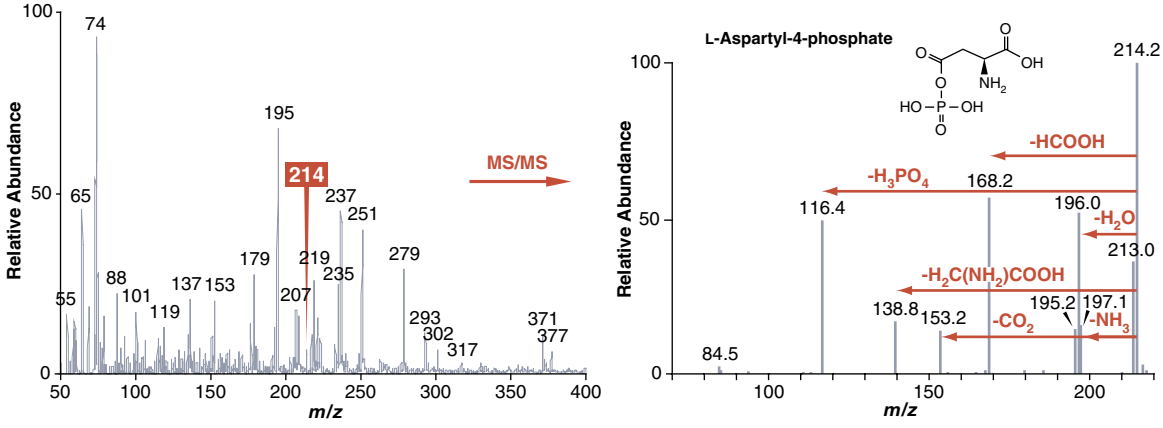

Fig. 2. DESI mass spectrum of dried, 2-μL, raw urine spots on paper, sprayed with 1:1 methanol:water containing 1% acetic acid. The product ion MS/MS spectrum identifies one of the minor components, with *m/z* = 214, as aspartyl-4-phosphate.

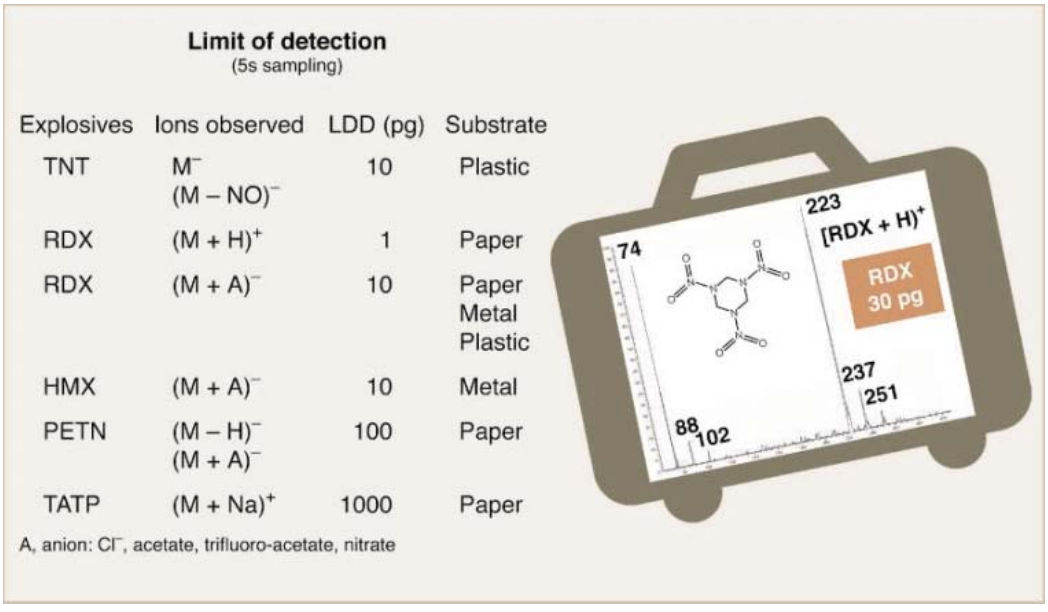

Fig. 3. Explosives detected at low levels on various surfaces, in the positive- and negative-ion modes, showing the mass spectrum of 30-pg RDX (TNT, trinitrotoluene; RDX, hexahydrotrinitro-1,3,5-triazine; HMX, octahydro-MX H1,3,5,7-tetranitro-1,3,5,7-tetrazocine; PETN, pentaerythritol tetranitrate; TATP, triacetonetriperoxide).

it is expected and observed that the DESI and ESI spectra of proteins are very similar, even though the protein being analyzed is in a different physical phase. Momentum transfer from impacting droplets may contribute to the desorption of larger molecules such as proteins, together with electrostatic repulsion caused by charge accumulation on the surface, whereas the force responsible for transfer to the mass spectrometer is suction from the vacuum system.

One consequence of these mechanistic considerations is that the range of applications and the ion formation mechanism of DESI (and presumably of ELDI, although this has not been investigated fully) is wider than but includes those of DAPCI and DART, because the conditions of the electrospray used in DESI can be selected to favor either dry ion or droplet impact by adjusting the distance to the sample or the nebulizing gas flow rate. It is the presence of charged aqueous liquid droplets that allows the ionization of highly polar species independent of molecular weight, therefore readily allowing DESI ionization of proteins, peptides, carbohydrates, polar lipids, and nucleic acids (*13*). As a consequence, the overwhelming majority of known molecular or ionic species can be ionized and detected by DESI-MS, from single metal ions to large proteins and from unsaturated hydrocarbons to complex polysaccharides.

Quantitative accuracy of the ambient MS methods is limited by matrix effects, which vary with the analyte. Internal standards increase accuracy and precision for solutions but cannot be used for solid samples. The surface-derived ion current is somewhat transitory in nature and is perhaps associated with surface-charging effects and the turbulent nature of high-velocity gas streams. Although detection limits are remarkably low, peak stability is not high, so some averaging of data is necessary for quantitation, the precision of which can be as low as a few percent relative standard deviation (RSD) but commonly is as high as 20%.

Applications

DESI experiments can be performed on a very wide range of samples to give information on many types of compounds (polar and nonpolar, low and high molecular weight) present in a wide range of matrices and in various physical states. As a consequence, the range of applications of DESI is extraordinarily wide and covers many scientific fields (Fig. 4). Applications include the following: (i) the examination of native surfaces for forensics, security, and environmental studies; (ii) the examination of biological surfaces, especially imaging of particular compounds in intact tissue; and (iii) high-throughput examination of solutions (after transfer onto a surface like paper), for example, in disease-state recognition using metabolomics.

Several groups have reported encouraging results with ambient MS of intact pharmaceutical products and in drug discovery (*17*–*23*). Pharmaceutical applications include high-throughput DESI analysis (rates of up to 10 tablets per second for simple MS scans and about 1 per second for more complex experiments, in which MS/MS spectra are recorded to confirm the identity of particular ions in the original mass spectra) (*17*). These experiments suggest the potential value of ambient MS in a wider range of industrial and laboratory process-monitoring applications, including its use as a chromatographic detector (*24*). Related applications are to natural products, including active components present in plant tissue. This type of study, e.g., on alkaloids in *Conium maculatum* (*25*), illustrates a number of important features of this ambient ionization method: (i) Mass and tandem mass spectral data take only a few seconds to acquire. (ii) The samples are examined as collected; there is no need for extraction or other work-up of the plant material. (iii) Isomers and congeners are readily distinguished. (iv) Trace constituents can be observed. (v) Quantitative reproducibility is adequate (20% RSD).

Recent advances in ambient ionization methods are providing sensitive, high-throughput means of analyzing biological samples at atmospheric pressure. Biological and biochemical applications of DESI include pharmacokinetics (*5*) and high-throughput medical screening. The best established high-throughput DESI experiments are in

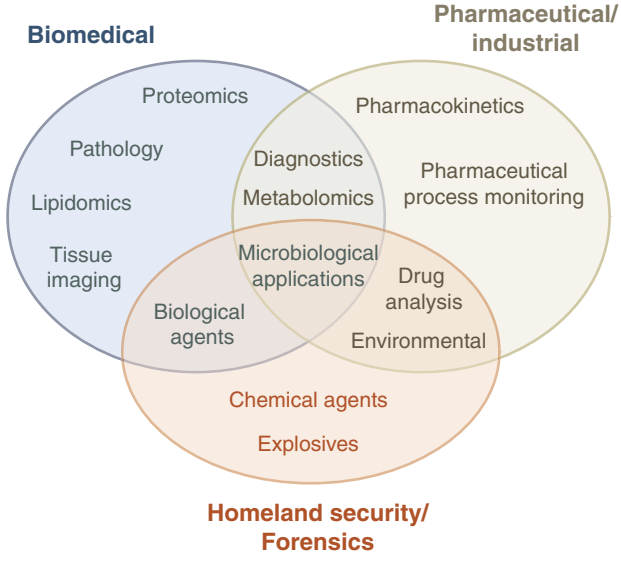

Fig. 4. Areas of application of the ambient MS method of DESI, grouped into three broad overlapping classes.

metabolomics, where quantitative pattern recognition techniques have been applied. By using principal component analysis, for example, it has been found that mice in different disease states can be distinguished by DESI urine analysis. This method identifies many more metabolites, and it is much faster than are corresponding nuclear magnetic resonance measurements made on the same samples (*26*). Although it is not necessary to identify particular up- or down-regulated metabolites to distinguish specific subpopulations, tandem mass spectrometry can provide this information (Fig. 2), and there is the potential to contribute to a more fundamental understanding of metabolism by focusing attention on particular compounds that participate in known metabolic pathways. Surveys for inborn errors of metabolism require high sensitivity, minimal sample clean up, chemical specificity, and high-throughput capabilities, all demonstrated characteristics of the DESI method.

The application of DESI to microbiological sample screening (for toxicity, clinical microorganism identification, etc.) has seen limited application, but information-rich spectra are recorded for bacteria and bacterial spores even in the presence of growth media. Distinctions between species are readily made, and it remains to be seen whether the more interesting subspecies distinctions can be made, and if so, in what times and at what levels.

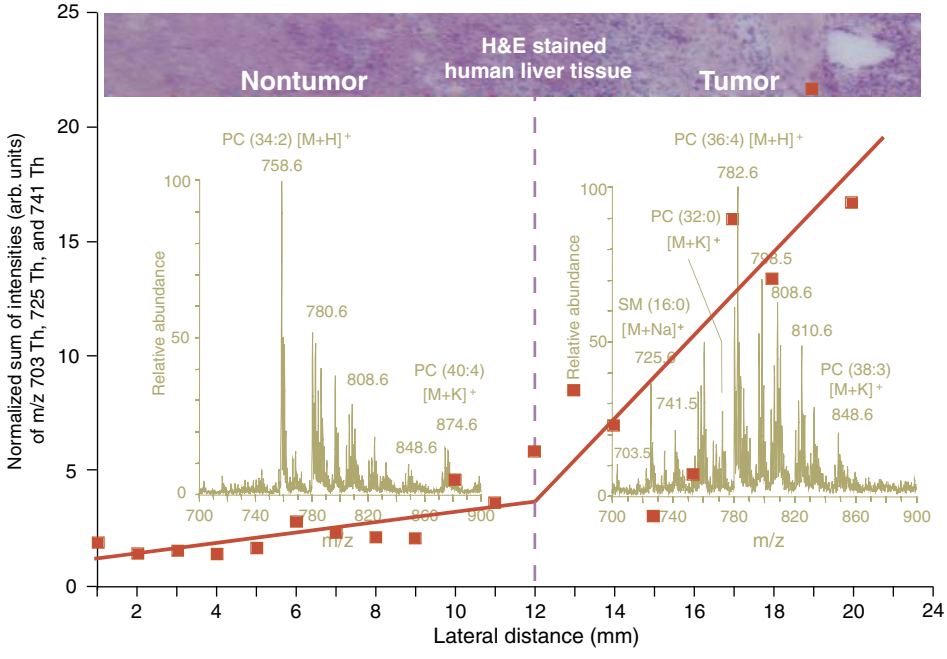

Fig. 5. Direct tissue profiling of human liver adenocarcinoma using DESI in the positive-ion mode. The tissue was sectioned and untreated, and it was subjected to a spray of 1:1 methanol:water containing 0.1% ammonium hydroxide. Adapted from (*32*).

Biological Tissue Analysis

Among the many biomedical problems to which DESI could be applied, in vivo real-time tissue imaging by MS could prove to be the most challenging and the most useful. Like other DI methods, DESI gives information on the spatial distribution of analytes on a surface, not only on their molecular identity but on the amounts present. Biological imaging by MS is achieved currently either through the irradiation of a thin, matrix-coated tissue section using a laser (*27*, *28*) [UV- or infrared (IR)-MALDI] or by particle bombardment as in SIMS (*6*, *29*, *30*) and now DESI (*31*). Each of these methods provides spatially defined chemical information on a tissue sample that can be correlated to cell morphology or the biological state of the tissue. Chemical imaging of this type is not only complementary to traditional histopathological protocols but has the potential to provide specific chemical information that reveals disease progression and prognosis.

The simplest way to perform DESI imaging is to use a microprobe beam of solvent microdroplets and to raster this across the surface. Tissue imaging by DESI shows only modest spatial resolution (spot sizes 0.5 to 1.0 mm), but it removes the constraints of the high vacuum met in SIMS imaging (*29*) and that of sample preparation, which is a requirement for MALDI imaging (*30*). This allows for analysis of the sample surface in the free ambient environment at atmospheric pressure.

DESI-MS studies of various biological tissues and whole organs, including cancerous human liver tissue, revealed differences in the distributions of compounds, including elevated levels of certain phospholipids in the tumor region as compared with the nontumor region (Fig. 5) (*31*). These initial results suggest, for the longer term, the development of ambient MS techniques for routine use in surgery or histology.

Reactive DESI

It is straightforward to add reagents to the DESI spray solvent to mediate the interfacial reactions of solution-phase reactants with condensed-phase analytes to yield gas-phase ions. These experiments (so-called reactive DESI) add chemical selectivity to the DESI experiment, just as the ability to choose a chemical ionization gas adds chemical selectivity to conventional chemical ionization MS. A wide range of reaction types can be used, including redox reactions of metal complexes (*32*), covalent modification of particular functional groups, and the formation of noncovalent complexes (*5*). Specific examples include the formation of specific enzyme substrate complex ions by doping the spray solvent with substrate (*5*) and the formation of cyclic boronates for identification of the cis-diol functional group. For example, when solid-phase glucose, glycosides, steroids, and other compounds with the cis-diol functionality are subjected to a spray containing phenylboronic acid, cyclic boronates are generated and easily recognized by the mass shift seen (*33*). Future applications are likely to focus on drug target screening, using reactive DESI in a high-throughput fashion to screen for drug candidate activity through the formation of noncovalent complexes.

Future

The emergence of MS as a tool for the biological sciences is the result of a series of remarkable developments, occurring over several decades. They include the following: (i) sensitive mass analyzers capable of appropriate resolution and mass range, (ii) MS/chromatography combinations, (iii) tandem mass spectrometry, and (iv) new ionization methods. MS is now an indispensable tool in the fields of proteomics, lipidomics, and metabolomics; on the basis of the detection, identification, quantification, and structural characterization of peptides, lipids, and metabolites derived from biological sources. In addition to these small-molecule applications, intact biomolecules such as proteins and protein complexes (enzyme-substrate, protein-protein, and protein-DNA) (*34*, *35*) are increasingly falling within the scope of MS, which is providing information such as molecular weight, stoichiometry, and binding affinity. All of these developments seem likely to be accelerated by the advent of ambient MS techniques, which allow compounds ranging from biopolymers to small drugs to endogenous

biochemicals to be analyzed in unprepared samples, very rapidly and with high specificity.

The rapid development of ambient MS likely will accelerate interest in miniature mass spectrometers. We can foresee handheld mass spectrometers equipped with DESI ion sources. The current trend in MS miniaturization is driven by the desire to perform in situ chemical analysis and facilitated in large measure by the development of small ion-trap analyzers, which have led to tandem mass spectrometers in the 10-kg (total system) weight range (*36*). These developments have been extended to instruments fitted with ambient ion sources, and a portable DESI ion-trap system based on a cylindrical ion-trap analyzer has been built. The drive toward miniature instruments, in parallel with the drive toward ambient mass spectrometers, has created technology that now allows ambient ionization methods to be used with instruments small enough to serve as personal mass spectrometers for individuals. It is likely that chemical measurements could be made soon by individuals with the ease with which, a generation ago, mathematical computational power became widely available with the development of the electronic calculator and the personal computer. Suitable ambient mass spectrometers would allow many of the environmental, pharmaceutical, and physiological measurements described in this article, and these could be of intense personal interest to individuals. The confluence of ambient and miniature MS has the potential to change not just MS but the whole subject of analytical chemistry.

References and Notes

1. J. B. Fenn, M. Mann, C. K. Meng, S. F. Wong, C. M. Whitehouse, *Science* **246**, 64 (1989).
2. S. J. Pachuta, R. G. Cooks, *Chem. Rev.* **87**, 647 (1987).
3. M. Karas, F. Hillenkamp, *Anal. Chem.* **60**, 2299 (1988).
4. V. V. Laiko, M. A. Baldwin, A. L. Burlingame, *Anal. Chem.* **72**, 652 (2000).
5. Z. Takats, J. M. Wiseman, B. Gologan, R. G. Cooks, *Science* **306**, 471 (2004).
6. M. L. Pacholski, N. Winograd, *Chem. Rev.* **99**, 2977 (1999).
7. J. F. Mahoney *et al.*, *Rapid Commun. Mass Spectrom.* **5**, 441 (1991).
8. R. B. Cody, J. A. Laramee, H. D. Durst, *Anal. Chem.* **77**, 2297 (2005).
9. Z. Takats, I. Cotte-Rodriguez, N. Talaty, H. W. Chen, R. G. Cooks, *Chem. Commun.* 1950 (2005).
10. J. Shiea *et al.*, *Rapid Commun. Mass Spectrom.* **19**, 3701 (2005).
11. C. N. McEwen, R. G. McKay, B. S. Larsen, *Anal. Chem.* **77**, 7826 (2005).
12. I. Cotte-Rodriguez, Z. Takats, N. N. Talaty, H. Chen, R. G. Cooks, *Anal. Chem.* **77**, 6755 (2005).
13. Z. Takats, J. M. Wiseman, R. G. Cooks, *J. Mass Spectrom.* **40**, 1261 (2005).
14. M. Nefliu, A. Venter, R. G. Cooks, *Chem. Commun.*, 888 (2006).
15. M. Vincenti, R. G. Cooks, *Org. Mass Spectrom.* **23**, 317 (1988).
16. P. Kebarle, *J. Mass Spectrom.* **35**, 804 (2000).
17. H. Chen, N. Talaty, Z. Takats, R. G. Cooks, *Anal. Chem.* **77**, 6915 (2005).
18. S. Rodriguez-Cruz, *Rapid Commun. Mass Spectrom.* **20**, 53 (2005).
19. D. J. Weston, R. Bateman, I. D. Wilson, T. R. Wood, C. S. Creaser, *Anal. Chem.* **77**, 7572 (2005).
20. J. P. Williams, J. H. Scrivens, *Rapid Commun. Mass Spectrom.* **19**, 3643 (2005).
21. K. A. Hall, M. Green, P. Newton, F. Fernandez, paper presented at the 53rd American Society for Mass Spectrometry, San Antonio, TX, June 5–9 2005.
22. J. Henion, C. Van Pelt, T. Corso, G. Schultz, X. Huang, paper presented at the 53rd American Society for Mass Spectrometry, San Antonio, TX 2005.
23. L. A. Leuthold *et al.*, *Rapid Commun. Mass Spectrom.* **20**, 103 (2006).
24. G. J. Van Berkel, M. J. Ford, M. A. Deibel, *Anal. Chem.* **77**, 1207 (2005).
25. N. Talaty, Z. Takats, R. G. Cooks, *Analyst* **130**, 1624 (2005).
26. H. Chen, Z. Pan, N. Talaty, R. G. Cooks, D. Raftery, *Rapid Commun. Mass Spectrom.*, in press.
27. R. M. Caprioli, T. B. Farmer, J. Gile, *Anal. Chem.* **69**, 4751 (1997).
28. L. A. McDonnell *et al.*, *J. Mass Spectrom.* **40**, 160 (2005).
29. D. Touboul, F. Kollmer, E. Niehuis, A. Brunelle, O. Laprevote, *J. Am. Soc. Mass Spectrom.* **16**, 1608 (2005).
30. P. J. Todd, T. G. Schaaff, P. Chaurand, R. M. Caprioli, *J. Mass Spectrom.* **36**, 355 (2001).
31. J. M. Wiseman, S. M. Puolitaival, Z. Takats, R. M. Caprioli, R. G. Cooks, *Angew. Chem. Int. Ed.* **44**, 7094 (2005).
32. M. Nefliu, C. Moore, R. G. Cooks, in preparation.
33. H. Chen, I. Cotte-Rodriguez, R. G. Cooks, *Chem. Commun.*, in press.
34. J. A. Loo, *Mass Spectrom. Rev.* **16**, 1 (1997).
35. B. T. Ruotolo *et al.*, *Science* **310**, 1658 (2005).
36. L. Gao, Q. Song, R. G. Cooks, Z. Ouyang, in preparation.

37. This work was supported by grants from NSF, the Office of Naval Research, and Prosolia, Inc. (through the Indiana 21st Century Fund). We acknowledge the contributions of collaborators cited in the references.

10.1126/science.1119426

REVIEW

Probing Cellular Chemistry in Biological Systems with Microelectrodes

R. Mark Wightman

Over the past 20 years, the technological impediments to fabricating electrodes of micrometer dimensions have been largely overcome. These small electrodes can be readily applied to probe chemical events at the surface of tissues or individual biological cells; they can even be used to monitor concentration changes within intact animals. These measurements can be made on rapid time scales and with minimal perturbation of the system under study. Several recent applications have provided important insights into chemical processes at cells and in tissues. Examples include molecular flux measurements at the surface of single cells and through skin—which can offer insights into oxidative stress, exocytosis, and drug delivery—and real-time brain neurotransmitter monitoring in living rats, which reveals correlations between behavior and molecular events in the brain. Such findings can promote interdisciplinary collaborations and may lead to a broader understanding of the chemical aspects of biology.

Microelectrodes, sometimes termed ultramicroelectrodes, are chemical sensors with micrometer or smaller dimensions. Very small microelectrodes that report concentrations on the basis of potential changes across chemically selective membranes at their tip, termed potentiometric electrodes, have been in use for decades. However, this review concerns voltammetric microelectrodes, microscopic devices that sense substances on the basis of their oxidation or reduction and that were introduced in the early 1980s (*1*). More recently, voltammetric microelectrodes—dynamic devices that allow control of chemical environments as well as chemical sensing—have been used in a variety of unusual applications, including fabrication of microstructures and investigation of chemical fluctuations at the surface of single biological cells and in the living brain. They offer considerable advantages relative to voltammetric electrodes of conventional (millimeter) size. The small double-layer capacitance of microelectrodes enables chemical events occurring on the submicrosecond time scale to be monitored (*2*). Their small currents facilitate measurements in highly resistive media such as solvents without electrolyte and supercritical fluids (*3*). Unlike electrodes of conventional size, microelectrodes can be used in measurements on longer time scales, when the distance across which reactive molecules diffuse to the electrode is much greater than the electrode dimensions. Thus, very small electrodes can have markedly enhanced fluxes, which can enhance signal-to-noise ratios in trace metal ion determinations (*1*). In general, microelectrodes allow chemical measurements

Department of Chemistry, University of North Carolina at Chapel Hill, Chapel Hill, NC 27599, USA. E-mail: rmw@unc.edu

in spatial and temporal domains that were previously inaccessible.

When voltammetric microelectrodes were last reviewed in this journal, almost 20 years ago (*4*), researchers were still examining methods to construct them in different geometries. Today these methods are quite well developed. Fabrication of micrometer-sized electrodes can be as simple as sealing microwires or carbon fibers into a suitable insulator; alternatively, present-day lithographic techniques can be used to construct microelectrodes suitable for simultaneous electrochemistry and atomic force microscopy measurements (*5*). Methods for constructing electrodes with submicrometer dimensions were slower to develop but now are commonplace (*6*). The diffusional concepts are now well understood and are discussed fully in a textbook of electrochemistry (*7*). Today, much of the use of microelectrodes exploits their ability to explore chemistry in very small domains, especially those associated with biological systems. For example, microelectrodes can be coupled to a micropositioner that can be moved in three dimensions to provide a spatially resolved view of chemical events much like the physical characterization provided by other scanning probe microscopies. This approach, termed scanning electrochemical microscopy (SECM), was the subject of a recent monograph (*8*).

Although many interesting systems have been explored with microelectrodes, this review focuses on their use at single cells and in intact tissue, where considerable recent progress has been made.

Determining Molecular and Ionic Fluxes in Biological Systems

Ion and molecule transport are essential for the maintenance of homeostasis in biological systems. The small size of microelectrodes has allowed site-specific molecular flux measurements in biological systems ranging from single cells to intact tissue. A prime target has been molecular oxygen. Amperometric sensing of O_2 by its electroreduction at a membrane-covered electrode with a surface area of a few square millimeters, the Clark electrode, is a well-established technique. Miniaturization of such an assembly to micrometer dimensions provides a way to measure O_2 flux with high spatial resolution. This technique has been used in suspensions of *Escherichia coli* to examine the effects of Ag^+ on the bacteria's respiration (*9*). Ag^+ initially increased the respiration rate because it uncoupled the respiratory chain.

When biological cells are under metabolic stress, various molecular fluxes adjust to remove the stress. For example, menadione is toxic to hepatocytes because it can diffuse into cells and generate reactive oxygen species (*10*). Within a cell, menadione is metabolized to the menadione-S-glutathione conjugate (thiodione) that is exported from the cell by an adenosine triphosphate–dependent pump. This pump-mediated efflux of thiodione was detected with a microelectrode by SECM both at single cells and at groups of highly confluent cells. The results quantified the flux of thiodione from a single cell. Oxidative stress causes increased generation of superoxide and nitric oxide derivatives, and these species can be individually monitored at the single cell level with a platinized carbon-fiber microelectrode (*11*). The bursts of reactive species generated by fibroblasts from normal strains under oxidative stress are considerably different from those measured at cancer-prone fibroblasts. The latter generated greater amounts of O_2^- and H_2O_2 and smaller amounts of $NO^\bullet$ and ONOO relative to normal fibroblasts.

Microelectrodes can also be used with intact biological tissue. For example, microelectrodes have provided fundamental information on transdermal drug delivery in research that involved the collaboration of electrochemists with a pharmaceutical company. Applied electric fields affect transport of the drugs through the skin in two ways: They induce electro-osmotic flow to propel neutral and charged species, and they induce iontophoretic mass transport to modulate the flux of charged species. SECM was used to measure transport rates in hairless mouse skin (*12*, *13*). The direction of electro-osmotic transport indicated that the skin has a negative charge at physiological pH. Electro-osmosis induced by an applied electric field enhanced the transport rate of hydroquinone, a neutral molecule (Fig. 1). Mass transport could be enhanced further for ions because of the additional migrational component to mass transport. The results revealed that the major sites for electro-osmotic transport of reagents are found at hair follicles that have a radius of 21 μm. This fundamental research demonstrating the nonuniformity of the molecular fluxes across skin was used by pharmacists to develop an FDA-approved drug delivery device for fentanyl, an opioid analgesic.

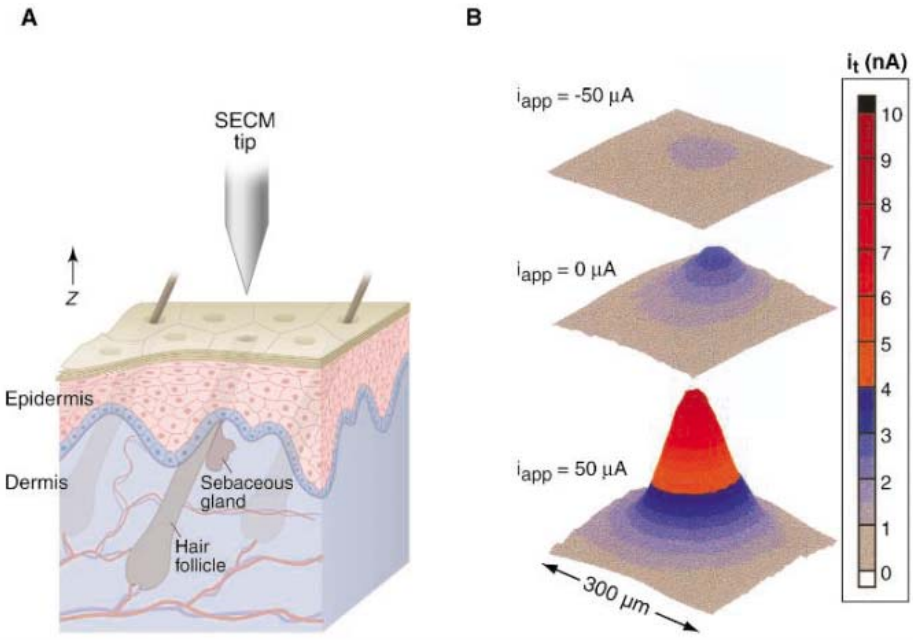

Fig. 1. (**A**) Schematic drawing illustrating the SECM tip positioned directly above the opening of a hair follicle. (**B**) SECM images of hydroquinone emerging from the opening of a hair follicle as a function of the applied iontophoretic current at pH = 6.0. The center image corresponds to diffusion of hydroquinone from the donor to receptor solutions without iontophoretic current. The lower image corresponds to positive iontophoretic current (i_{app} = 50 μA), inducing electro-osmotic flow in the same direction as diffusion. The upper image corresponds to a negative current (i_{app} = –50 μA), resulting in electro-osmotic flow opposing diffusion. A SECM tip of radius 2.6 μm, biased at 0.9 V versus Ag/AgCl, was used to record the images. Reprinted with permission from (*13*).

permeate the cartilage, and therefore fluctuations in the oxidation current during the positional scanning of the tip reflected the proximity of the surface. The topographic map of cartilage revealed depressions with diameters of 15 to 25 μm, which were attributed to chondrocytes because their distribution was similar to that observed with atomic force and light microscopy. Subsequent imaging of the same area of the cartilage sample for the flux of O_2, again detected by its electroreduction, showed heterogeneous permeability of O_2 across the cartilage surface. The regions of high permeability were localized to the cellular and pericellular regions.

In the previous example of O_2 transport through cartilage, a concentration gradient was generated by the consumption of O_2 during its electroreduction, and the gradient induced the flux that was measured. However, within a living animal, O_2 flux is adjusted by fluctuations in blood flow, a process that is dynamically regulated by blood vessel dilation and constriction. In the brain, increased neuronal activity results in secretion of chemical messengers that cause blood vessels to dilate so that additional glucose is supplied to compensate for the increased metabolism. Positron emission tomography studies have shown that glucose metabolism becomes anaerobic during periods of high neuronal activity. Thus, during such periods, O_2 levels are predicted to increase in the extracellular fluid of the brain because of increased blood flow and decreased usage by oxidative metabolism (*15*).

With the use of a carbon-fiber microelectrode inserted into the rat striatum, this phenomenon could be directly observed after electrical stimulation of the medial forebrain bundle, a neuronal pathway into the striatum (*16*). The local O_2 concentration was measured with fast-scan cyclic voltammetry, using a voltage scan to negative potentials to detect O_2 and a positive scan to detect release of the neurotransmitter dopamine. The background subtraction procedure used with this technique also revealed pH changes, because they cause a shift in the background that leads to a differential alteration of the cyclic voltammograms. The O_2 increase and the basic pH shift induced by the stimulation both occurred a few seconds after neurotransmitter release, and their changes were inhibited by pharmacological agents known to attenuate vasodilation, such as adenosine-receptor antagonists and NO-synthase inhibitors. These O_2 and pH changes correlate in the living brain because carbon dioxide, a central component of the physiological pH buffering system, is removed by the increased blood flow. Similar changes did not occur in excised slices of brain tissue, even though neurotransmitter release is still viable in this preparation, presumably because there was no blood flow.

Chemical Sensing at Individual Biological Cells During Exocytosis

Neurons and other cells communicate with each other through the triggered secretion of small molecules. A primary means by which these molecules are secreted is exocytosis, the regulated process in which a membrane-bound vesicle in the cytoplasm fuses with the plasma membrane via a Ca^{2+}-dependent mechanism. This fusion leads to the extrusion of the intravesicular contents, including the chemical messengers, into the extracellular space (*17*). This concept is thought to be governed by the quantal hypothesis, which asserts that chemical transmitters are stored and released in predetermined unit amounts that are independent of the event initiating release. Measurements with microelectrodes provided chemical evidence that directly demonstrated the outcome of exocytosis.

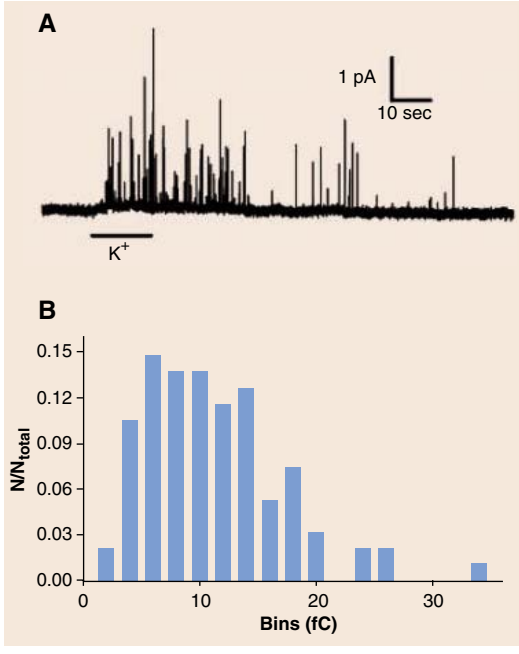

Fig. 2. Exocytotic current spikes from dopaminergic neurons isolated from mouse retina. **(A)** Application of an elevated K^+ solution depolarizes the cell membrane and results in a series of sharp amperometric spikes, each corresponding to a single exocytotic event. **(B)** Histogram of the distribution of charges of the spikes in (A); bins are in units of femtocoulombs. Reprinted with permission from (*22*).

Because the size of carbon-fiber microelectrodes is similar to that of many biological cells, they are well suited to examine the chemical and temporal characteristics of secretory events at the cell surface (*18*). With the use of a micropositioner mounted on a microscope stage, the microelectrode can be placed directly in contact with the cell to monitor secretion. The simplest approach is to use amperometry with a fixed applied potential while the current resulting from electrolysis of adjacent species is measured. A number of chemical messengers secreted by cells are electroactive and can be detected in this way. These include the catecholamines (dopamine, epinephrine, and norepinephrine), 5-hydroxytryptamine (5-HT or serotonin), and histamine. Peptides containing a tryptophan or tyrosine residue are also electroactive, as is nitric oxide. Alternatively, surface modification has been used for peptides such as insulin, whose detection by amperometry is facilitated by a ruthenium oxide coating (*19*). Because the secreted molecules detected are in the microscopic space between the electrode and the cell, all of the released contents are oxidized, yielding a quantitative measure of the number of molecules secreted per vesicle (*20*). An alternate method that provides the identity of the species detected is cyclic voltammetry (*21*). In this technique, the current is measured while the applied potential is swept over a range of interest.

A variety of evidence has established that the spikes observed upon stimulation of a secretory cell (Fig. 2) are of vesicular origin. They occur only after stimulation that promotes an elevated intracellular Ca^{2+} concentration, and they originate from spatially localized sites on the cell surface (*18*). In contrast, efflux of a predominantly nonvesicular component, ascorbate, is observed as a broad envelope rather than a discrete spike. Taken together, these measurements confirmed the quantal nature of chemical release by exocytosis. This approach was later used to measure exocytosis from a variety of cells (*18*) including mast cells from the immune system, immortal neuronal-like cells, insulin-secreting β cells from the pancreas, and invertebrate and mammalian neurons (*22*). In mammalian neurons, the amounts released from each vesicle are fewer than 50,000 molecules, so high-sensitivity recordings are required (Fig. 2).

This technique is noninvasive because measurements are made exterior to the cell. When the microelectrode is used with SECM, a map of the cell can be obtained and release sites across the cell surface can be probed (*23*, *24*). Alternatively, very small (micrometer or smaller) electrodes can be used to spatially resolve exocytosis from well-defined regions of a single cell. With the use of a sensor incorporating four microelectrodes, the location of release sites on bovine chromaffin cells can be continuously monitored (*25*). Access to the interior of the cell can be achieved with a patch-clamp pipette containing a microelectrode, allowing recordings of the cytoplasmic levels of chemical messengers (*26*).

Microelectrode recordings at single cells have exposed a number of previously unknown features of exocytosis. In many cells with large vesicles (vesicle radius >100 nm), especially those with dense core vesicles, individual secretory events are prolonged relative to the time scale expected for simple diffusional dispersion, and vesicle extrusion is dominated by the time course needed for dissociation of the vesicle contents (*27*). At neurons (vesicle radius ~25 nm) as well as cells with large vesicles, the secretory packets are not quantized in a tight fashion (Fig. 2, for example). Rather, a broad distribution is found for the amounts released by exocytosis (*18*). Furthermore, quantal size can be adjusted pharmacologically with a concomitant change in vesicle volume (*28*). Recordings at cells with large vesicles reveal, at the initial stages of some exocytotic release events, a "foot"-like feature that reflects diffusion of the vesicular contents through an initially formed fusion pore (*29*). The foot can be reproduced in liposome preparations composed of nanotubes connecting different compartments (*30*). This foot occasionally flickers, which implies that the fusion pore has a fluctuating diameter. Release from neurons shows several events that appear to flicker, which suggests repeated, partial exocytotic events from the same vesicle (*31*)—a process termed "kiss and run" exocytosis that may arise from opening and closing of the fusion pore.

Measuring Dopamine Neurotransmission During Behavior

The process of neurotransmission governs virtually all functional aspects of the nervous system, including the triggering of contraction at neuromuscular junctions, activation of emotional responses in the amygdala, and the processing of memories in the hippocampus. Within the intact brain, neurons release neurotransmitters by the exocytotic process that has been characterized with microelectrodes at isolated cells. The specific site of release is the synapse, a narrow (10 to 100 nm) space between neurons. Once released, the neurotransmitter diffuses to its receptors—membrane-bound proteins that can recognize the specific neurotransmitter. For catecholamines and 5-HT, these receptors are distributed throughout the extracellular space, and neurotransmission is not restricted to the synaptic region (*32*). The binding of a neurotransmitter to its receptor triggers specific intracellular processes (opening of an ion channel, activation of cyclic adenosine monophosphate, etc.) that lead to information transfer between neurons. Neurotransmitter lifetimes in the extracellular space are short because metabolism or cellular uptake rapidly restores neurotransmitter concentrations to their original low levels.

To monitor neurotransmission, a chemical sensor must provide information from the micrometer dimensions and the millisecond time scale over which communication occurs. Sensing also requires high chemical specificity to allow selective monitoring, as well as a sensitivity for the neurotransmitter that is similar to the affinity of its natural biological receptors, often in the nanomolar range. Carbon-fiber microelectrodes have many of the properties required for such sensing, and for some years they have been used to monitor neurotransmission in the brains of living but anesthetized organisms (*33*). In these experiments, the animal is placed in a stereotaxic frame and the electrode is lowered through a hole drilled in the skull to the region of interest. Dopamine has been a popular target of such studies because it plays several roles in the brain (*34*). Normal dopamine functioning is essential for coordinated motor movement; the symptoms of Parkinson's disease arise because of a shortage of this neurotransmitter. In addition, dopamine is a neurotransmitter in the brain reward pathway. Many drugs of abuse such as cocaine and amphetamine, which can evoke profound behavioral changes, appear to tap into the brain reward circuitry through dopaminergic neurons.

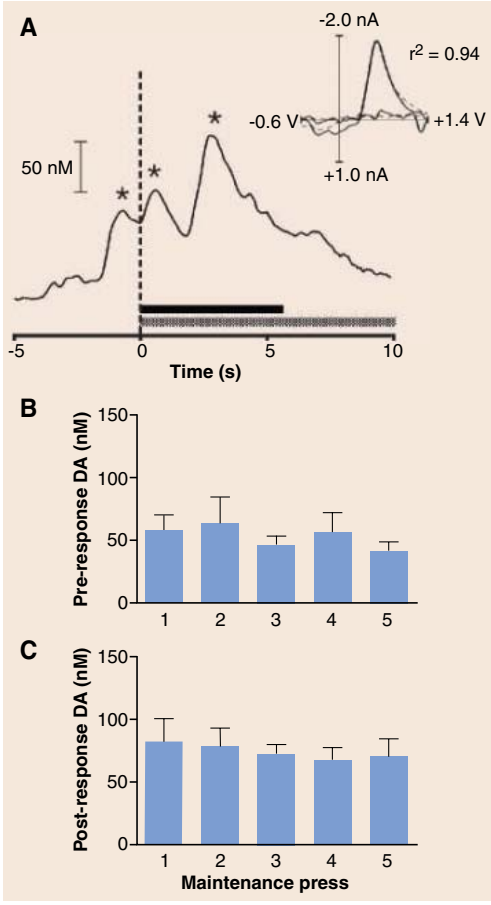

Fig. 3. Dopamine concentration in the rat nucleus accumbens at the time of the lever press for cocaine self-administration. **(A)** Pre- and postresponse dopamine transients associated with the operant response during a single trial. The lever press response occurs at $t = 0$, the black bar indicates the duration of the 0.33-mg cocaine infusion, and the shaded bar indicates the presentation of the drug-associated cues, which lasts for 20 s after the lever press response. Inset shows the cyclic voltammogram from the maximum dopamine change (solid line) compared to the voltammogram for electrically evoked dopamine release from the same animal. Linear regression analysis revealed a high correlation ($r^2 = 0.94$) between the voltammograms. **(B** and **C)** Mean (± SEM) preresponse (B) or postresponse (C) of dopamine concentrations during maintenance of cocaine self-administration. Data are from eight animals. Reprinted with permission from (*40*).

With dopamine. A cyclic voltammetry study in rats revealed that dopamine was released during electrical depolarization of its neurons—a procedure that generates action potentials, the normal mode of intracellular information transfer. When the depolarization was terminated, release ceased and dopamine was cleared by the dopamine transporter (*36*). Amperometry provides better time resolution in these experiments, allowing a clearer view of the rapidity of dopamine uptake (half-time $t_{1/2}$ = 20 to 40 ms) (*37*). The importance of the dopamine transporter was unequivocally established with genetic knockout technology: In mouse brains lacking the transporter, dopamine clearance took 100 times as long as in normal mice (*38*). The control of extracellular dopamine as a balance between release and uptake is similar throughout the striatum, an area composed of the caudate-putamen and nucleus accumbens, as well as other dopaminergic regions (prefrontal cortex, amygdala), although the specific rates of release and uptake are regionally specific. The measured rates are also sensitive to pharmacological

substances such as cocaine, amphetamine, and neuroleptic drugs, and the alterations in dopamine responses caused by these drugs reveal the chemical imbalances that they can generate.

Today the technology has advanced so that carbon-fiber microelectrodes can be used to measure dopamine concentration fluctuations in the brain during behavior. Working in collaboration with psychologists, voltammetrists have gleaned insights into the role of this neurotransmitter during reward-seeking. For example, in a rat trained to self-administer cocaine by pressing a lever, a dopamine transient occurs in the nucleus accumbens as the animal begins its approach to the lever (*39*). In addition, another dopamine transient occurs after the lever press in response to a cue (light and tone) that is associated with the lever press. These results can be seen on individual trials and remain constant in amplitude during repeated trials (Fig. 3). However, when the animal presses the lever but the cocaine is withheld, a protocol termed extinction, the dopamine transient associated with the cue diminishes in amplitude, even though the dopamine transients associated with approaching the lever remain (*40*). These dopamine fluctuations last for only a few seconds and so would be undetectable without the rapid chemical sampling that is provided by the microelectrode.

Although dopamine had long been implicated in reward-seeking as well as drug-taking, these results provide a high-resolution view of the specific role of this neurotransmitter in this well-characterized behavioral condition. For example, the findings during extinction suggest that dopamine transients encode the learned association between environmental cues and cocaine. Future investigations with this technology should enable probes of the role of dopamine in other behaviors such as learning and memory, as well as the role of 5-HT in sleep. However, such research requires close interactions between chemists and psychologists to ensure the validity of the experimental design as well as appropriate interpretation of the results.

Conclusions

As is clear from the experiments summarized here, microelectrodes allow an unparalleled view of the dynamic chemical events that occur at the surface of cells and in intact tissue. These sensors allow for the observation of real-time chemical communication between neurons and of fundamental processes associated with oxidative metabolism. The results from these studies contribute to fields as diverse as drug delivery and neurochemical responses during substance abuse. Microelectrodes clearly enable interdisciplinary studies because they allow chemistry to be probed in unique microdomains in biological systems.

References and Notes

1. R. M. Wightman, D. O. Wipf, *Electroanal. Chem.* **15**, 267 (1989).
2. C. Amatore, E. Maisonhaute, *Anal. Chem.* **77**, 303A (2005).
3. N. Baltes, L. Thouin, C. Amatore, J. Heinze, *Angew. Chem. Int. Ed. Engl.* **43**, 1431 (2004).
4. R. M. Wightman, *Science* **240**, 415 (1988).
5. P. S. Dobson, J. M. R. Weaver, M. N. Holder, P. R. Unwin, J. V. Macpherson, *Anal. Chem.* **77**, 424 (2005).
6. B. Liu, J. P. Rolland, J. M. DeSimone, A. J. Bard, *Anal. Chem.* **77**, 3013 (2005).
7. A. J. Bard, L. R. Faulkner, *Electrochemical Methods, Fundamentals and Applications* (Wiley, New York, ed. 2, 2001).
8. M. V. Mirkin, A. J. Bard, *Scanning Electrochemical Microscopy* (Dekker, New York, 2001).
9. K. B. Holt, A. J. Bard, *Biochemistry* **44**, 13214 (2005).
10. J. Mauzeroll, A. J. Bard, O. Owhadian, T. J. Monks, *Proc. Natl. Acad. Sci. U.S.A.* **101**, 17582 (2004).
11. S. Arbault *et al.*, *Carcinogenesis* **25**, 509 (2004).
12. B. D. Bath, E. R. Scott, J. B. Phipps, H. S. White, *J. Pharm. Sci.* **89**, 1537 (2000).
13. B. D. Bath, H. S. White, E. R. Scott, *Pharm. Res.* **17**, 471 (2000).
14. M. Gonsalves *et al.*, *Biophys. J.* **78**, 1578 (2000).
15. N. K. Logothetis, B. A. Wandell, *Annu. Rev. Physiol.* **66**, 735 (2004).
16. B. J. Venton, D. J. Michael, R. M. Wightman, *J. Neurochem.* **84**, 373 (2003).
17. D. Sulzer, E. N. Pothos, *Rev. Neurosci.* **11**, 159 (2000).
18. E. R. Travis, R. M. Wightman, *Annu. Rev. Biophys. Biomol. Struct.* **27**, 77 (1998).
19. R. T. Kennedy, H. A. Lan, C. A. Aspinwall, *J. Am. Chem. Soc.* **118**, 1795 (1996).
20. R. M. Wightman *et al.*, *Proc. Natl. Acad. Sci. U.S.A.* **88**, 10754 (1991).
21. K. P. Troyer, R. M. Wightman, *J. Biol. Chem.* **277**, 29101 (2002).
22. S. E. Hochstetler, M. Puopolo, S. Gustincich, E. Raviola, R. M. Wightman, *Anal. Chem.* **72**, 489 (2000).
23. A. Hengstenberg, A. Blochl, I. D. Dietzel, W. Schuhmann, *Angew. Chem. Int. Ed. Engl.* **40**, 905 (2001).
24. J. M. Liebetrau *et al.*, *Anal. Chem.* **75**, 563 (2003).
25. I. Hafez *et al.*, *Proc. Natl. Acad. Sci. U.S.A.* **102**, 13879 (2005).
26. E. V. Mosharov, L. W. Gong, B. Khanna, D. Sulzer, M. Lindau, *J. Neurosci.* **23**, 5835 (2003).
27. C. Amatore, Y. Bouret, E. R. Travis, R. M. Wightman, *Angew. Chem. Int. Ed. Engl.* **39**, 1952 (2000).
28. T. L. Colliver, E. J. Hess, E. N. Pothos, D. Sulzer, A. G. Ewing, *J. Neurochem.* **74**, 1086 (2000).
29. R. H. Chow, L. Von Rüden, E. Neher, *Nature* **356**, 60 (1992).
30. A. S. Cans *et al.*, *Proc. Natl. Acad. Sci. U.S.A.* **100**, 400 (2003).
31. R. G. W. Staal, E. V. Mosharov, D. Sulzer, *Nat. Neurosci.* **7**, 341 (2004).
32. S. J. Cragg, M. E. Rice, *Trends Neurosci.* **27**, 270 (2004).
33. R. N. Adams, *Prog. Neurobiol.* **35**, 297 (1990).
34. R. M. Wightman, D. L. Robinson, *J. Neurochem.* **82**, 721 (2002).
35. M. L. Heien *et al.*, *Proc. Natl. Acad. Sci. U.S.A.* **102**, 10023 (2005).
36. B. J. Venton *et al.*, *J. Neurochem.* **87**, 1284 (2003).
37. A. N. Samaha, N. Mallet, S. M. Ferguson, F. Gonon, T. E. Robinson, *J. Neurosci.* **24**, 6362 (2004).
38. B. Giros, M. Jaber, S. R. Jones, R. M. Wightman, M. G. Caron, *Nature* **379**, 606 (1996).
39. P. E. Phillips, G. D. Stuber, M. L. Heien, R. M. Wightman, R. M. Carelli, *Nature* **422**, 614 (2003).
40. G. D. Stuber, R. M. Wightman, R. M. Carelli, *Neuron* **46**, 661 (2005).

41. Research in this laboratory concerning microelectrodes in biological systems has been supported by NIH grants NS 15841, NS 38879, and DA 10900.

10.1126/science.1120027

Seed Dispersal by Weta

Catherine Duthie, George Gibbs, K. C. Burns*

Natural selection on islands often produces unusual solutions to common ecological problems. Species that are widespread on continents often fail to reach isolated islands, where their niches are filled by other species. As one of the world's most isolated landmasses, New Zealand is a storehouse of unusual niche shifts. Giant, flightless grasshoppers called weta (Fig. 1) appear to have taken on the distinctive ecological niche of small mammals in New Zealand (*1*). Yet if weta truly are ecological equivalents of small mammals, they should form mutualistic partnerships with plants as seed dispersers. However, no insect is known to consume fleshy fruits and to disperse seeds after gut passage.

In a series of experiments and field observations, we tested whether weta are legitimate seed dispersers of fleshy-fruited plants. First, we presented fleshy fruits from 19 New Zealand plant species to captive Wellington tree weta (*Hemidenina crassidens*) in laboratory enclosures. Weta consumed the flesh of all 19 fruit species. Although seeds were frequently ingested, many were destroyed, in common with the actions of small mammals elsewhere (*2*, *3*). The seeds of five plant species (*Fuchsia excorticata, F. procumbens, Gaultheria antipoda, Pratia angulata*, and *P. physaloides*) passed through weta intact. Next, we compared germination rates of weta-dispersed seeds to those manually extracted from pulp. Results showed that seeds ingested by weta had higher germination rates relative to controls (Fig. 1), suggesting that weta-dispersed seeds have a fitness advantage over undispersed seeds. We then asked whether weta-dispersed fruits are morphologically distinct from other fruit species by comparing fruit length, pulp mass, water content, fruit pulp percentage, and seed length between dispersed and undispersed species. Morphological differences were observed [multivariate analysis of variance (MANOVA), $F_{5,13} = 9.6$, $P < 0.01$]. Fruits dispersed by weta had smaller seeds (ANOVA, $F_{1,17}$, $P < 0.01$), lower water content (ANOVA, $F_{1,17}$, $P < 0.01$), and higher fruit pulp percentages (ANOVA, $F_{1,17}$, $P = 0.04$), suggesting that a "syndrome" of fruit traits is associated with weta seed dispersal. Lastly, we tested whether weta actually disperse seeds in the wild. We collected 104 scat from a natural population of Wellington tree weta inhabiting a grove of *F. excorticata*. 64% contained seeds or seed fragments, and 49 intact seeds were recovered. Seeds collected from scat obtained in the field also germinated in laboratory trials, confirming that weta are legitimate seed dispersers. If overall fitness gains from seed dispersal outweigh losses due to seed predation, then our results provide the first example of a mutualistic association between fleshy fruits and an insect fruit consumer.

Fleshy fruits are typically dispersed by birds and mammals. Some insects, such as dung beetles and ants, also disperse seeds externally (*4*, *5*). The only other example of insects ingesting and dispersing seeds apparently comes from Charles Darwin (*6*). In 1881, a farmer from Natal sent Darwin scat from locusts that he collected from his fields, which contained the seeds of two grass species. However, grass seeds are not adapted to this mode of transport, so Darwin's finding represents a different sort of interaction than that discovered here. Our results show that weta form mutualistic partnerships with fleshy-fruited plants, characteristic of relationships between plants and small mammals on continents, providing a striking example of ecological convergence between unrelated organisms. Unfortunately, many weta species are currently threatened with extinction by mammal predators introduced to New Zealand by humans in the 19th and 20th centuries. Therefore, more detailed information on the effects of weta seed dispersal on plant recruitment dynamics is needed to determine if the loss of weta from natural ecosystems will generate cascading effects on the structure and function of New Zealand forests.

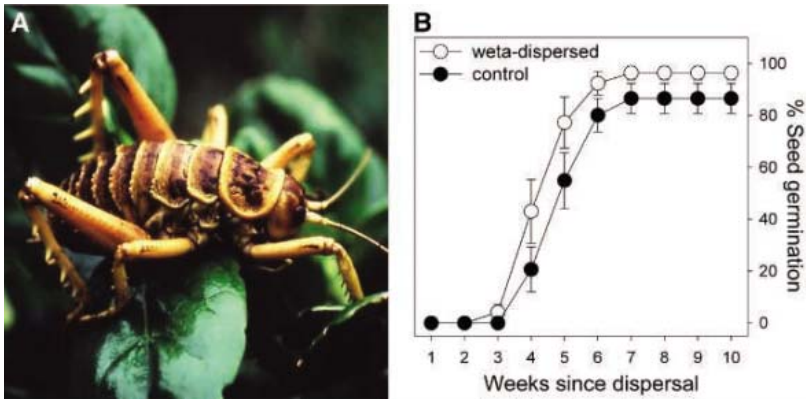

Fig. 1. (**A**) New Zealand weta (*Deinacrida rugosa*, ≈70 mm). [Photograph by B. Robertson] (**B**) The effect of weta ingestion on seed germination. Average percent germination of *P. physaloides* (±SE) seeds dispersed by New Zealand weta versus seeds manually extracted from pulp (control). Germination increased through time (repeated measures ANOVA, $F_{3,23} = 148.3$, $P < 0.001$) and was enhanced by weta ingestion ($F_{1,9} = 8.3$, $P < 0.05$). Both factors did not interact ($F_{3,26} = 1.0$, $P > 0.10$). Statistically similar results were obtained for *F. excorticata*.

References and Notes

1. G. Gibbs, *The New Zealand Weta* (Reed Publishing, New Zealand, 2001).
2. G. Amico, M. A. Aizen, *Nature* **408**, 929 (2000).
3. P. A. Williams, B. J. Karl, P. Bannister, W. G. Lee, *Austral. Ecol.* **25**, 523 (2000).
4. C. E. Christian, *Nature* **413**, 635 (2001).
5. K. Vulinec, *Biotropica* **34**, 297 (2002).
6. C. Darwin, *Origin of Species* (Dent Ltd., UK, 1866).
7. Funding for this study was provided by an Alison Morton Scholarship to C.D. and by the Victoria University of Wellington.

Supporting Online Material

www.sciencemag.org/cgi/content/full/311/5767/1575/DC1
Materials and Methods

7 December 2005; accepted 3 February 2006
10.1126/science.1123544

School of Biological Sciences, Victoria University of Wellington, Post Office Box 600, Wellington, New Zealand.

*To whom correspondence should be addressed. E-mail: kevin.burns@vuw.ac.nz

Large-Scale Sequence Analysis of Avian Influenza Isolates

John C. Obenauer,[1] Jackie Denson,[1] Perdeep K. Mehta,[1] Xiaoping Su,[1] Suraj Mukatira,[1] David B. Finkelstein,[1] Xiequn Xu,[1] Jinhua Wang,[1] Jing Ma,[1] Yiping Fan,[1] Karen M. Rakestraw,[1] Robert G. Webster,[2,4] Erich Hoffmann,[2] Scott Krauss,[2] Jie Zheng,[3] Ziwei Zhang,[3] Clayton W. Naeve[1,4]*

The spread of H5N1 avian influenza viruses (AIVs) from China to Europe has raised global concern about their potential to infect humans and cause a pandemic. In spite of their substantial threat to human health, remarkably little AIV whole-genome information is available. We report here a preliminary analysis of the first large-scale sequencing of AIVs, including 2196 AIV genes and 169 complete genomes. We combine this new information with public AIV data to identify new gene alleles, persistent genotypes, compensatory mutations, and a potential virulence determinant.

Influenza A viruses are endemic in the wild aquatic birds of the world and are occasionally transmitted to humans with catastrophic results (*1*). The outbreak of H5N1 avian influenza virus (AIV) infection in humans in Southeast Asia starting in 2003 has resulted in 76 deaths among 144 infected individuals (*2*) and the slaughter of millions of birds. The virus is clearly present in the wild duck population in China (*3*, *4*) and has spread to Romania, Turkey (*5*), Croatia, and Russia. These events have led to substantial global concern about the potential for this virus to evolve to pandemic proportions, with the capacity to cause millions of deaths. Remarkably, little AIV whole-genome data are available, and the public repositories of sequence data are skewed toward the shorter genes (*Matrix* and *Nonstructural*) and surface glycoproteins [hemagglutinin (HA) and neuraminidase (NA)]. A more comprehensive collection of data and analysis at the gene and whole-genome level are critical needs as we search for answers to questions regarding the virulence and transmissibility of these viruses from avian species to humans.

To address this need, we established the first large-scale sequencing effort to collect additional genomic data on the avian population of influenza A viruses. The AIV genome consists of eight RNA segments that range in size from 890 to 2341 bases and code for 11 known proteins. We developed a primer library specific for each of these eight genes and suitable for our remarkably diverse virus collection, as well as a pipeline for assembly, finishing, and quality control (*6*). Our sequences are of high quality, averaging 8.8 reads per base and mean Phred quality values of 51.2, indicating an average base-calling accuracy of 99.999% (*7*). We provide complete gene sequences, including 5′ and 3′ untranslated regions. All sequences produced by the St. Jude Influenza Genome Project have been submitted to GenBank and are available for study.

Study population and sequencing results. The St. Jude Influenza Repository currently contains ~11,000 influenza viruses, including ~7000 AIVs. We have sequenced a diverse sampling of 336 AIVs from this collection, including isolates from ducks, gulls, shorebirds, and poultry collected in North American, Eurasian, and Australasian countries, primarily during the years from 1976 to 2004. Our sampling includes representatives of all 25 known HA and NA serotypes. We report here the analysis of 2196 new AIV gene sequences and 169 complete AIV genomes (listed in table S1), doubling the amount of publicly available genetic information for AIVs (3,702,178 bases of finished data). We also include in our analysis 2143 AIV sequences retrieved from GenBank (table S2) for a total of 4339 AIV genes. We calculated (Table 1) the nonsynonymous/synonymous substitution rate ratios (dN/dS) in our population (*8*) and find that only the gene encoding the recently reported alternative PB1 transcript PB1-F2 (*9*) is under positive selection pressure. The ratio for PB1-F2 is extreme; values greater than 1.0 are considered positive selection, and this gene's ratio is 9.36; furthermore, this open reading frame is conserved in 281 of 284 of the PB1 sequences in our study. Thus, this protein's reported role in apoptosis appears to be critical. We calculated the number of variants per position in the amino acid sequence of each protein and find that avian viruses exhibit greater variability in their PB1-F2, HA, NS1, and NA proteins than do their non-avian counterparts (table S2 lists the accession numbers for the avian and non-avian samples). An analysis of concatenated genomes showed that HA, NA, and NS1 contribute the most to the variability of avian virus genomes, and that multiple viral lineages co-circulate (supporting online material text). HA and NA are considered highly variable because of immune pressure; it is not known what drives NS1 variability, but this variation appears to be important in the virus life cycle.

We inferred phylogenetic trees for each of the eight individual gene segments, using our 2196 genes and 2143 full or nearly full-length genes retrieved from GenBank (fig. S1). We observed eight novel clades; two in PB1, one in PB2, two in PA, and three in NP genes (blue brackets). These constitute completely new North American clades that are distinct from

Table 1. Project summary. All 11 transcripts from the eight gene segments of AIV are listed along with their lengths in nucleotides (nt), the number of complete gene sequences produced in this study, and the total number of finished nucleotides by segment. The nonsynonymous/synonymous substitution rate ratio (dN/dS), transition/transversion rate ratio (ts/tv), variability of each segment at the amino acid level expressed as a percentage of total ("variability"), and the number of amino acid variations per position in avian versus non-avian hosts are also shown. The asterisks in the length column indicate that this is an average value, because the genes encoding HA, NA, and NS1 have variable lengths.

Segment	Length (nt)	Segments completed	Finished sequence (nt)	dN/dS	ts/tv	Variability (%)	Variants/position	
							Avian	Non-avian
PB1	2341	284	664,844	0.03	8.0	3.5	1.52	1.52
PB1-F2				9.36	33.3	10.2	3.54	2.45
PB2	2341	272	636,752	0.03	7.9	3.7	1.67	1.66
PA	2233	272	607,376	0.04	7.3	3.7	1.74	1.70
HA	1770*	219	387,630	0.14	2.7	28.0	5.52	4.42
NP	1565	292	456,980	0.03	6.9	3.7	1.81	1.85
NA	1450*	259	375,550	0.14	3.5	28.0	5.09	4.38
M1	1027	298	306,046	0.03	8.1	3.4	1.84	1.77
M2				0.39	12.5	4.2	3.50	3.42
NS1	890*	300	267,000	0.16	5.5	6.5	3.40	2.89
NS2				0.12	5.9	4.7	2.81	2.68
Total	13617	2196	3,702,178					

[1]Hartwell Center for Bioinformatics and Biotechnology, [2]Department of Infectious Diseases, Division of Virology, [3]Department of Structural Biology, St. Jude Children's Research Hospital, Memphis, TN 38105, USA. [4]Department of Pathology, University of Tennessee Health Science Center, Memphis, TN 38163, USA.

*To whom correspondence should be addressed. E-mail: clayton.naeve@stjude.org

Asian isolates in the trees. The new surface glycoprotein HA and NA sequences merge with existing clades as defined by serotype; no new clades/serotypes were observed. Likewise, no novel clades were observed for M. The NS tree clearly retains two primary clades (A and B) as previously published (*10*); however, we observed that the viruses in an emerging branch of the A clade are the same viruses present in branches of clades in other gene segments (boxed in red). This is a family of gull and shorebird viruses (Ciconiiformes) that share genes for NS, M2, NP, PA, and PB2 in our trees. We anticipate that this family, and others found to share genes, will be valuable in correlating genotype with phenotype. To identify other viruses that share genes but do not present obvious branches on a DNA tree, we developed a simple method to visualize unique amino acid signatures.

Persistence and compensatory mutations revealed by proteotyping. Traditionally one would assign numbers to all clades in the phylogenetic analysis of individual gene segments and use those numbers to represent and compare genotypes across multiple viruses. In our experience, this approach does not provide the granularity one needs to distinguish subtle, though probably important, differences among these viral gene products. We introduce the concept of proteotyping, in which we identify and number unique amino acid signatures (proteotypes) for sequences that may or may not be distinguished by branches on a phylogenetic tree. We align all sequences of a given segment, manually curate the alignments, generate a maximum likelihood (ML) tree, and then re-sort the alignment to match the order in the tree. We produce an image of the clade-guided sequence alignment by assigning a unique color to each amino acid. Finally, we calculate a consensus sequence for the alignment, hide all the consensus amino acids (colored white to match the background), and remove completely invariant residue positions. By our method, a residue does not have to occur in the majority of sequences to be the consensus; it only has to occur more than any other residue (*6*). This leaves only those amino acids that uniquely define a proteotype. Figure 1 illustrates this process for a small portion of the NS tree. From left to right, we illustrate part of the ML tree's clade A with a region of the aligned NS1 sequences and their assigned proteotype numbers. One can clearly identify amino acid signatures that are distinct from consensus despite being grouped in the same tree clade (p1.1 to p1.4). Potential proteotypes were excluded if the sequences were identical or the isolates were consecutive samples from the same location and year. The gull family of viruses, found by chance to share genes in our phylogenetic analysis, is proteotype NSp1.1 and clearly has a distinct amino acid signature. We assigned clade and proteotype numbers to all visually distinct amino acid signatures for all eight gene segments (figs. S2 to S9). Even the highly variable genes encoding HA and NA can be classified in this manner; for example, H6 hemagglutinins clearly have six distinct proteotypes within the H6 clade (fig. S6). Figure S10 presents the compiled proteotype data for all AIV complete genomes, where each column represents a specific gene product in the order PB1, PB2, PA, HA, NP, NA, M, and NS. Each proteotype is assigned a unique color to facilitate the identification of patterns. Using this approach has allowed us to observe for the first time viruses sharing not only specific genes but genes coding for specific proteotypes.

If one sorts the proteotype table by NS type (Fig. 2A), one can easily identify the gull family of viruses we identified first in our phylogenetic analysis (NSp1.1), in addition to two families not previously observed (NSp1.4 and NSp1.5). The NS, M, NP, and PB2 proteotypes in the NSp1.1 family are rare and always occur together, suggesting functionally important cosegregation. The NSp1.4 family shares HA, NA, M, and NS proteotypes, whereas the NSp1.5 family shares PB1, PA, M, and NS proteotypes. Each family includes viruses isolated from multiple years and each includes proteins with novel signatures pairing with each other. It appears that specific combinations of proteotypes persist over time and may be needed to assemble functional complexes or to maintain specific functional interactions. Sorting this data by each of the remaining seven genes reveals many other instances of virus families sharing specific proteotypes. We anticipate that this method will be useful in identifying AIV protein interactions occurring during infection.

The exchange of gene segments among influenza viruses (reassortment) is one of the hallmarks of influenza virus variation, and these events are rampant in this population. One can see evidence of this in family NSp1.5 in Fig. 2A. Over

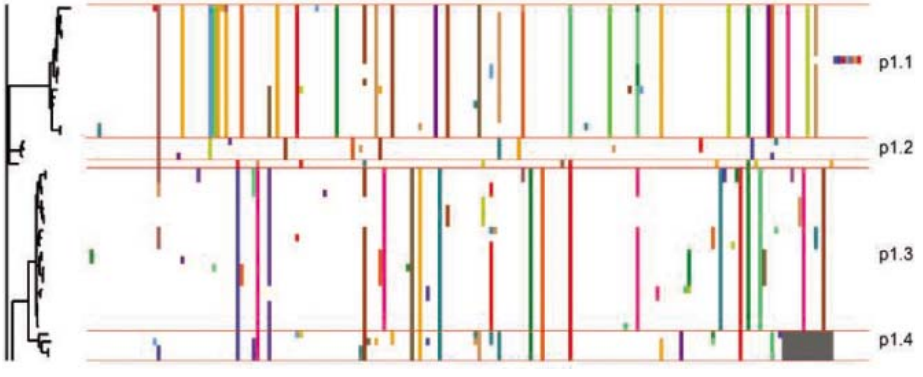

Fig. 1. Proteotype assignment for the NS gene/protein. Part of the maximum-likelihood tree within NS's clade A is shown on the left. The amino acid signatures are in the center, and proteotype assignments are shown on the right. White regions in each sequence match the consensus. Proteotypes appear as aligned vertical colored bars, are numbered in order from top to bottom, and are separated by horizontal red lines. The proteotype assignments for the complete NS gene are shown in fig. S2. Clade and proteotype assignments for all eight gene segments are shown in figs. S2 to S9.

Table 2. Distribution of PL motifs in 1196 influenza NS1 proteins. PDZ-domain ligand sequences found in this population are listed in the PL column; the top blank entry refers to sequences in which the C terminus is truncated to varying extents. The distribution of each PL sequence in avian, human, swine, and equine AIV isolates is shown. The residue at the −3 position from COOH clearly distinguishes these populations, avian and equine always having E/G at −3 and human almost never having E/G at −3. In contrast, human signatures have R/K at −3 92% of the time; the remaining 8% have avian signatures and are known to be of avian origin. Swine isolates can accommodate both PL motifs. The single isolate with the PL motif KSEV is from the 1918 NS1 sequence. Accession numbers for the public sequences used in this analysis are listed in table S4. Numbers in bold indicate the most frequent motif in avian, human, and swine viruses.

PL	Avian	Human	Swine	Equine	−3
	5	2	4		
EPEV	23	21	1	14	
EPKV				1	
ESEI	48		4		
ESEV	**483**	12	7	10	
ESKV	55				E/G
GPEV	2	1	**19**	2	
GPKV			6		
GSEA	1				
GSEI			1		
GSEV	4		4		
GSKV	1	2			
KSEV		1			
RPKV		1			
RSEA			1		R/K
RSEV		22	4		
RSKI		9			
RSKV		**403**	**21**		
TSEV			1		
Totals	622	474	73	27	

the period 1986–1989 the core genes in this family (all those except the surface genes HA and NA) have remained fairly constant, with only a single change in PB2 and NP proteotypes. In contrast, these viruses have acquired four different HAs and six different NAs during this same period.

The data in fig. S10 were re-sorted by HA type, and we illustrate in Fig. 2B the genotype (left) and proteotype (right) for the H6 serotype viruses. The genotyping data show only that these isolates share the H6 serotype/clade HA and M clade 2.0. In contrast, the proteotyping data shows that these viruses can be subclassed into four HA types and two M types and that Mp2.2 is found to pair only with HAp6.2. We propose that the specific pairing we observe in this example results from a change in HA or M requiring the selection of genes encoding proteins with compensating mutations. A number of genetic studies have indicated functional cooperativity between the three polymerase proteins (PB1, PB2, and PA), between NP and M, and between HA and NA (*11*). Such relationships are clearly observed in our data using proteotypes. The method of assigning proteotypes introduced here has advantages over using traditional clade assignment and phylogenetic analysis alone. Proteotypes provide a higher-resolution view of protein variability, potential protein interactions, and the identity of residues that are likely to be functionally important.

Overall, we are struck by the high frequency of reassortment among the surface glycoproteins and, at the same time, the specific pairing and the conservation seen among the core proteins of AIV. 167 of our 169 complete genomes share five or more genes with at least two additional viruses in our sampling. This is not a sampling artifact, because only four of these isolates have identical genomes and presumably represent multiple sampling of the same virus; the rest clearly share genes with other isolates. The virus families we observed tend to have multiple core genes that specifically pair at the proteotype level, indicating that mutations in these highly conserved genes may be complemented by corresponding mutations in one or more binding or interaction partners in order to result in viable virus. The surface glycoproteins appear to be more freely exchanged than core proteins, most likely because of immune pressure. In addition, any instances of homologous recombination should be easily seen in our proteotypes as contiguous residues that are different from the consensus, but at least among the more conserved internal genes, we have not observed such instances in this preliminary analysis. Our

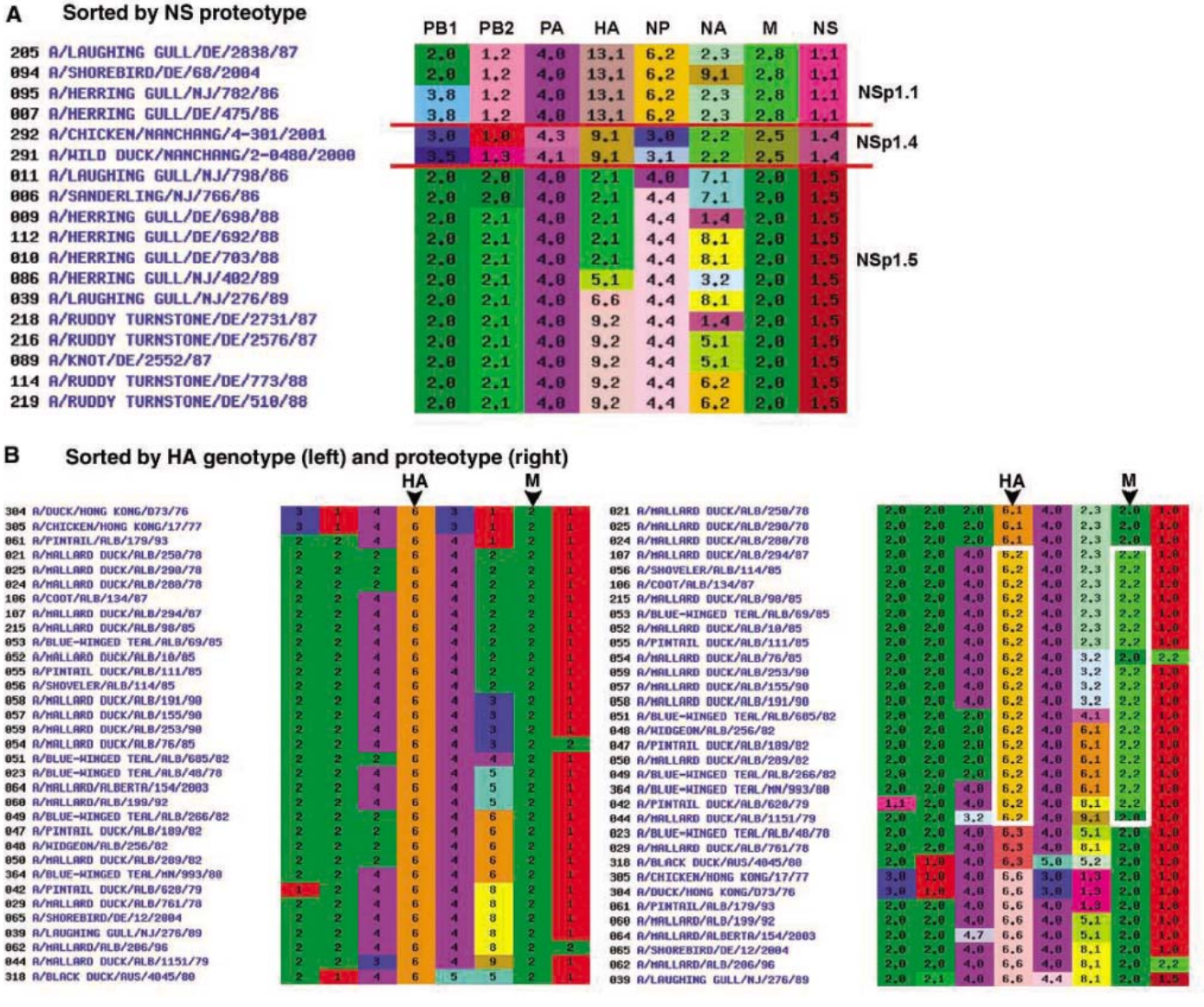

Fig. 2. Proteotyping complete genomes. (**A**) Magnified view of a portion of fig. S10 illustrating three NS families, each sharing different combinations of proteotypes. (**B**) Proteotype data in fig. S10 sorted by HA genotype (left) and proteotype (right). HA and M genotypes and proteotypes are marked to illustrate the detail provided by proteotyping and the recognition that Mp2.2 pairs only with HAp6.2 (white boxes), a feature not seen at the nucleotide level.

findings suggest that homologous recombination is a rare occurrence in AIV evolution.

PDZ ligand motif in NS1 as a potential virulence determinant. The contribution of NS to the genetic variability of AIV and the discovery of NS families with unique proteotype combinations prompted us to examine this gene in detail. The NS gene encodes the proteins NS1 and NS2. NS1 is found only in infected cells and regulates many cell functions during infection (*12*). Substantial evidence suggests that NS1 plays a role in virulence by abrogating the expression of antiviral genes in host cells, including interferon (IFN), nuclear factor kappa B (NF-κB), and RNA-activated protein kinase (PKR) pathways (*13*–*17*). We examined our collection of new AIV NS data and identified a previously unrecognized canonical PDZ domain ligand (PL) (*18*) at the C terminus of NS1 (ESEV-COOH). PDZ domains are modular protein interaction domains that bind in sequence-specific fashion to short C-terminal peptides. They are known to function as scaffold proteins that coordinate the assembly of supramolecular complexes that perform localized signaling at particular subcellular locations (*19*). Proteins that contain PDZ domains play important roles in many key signaling pathways, including regulating the activity and trafficking of membrane proteins, maintaining cell polarity and morphology, and organizing the postsynaptic density in neuronal cells.

We examined the distribution of the four C-terminal amino acids of 1196 NS1 sequences from avian, human, swine, and equine isolates (Table 2). The PL motif contains E/G (*20*) at the –3 position in 100% of all 622 available avian and 27 equine NS sequences. In contrast, 436 of 474 human NS1 sequences (92%) have R/K at the –3 position of this motif, and this motif is not seen in avian or equine isolates. Isolates from swine, which can host both avian and human influenza viruses, show instances of both motifs. The sources of the 38 (8%) human isolates with "avian" PL motifs are predominantly H5N1 Asian isolates known to be of avian origin. The human viruses with the EPEV motif (n = 21) are highly virulent isolates from the 1997–1999 outbreaks in Hong Kong. The human isolates with the PL motif ESEV (n = 12) are from the 2003–2004 outbreak in Hong Kong, Vietnam, and Thailand. The 1918 virus NS1 protein has a unique PL motif, KSEV. Thus, the recent high-mortality H5N1 outbreaks are all characterized by NS1 proteins with "avian" PL motifs, whereas previous low-mortality human pandemics (in 1957 and 1968) are characterized by NS1 proteins with "human" PL motifs.

To determine whether these NS1 PL motifs actually bind to PDZ domains and could potentially disrupt key cell pathways, we analyzed the interactions between three known PDZ domains and four synthetic peptides: the two characteristically avian PL motifs found in highly pathogenic human infections in 1997 (EPEV) and 2003 (ESEV); the unique 1918 pandemic virus motif (KSEV); and the predominant motif in low-pathogenic human infections (RSKV). Peptides were produced to contain each motif at the C terminus but were extended by two amino acids (G and S) at the N terminus to increase their length without interfering with binding specificity. Interactions were measured by chemical-shift perturbation nuclear magnetic resonance (NMR) spectroscopy as described by Wuthrich (*21*) and Wong (*22*). The results are summarized in Table 3 (NMR data are shown in figs. S11 to S14). The highly pathogenic virus sequences from 2003, 1997, and 1918 bind to the PDZ domain from the protein Disheveled (Dsh), whereas the low-pathogenic human virus sequence (GSRSKV) does not. Similarly, the motif representing low-pathogenic strains shows little or no binding to the first PDZ domain in postsynaptic density protein 95 (PSD-95), but the 2003 and 1918 motifs show strong binding affinities. None of our peptides were found to bind to the seventh PDZ domain in glutamate receptor–interacting protein 1 (GRIP1). Our results suggest that the C terminus of NS1 in low-pathogenic human influenza viruses has no interaction with PDZ domains, but the highly pathogenic viruses from 2003, 1997, and 1918 are all able to interact with some PDZ proteins.

To confirm the peptide results, we expressed histidine-tagged full-length versions of both avian and human NS1 proteins in *Escherichia coli* (Fig. 3A) and assessed their ability to bind to four protein arrays containing 123 human PDZ domains (from TranSignal, Panomics, Fremont, CA). The NS1 protein from A/Blue-winged teal/MN/993/80 (H6N6) contained the predominant avian motif ESEV, and the NS1 protein from A/Memphis/14/98 (H3N2) contained the predominant human motif RSKV. The results demonstrate that the full-length avian NS1 protein

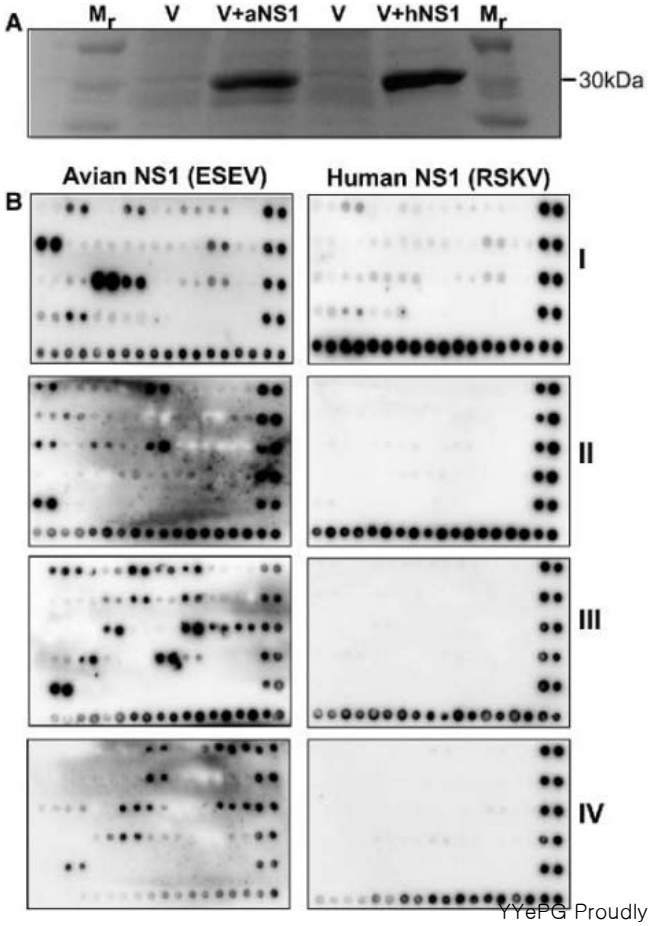

Fig. 3. PDZ domain array analysis. (**A**) Avian (V+aNS1) and human (V+hNS1) NS1 clones were expressed as His-tagged proteins in *E. coli* (*6*). The control lanes are a molecular weight marker (M_r) and vector without insert (V). (**B**) The expressed avian and human NS1 proteins were assayed for their ability to bind 123 human PDZ domains on four membrane filters (I to IV; from Panomics).

Table 3. PDZ binding studies. Synthetic peptides corresponding to the two avian PL signatures seen in highly pathogenic human infections in 1997 (GSEPEV) and 2003 (GSESEV), the 1918 pandemic signature (GSKSEV), and the most common low-pathogenic human signature (GSRKSV) were tested for their ability to bind three known human PDZ domains by chemical-shift perturbation NMR. The domains represented are the PDZ domain in Dsh (residues 251 to 345), the first PDZ in PSD-95 (residues 61 to 151), and the seventh PDZ in GRIP1 (residues 980 to 1070). The results are summarized here in terms of relative binding strength. NMR data are shown in figs. S10 to S13.

	GSESEV (2003)	GSEPEV (1997)	GSKSEV (1918)	GSRSKV (low-pathogenic)
Dsh	++	++	++	-
PSD-95	+++	±	++	±
GRIP1	-	-	-	-

binds to 30 different human PDZ domains, whereas the expressed human NS1 protein binds at a very low level or not at all (Fig. 3B). The identities of these 30 PDZ domain–containing proteins are shown in table S3 and include members of all classes of PDZ domain proteins with roles in cell polarity, T cell proliferation, and mitochondrial localization, among others.

Thus, although the molecular consequences of these interactions are as yet unknown, it appears that avian NS1 proteins, when introduced into human cells, have the opportunity to bind to and presumably disrupt many PDZ domain protein–mediated pathways that the human NS1 protein cannot. The 1957 H2N2 and the 1968 H3N2 influenza pandemics were caused by viruses in which only the surface glycoproteins HA and NA and the polymerase protein PB1 of the prevalent human strains were replaced by avian-like molecules, while the remaining core genes remained of human virus origin. In contrast, the recent H5, H7, and H9 outbreaks in Asia were caused by viruses in which the entire complement of influenza genes, including those encoding NS, were derived from an avian source. We propose that the introduction of avian NS1 into human cells can potentially disrupt many cell pathways via binding to PDZ domain–containing proteins, whereas the human NS1 does not. Disruption of these pathways at the cellular level may well contribute to the higher mortality rates reported in the recent outbreaks as compared to those seen in previous pandemics, though it is clear that multiple genes and gene products are involved. This finding reveals an entirely new means by which AIV may interact with host cell proteins, and these proteins may prove valuable as targets for antiviral therapy.

The wealth of AIV genome data provided by this sequencing project has revealed virus families showing conserved combinations of core proteins; frequent reassortment among the surface proteins; newly observed clades of the PB1, PB2, PA, and NP genes; and a possible virulence marker in NS1. We expect that further analysis of this data by the research community will be valuable in understanding AIVs and how they contribute to human disease.

References and Notes

1. T. Horimoto, Y. Kawaoka, *Nat. Rev. Microbiol.* **3**, 591 (2005).
2. The World Health Organization maintains an updated Web site of the human H5N1 cases and deaths at www.who.int/csr/disease/avian_influenza/country. The figures given here are from the 5 January 2006 update.
3. J. Liu *et al.*, *Science* **309**, 1206 (2005).
4. H. Chen *et al.*, *Nature* **436**, 191 (2005).
5. M. Enserink, *Science* **310**, 209 (2005).
6. Information on materials and methods is available as supporting material on *Science* Online.
7. P. Richterich, *Genome Res.* **8**, 251 (1998).
8. Z. Yang, *Comput. Appl. Biosci.* **13**, 555 (1997).
9. W. Chen *et al.*, *Nat. Med.* **7**, 1306 (2001).
10. Y. Kawaoka *et al.*, *Virus Res.* **55**, 143 (1998).
11. B. W. J. Mahy, in *Genetics of Influenza Viruses*, D. W. Kingsbury, P. Palese, Eds. (Springer-Verlag, Berlin, 1983), pp. 192–254.
12. R. M. Krug *et al.*, *Virology* **309**, 181 (2003).
13. S. Schultz-Cherry *et al.*, *J. Virol.* **75**, 7875 (2001).
14. A. Garcia-Sastre *et al.*, *Virology* **252**, 324 (1998).
15. S. H. Seo, R. G. Webster, *Virus Res.* **103**, 107 (2004).
16. G. K. Geiss *et al.*, *Proc. Natl. Acad. Sci. U.S.A.* **99**, 10736 (2002).
17. A. S. Lipatov *et al.*, *J. Gen. Virol.* **86**, 1121 (2005).
18. Z. Songyang *et al.*, *Science* **275**, 73 (1997).
19. M. Sheng, C. Sala, *Annu. Rev. Neurosci.* **24**, 1 (2001).
20. Single-letter abbreviations for the amino acid residues are as follows: A, Ala; C, Cys; D, Asp; E, Glu; F, Phe; G, Gly; H, His; I, Ile; K, Lys; L, Leu; M, Met; N, Asn; P, Pro; Q, Gln; R, Arg; S, Ser; T, Thr; V, Val; W, Trp; and Y, Tyr.
21. K. Wuthrich, *Nat. Struct. Biol.* **7**, 188 (2000).
22. H.-C. Wong *et al.*, *Mol. Cell* **12**, 1251 (2003).

23. We thank the following Hartwell Center staff for superb support: J. Armstrong, S. Tate, and C. Aldridge (HT Sequencing); M. Sanyang (Software Development); S. Olsen, P. Rodrigues, and B. Cassell (Macromolecular Synthesis); and S. Malone and B. Pappas (Operations). Sequences from this study have been deposited in GenBank under accession numbers CY003847 to CY006042. This work was supported by the American Lebanese Syrian Associated Charities, a Cancer Center Support Grant (CA 21765), the U.S. Public Health Service (grant AI95357), and the Hartwell Foundation.

Supporting Online Material

www.sciencemag.org/cgi/content/full/1121586/DC1
Materials and Methods
SOM Text
Figs. S1 to S15
Tables S1 to S6
References

20 October 2005; accepted 17 January 2006
Published online 26 January 2006;
10.1126/science.1121586
Include this information when citing this paper.

REPORTS

Fuel-Powered Artificial Muscles

Von Howard Ebron,[1] Zhiwei Yang,[1] Daniel J. Seyer,[1] Mikhail E. Kozlov,[1] Jiyoung Oh,[1,2] Hui Xie,[1] Joselito Razal,[1] Lee J. Hall,[1] John P. Ferraris,[1] Alan G. MacDiarmid,[1] Ray H. Baughman[1]*

Artificial muscles and electric motors found in autonomous robots and prosthetic limbs are typically battery-powered, which severely restricts the duration of their performance and can necessitate long inactivity during battery recharge. To help solve these problems, we demonstrated two types of artificial muscles that convert the chemical energy of high–energy-density fuels to mechanical energy. The first type stores electrical charge and uses changes in stored charge for mechanical actuation. In contrast with electrically powered electrochemical muscles, only half of the actuator cycle is electrochemical. The second type of fuel-powered muscle provides a demonstrated actuator stroke and power density comparable to those of natural skeletal muscle and generated stresses that are over a hundred times higher.

Although nature's choice is to chemically power the diverse muscles of her design with a high–energy-density fuel, humankind has largely taken another route. In those systems, electrical energy is typically converted to mechanical energy by means of motors, hydraulic systems, or piezoelectric, electrostrictive, or electrochemical actuators (*1*–*9*). Because of high electrical power needs, some of the most athletically capable robots cannot freely prance around because they are wired to a stationary power source.

There are exceptions to this use of electrically powered actuators: Chemically powered artificial muscles based on polymer gels were demonstrated over 50 years ago and remain of practical interest for both chemically and electrically powered actuators (*10*–*12*). Although actuator strains can be very large, their application has been limited by low response rates, low stress generation, and the low energy densities of the chemicals used for driving actuation. The combustion of fuels in a preburner has been used to indirectly power actuation of shape-memory alloys (*13*), and muscles that act as fuel cells have been proposed (*14*, *15*) but not experimentally demonstrated. Also, nanoscale and larger actuators that are powered by oxygen gas released by the catalytic decomposition of hydrogen peroxide have been described (*16*–*20*).

We experimentally demonstrated two types of artificial muscles that are powered by high–energy-density fuels (hydrogen, methanol, or formic acid). The first type uses a catalyst-containing carbon nanotube electrode that simultaneously functions as a muscle, a fuel-cell electrode, and a supercapacitor electrode. The result is a muscle that converts chemical energy in a fuel to electrical energy and can use this electrical energy for actuation, store it, or potentially use it for other energy needs. The

[1]Department of Chemistry and NanoTech Institute, University of Texas at Dallas, Richardson, TX 75083–0688, USA. [2]Research Center of Dielectric and Advanced Matter Physics and Department of Physics, Pusan National University, Busan 609–735, Korea.

*To whom correspondence should be addressed. E-mail: ray.baughman@utdallas.edu

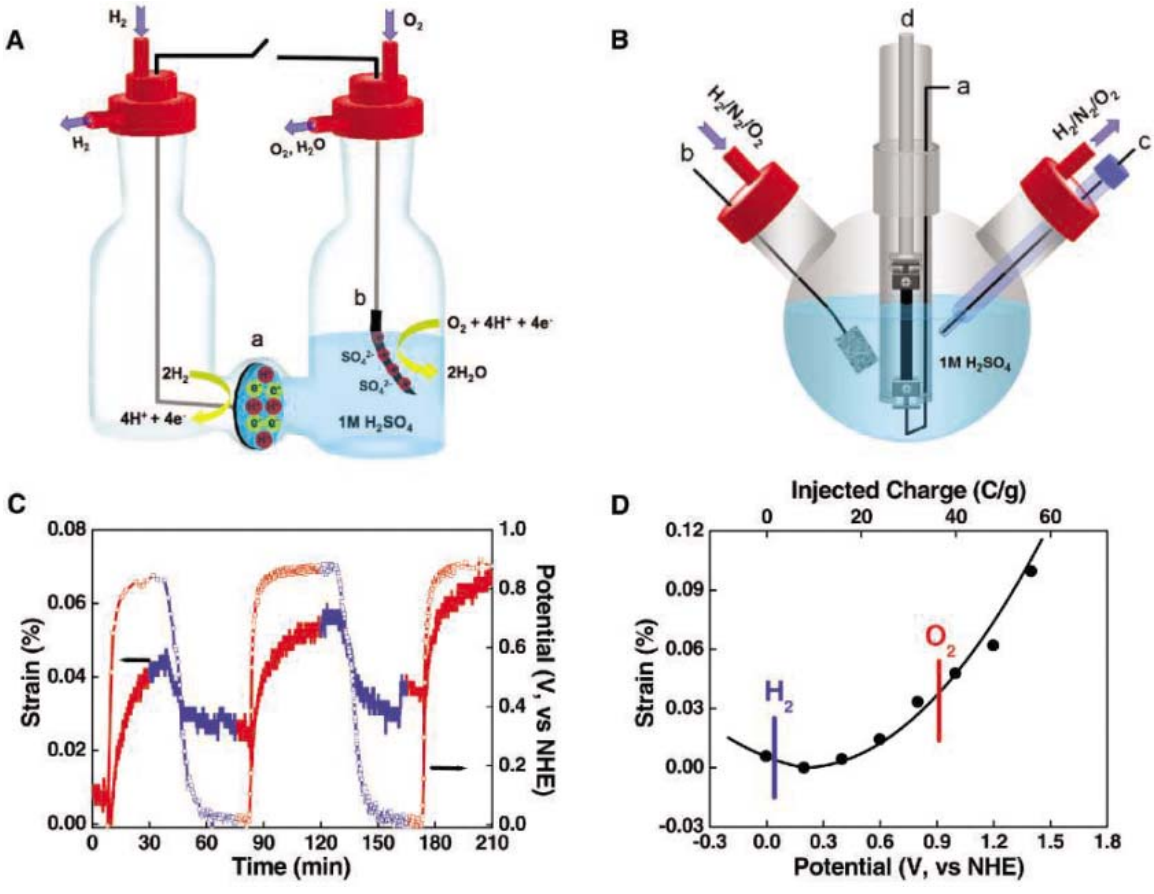

Fig. 1. Nanotube-based fuel-cell muscles. (**A**) Schematic illustration of the apparatus used for demonstration of a cantilever-based nanotube fuel-cell muscle. Element a is the membrane electrode assembly (composed of a porous carbon bilayer, a Pt-C-ionomer layer, and a Nafion-117 membrane) that is the counter-electrode to the actuating Pt-containing nanotube cantilever strip (element b). (**B**) Schematic illustration of a one-compartment cell mounted in a dynamic mechanical analyzer (DMA) for tensile measurements during either fuel-driven or electrically driven actuation. Elements a, b, and c are electrical wires connecting to the fuel-cell muscle working electrode (catalyst-containing nanotube sheet), the carbon felt counter-electrode, and the Ag/AgCl reference electrode, respectively. Element d is the measurement probe assembly of the DMA. (**C**) Potential and actuator strain versus time for a tensile nanotube actuator that is alternately exposed to pure O_2 (red) or a mixture of 5 volume % H_2 in inert gas (blue). An N_2 purge between the O_2 and H_2 purges has negligible duration on this time scale. The slow actuator response results from the present need to dissolve different gases in relatively massive amounts of electrolyte in different parts of the actuation cycle. Creep, which is also a problem for electrically powered nanotube sheet actuators, causes the irreversible component of actuator strain. (**D**) Measured tensile actuator strain versus potential and injected charge for an electrically powered nanotube actuator, indicating the measured hydrogen and oxygen potentials for the chemical actuator experiment. There is agreement between the strain change ongoing between these potentials in the fuel-powered and electrically powered actuator experiments.

second type of artificial muscle functions as a "continuously shorted fuel cell" that converts chemical energy in a fuel to thermal energy that produces actuation.

The first demonstration was of a cantilever actuator (Fig. 1A) in which a nanotube sheet strip was laminated with a mixture of Pt-coated carbon and Nafion ionomer (*21*). The actuating cantilever electrode was immersed in 1 M H_2SO_4, and the counter-electrode was a Pt-C-Nafion ionomer layer deposited on a Nafion-117 membrane, which separated the fuel (hydrogen, at the counter-electrode) from the oxidant (oxygen, at the nanotube actuator electrode) and enabled hydrogen ion diffusion between electrodes when the electrodes were shorted. Unlike traditional fuel cells, where the anode and cathode are deposited on each side of a proton-conducting membrane (such as Nafion), the anode and the cantilever-type cathode in our design are mechanically uncoupled but ionically connected to each other by a liquid electrolyte, enabling actuation during charge/discharge operation of the cell.

This fuel-cell muscle type is in part electrochemical and uses the catalyst-containing carbon nanotube sheet electrode as an artificial muscle. Although both the working and counter-electrodes can actuate, only one electrode was used for actuation in this initial demonstration. Reversible actuator strokes result from electronic charge injection into carbon nanotubes (*22*, *23*). The simultaneous movement of ions of the electrolyte into close proximity to the injected electronic charge forms the so-called electrochemical double layer, which enables high charge injection by maintaining overall charge neutrality. This close proximity of electronic charge on the carbon nanotubes and counter-ions in the electrolyte is enabled by the nanoscale porosity of the carbon single-walled nanotube (SWNT) sheets and the corresponding high surface area, ~300 $m^2\ g^{-1}$ (*23*).

Instead of actuating in response to an applied inter-electrode voltage, the chemically powered actuator electrode generates a potential by acting as a fuel-cell electrode. The fuel-cell muscle generates and capacitively stores electrical energy (which simultaneously causes actuation) when the inter-electrode circuit is open. Oxygen gas at the cantilevered nanotube electrode is reduced in the presence of Pt. Four protons in the H_2SO_4 combine with an O_2 and four electrons extracted from the carbon nanotube electrode to produce two water molecules. The resulting injection of positive charge (holes) into the nanotube sheet causes actuation, with the SO_4^{2-} ions serving as countercharges. Reaction continues until the nanotube electrode is fully charged, generating a half-cell potential of ~0.9 V versus that of a normal hydrogen electrode (NHE) (Fig. 1A). This differs from the continuous power production process of an ordinary hydrogen fuel cell, where the protons and electrons needed to produce water come from the hydrogen electrode. Also, unlike the case of electrically powered actuation using double-layer charge injection, the amount of charge injected into the two electrodes depends only on their individual charge storage capability.

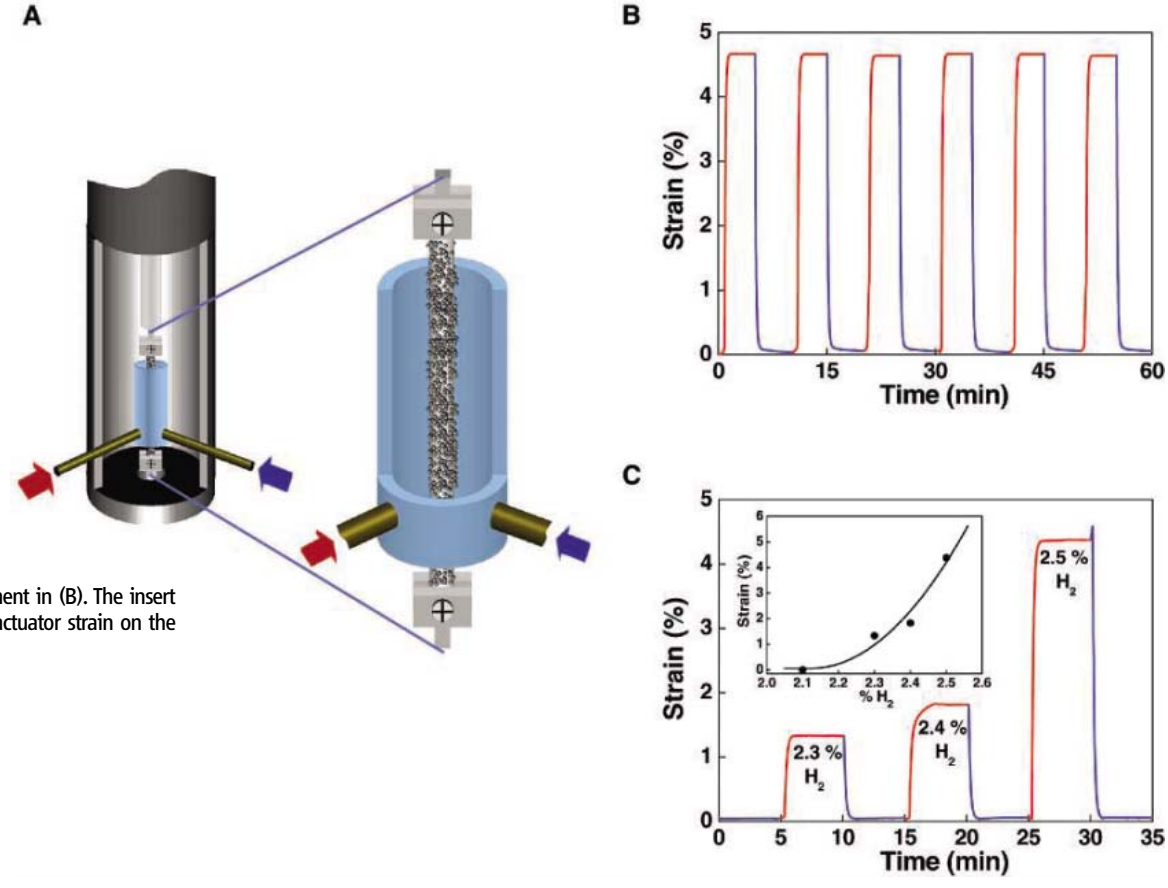

Fig. 2. Continuously shorted fuel-cell muscle based on a NiTi shape-memory alloy. (**A**) Schematic illustration, with cutaway to reveal details, of the fuel-powered artificial muscle mounted in the dynamic mechanical analyzer used for measurements. (**B**) Actuator strain versus time during exposure of the chemically powered actuator to a mixture of N_2, 2.5% by volume hydrogen and 50% oxygen (red curves) and during exposure to pure oxygen (blue curves). (**C**) Actuator strain versus time for different volume percents of H_2 for the experiment in (B). The insert shows the dependence of actuator strain on the H_2 volume % in the fuel.

At the opposite electrode, again under open circuit conditions, hydrogen is oxidized to produce protons and electrons that form an electrochemical double layer, generating a half-cell potential of 0.0 V versus NHE (Fig. 1A). The discharge of the fuel-cell muscle, where actuation is reversed, corresponds to the recombination of electrons on the hydrogen electrode with the holes on the oxygen electrode (the actuating nanotube sheet) when the inter-electrode circuit is closed. Simultaneously, the H_2-derived protons diffuse to the carbon nanotube cathode to replace H^+ ions in the liquid electrolyte that were used to make water during the hole-injection part of the actuator cycle.

The observed actuator stroke during chemically driven charge injection was a 2-mm deflection of a 3-cm-long nanotube cantilever in ~5 s, as the nanotube electrode potential increased to ~0.8 V (versus NHE) (fig. S1). The opposite actuator deflection, obtained when the hydrogen and oxygen electrodes were shorted, occurred in ~1 s (fig. S1). Breaking the connection between electrodes caused recharging of the nanotube muscle and return to the deflection of the initially charged state.

Although this fuel-cell muscle uses only one electrode for actuation, both electrodes can simultaneously serve as muscles. To demonstrate this, we switched the oxygen and hydrogen delivery, so that the actuator electrode became the hydrogen electrode. This causes a decrease in the time required for the charge-injection stroke to 1 to 2 s and a 180° phase shift in actuator response direction. This phase shift and unchanged actuation amplitude result from the low charge-storage capacity of the nanotube sheet as compared to that of the much larger counter-electrode. As a result, the nanotube electrode potential cycles between ~0 and ~0.9 V (versus NHE) during charge and discharge, and only the direction of this shift depends on the gas at the actuating electrode.

Again using hydrogen as the fuel, oxygen as the oxidant, and 1 M H_2SO_4 as the electrolyte, we also drove forward and reverse actuation of a Pt-containing nanotube sheet in a one-compartment cell (Fig. 1B). The fuel and oxidant were introduced one at a time, with an N_2 purge in between. Instead of using a cantilever actuator as the electrode, we used a nanotube sheet that was uniformly filled with catalyst and characterized actuation in tension (*21*). The actuation observed in this setup is driven by the same half-cell reactions as described in the previous two-compartment cell (Fig. 1A), where the fuel and oxidant are continuously present in separate compartments. Because the driving potential and electrolyte are unchanged, the basic mechanisms (quantum-mechanical and coulombic) (*23*) for causing changes in nanotube dimension should be identical.

In the forward actuation step, the nanotube sheet was double-layer charged to 0 V (versus NHE) by filling the cell with hydrogen. After purging the cell with N_2 to avoid direct contact of a H_2 and O_2 mixture with the catalyst, we filled the cell with O_2, which reversed the charging and actuation direction as the nanotube electrode went to a potential of ~0.9 V (versus NHE). Although very long actuation times result in this configuration from the need to periodically dissolve gases in relatively massive amounts of electrolyte, this experiment enabled a reliable comparison between chemically driven and electrically driven actuation in one electrolyte for the same type of Pt-infiltrated nanotube sheet. The obtained results (Fig. 1C) show that the potential changed from ~0.0 to ~0.9 V (versus NHE) as the hydrogen gas in the cell was switched to oxygen, and that the length increase of the nanotube sheet was ~0.035%. Essentially the same length change resulted for electrically driven actuation between these potentials in the utilized electrolyte (Fig. 1D). This actuation strain is within a factor of 3 of the typically 0.1% maximum strain for commercial high-modulus ferroelectrics, which usually require about 100 V of externally applied potential for operation (*1*).

Although the efficiencies of polymer electrolyte fuel cells do not exceed 40% at peak power (*24*), the second type of fuel-powered

muscle can use essentially all of the energy produced by fuel oxidation to produce the heating needed for actuation (*15*). This muscle is called a continuously shorted fuel-cell muscle because the effective redox reactions occur on a catalyst-coated shape-memory metal. Unlike the situation in a classical fuel cell, both fuel and oxidant are simultaneously delivered to a single electrode (a Pt-coated shape-memory wire), which functions as a shorted electrode pair.

Our demonstrations used a NiTi shape-memory wire coated with Pt catalyst particles as the fuel-cell muscle and either hydrogen, methanol, or formic acid as fuel (*21*). The Pt-coated shape-memory wire was attached to a sample holder of a dynamic mechanical analyzer and placed in an enclosure with provision for the simultaneous introduction of fuel and oxidant (Fig. 2A). Contact of the fuel and an oxidant (oxygen or air) causes the mechanically loaded wire to heat to above the austenitic phase-transition temperature and do mechanical work during the resulting contraction. Upon interruption of the fuel, the wire cools to below its martensitic phase-transition temperature and returns to its original length (Fig. 2, B and C).

This fuel-powered muscle (Fig. 2B) supported stress of ~150 MPa or more while undergoing ~5% contraction when powered by a mixture of oxygen (or air) and either methanol vapor, formic acid vapor, or a noncombustible mixture of hydrogen in inert gas. This stress-generation capability is ~500 times that which is typical for human skeletal muscle (0.3 MPa), whereas the percent stroke is ~25% that of this natural muscle (*1*). Hence, the work capability of the continuously shorted fuel-cell muscle on lifting a weight (5300 kJ m^{-3} for methanol and 6800 kJ m^{-3} for hydrogen or formic acid) is over 100 times that of skeletal muscle (~40 kJ m^{-3}) (*1*). The percent contraction (5, 7, and 8% observed for 150-, 122-, and 98-MPa loads, respectively, using 2.5 volume % hydrogen in inert gas as fuel) can be increased to far above the ~20% typical of skeletal muscle (*1*) by simply coiling the shape-memory wire, albeit with a proportional decrease in stress generation. The presently achieved power density (68 W kg^{-1} during the work part of the cycle for hydrogen fuel) is similar to that of natural skeletal muscle (typically about 50 W kg^{-1}) (*1*). By increasing the fuel delivery rate and optimizing fuel composition and catalyst loading, it should be possible to dramatically increase power density.

References and Notes

1. J. D. W. Madden *et al.*, *IEEE J. Oceanic Eng.* **29**, 706 (2004).
2. R. H. Baughman, *Science* **308**, 63 (2005).
3. E. Smela, *Adv. Mater.* **15**, 481 (2003).
4. R. Pelrine, R. Kornbluh, Q. Pei, J. Joseph, *Science* **287**, 836 (2000).
5. Q. M. Zhang, V. Bharti, X. Zhao, *Science* **280**, 2101 (1998).
6. S. Nemat-Nasser, *J. Appl. Phys.* **92**, 2899 (2003).
7. J. Weissmüller *et al.*, *Science* **300**, 312 (2003).
8. S. Hara, T. Zama, W. Takashima, K. Kaneto, *J. Mater. Chem.* **14**, 1516 (2004).
9. K. Asaka, K. Oguro, Y. Nishimura, M. Mizuhata, H. Takenaka, *Polym. J.* **27**, 436 (1995).
10. H. B. Schreyer, N. Gebhart, K. J. Kim, M. Shahinpoor, *Biomacromolecules* **1**, 642 (2000).
11. D. Kaneto, J. P. Gong, Y. Osada, *J. Mater. Chem.* **12**, 2169 (2002).
12. Y. Osada, H. Okuzaki, H. Hori, *Nature* **355**, 242 (1992).
13. O. K. Rediniotis, D. C. Lagoudas, H. Y. Jun, R. D. Allen, *Proc. SPIE* **4698**, 441 (2002).
14. R. H. Baughman, C. Cui, J. Su, Z. Iqbal, A. A. Zakhidov, U.S. patent 6,555,945 (2003).
15. R. J. Howard, U.S. Patent Application Publication U.S. 2005/0028901 (2005).
16. W. F. Paxton *et al.*, *J. Am. Chem. Soc.* **126**, 13424 (2004).
17. S. Fournier-Bidoz, A. C. Arsenault, I. Manners, G. A. Ozin, *Chem. Commun.* 441 (2005).
18. T. R. Kline, W. F. Paxton, T. E. Mallouk, A. Sen, *Angew. Chem. Int. Ed. Engl.* **44**, 744 (2005).
19. J. M. Catchmark, S. Subramanian, A. Sen, *Small* **1**, 202 (2005).
20. R. F. Ismagilov, A. Schwartz, N. Bowden, G. M. Whitesides, *Angew. Chem. Int. Ed. Engl.* **41**, 652 (2002).
21. Materials and methods are available as supporting material on ***Science*** Online.
22. R. H. Baughman *et al.*, *Science* **284**, 1340 (1999).
23. R. H. Baughman, A. A. Zakhidov, W. de Heer, *Science* **297**, 787 (2002).
24. F. Barbir, T. Gómez, *Int. J. Hydrogen Energy* **22**, 1027 (1997).

25. The authors thank J. A. Main for describing needs that led to this work and B. L. Lee for discussions of actuator energy harvesting. This work was supported by the Defense Advanced Research Projects Agency/U.S. Army Research Office (grant W911NF-04-1-0174), the Robert A. Welch Foundation (grant AT-0029), and the Strategic Partnership for Research in Nanotechnology (SPRING) consortium in Texas.

Supporting Online Material

www.sciencemag.org/cgi/content/full/311/5767/1580/DC1
Materials and Methods
Fig. S1

14 September 2005; accepted 19 January 2006
10.1126/science.1120182

Microstructured Optical Fibers as High-Pressure Microfluidic Reactors

Pier J. A. Sazio,[1*] Adrian Amezcua-Correa,[1] Chris E. Finlayson,[1†] John R. Hayes,[1] Thomas J. Scheidemantel,[2,3] Neil F. Baril,[2,4] Bryan R. Jackson,[2,4] Dong-Jin Won,[2,5] Feng Zhang,[2,3] Elena R. Margine,[2,3] Venkatraman Gopalan,[2,5] Vincent H. Crespi,[2,3,5] John V. Badding[2,4*]

Deposition of semiconductors and metals from chemical precursors onto planar substrates is a well-developed science and technology for microelectronics. Optical fibers are an established platform for both communications technology and fundamental research in photonics. Here, we describe a hybrid technology that integrates key aspects of both engineering disciplines, demonstrating the fabrication of tubes, solid nanowires, coaxial heterojunctions, and longitudinally patterned structures composed of metals, single-crystal semiconductors, and polycrystalline elemental or compound semiconductors within microstructured silica optical fibers. Because the optical fibers are constructed and the functional materials are chemically deposited in distinct and independent steps, the full design flexibilities of both platforms can now be exploited simultaneously for fiber-integrated optoelectronic materials and devices.

Optical fibers provide ideal hosts for the manipulation of photons, especially when formed into microstructured optical fibers (MOFs) that enable precise control of photon dispersion (*1*). Crystalline semiconductors such as silicon provide ideal hosts for the manipulation of electrons, especially when formed into heterostructures that enable precise control of electron transport. It has thus far not been possible to integrate the crystalline semiconductors that form the basis for modern optoelectronics into MOFs, allowing for interaction of such materials with waveguided electromagnetic radiation over much longer length scales than can be realized in typical planar device geometries (*2*). Fabrication of such structures would be a major step forward toward all-fiber optoelectronics. The preferred method for depositing semiconductors and metals, including nearly all of the technologically important semiconductors, is chemical vapor deposition (CVD) (*3*). However, CVD onto the walls of the long, extremely narrow pores in a MOF presents two challenges: Small deviation from perfect conformal deposition anywhere along the length of the pore would immediately arrest deposition, and mass transport of the reactants into and by-products out of such a confined space is prohibitively slow using traditional techniques. We report the fabrication of high-quality polycrystalline and single-crystal semiconductors within the voids of MOFs by high-pressure microfluidic chemical deposition. High-pressure flow, which can be sustained because of the very

high mechanical strength of optical fibers (*4*), overcomes mass-transport constraints and also enables a strikingly uniform, dense, and conformal annular deposition onto the capillary walls, even for pores that reduce to less than 10 nm in diameter.

MOFs are typically fabricated by stacking and fusing arrays of capillaries into preforms centimeters in diameter that are drawn at high temperature (*1*, *5*). This approach allows the complex preform structure to be scalably replicated in fibers that are four orders of magnitude longer and two orders of magnitude smaller in diameter. By appropriately designing the stacked preform, the capillary holes within a single MOF can have a wide range of shapes and sizes in precisely engineered periodic or aperiodic spatial configurations.

We treat the empty pores in a MOF as micro/nanoscale reaction chambers into which we can directly deposit a wide range of technologically important semiconductors and metals with exceptional control, because we can now exploit the decades-long knowledge base developed for CVD onto planar substrates. Very high pressures (10 to 100 MPa) facilitate rapid mass transport through the fiber pores. In a typical experiment (*6*), a germanium precursor GeH_4 flows through the heated MOF at a partial pressure of 2 MPa [much higher than in traditional CVD (*3*)], along with an inert carrier gas. High pressures and toxic precursors such as GeH_4 are safe and practical because the pressure reservoir and the fiber pores have a very small volume. A smooth layer of amorphous germanium begins to deposit on the pore walls as the temperature is ramped up past 300°C. Crystalline grains then nucleate and grow as the temperature exceeds the crystallization point of ~375°C. As growth proceeds, a remarkably uniform tube forms (see Fig. 1, A to D); as it fills with germanium, a 1.0-μm diameter pore can be narrowed by a factor of 100 down to 25 nm or smaller, tapering open gradually over a deposition length of 70 cm. Silica capillaries drawn to a 100-nm diameter were also successfully filled with germanium to form nanotubes over macroscopic lengths of up to 30 cm, with an inner diameter of less than 10 nm (Fig. 1D).

Deposition into more highly structured pores reveals additional information about this conformal filling. When a large-air-fraction fiber with a honeycomb pattern of holes is filled (Fig. 1E), a spatially ordered array of hexagonal germanium tubes is formed (Fig. 1F). The interior vertices of the hexagonal holes, originally defined by the rounded silica template (Fig. 1, E and G), actually sharpen (Fig. 1F) as growth proceeds. If we assume uniform inward motion of the surface along the local normal during deposition, then the rounded corners of a polygon will become sharp as the thickness of the deposited layer exceeds the radius of curvature of the corner (Fig. 1E, inset). The resulting faceted tubes resemble lithographically patterned micro and nanostructures but are formed in a simple single-stage deposition.

This uniform annular growth down to very small inner diameters, with sharp geometric features, is particularly striking when one considers that the germanium is polycrystalline, with a grain size much larger than the dimensions of these features. Transmission electron microscopy (TEM) and selected-area diffraction patterns (Fig. 1, G and H) reveal that upon heating up to 500°C, the originally amorphous germanium converts into crystalline grains more than 500 nm across (*6*). These grains are much larger than the final inner diameter of the hexagonal tubes, yet the inner walls remain smooth. micro-Raman spectra of wires inside the silica matrix show just a single mode at 300.8 cm^{-1}, characteristic of pure crystalline germanium.

To demonstrate that we have integrated continuous, electrically active germanium into optical fibers over macroscopic lengths, we have fabricated an 11-mm-long, 5-μm-diameter field-effect transistor (FET) inside a single silica capillary of 94-μm outer diameter (Fig. 2). Transconductance measurements (*6*) reveal the carriers to be n-type; by interpolating the linear slope of dI_{drain}/dV_{gate} for a given V_{source} (*7*), the carrier mobility is calculated to be 1.05 cm^2/Vs at room temperature. The samples were not intentionally doped, although it should be possible to extrinsically dope during deposition. We can modulate the channel conductance over several orders of magnitude to obtain pinch-off, yielding an estimate of the carrier concentration of 2×10^{15} cm^{-3} (*7*). We anticipate that

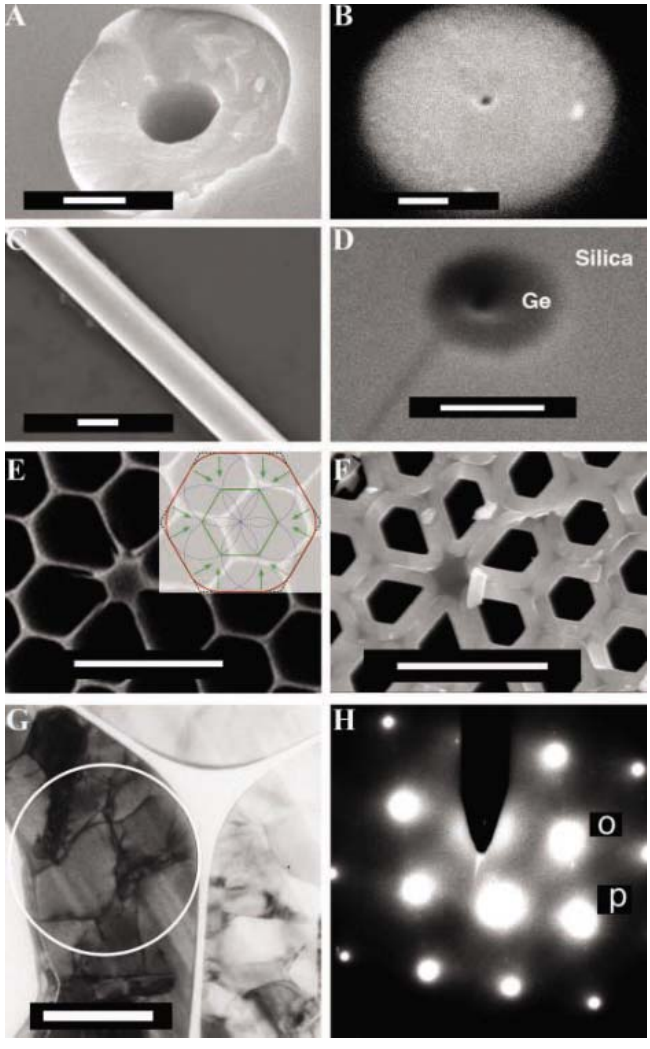

Fig. 1. Germanium integrated into MOFs. (**A**) Scanning electron microscopy (SEM) cross section of a germanium tube within a silica capillary. Scale bar, 500 nm. (**B**) Germanium deposited within a 1.0-μm pore, with a central hole ~25 nm in diameter. Scale bar, 200 nm. (**C**) A germanium wire etched out of a MOF. Scale bar, 2 μm. (**D**) Field-emission SEM cross section of a germanium nanotube within a MOF. Scale bar, 100 nm. (**E**) Unfilled honeycomb MOF template. Scale bar, 5 μm. (Inset) Schematic indicating surfaces growing inward at a uniform rate, in a direction parallel to the local normal (green arrows). When the deposition reaches the thickness indicated by the green inner hexagon, the rounded corners have disappeared and the cross section is a perfect hexagon. (**F**) Honeycomb template after germanium deposition. Scale bar, 5 μm. (**G**) Cross-sectional TEM of a germanium-filled honeycomb MOF, showing thread-like dislocations within the grains. Scale bar, 500 nm. (**H**) Selected-area diffraction pattern of the region circled in (G). o is $\bar{1}11$; p is $\bar{2}20$. Zone axis is <110>.

[1]Optoelectronics Research Centre, University of Southampton, Highfield, Southampton SO17 1BJ, UK. [2]Materials Research Institute, [3]Department of Physics, [4]Department of Chemistry, [5]Department of Materials Science and Engineering, Pennsylvania State University, University Park, PA 16802, USA.

*To whom correspondence should be addressed. E-mail: pjas@orc.soton.ac.uk (P.J.A.S.); jbadding@chem.psu.edu (J.V.B.)

†Present address: Department of Physics, Cavendish Laboratory, University of Cambridge, Cambridge CB3 0HE, UK.

the mobility will approach values more typical of bulk n-type polycrystalline Ge [100 cm^2/Vs (*8*)] upon further optimization of the deposition conditions (e.g., precursor and carrier gas purity and thermal treatment for grain growth).

Electrical characterization of individual wires and tubes within MOF templates is straightforward in comparison with transport measurements on "loose" vapor-liquid-solid (VLS)–grown wires (*9*, *10*), because it does not require lithographic patterning or micromanipulation. An additional advantage is the ease of forming low-resistance ohmic contacts, because up to several millimeters of the protective silica cladding can be etched away (Fig. 2, upper inset) to reveal long sections of bare nano/microwires for metallization by standard techniques. The resulting contacts are thus well decoupled from the transfer characteristics of the device. In contrast, the formation of high-quality ohmic contacts to VLS nanowire devices remains challenging (*11*). In particular, if sufficiently high-quality contacts are not formed, modulation of the contact resistance by the source-drain bias can give rise to nongated transconduction in such systems. Furthermore, lithographically processed VLS nanowire devices are often annealed to reduce the contact resistance. This annealing can lead to chemical diffusion along the wire (given the proximity of the contacts) and thus make it difficult to control the doping type and level (*11*). Our approach precludes any contact-induced changes in device behavior because of the large distance between the source, drain, and gate. Such decoupling of extraneous contact effects is critical for obtaining a fundamental understanding of device behavior.

Deposition of silicon from a SiH_4 precursor into a honeycomb fiber at 700°C also forms long, smooth hexagonal tubes with sharp vertices (see Fig. 3, A and B). The peak in micro-Raman spectra collected on these silicon wires is downshifted by 2 cm^{-1} from that expected for bulk silicon (521 cm^{-1}). This downshift is consistent with the differential thermal expansion of silica and silicon between 700°C and room temperature. First-principles total energy calculations of bulk silicon under tensile stress produce a comparable Raman downshift at an isotropic dilation of 0.15%. A roughly isotropic thermal dilation is expected, even though the fiber container is elongated. Taking the silicon bulk modulus of 98.9 GPa, the fiber-integrated silicon wire experiences a substantial negative pressure, –0.15 GPa. A uniaxial or biaxial tensile stress is inconsistent with the maximum possible differential thermal expansion, because the positive Poisson's ratio of silicon ensures that the pressure dependence of the Raman mode is much weaker under such conditions (*12*). If the wires are etched out of the silica matrix, this stress is relieved and the mode returns to 521 cm^{-1}. In contrast, the germanium tubes show no stress-induced Raman shifts, even though the thermal-expansion coefficient for germanium is 2.3 times as high as that of silicon. The germanium-silica interface does not transfer as large tensile and extensional shear forces as does the silicon-silica interface.

A major advantage of the fiber-integrated geometry is the strong coupling of propagating photons to electronic degrees of freedom in the deposited material along the long interaction length of the fiber. Therefore, the waveguiding properties of semiconductor MOF metamaterials are key to their exploitation in the next generation of photonic devices. Approximately 2 mm of the 125-μm diameter silica cladding of a 5-cm-long sample was chemically etched away at one end to allow its optical characteristics to be decoupled from those of the 2-μm diameter silicon core. A 633-nm laser light launched into the other cleaved end-face of the composite fiber cannot propagate beyond the cladding region and into the core (Fig. 3, C and D) because silicon absorbs strongly at visible wavelengths. However, for near-infrared light at energies below the silicon bandgap (1.07 eV), the core is transparent and 1.55-μm radiation can be observed propagating through it (Fig. 3E). By measuring the output power waveguided through the isolated silicon core (*6*), we place an upper bound of 7 dB cm^{-1} on the loss within it, comparing favorably to losses of 7 to 9 dB cm^{-1} reported thus far for optimized planar polycrystalline silicon waveguides (*13*, *14*). The optical losses in semiconductor devices are a strong function of the surface roughness (*15*), which can limit the performance of lithographically defined rectilinear waveguides because they have an exposed upper surface. However, as material deposits inside a MOF, the area of the exposed growth surface decreases linearly with the inner diameter and becomes zero in the limit of a fully filled pore. In addition, the outer surface of the fiber-integrated semiconductor waveguide is defined by the extremely smooth silica surface of the MOF pore [0.1-nm root mean square roughness (*16*)]. Therefore, boundary scattering from both inner and outer surfaces is minimized.

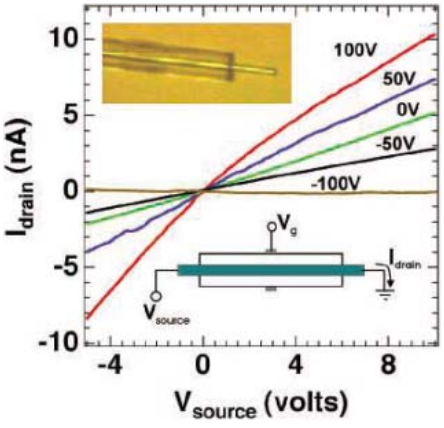

Fig. 2. A fiber-integrated germanium FET. The current-voltage characteristics of the FET show the effect of gate bias (as labeled for each curve), with complete pinch-off at –100V. (**Upper inset**) Etched end of the germanium-filled capillary. (**Lower inset**) Schematic circuit diagram of the FET.

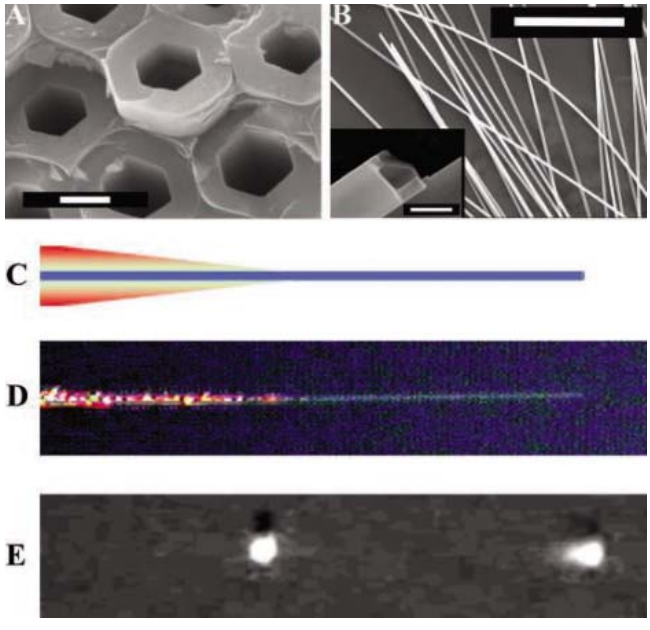

Fig. 3. Fiber-integrated silicon structures. (**A**) Hexagonal silicon tubes in a honeycomb MOF template. Scale bar, 1 μm. (**B**) Long silicon tubes etched out of the template. Scale bar, 100 μm. (Inset) One of these tubes at higher magnification, showing the flat sides of the hexagon. Scale bar, 2 μm. (**C**) Schematic of light-guiding experiment. The end of a filled fiber is etched to completely expose 2 mm of the central silicon core (blue) and taper a portion of the silica cladding (red). (**D**) A 633-nm light is guided in the tapered silica cladding but not in the exposed silicon. (**E**) A 1.55-μm light propagating through the same etched fiber. The light is scattered at the end of the silica cladding but continues to propagate the full length of the silicon core.

Fiber-integrated compound semiconductors, semiconductor heterostructures, and metal-semiconductor heterostructures are also possible. For example, we have integrated annular layers of mid-infrared transparent GeS_2 (*17*), coaxial SiGe heterojunctions, and annular gold/silicon Schottky junctions into MOFs by sequential deposition (Fig. 4). The large discontinuities in refractive index and electronic bandgap in, for example, SiGe heterostructures are a prerequisite for devices such as high-frequency electro-optic modulators that span the mid- to far-infrared (*14*, *18*). Many of the known CVD chemistries for other compound semiconductors (*3*) and metals (*19*) can be adapted to the high-pressure microfluidic chemical deposition technique. Perfect crystallinity is not required for many high-quality devices; suitably engineered polycrystalline materials systems can have optical properties nearly equivalent to those of single crystals (*20*).

The high transparency of the MOF templates can be exploited to pattern thermally sensitive or photosensitive precursors along the fiber axis. When combined with the ability to individually address capillaries within spatially ordered arrays (either serially or in parallel), this capability enables patterning in all three spatial dimensions. For example, using a laser oriented perpendicular to the fiber axis and focused through the cladding, we have directly written gold (Fig. 4D) and silicon particles (*6*) as small as 1.0-μm long at precise locations along the axis of a 1.6-μm diameter capillary.

The superior electron transport and photonic properties of single-crystal semiconductors are desirable for many high-performance devices such as lasers (*10*) and FETs. To this end, we have modified our high-pressure microfluidic process to enable the template-directed growth of single-crystal semiconductor wires in a manner analogous to VLS growth techniques (*9*) for single-crystal nanowires, which can be assembled into devices (*10*, *21*, *22*). We used laser-written gold plugs inside a 1.6-μm silica capillary to decompose high-pressure silane at 370°C for growth of single-crystal silicon wires. The resulting wires, also 1.6 μm in diameter, grow in the <112> direction (Fig. 4, E and F).

Hierarchical bottom-up organization of nanomaterials into device configurations remains a central challenge in nanotechnology. The CVD deposition and VLS growth of materials within the ordered arrays of capillary holes in MOFs demonstrated here provide an elegant and powerful method to spatially organize functional materials at dimensions down to the nanoscale and allow for cooperative photonic and electronic processes between them. For example, the selective filling [by masking techniques (*23*)] of adjacent capillary holes in photonic-bandgap fiber waveguides with semiconductor/metallic electrodes (*24*) can enable electro-optic modulation (*14*) of the semiconductor refractive index and, therefore, bandgap tuning. In addition, polycrystalline or single-crystal semiconductors, deposited within MOFs, can enable nonlinear frequency conversion in the near- to mid-infrared (*25*) and serve as direct bandgap gain media for fiber lasers that operate over a range of wavelengths not previously possible. Such devices could be robust, inexpensive, and seamlessly integrated into the existing fiber-based infrastructure. More generally, the ability to simultaneously engineer radial, longitudinal, and compositional complexity within optical fibers, whose own microstructure can be engineered independently, heralds an opportunity to fabricate sophisticated three-dimensional optoelectronic device structures within the fiber geometry.

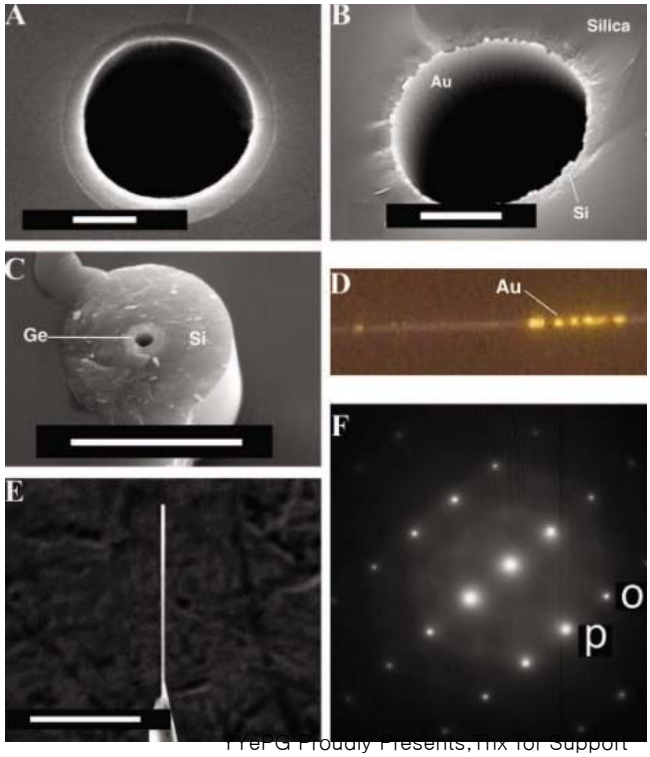

Fig. 4. Heterostructures and single crystals within MOFs. (**A**) Compound semiconductor GeS_2 tube. Scale bar, 500 nm. (**B**) An 80-nm-thick smooth gold annulus deposited within a silicon tube. Contrast between silica and silicon is low. Scale bar, 2 μm. (**C**) Silicon cladding on a germanium core. Scale bar, 6 μm. (**D**) Optical micrograph of an array of gold particles written with a focused 514.5-nm laser beam within a 1.6-μm capillary. (**E**) SEM micrograph of an 80-μm-long section of a single-crystal silicon wire protruding out of an MOF after etching away the silica cladding. Scale bar, 50 μm. (**F**) Electron diffraction pattern collected on a cross-sectional slice of the single-crystal wire. o is $13\bar{1}$; p is $\bar{2}20$.

References and Notes

1. J. C. Knight, *Nature* **424**, 847 (2003).
2. M. Bayindir *et al.*, *Nature* **431**, 826 (2004).
3. A. C. Jones, P. O'Brien, *CVD of Compound Semiconductors: Precursor Synthesis, Development and Applications* (VCH, Weinheim, Germany; Cambridge, 1997).
4. C. R. Kurkjian, J. T. Krause, M. J. Matthewson, *J. Lightwave Technol.* **7**, 1360 (1989).
5. D. J. Richardson *et al.*, *Proceedings of 2005 Institute of Electronic and Electrical Engineers/Lasers and Electro-Optics Society Workshop on Fibres and Optical Passive Components*, 1 (2005).
6. Materials and methods are available as supporting material on *Science* Online.
7. R. Martel, T. Schmidt, H. R. Shea, T. Hertel, P. Avouris, *Appl. Phys. Lett.* **73**, 2447 (1998).
8. Z. G. Meng *et al.*, *J. Mater. Res.* **12**, 2548 (1997).
9. T. E. Bogart, S. Dey, K. K. Lew, S. E. Mohney, J. M. Redwing, *Adv. Mater.* **17**, 114 (2005).
10. X. F. Duan, Y. Huang, R. Agarwal, C. M. Lieber, *Nature* **421**, 241 (2003).
11. S. M. Koo, M. D. Edelstein, Q. L. Li, C. A. Richter, E. M. Vogel, *Nanotechnology* **16**, 1482 (2005).
12. E. Anastassakis, E. Liarokapis, *J. Appl. Phys.* **62**, 3346 (1987).
13. L. Liao *et al.*, *J. Electron. Mater.* **29**, 1380 (2000).
14. A. S. Liu *et al.*, *Nature* **427**, 615 (2004).
15. J. S. Foresi, M. R. Black, A. M. Agarwal, L. C. Kimerling, *Appl. Phys. Lett.* **68**, 2052 (1996).
16. P. J. Roberts *et al.*, *Opt. Express* **13**, 236 (2005).
17. C. C. Huang, D. W. Hewak, J. V. Badding, *Opt. Express* **12**, 2501 (2004).
18. Y.-H. Kuo *et al.*, *Nature* **437**, 1334 (2005).
19. A. Cabanas, D. P. Long, J. J. Watkins, *Chem. Mater.* **16**, 2028 (2004).
20. G. A. Kumar *et al.*, *IEEE J. Quant. Elect.* **40**, 747 (2004).
21. M. S. Gudiksen, L. J. Lauhon, J. Wang, D. C. Smith, C. M. Lieber, *Nature* **415**, 617 (2002).
22. L. J. Lauhon, M. S. Gudiksen, C. L. Wang, C. M. Lieber, *Nature* **420**, 57 (2002).
23. Y. Y. Huang, Y. Xu, A. Yariv, *Appl. Phys. Lett.* **85**, 5182 (2004).
24. M. Fokine *et al.*, *Opt. Lett.* **27**, 1643 (2002).
25. M. Baudrier-Raybaut, R. Haidar, P. Kupecek, P. Lemasson, E. Rosencher, *Nature* **432**, 374 (2004).

26. J.V.B., V.G., and V.H.C. thank the National Science Foundation, the Penn State Materials Research Science and Engineering Center, funded by NSF grant DMR-0213623, and the Penn State-Lehigh Center for Optical Technologies for support. TEM work was performed at the EM facility of the Materials Research Institute at Penn State by J. Kulik. P.J.A.S. thanks the Engineering and Physical Sciences Research Council for support, D. C. Smith and R. T. Harley for assistance with electron transport measurements, and J. J. Baumberg for discussions. A.A.C. thanks the Mexican Council for Science and Technology for support. We thank J. A. Calkins for the direct writing of gold structures.

Supporting Online Material

www.sciencemag.org/cgi/content/full/311/5767/1583/DC1
Materials and Methods
References

23 December 2005; accepted 21 February 2006
10.1126/science.1124281

Saturn's Spokes: Lost and Found

C. J. Mitchell,[1] M. Horányi,[1]* O. Havnes,[2] C. C. Porco[3]

The spokes are intermittently appearing radial markings in Saturn's B ring that are believed to form when micrometer-sized dust particles are levitated above the ring by electrostatic forces. First observed by the Voyagers, the spokes disappeared from October 1998 until September 2005, when the Cassini spacecraft saw them reappear. The trajectories of the charged dust particles comprising the spokes depend critically on the background plasma density above the rings, which is a function of the solar elevation angle. Because the rings are more open to the Sun now than when Voyager flew by, the charging environment above the rings has prevented the formation of spokes until very recently. We show that this notable effect is capable of stopping spoke formation entirely and restricting the size of the particles in the spokes.

Voyagers and Cassini have collected images of spokes at Saturn (Fig. 1). These features, which are composed of micrometer-sized dust particles, are typically 10,000 km in length and 2000 km in width. Although they last for hours, there are indications that spokes form very rapidly (*1*, *2*). Observations of Saturn's rings by the Hubble Space Telescope (HST) (*3*) started around the time when Earth crossed Saturn's ring plane in 1995 and continued through 2004. The spokes were observed to fade as the ring opening angle (B') increased, which resulted from Saturn's orbital motion and its tilted axis of rotation changing the light-scattering geometry. The changing geometry accounted for the diminishing visibility of the spokes in the HST observations, because light must pass through the spokes at a shallow angle for them to be observed. On the basis of these arguments, Cassini was expected to see spokes during periods when it was near the ring plane (*3*). Contrary to these expectations (*4*), Cassini has not yet seen spokes on the illuminated side of the rings, despite many dedicated observations during its first 15 months in orbit, indicating that the spokes were largely absent. Here, we extend an earlier suggestion that the value of B' may affect spoke activity (*5*) and show that for large values of B', spokes cannot form at all.

Electrostatic interactions were suggested early on to explain spoke formation (*6*–*8*). The interactions involved a transient event to charge grains to sufficiently large potentials for lift-off from the ring. Meteorite impacts (*6*, *7*) or high-energy auroral electron beams (*8*) could create a region of sufficiently dense plasma immediately above the ring. This short-lived transient plasma charges the boulders of the main ring to a negative potential due to electron collection. A small fraction of the dust grains on the surface of the boulders collect an extra electron and are repelled from the surface by the electrostatic forces. For a few seconds after lift-off, the dust grains remain immersed in the short-lived dense plasma and are accelerated away from the ring. Subsequently, they leave the dense transient plasma cloud and enter the permanently present background plasma environment.

Voyager took spoke images that were separated by several minutes and observed fully formed spokes that were absent in the image taken just moments before (*2*). These observations indicate that spokes could form instantaneously over a large radial distance, as expected if they were triggered by a sheet of high-energy auroral electrons connecting the ionosphere to the ring (*8*). Alternatively, if spoke formation were triggered by meteorite impacts, the transient plasma cloud would have to drift along the full radial extent of the spokes in minutes (*6*, *7*, *9*, *10*). Cassini is capable of taking images at a much higher rate than Voyager and will be able to distinguish between these two models.

For our simulations, we assume that the meteorite impact model is correct and use the expected properties of the ambient and transient plasmas to calculate the potential on the ring, the charging of the dust grains, and the electrostatic forces acting on the grains, as well as to follow their trajectories above the ring. The source of the background plasma is believed to be photosputtering off the main ring followed by photoionization of the subsequent neutral exosphere (*11*). We take the plasma density to be proportional to $\sin(B')$ and use this density at the maximum opening angle ($B'_{\max} \cong 27°$) as a parameter, $n_{\max} = n_{H^+}(B' = B'_{\max})$, where n_{H^+} is the density of hydrogen ions. During Cassini's orbit insertion in July 2004 ($B' = 24.4°$), the density and the composition of the plasma above the main rings were measured (*12*). The plasma is composed of H^+ and $O_2{}^+$, as well as O^+ ions, with a density of $0.1 < n_{H^+} < 1$ cm^{-3} and mixing ratios of $n_{H^+}:n_{O^+}:n_{O_2{}^+} = 1:0.3:1$.

The equilibrium potential of the ring itself can be calculated by setting the sum of the currents equal to zero, $\sum_j I_j = 0$, where I_j represents the collection of electrons and ions, as well as the production of photoelectrons, all of which are functions of the potential of the ring, ϕ_r. The ring potential itself is a function of $n_{\max}$, and it remains independent of B', because all of the charging currents are proportional to $\sin(B')$. Based on Cassini plasma measurements, the ring potential is expected to be in the range of $-1.7 < \phi_r < 1.6$ V.

Because of the charging of the ring and the resulting electric field, the electron and ion densities immediately above the ring will not be equal. These densities can be calculated by considering the conservation of energy and flux, resulting in densities for all the species considered (*5*) as functions of ϕ. The potential in the plasma as a function of height above the ring is the solution of Poisson's equation

$$\frac{d^2\phi}{dz^2} = -4\pi e\left(n_{H^+} + n_{O^+} + n_{O_2^+} - n_e - n_v\right) \quad (1)$$

where e is the charge of an electron, and where in addition to the ion densities, we also consider

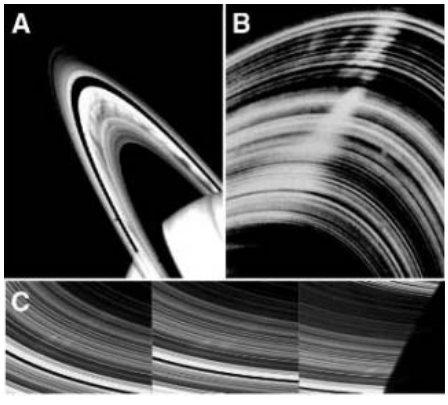

Fig. 1. (**A** and **B**) Voyager 2 images of spokes in the B ring (*1*, *2*). (A) An image captured in backscattered light before the closest encounter; the spokes appear as dark radial features across the ring plane. (B) An image taken in forward-scattered light after Voyager crossed the ring plane, looking back toward the Sun; the spokes appear as bright markings. Typical dimensions of these spokes are 10,000 km in length and 2000 km in width. The changing brightness indicates that spokes consist of small grains with radii comparable to the wavelength of the visible light (<1 μm). At the time these images were taken, the rings' opening angle to the sun was $B' = 8°$. (**C**) The first set of spoke observations by Cassini taken on 5 September 2005 ($B' = 20.4°$) over a span of 27 min. These faint and narrow spokes were seen from the unilluminated side of the B ring. These spokes are ≈3500 km long and ≈100 km wide, much smaller than the average spokes seen by Voyager. These images were taken with a resolution of 17 km per pixel at a phase angle of 145° when Cassini was 13.5° above the dark side of the rings as the spokes were about to enter Saturn's shadow. [Images courtesy NASA/Jet Propulsion Laboratory (JPL)–California Institute of Technology and NASA/JPL/Space Science Institute]

[1]Laboratory for Atmospheric and Space Physics, and Department of Physics, University of Colorado, Boulder, CO 80304–0392, USA. [2]Department of Physics, The Auroral Observatory, University of Tromsø, 9000 Tromsø, Norway. [3]Cassini Imaging Central Laboratory for Operations, Space Science Institute, Boulder, CO 80301, USA.

*To whom correspondence should be addressed. E-mail: horanyi@colorado.edu

the densities of the ambient electrons (n_e) and the photoelectrons (n_v) released from the ring. The boundary conditions for ϕ are $\phi(z = o) = \phi_r$, where z is the height above the ring, and there is no electric field far from the ring so that $\nabla\phi = 0$ at $z = 10\ \lambda_D$, where λ_D is the Debye length in the plasma. This length is typically tens of meters at the maximum plasma density and is a function of the plasma density ($\lambda_D \sim \sqrt{kT_e/n_e}$, where k is the Boltzmann constant, and T_e is the electron temperature), which varies as $\sin(B')$. Hence, the electric field, $E \cong \phi_r/\lambda_D$, increases as B' increases, even though the potential of the ring, ϕ_r, does not depend on this angle.

The motion of a spoke particle in one dimension can be followed by simultaneously integrating its equation of motion and the charging currents, including the effects of the electric field in the plasma sheath, gravity from the ring, and the z component of Saturn's gravitational field

$$\frac{d^2z}{dt^2} = \frac{-GMz}{r^3} - 2\pi G\sigma + \frac{q(t)}{m}E \qquad (2)$$

where G is the gravitational constant, M is Saturn's mass (5.8×10^{29} g), m is the grain's mass, r is the distance from Saturn, σ is the ring's surface-mass density (100 g/cm^2) (*13*), q is the charge on the dust grain, and E is the electric field. Initially, the electric field and the charging currents are set by the transient plasma cloud, and later by the ambient plasma environment.

Because we expect the transient plasma to be short lived, we subjected the dust grains to a dense plasma for a few seconds before switching to the ambient plasma environment. The transient plasma has a density of $n_T = 100$ cm^{-3} and is assumed to be dominated by oxygen ions with a temperature of 2 eV (*7*). Independently of B', this produces a negatively charged ring with a potential of about $\phi_r \cong -9$ V and a plasma sheath with a Debye length of $\lambda_D \cong 1$ m. Even in this dense plasma, the surface charge density on the ring remains low and most dust particles on the boulders remain uncharged. The small fraction of the grains that collect an electron will be lifted off the ring by the electric field. Although the source of the dense plasma and its dynamics are still being debated (*9*, *10*), the details are unimportant to our model because the dust grains will be singly charged and exposed to a short-lived electric field regardless of which formation theory is correct.

For a low ambient plasma density (*12*), the ring remains at a positive potential, independent of B'. For example, when $n_{max} = 0.11$ cm^{-3}, $\phi_r = 1.5$ V, and there is an abrupt change in the lifetime of the dust grains as a function of B' (Fig. 2). In the transient plasma, the characteristic time for a grain with a radius of 0.5 μm to lose its excess electron and collect an ion is about 10 s. Because this transient plasma is expected to dissipate in seconds (*6*), most of the small grains will emerge either with their excess negative charge or neutral. Grains that are too large quickly collect an excess ion and immediately fall back down to the ring, never leaving the transient plasma cloud. The subsequent charging of the small grains that escape the transient plasma cloud depends on the ambient plasma density. If this plasma density were high, the grain charging would be dominated by electron collection and the grains would collect a negative charge and fall back down to the ring, which by this time would have returned to its usual positive potential. In a low plasma density environment, the small grains would charge positively, due to the dominating photoelectron current. In this case, the grains continue to be repelled by the ring and can form spokes.

We followed the trajectories of grains with radii up to 10 μm in diameter (Fig. 3). For $n_{max} = 0.11$ cm^{-3}, there is an abrupt increase of the lifetime as B' drops below 20°, indicating the transition between periods when spokes cannot form and when they will be abundant. The value of B' at which the spokes turn on and off is a function of n_{max}. From the Cassini plasma measurements (*12*), the maximum plasma density is in the range of $0.1 < n_{max} < 1$ cm^{-3}. Taking $n_{max} = 0.11$ cm^{-3}, we can match the Cassini imaging observations of the recent reappearance of the spokes in September of 2005 on the unilluminated rings if we assume that these dark-side spoke sightings are indeed observations of day-side spokes seen through the rings. For different values of n_{max}, the behavior can be markedly different. For example, for $n_{max} \approx 0.23$ cm^{-3}, $\phi_r \cong 0$, and spokes would form for any value of B'. For even larger values of n_{max}, spokes would form only for large values of B', contradicting the observations. For the range $0.1 < n_{max} < 0.2$, the onset of the spoke activity shifts by several degrees and the higher plasma densities reduce the range of B' where spokes can form.

The upper cut-off in the lifetime of particles as a function of their size depends on the properties of the transient plasma. The larger particles that lose their excess electron too quickly are rapidly pulled back down to the ring without ever leaving the transient plasma cloud. This is consistent with the photometry of the spokes indicating the lack of particles bigger than a few micrometers (*14*).

The sudden reappearance of the spokes to Cassini at $B' \cong 20°$ indicates that the plasma density above the rings must be close to the lower limit indicated by the in situ measurements (*12*). Notably, if spoke activity switches

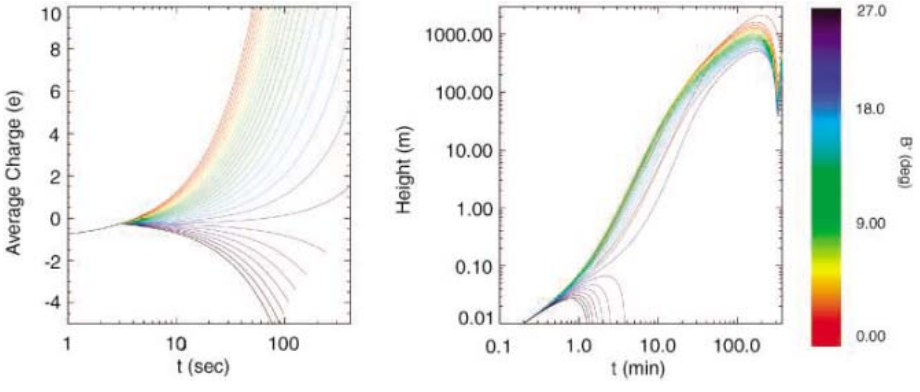

Fig. 2. Charging histories (**left**) and trajectories (**right**) for 0.5-μm dust grains started with one excess electron for different values of B'. The particles are initially in the transient dense (n_T = 100 cm^{-3}) plasma for 3 s, after which the plasma is changed to the ambient plasma sheath with n_{max} = 0.11 cm^{-3}. Color denotes B'. For opening angles smaller than $B' \approx 20°$, particles in the ambient plasma are charged positively because the photoelectric effect produces a larger current than that produced by electron collection. Because the electric field points away from the ring, the grains are accelerated upward and form a spoke. For larger values of B', the plasma density increases enough to charge the grains negatively as the electron collection current becomes dominant. In this case, the dust grains are quickly pulled back down onto the ring, preventing the formation of spokes.

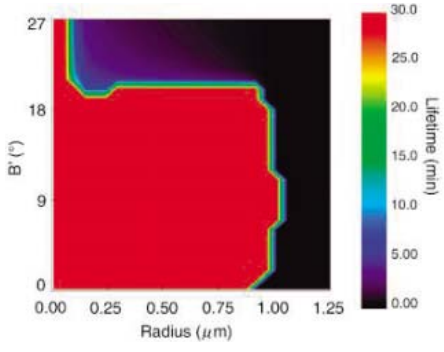

Fig. 3. The lifetime of dust particles above the ring as a function of B' and particle size. The abrupt change in the lifetime of the particles with radii $0.1 < a < 1$ μm, as indicated by the sharp color transition from red to purple at $B' = 20°$, indicates that spoke activity is expected to turn on and off rapidly as a function of B'. The exact value at which this transition happens is a function of the ambient plasma density n_{max}. The cut-off for large particles is a function of the amount of time the grains spend in the transient plasma.

off for $|B'| > 20°$, we expect spoke activity for about 8 years at a time, followed by a period without spokes that lasts 6 to 7 years. Within a few days of the dark-side spoke sightings on 5 September (Fig. 1), Cassini captured several series of excellent images of the lit side without any indications of spokes. Hence, the recently seen spokes might just represent an "early-bird" event, before the onset of the main spoke season. If these 5 September spokes were indeed the start of the main season, the background plasma density must be on the order of $n_{max} \approx 0.1\ cm^{-3}$. However, if the HST observations of the last spoke sighting ($B' = 15°$) correspond to the start of the off season, this would require $n_{max} \approx 0.2\ cm^{-3}$, and spoke activity will not be expected to return until late 2006. In summary, spokes are expected to be seen if the plasma conditions are favorable for their formation and either the observer or the Sun is near the ring plane. Currently, Cassini is orbiting too close to the ring plane and cannot make any observations. We expect that spoke activity will have returned by the time its inclination increases again in July of 2006.

References and Notes

1. B. A. Smith *et al.*, *Science* **212**, 163 (1981).
2. B. A. Smith *et al.*, *Science* **215**, 504 (1982).
3. C. A. McGhee *et al.*, *Icarus* **173**, 508 (2005).
4. M. Horányi, T. W. Hartquist, O. Havnes, D. A. Mendis, G. E. Morfill, *Rev. Geophys.* **42**, RG4002 (2004).
5. T. Nitter, O. Havnes, F. Melandsø, *J. Geophys. Res.* **103**, 6605 (1998).
6. G. E. Morfill, C. K. Goertz, *Icarus* **55**, 111 (1983).
7. C. K. Goertz, G. Morfill, *Icarus* **53**, 219 (1983).
8. J. R. Hill, D. A. Mendis, *Moon Planets* **24**, 431 (1981).
9. A. J. Farmer, P. Goldreich, *Icarus* **179**, 535 (2005).
10. G. E. Morfill, H. M. Thomas, *Icarus* **179**, 539 (2005).
11. R. L. Tokar *et al.*, *Geophys. Res. Lett.* **32**, L14S04 (2005).
12. J. H. Waite Jr. *et al.*, *Science* **307**, 1260 (2005).
13. J. N. Cuzzi *et al.*, in *Planetary Rings*, R. Greenberg, A. Brahic, Eds. (Univ. of Arizona Press, Tucson, AZ, 1984), pp. 73–199.
14. L. R. Doyle, E. Grün, *Icarus* **85**, 168 (1990).

15. This work was supported by the Cassini project. We benefited from discussions on ring dynamics at the Second Midnight Sun Workshop in Tromsø, supported by the Norwegian Research Council.

13 December 2005; accepted 13 February 2006
10.1126/science.1123783

Visualizing Picometric Quantum Ripples of Ultrafast Wave-Packet Interference

Hiroyuki Katsuki,[1,2,3] Hisashi Chiba,[1,2] Bertrand Girard,[4] Christoph Meier,[4]* Kenji Ohmori[1,2,3]*

Interference fringes in vibrating molecules are a signature of quantum mechanics, but are often so short-lived and closely spaced that they elude visualization. We have experimentally visualized dynamical quantum interferences, which appear and disappear in less than 100 femtoseconds in the iodine molecule synchronously with the periodic crossing of two counterpropagating nuclear wave packets. The obtained images have picometer and femtosecond spatiotemporal resolution, representing a detailed picture of the quantum interference.

Interference is a clear manifestation of the quantum-mechanical wave character of a physical system (*1*, *2*). It has been visualized in the past decade through compelling experiments involving the translational degree of freedom of atoms (*3*–*6*), complex molecules (*7*), and even Bose-Einstein condensates (*8*).

Interferences have also been observed in the relative motion of the nuclei in molecules. In predissociative states, partial reflection of the oscillating wave packet produces a sequence of equally spaced partial wave packets on the dissociative part of the potential. Interferences of these wave packets are a direct consequence of the natural spreading of matter waves (*9*). Interferences can also be produced by creating a sequence of two partial wave packets on the same dissociative potential. Again, overlap and interferences result from natural spreading of the wave packets during their propagation (*10*, *11*).

In all these examples, the partial wave packets are propagating in the same direction, and the interference pattern, which involves components from the different partial waves having the same momentum, is very stable in time. The situation for counterpropagating wave packets is completely different. The interference pattern is localized in space only during the crossing time. High temporal and spatial resolutions, and strong robustness toward averaging effects, are required to observe it. A wave packet oscillating in an anharmonic well provides a natural situation for such interferences.

When several quantum states of a weakly anharmonic system are excited coherently, the time evolution of such a system is characterized by a "revival" phenomenon: An initially well-localized wave packet at first disperses, and then relocalizes after some well-defined revival time and regains its original shape. This effect had been theoretically predicted (*12*–*14*) and was later experimentally verified for a large number of very different quantum systems, e.g., atomic Rydberg states (*15*, *16*) or molecular vibrational levels (*17*–*24*) excited by broadband ultrashort laser pulses. Furthermore, at a certain, well-defined earlier time (half-revival time), the wave packet consists of two copies of the initial wave packet, shifted by half a vibrational period. As has been shown theoretically (*25*), in this special situation, the two counterpropagating wave packets produce pronounced interference structures when they cross. Additionally, a detailed theoretical treatment shows that the fringes are out of phase for subsequent crossing events.

Here, we use a laser pump-probe scheme to visualize this event. The interaction with the pump pulse centered around 587 nm creates a vibrational wave packet in the electronic B state of I_2, widely studied in the gas phase (*17*–*21*) as

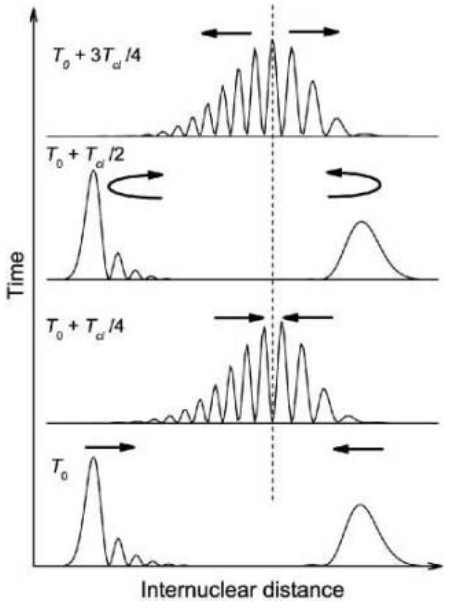

Fig. 1. Evolution of the two wave packets (probability distributions $|\Psi(r,T)|^2$) around the half-revival time ($T_0 = pT_{cl} \cong T_{rev}/4$, p integer). At T_0, the two wave packets are localized at the turning points and start to propagate toward each other. At $T_0 + T_{cl}/4$, the two wave packets overlap and interfere, creating a stationary wave that lasts during their whole crossing. At $T_0 + T_{cl}/2$, the two wave packets are at the opposite turning points and start to come back. At $T_0 + 3T_{cl}/4$, the wave packets intersect once more. The stationary wave resulting from their interference is phase shifted by π as compared to the previous crossing (see the vertical dashed line).

[1]Institute for Molecular Science, Myodaiji, Okazaki 444-8585, Japan. [2]Core Research for Evolution of Science and Technology, Japan Science and Technology Agency, Japan. [3]The Graduate University for Advanced Studies (SOKENDAI), Myodaiji, Okazaki 444–8585, Japan. [4]Laboratoire Collisions, Agrégats, Réactivité, CNRS UMR 5589, Institut de Recherche sur les Systèmes Atomiques et Moléculaires Complexes, Université Paul Sabatier–Toulouse 3, France.

*To whom correspondence should be addressed. E-mail: chris@irsamc.ups-tlse.fr (C.M.), ohmori@ims.ac.jp (K.O.)

well as in a solid matrix environment (*26*). Due to the large spectral width of the laser pulse, several vibrational levels around $\tilde{n} \sim 14$ are excited coherently to form a localized wave packet, which is a superposition of vibrational eigenstates of energy E_n. The classical vibrational period (T_{cl}) and the revival time (T_{rev}) are given by (*12*, *27*)

$$\left(\frac{dE_n}{dn}\right)_{n=\tilde{n}} = \frac{2\pi\hbar}{T_{cl}}, \left|\left(\frac{d^2E_n}{dn^2}\right)_{n=\tilde{n}}\right| = \frac{4\pi\hbar}{T_{rev}} \quad (1)$$

The iodine B state is spectroscopically well known, and for $\tilde{n} \sim 14$ we find the values of $T_{cl} \sim 0.3$ ps and $T_{rev} \sim 37$ ps (*28*). Here $T_{rev} \gg T_{cl}$, which results from the weak anharmonicity in the excitation region. At times around $T_{rev}/4 \sim 9.3$ ps, the half-revival occurs as described above. Two wave packets, shifted by half the vibrational period, oscillate in the potential well (Fig. 1). Theory predicts a spatial nodal structure for internuclear distances between 3.1 and 3.4 Å, where the two fractional wave packets cross. The important point is that, due to phase shifts at reflection [for a detailed discussion, see (*25*, *29*)], the nodal structure being formed when the two partial wave packets intercept differs for two subsequent passages: Maxima turn into minima and vice versa (see the vertical dashed line in Fig. 1).

Observing these nodal structures experimentally is challenging. Coulomb explosion methods (*30*) have the advantage of taking snapshots of the whole wave function at once and have been used to image nuclear wave functions (*10*). However, the demonstrated resolution is not sufficient and is better suited for longer internuclear distances; strong bias is present at small distances due to deviations from Coulombic potential (*11*). Also, time-resolved photoelectron spectroscopy has successfully been used to map moving vibrational wave packets (*31*), but the energy resolution did not allow for the observation of details of the wave functions on a picometric scale. Alternatively, using an optical probe transition between two neutral molecular states offers excellent selectivity. The difficulty is to achieve the required spatial and temporal resolutions.

Our scheme (Fig. 2) maps the vibrational wave-packet motion into a measurable signal by using a probe pulse resonant to some higher-lying electronic state at an internuclear distance called the "transient Franck-Condon point." Probe wavelengths (λ_{pr}) between 382 and 391 nm induce a transition to the E state, from which fluorescence is observed as a function of delay time between the pump and probe pulses. By varying the probe wavelength, we selectively excite the molecule at different internuclear distances. Each probe wavelength intercepts a different slice of the wave function, allowing us to monitor the crossing in time and space. Under the conditions of the experiment to be described below, and considering a Gaussian probe pulse $\mathcal{E}(t) = \mathcal{E}_0 e^{-t^2/\tau_{pr}^2} e^{-i\omega_{pr}t}$ of duration τ_{pr}, the pump-probe signal $P_{\lambda_{pr}}$ for a probe frequency

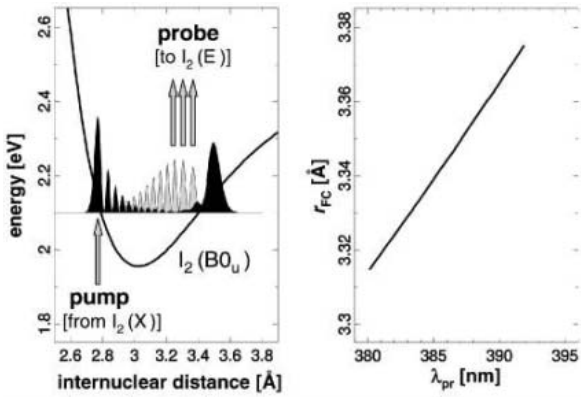

Fig. 2. (**Left**) Potential energy surface of the $B0_u^+$-state of I_2 together with the vibrational wave packet (probability density $|\Psi(r,T)|^2$) at two times around the half-revival time, showing two moving wave packets creating an interference pattern while intercepting each other. (**Right**) Transient Franck-Condon point (r_{FC}) as a function of probe wavelength (λ_{pr}).

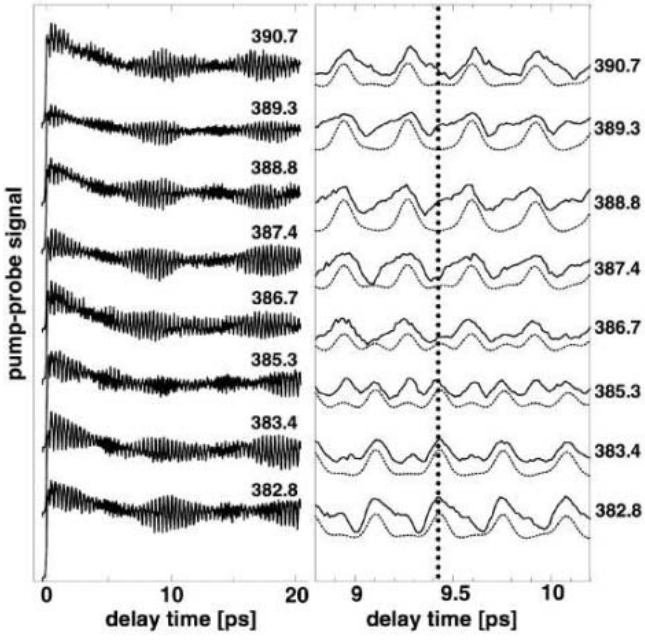

Fig. 3. (**Left**) Experimental pump-probe signals, using a 587-nm pump pulse and probe pulses with different central wavelengths, as indicated (in nm). Each experimental curve was normalized by the signal intensities around its first three oscillations, and its zero delay was adjusted to superimpose its first three oscillations to those of the theoretical one. (**Right**) Magnified area of the experimental results between 9 and 10 ps, together with theoretical simulations (dashed lines), showing the change from maxima into minima as the probe wavelength is changed.

ω_{pr} as a function of the delay time T can be shown to be given by (*32*, *33*)

$$P_{\lambda_{pr}}(T) \sim \int dr\, e^{-\frac{\tau_{pr}^2}{2\hbar^2}[V_E(r) - V_B(r) - \hbar\omega_{pr}]^2} \left|\psi(r,T)\right|^2 \quad (2)$$

where $V_B(r)$ and $V_E(r)$ are the potentials of the B and E electronic states, respectively. This expression clearly reflects the fact that the pump-probe signal measures the modulus square of the vibrational wave packet within a Franck-Condon window Δr_{FC}, around the Franck-Condon point r_{FC}, defined as the internuclear distance where $V_E(r_{FC}) - V_B(r_{FC}) = \hbar\omega_{pr}$ holds. The dependence of the Franck-Condon point on the probe wavelength is found to be almost linear (Fig. 2, right panel). To resolve the nodal structure, we require the width of the Franck-Condon window

$$\Delta r_{FC} = \frac{2\hbar\sqrt{2\ln 2}}{\tau_{pr}\left|\frac{d}{dr}[V_E(r) - V_B(r)]\right|} \quad (3)$$

to be smaller than half of the de Broglie wavelength (λ_{dB}) of the moving wave packet. This relation sets an upper limit to the pulse spectral width and therefore a lower limit for the pulse duration. On the other hand, to observe the π-phase shift at two subsequent crossings requires the pulse duration to be shorter than half the vibrational period.

Under these conditions, the pump-probe spectrum is approximately given by

$$P_{\lambda_{pr}}(T) \sim \left|\psi\left(r_{FC}(\lambda_{pr}), T\right)\right|^2 \quad (4)$$

and it is clear from Fig. 2 (right panel) that by scanning the probe wavelength from 382 to 391 nm, one can measure the modulus square of the vibrational wave packet at internuclear distances between 3.32 and 3.37 Å.

Based on the experimental parameters (see below), one can estimate $\lambda_{dB} \sim 0.08$ Å and $\Delta r_{FC} \sim 0.014$ Å, deduced from the probe bandwidth and from Fig. 2. Furthermore, because $T_{cl} \sim 330$ fs, the condition $\tau_{pr} < T_{cl}/2$ is also satisfied. Hence, we see that under these experimental conditions, an observation of the transient,

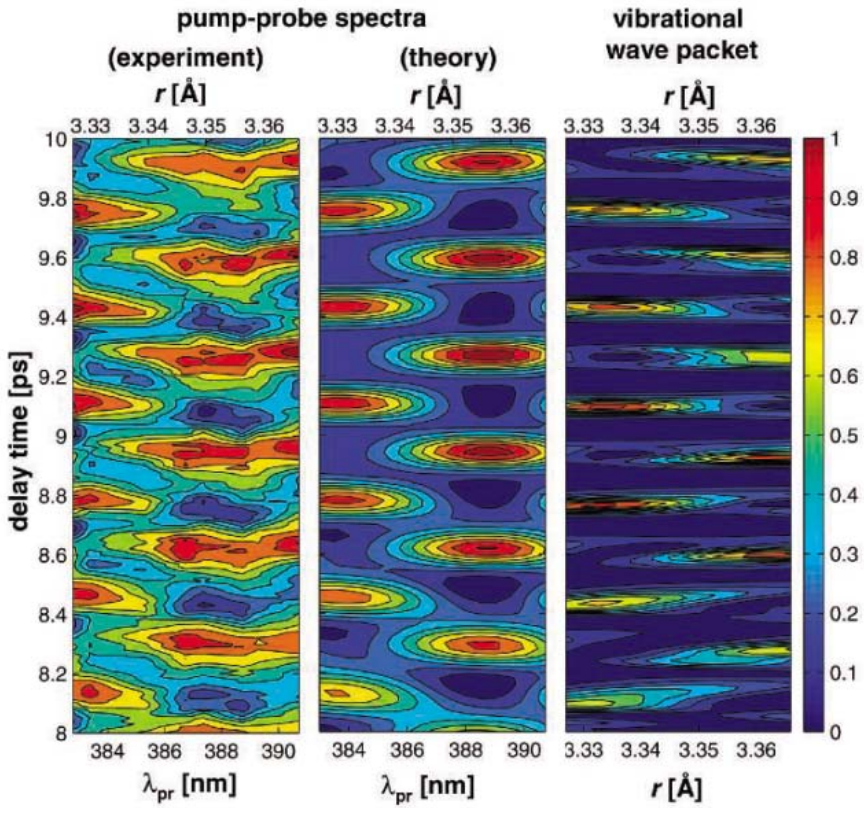

Fig. 4. Contour plots of the experimental pump-probe signal (**left**), the simulated pump-probe signal (**middle**), and parts of the vibrational wave packet (**right**). The pump-probe spectra clearly reflect the spatiotemporal nodal structure of the wave-packet interferences.

picometric interference structures that appear at delay times of ~9.3 ps and at internuclear distances around 3.3 Å should be possible.

The experimental setup is similar to the one described elsewhere (*29*, *34*). The I_2 molecule was prepared in the electronic ground state X by expansion of a heated I_2/Ar mixture (~310 K, ~1 atm) into a vacuum chamber through a nozzle. The output of a Ti:sapphire laser system (pulse width ~100 fs, repetition rate 1 kHz; Quantronix, Titan) was used to pump two Optical Parametric Amplifiers (Quantronix, TOPAS). Their outputs were used as the pump and probe pulses, tuned around 587 nm and 382 to 391 nm, respectively, and polarized parallel to each other. The typical bandwidths were ~10 nm for the pump pulse and ~2.6 nm for the probe pulse. The rotational and vibrational temperatures of the ensemble of I_2 molecules were estimated to be ~15 K and ~220 ± 40 K, respectively, from the B-X fluorescence excitation spectra measured with another narrow-band dye laser under similar conditions (*35*). Therefore, the observed signal was the sum of the contributions from the initial rotational and vibrational levels distributed under the present temperatures, weighted by the Franck-Condon factors of the relevant transitions.

At short times, the oscillating signal reflecting the vibrational wave-packet motion is clearly visible (Fig. 3). After about 5 ps, the clear oscillation vanishes due to the dispersion of the wave packet. Around ~9 ps, the oscillations become pronounced again, but at this time, they are very sensitive to the probe wavelength, as evidenced in an expanded plot between 9 and 10 ps (Fig. 3, right panel, solid lines). A careful inspection of the maxima and minima (guided by the dotted line in the figure) reveals that as the probe wavelength is tuned from 382 to 391 nm, the maxima smoothly turn into minima, while passing through a double-peak structure at 385.3 nm. The reason for this behavior can be understood from Fig. 2: While scanning from 382 to 391 nm, the probe has swept the internuclear distance from 3.32 to 3.37 Å, thus detecting the nodal structure of the wave packet in this spatiotemporal region. This interpretation also explains the extreme sensitivity to the probe parameters used. Furthermore, the finding confirms that a pump-probe spectrum cannot be interpreted without taking the probe step carefully into account (*21*, *36*, *37*).

A theoretical simulation (Fig. 3, right panel, dotted lines) reproduces well the gradual change from maxima to minima as the probe wavelength is tuned from 382 to 391 nm. These simulations are performed along the lines described in (*25*, *29*), including the pump and probe polarizations, rotations, and vibrations, as well as a statistical ensemble of initially prepared rovibrational levels (vibrational temperature of 170 K, rotational temperature of 15 K). The very good agreement with the experimental results clearly confirms the interpretation of the measured signals.

An especially interesting situation occurs when the detection is tuned to a node in the interference structure, e.g., at 9.42 ps and for probe wavelengths between 387 and 389 nm. In this case, the two wave packets pass the detection window simultaneously, but without being detected, leading to a minimum in the pump-probe signal (see the vertical dotted line in Fig. 3, right panel). The detection of the moving wave packets only takes place when the modulus square of the wave function is nonzero at the detection point. Because the same interference structure appears in steps of T_{cl}, the signal exhibits a periodicity of T_{cl}, despite the presence of two fractional wave packets at that time. Every second passage, the two oscillating wave packets are not detected due to the nodal structure of the moving wave packets at the intersection region.

Based on the experimental data shown in Fig. 3 (after subtraction of a slowly varying background), Fig. 4 gives a contour plot of the experimental results (left panel), the simulated pump-probe signals (middle panel), and a vibrational wave packet (right panel) around 8 to 10 ps at the region of interest. The wave packet shown in the right panel corresponds to the one calculated by laser excitation from the initial vibrational level $n_X = 1$, which yields the highest contribution to the signal. The simulated pump-probe spectrum (middle panel) is calculated as a Boltzmann average over all initial rovibrational levels corresponding to a rotational and vibrational temperature of 15 and 170 K, respectively. A slight shift (by ~0.8 nm) is observed between the experimental (left panel) and simulated (middle panel) plots. It may be partly attributed to asymmetries in the pump spectrum, which were not taken into account in the simulation. Other possible reasons for this shift are errors in the probe wavelength calibration. This shift also explains slight discrepancies observed in the comparison between experimental data and theoretical simulations shown in Fig. 3.

Using the relationship between r_{FC} and the probe wavelength (Fig. 2, right panel), the probe wavelengths of both the experimental and simulated spectra can be directly translated into an internuclear distance, shown on the upper horizontal axis of Fig. 4. Using this correspondence, a direct comparison with the moving wave packet clearly shows that we have succeeded in measuring the nodal structure of the quantum matter interferences as implied by Eq. 4. The features are resolved on a picometer length scale, and evolve dynamically on the femtosecond time scale.

References and Notes

1. L. Marton, J. Arol Simpson, J. A. Suddeth, *Phys. Rev.* **90**, 490 (1953).
2. C. Davisson, L. H. Germer, *Phys. Rev.* **30**, 705 (1927).
3. O. Carnal, J. Mlynek, *Phys. Rev. Lett.* **66**, 2689 (1991).

4. D. W. Keith, C. R. Ekstrom, Q. A. Turchette, D. E. Pritchard, *Phys. Rev. Lett.* **66**, 2693 (1991).
5. M. Kasevich, S. Chu, *Phys. Rev. Lett.* **67**, 181 (1991).
6. P. Szriftgiser, D. Guery-Odelin, M. Arndt, J. Dalibard, *Phys. Rev. Lett.* **77**, 4 (1996).
7. B. Brezger *et al.*, *Phys. Rev. Lett.* **88**, 100404 (2002).
8. M. R. Andrews *et al.*, *Science* **275**, 637 (1997).
9. J. Degert, C. Meier, B. Chatel, B. Girard, *Phys. Rev. A.* **67**, 041402 (2003).
10. E. Skovsen, M. Machholm, T. Ejdrup, J. Thøgersen, H. Stapelfeldt, *Phys. Rev. Lett.* **89**, 133004 (2002).
11. C. Petersen, E. Péronne, J. Thøgersen, H. Stapelfeldt, M. Machholm, *Phys. Rev. A.* **70**, 033404 (2004).
12. I. S. Averbukh, N. F. Perelman, *Phys. Lett. A* **139**, 449 (1989).
13. O. Knospe, R. Schmidt, *Phys. Rev. A.* **54**, 1154 (1996).
14. C. Leichtle, I. S. Averbukh, W. P. Schleich, *Phys. Rev. Lett.* **77**, 3999 (1996).
15. J. A. Yeazell, M. Mallalieu, C. R. Stroud Jr., *Phys. Rev. Lett.* **64**, 2007 (1990).
16. J. A. Yeazell, C. R. Stroud Jr., *Phys. Rev. A.* **43**, 5153 (1991).
17. R. M. Bowman, M. Dantus, A. H. Zewail, *Chem. Phys. Lett.* **161**, 297 (1989).
18. M. Gruebele, A. H. Zewail, *J. Chem. Phys.* **98**, 883 (1993).
19. I. Fischer, D. M. Villeneuve, M. J. J. Vrakking, A. Stolow, *J. Chem. Phys.* **102**, 5566 (1995).
20. M. J. J. Vrakking, D. M. Villeneuve, A. Stolow, *Phys. Rev. A.* **54**, R37 (1996).
21. I. Fischer, M. J. J. Vrakking, D. M. Villeneuve, A. Stolow, *Chem. Phys.* **207**, 331 (1996).
22. T. Baumert, V. Engel, C. Röttgermann, W. T. Strunz, G. Gerber, *Chem. Phys. Lett.* **191**, 639 (1992).
23. I. S. Averbukh, M. J. J. Vrakking, D. M. Villeneuve, A. Stolow, *Phys. Rev. Lett.* **77**, 3518 (1996).
24. J. Heufelder, H. Ruppe, S. Rutz, E. Schreiber, L. Wöste, *Chem. Phys. Lett.* **269**, 1 (1997).
25. T. Lohmüller, V. Engel, J. A. Beswick, C. Meier, *J. Chem. Phys.* **120**, 10442 (2004).
26. Z. Bihary, R. Zadoyan, M. Karavitis, V. A. Apkarian, *J. Chem. Phys.* **120**, 7576 (2004).
27. W. P. Schleich, *Quantum Optics in Phase Space* (Wiley-VCH, Berlin, 2001).
28. H. Knöckel, B. Bodermann, E. Tiemann, *Eur. Phys. J. D* **28**, 199 (2004).
29. Materials and methods are available as supporting material on *Science* Online.
30. H. Stapelfeldt, E. Constant, P. B. Corkum, *Phys. Rev. Lett.* **74**, 3780 (1995).
31. A. Assion, M. Geisler, J. Helbing, V. Seyfried, T. Baumert, *Phys. Rev. A.* **54**, R4605 (1996).
32. M. Braun, C. Meier, V. Engel, *J. Chem. Phys.* **103**, 7907 (1995).
33. L. W. Ungar, J. A. Cina, *Adv. Chem. Phys.* **100**, 171 (1997).
34. K. Ohmori *et al.*, *Phys. Rev. Lett.* **96**, 093002 (2006).
35. The rotational-level dependence of the predissociation yield of the B state was not taken into account.
36. G. Grégoire *et al.*, *Eur. Phys. J. D* **1**, 187 (1998).
37. C. Nicole *et al.*, *J. Chem. Phys.* **111**, 7857 (1999).

38. Fruitful discussions with A. Beswick, V. Blanchet, V. Engel, T. Lohmüller, and J. Vigué are gratefully acknowledged. This work has been supported by Institute for Molecular Science and by SAKURA (Ministère des Affaires étrangères–Japan Society for the Promotion of Science) international exchange programs, as well as by Grant-in Aid from the Ministry of Education, Culture, Sports, Science and Technology of Japan (15204034, and Priority Area: "Control of Molecules in Intense Laser Fields") and by Calcul en Midi-Pyrénées (Toulouse) and Centre Informatique National de l'Enseignement Supérieur (Montpellier) computer facilities.

Supporting Online Material

www.sciencemag.org/cgi/content/full/311/5767/1589/DC1
Materials and Methods
Figs. S1 and S2
References

11 October 2005; accepted 3 January 2006
10.1126/science.1121240

MOSFET-Embedded Microcantilevers for Measuring Deflection in Biomolecular Sensors

Gajendra Shekhawat,[1,2]* Soo-Hyun Tark,[3] Vinayak P. Dravid[1,2,3]*

A promising approach for detecting biomolecules follows their binding to immobilized probe molecules on microfabricated cantilevers; binding causes surface stresses that bend the cantilever. We measured this deflection, which is on the order of tens of nanometers, by embedding a metal-oxide semiconductor field-effect transistor (MOSFET) into the base of the cantilever and recording decreases in drain current with deflections as small as 5 nanometers. The gate region of the MOSFET responds to surface stresses and thus is embedded in silicon nitride so as to avoid direct contact with the sample solution. This approach, which offers low noise, high sensitivity, and direct readout, was used to detect specific binding events with biotin and antibodies.

The microcantilever detection approach has attracted considerable attention as a means of label-free detection of biomolecules (*1*–*6*) in recent years. The specific biomolecular binding between ligands and receptors on the surface of a microcantilever beam results in physical bending of the beam by some tens of nanometers (*2*–*6*). The origin of this nanomechanical bending of such a hybrid structure is driven by a change in the surface stress caused when ligands bind to receptors, which leads to a differential bending moment.

The prevailing methods for measuring the microcantilever bending involve optical (*1*–*6*), piezoresistive (*7*–*13*), and capacitance (*14*) detection technologies, but each method has some limitations. For example, Majumdar and coworkers (*6*) have developed a microcantilever array for multiplexed biomolecular analysis based on a two-dimensional (2D) charge-coupled device (CCD) optical readout to monitor the microcantilever deflection. Optical detection systems are less amenable to monolithic integration and are not readily amenable to massively parallel and highly multiplexed detection because of difficulties in laser alignment and power management. Also, optical detection systems have limited use in situations of turbid or opaque fluidic and smoky environment where light scattering can compromise detection.

Recently, piezoresistive detection (*7*–*13*) has emerged as an alternative to optical detection because it is compatible with aqueous media and allows parallel microcantilever arrays to be implemented for detecting multiple analytes at the same time. However, because the piezoresistors cover a large length of the cantilever and high doping levels are required, the stress measurement is not localized. Thus, piezoresistive detection suffers from inevitable thermal and electronic noise, thermal drifts, nonlinearity in piezo-response, conductance fluctuation noise (usually called flicker or 1/*f* noise), cycle fatigue, and inadequate sensitivity to very small cantilever deflections. Moreover, microcantilever bending of more than 50 nm is required to detect measurable and reproducible piezoresistance, so this method is insensitive to low concentrations of bimolecular species. Capacitance readout (*14*) is based on change in the gap due to microcantilever deflection, which results in the change in the capacitance between two conductor plates. Capacitance readout suffers from inevitable interference with the variations in the dielectric constant of the fluidic media.

Here, we report the use of 2D microcantilever arrays with geometrically configured metal-oxide semiconductor field-effect transistors (MOSFETs) embedded in the high-stress region of the microcantilevers to measure deflections induced by biomolecular binding. Finite-element modeling was used to optimize the change in the drain current of the MOSFETs buried in the microcantilevers.

FET-based stress sensors are widely reported for micromechanical devices such as accelerometers, resonators, and parallel cantilevers for scanning probe microscopy, as well as for residual stress measurements (*15*–*20*). When a microcantilever bends as a result of adsorption-induced surface stress, modulation of the channel current underneath the gate region results from altered channel mobility of the transistor due to increased channel resistance. As fixed biased voltages are applied on the gate and source-drain region of the transistor, any change in channel mobility will result in change in the drain current of the transistor. Apart from a decrease in channel conductivity, the channel mobility is also affected by the generation of trap states and band structure alteration. However, these stress sensors have not been configured for high sensitivity for small

[1]International Institute for Nanotechnology, [2]NU*ANCE* Center, [3]Department of Materials Science and Engineering, Northwestern University, Evanston, IL 60208, USA.

*To whom correspondence should be addressed. E-mail: g-shekhawat@northwestern.edu; v-dravid@northwestern.edu

changes in the drain current, nor used for nanomechanical biomolecular sensor applications. Because MOSFETs and contact pads are passivated with a thin coating of silicon nitride, they are inherently protected from any environmental influence; thus, their performance is not compromised by contact with gases or corrosive liquids such as saline solution.

The MOSFET-embedded microcantilever detection approach is illustrated in Fig. 1. To achieve high sensitivity, we must detect deflections as small as 5 to 10 nm (Table 1). The MOSFETs were engineered for optimal source-drain doping concentration and depth, channel doping, and transistor width/length ratio, taking into account their location at a high-stress region (the cantilever base) (*21*) and their geometrical configuration (i.e., thickness and length of the cantilever). The optimized design minimizes the electronic noise by (i) selecting localized doping regions on moderately resistive Si cantilevers (10 to 15 ohm·cm) to reduce unwanted noise due to carriers; (ii) precisely controlling the doping region thickness, width, and carriers to optimize the mobility; (iii) having a sharp dopant step profile; and (iv) using a large gate area to suppress $1/f$ noise. The optimized MOSFET-embedded microcantilevers exhibit measurable, consistent, and reproducible change in the drain current, even for deflections as small as 5 nm.

The microcantilevers were fabricated from SOI (silicon-on-insulator) wafers with a buried oxide etch-stop layer (2.5 μm) and an epitaxial silicon layer (1.5 μm). Initially, 50 × 1 cantilever arrays were fabricated with the standard microelectromechanical systems (MEMS) technology (*22*).

Embedded n-type MOSFET transistors were fabricated on each individual microcantilever by the standard complementary MOS (CMOS) approach, wherein the transistors were located at the rear part of the cantilever where surface stress is the highest (*21*). Once the process was completed and the MOSFETs were tested for their functionality, microcantilever shapes were defined. Metal contacts to the gate, source, and drain of individual microcantilevers were then made by contact lithography. Finally, the 2.5-μm oxide layer was etched to release the microcantilevers from the top. The transistor design process was simplified with only four masks and minimal process steps for ease of fabrication.

Scanning electron microscopy (SEM) images of one pair of identical cantilevers from an initial 50 × 1 microcantilever array are shown in Fig. 2A. The pair consists of one microcantilever coated with a thin film of gold for immobilization of probe molecules, typically with thiol chemistry, and the other is uncoated and acts as the reference. The differential drain current between the sensing and the reference microcantilevers, which further minimizes systematic noise and environmental perturbations, forms the basis for the MOSFET electronic detection (Fig. 1). The differential signal can be fed into a CMOS-based differential amplifier for electronic readout at the chip level for future development. A magnified view (Fig. 2B) shows the contact leads and the physical separation of the Cr/Au layer and the contacts. MOSFET-embedded microcantilevers with thickness of 1.5 to 2 μm and length ranging from 200 to 300 μm were fabricated. In each case, the separation between the reference and sensing microcantilevers was about 250 μm for simplicity, the transistor was located about 2 to 4 μm from the cantilever base, and the width/length ratio of source and drain was around 10 to allow for high transconductance. The resonance frequency of the MOSFET-embedded microcantilevers was around 100 to 150 kHz. Each array was designed to have identical sensor (i.e., Cr/Au-coated) and SiN_x reference microcantilevers for differential output to minimize systematic noise and possible false positives. The residual stress that may be introduced by applying a thin layer (30 nm) of gold coating on one side of the cantilever does not create a notable difference in MOSFET current-voltage characteristics when compared with those of SiN_x reference cantilevers.

We validated the drain current sensitivity of MOSFET-embedded microcantilevers to bending with the use of a high-resolution nanomanipulator with a vertical (z-axis) resolution of <5 nm. As the nanomanipulator bent the cantilever downward in steps of 5 nm, the corresponding current-voltage (I-V) characteristics were acquired at a fixed gate bias of 5 V in air. We observed (Fig. 3A) a decrease in drain current of 0.1 to 0.2 mA per nanometer of microcantilever

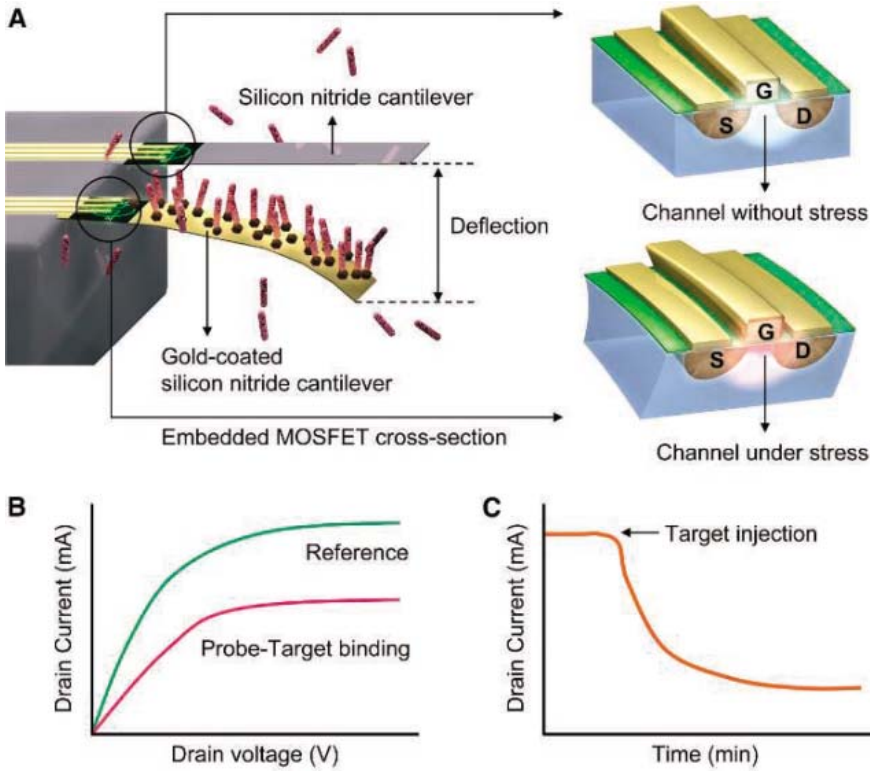

Fig. 1. (**A**) Schematic of the interaction between probe and target molecules on an embedded-MOSFET cantilever system. The silicon nitride cantilever is a reference, and the gold-coated one is used as a sensing cantilever. Specific biomolecular interactions between receptor and target bend the cantilever. Magnified view of embedded MOSFET in cross section shows stressed gate region when cantilever bends, resulting in change of drain current due to conductivity modulation of the channel underneath the gate. (**B**) Schematic of change in a MOSFET drain current upon probe-target binding. (**C**) Change in drain current over time due to deflection of a microcantilever.

Table 1. A few examples showing conversion of the probe-target biomolecular interactions into nanomechanical responses of microcantilevers (ssDNA, single-stranded DNA; fPSA, free prostate-specific antigen).

Probe-target system	Target molecule concentration	Deflection magnitude (nm)	References
Biotin-streptavidin	100 nM (6 μg/ml)	50	(*1*)
Biotin-neutravidin	25 μg/ml	20	(*2*)
ssDNA hybridization	40 μg/ml (3 μM)	15	(*2*)
ssDNA hybridization	500 nM	10	(*2*)
PSA antibody–fPSA	6 ng/ml	20	(*3*)

deflection. We note that the drain current changes by almost one order of magnitude between a few nanometers and 150 nm of microcantilever bending. The bending results indicate that the MOSFET deflection sensitivity is of the same order as that of optical detection, as inferred from the prior literature [shown in Table 1 and (*3*–*6*)], and is higher than that of existing active and passive detection technologies by one to two orders of magnitude (*7*–*14*).

Moreover, MOSFETs have large signal-to-noise (S/N) ratios caused by the large change in drain current relative to the concomitant small noise density (Fig. 3B). The three curves show 1/*f* or flicker noise—the dominant source of noise in MOSFETs at low frequencies—at three different voltages (*23*, *24*). The current noise of 40 to 60 nA, which is calculated by integrating the spectral power density over 1/*f* bandwidth for different gate voltages, is lower than the reported value of 2.7 μV for a piezoresistance-based microcantilever-type sensor (*25*). Given that MOSFET current sensitivity is around 0.1 to 0.2 mA per nanometer of cantilever deflection, a low detection limit can be readily achieved with a large S/N ratio. The noise density could likely be further reduced in future generations of these devices by standard processing steps that would optimize doping concentration and minimize the interface traps.

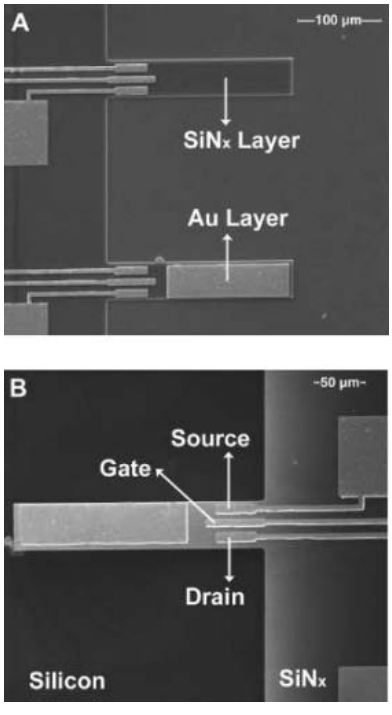

Fig. 2. (**A**) SEM image of two identical cantilevers (from a 50 × 1 array) displaying embedded MOSFET and geometry of the gold-coated and SiN_x cantilever beam pair; each cantilever is about 250 μm long, 1.5 μm thick, and 50 μm wide. (**B**) Details of MOSFET location on cantilever beam, which is released by etching a 2.5-μm sacrificial oxide layer.

Electronic measurements of the transistor characteristics revealed that the observed changes in the drain current at gate bias and while sweeping the drain voltage demonstrate the modulation of channel current with surface stress due to microcantilever bending. The large change in drain current results from the modulation of channel mobility because of surface stress, which increases the channel resistance. The mobility change may also arise from the changes in the interface charge densities, generation of trap states, band structure alteration, and generation of shallow defects due to localized bending stress.

For biomolecular binding experiments, the MOSFET-embedded microcantilevers were cleaned sequentially in acetone, isopropanol-2, and methanol for 10 min each, followed by ultraviolet cleaning for 25 min. They were then functionalized with DTSSP [3,3′-dithiobis (sulfosuccinimidylpropionate), Pierce Chemical Co.], a linker molecule involved in immobilizing streptavidin and antibodies to the gold-coated microcantilever surface. Streptavidin (Pierce) was later immobilized on the microcantilever surface by incubating overnight in a streptavidin solution (10 μg/ml) prepared with phosphate-buffered sa-

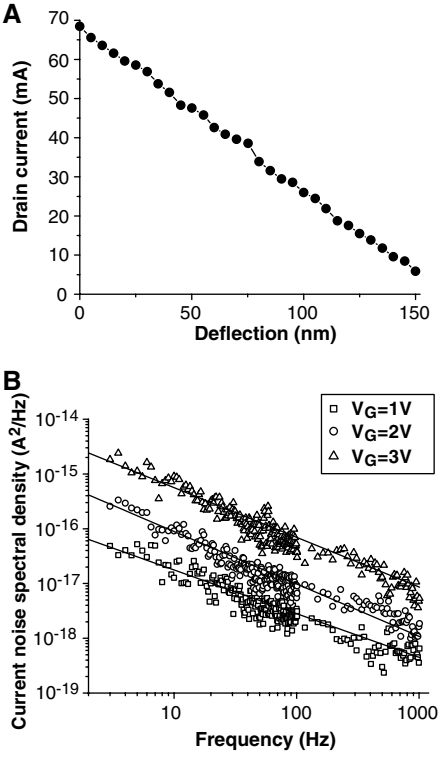

Fig. 3. (**A**) Plot of embedded MOSFET drain current with physical bending of a microcantilever by a nanomanipulator, in step size intervals of 5 nm. The decrease in drain current was 0.1 to 0.2 mA/nm of cantilever deflection. (**B**) Current noise power spectral densities measured from an embedded MOSFET at different gate voltages and at constant current level, which is inversely proportional to frequency. Current noise power spectral density was measured using a previously described setup (*24*) with a current preamplifier (DL Instruments, model 1211).The spectra show very low noise level in drain current, supporting high current sensitivity of the device. The drain voltage was fixed at 1 V.

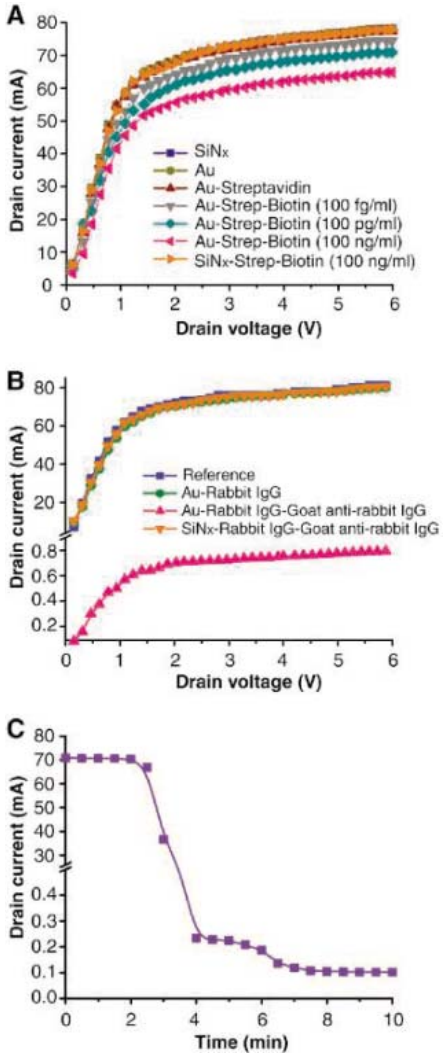

Fig. 4. (**A**) I_D versus V_D characteristics of gold-coated cantilever immobilized with streptavidin (10 μg/ml) immersed in PBS. The experiment was carried out to check whether the presence of ions caused any bending of the cantilever beam. Negligible change in drain current is observed on the cantilever coated with streptavidin (10 μg/ml) in absence of ligands (biotin). When biotin (100 fg/ml to 100 ng/ml) is added, current decreases as concentration increases; this is indicative of cantilever bending. No drain current decrease is observed in the silicon nitride reference cantilever, indicating no probe-target binding. (**B**) Measured I_D versus V_D characteristics for embedded n-MOSFET transistor at V_G = 5 V. There is negligible change in drain current on a cantilever coated with rabbit IgG (0.1 mg/ml) in absence of secondary antibody. When goat antibody to rabbit IgG (0.1 mg/ml) is added, a change in drain current of almost two orders of magnitude is observed, indicative of cantilever bending. (**C**) Interaction of rabbit IgG and goat antibody to rabbit IgG over time at a fixed drain voltage of 2 V.

line (PBS, pH = 7.4). This immobilization method provides a tight streptavidin layer with uniform density on gold for efficient binding of biotin. All of the nonspecific binding sites were blocked with bovine serum albumin (BSA). For detection experiments, the functionalized microcantilevers were exposed to target biotin concentrations (in PBS) of 100 fg/ml, 100 pg/ml, and 100 ng/ml.

MOSFET transistors were passivated with a thin coating of silicon nitride (30 nm), and electrical contacts were isolated for the binding measurements in the fluidic environment. The measured drain current (I_D) versus drain voltage (V_D) characteristics for the n-MOSFET–embedded transistor, at gate voltage V_G = 5 V, show a negligible change in I_D (Fig. 4A) when the streptavidin-immobilized gold microcantilevers are immersed in PBS. Microcantilever bending as a result of streptavidin-biotin binding leads to decreases in I_D as the concentration of biotin increases from 100 fg/ml to 100 ng/ml. The bending results from an increase in compressive stress, which in turn results from the repulsive electrostatic or steric intermolecular interactions (*2*–*6*) or from changes of the hydrophobicity of the surface (*1*–*6*). No drain current change was seen in SiN_x cantilevers with biotin, where no binding events occurred.

Similar experiments were performed for detection of goat antibodies [secondary immunoglobulin G (IgG)] by rabbit antibodies (primary IgG) with the embedded MOSFET. After the cleaning procedure, the MOSFET-embedded microcantilevers were first functionalized with DTSSP as a linker and then incubated overnight in rabbit IgG (0.1 mg/ml, Pierce) prepared in PBS for immobilization. BSA was again used as an agent to block nonspecific binding sites. The functionalized microcantilevers were exposed to goat antibody to rabbit IgG (0.1 mg/ml in PBS) for binding experiments.

The measured I_D versus V_D characteristics for V_G = 5 V (Fig. 4B) again showed no change in the drain current for the SiN_x cantilever and negligible change for the gold-coated cantilever with rabbit IgG immersed in PBS. When goat antibody to rabbit IgG (0.1 mg/ml) was introduced, a change in I_D of almost two orders of magnitude was observed, which is indicative of microcantilever bending as a result of antibody–secondary antibody binding. The SiN_x reference cantilever remained the same after injecting the target. The large change in I_D with time is shown in Fig. 4C; steady-state saturation is achieved when molecular and surface interactions are completed.

The MOSFET detection method offers a number of advantages over traditional piezoresistive or capacitive sensor elements because of its small size, high sensitivity, and uncomplicated current measurement as well as its full and seamless compatibility with direct monolithic integration for application-specific integrated circuits. Moreover, the small channel lengths of MOSFET devices provide more localized stress measurements. MOSFET-embedded microcantilever detection should allow for massively parallel on-chip signal sensing, multiplexing, and remote addressability via on-chip integration of radio-frequency elements as well as photovoltaics for local power supply.

References and Notes

1. R. Raiteri, M. Grattarola, H. J. Butt, P. Skladal, *Sens. Actuators B* **79**, 115 (2001).
2. G. Wu *et al.*, *Proc. Natl. Acad. Sci. U.S.A.* **98**, 1560 (2001).
3. G. Wu *et al.*, *Nat. Biotechnol.* **19**, 856 (2001).
4. J. Fritz *et al.*, *Science* **288**, 316 (2000).
5. N. V. Lavrik, M. J. Sepaniak, P. G. Datskos, *Rev. Sci. Instrum.* **75**, 2229 (2004).
6. M. Yue *et al.*, *J. Microelectromech. Syst.* **13**, 290 (2004).
7. A. Boisen, J. Thaysen, H. Jensenius, O. Hansen, *Ultramicroscopy* **82**, 11 (2000).
8. H. Jensenius *et al.*, *Appl. Phys. Lett.* **76**, 2615 (2000).
9. R. Marie, H. Jensenius, J. Thaysen, C. B. Christensen, A. Boisen, *Ultramicroscopy* **91**, 29 (2002).
10. S. C. Minne *et al.*, *Appl. Phys. Lett.* **72**, 2340 (1998).
11. S. C. Minne, S. R. Manalis, C. F. Quate, *Appl. Phys. Lett.* **67**, 3918 (1995).
12. D. R. Baselt, G. U. Lee, R. J. Colton, *J. Vac. Sci. Technol. B* **14**, 789 (1996).
13. D. R. Baselt, G. U. Lee, K. M. Hansen, L. A. Chrisey, R. J. Colton, *Proc. IEEE* **85**, 672 (1997).
14. C. L. Britton *et al.*, *Ultramicroscopy* **82**, 17 (2000).
15. A. Hamada, T. Furusawa, N. Saito, E. Takeda, *IEEE Trans. Electron Devices* **38**, 895 (1991).
16. R. C. Jaeger, J. C. Suhling, R. Ramani, A. T. Bradley, J. P. Xu, *IEEE J. Solid-State Circuits* **35**, 85 (2000).
17. Y. J. Yee, J. U. Bu, K. J. Chun, J. W. Lee, *J. Micromech. Microeng.* **10**, 350 (2000).
18. T. Akiyama *et al.*, *J. Vac. Sci. Technol. B* **18**, 2669 (2000).
19. D. Lange, C. Hagleitner, C. Herzog, O. Brand, H. Baltes, *Sens. Actuators A* **103**, 150 (2003).
20. T. Akiyama, U. Staufer, N. F. de Rooij, *Rev. Sci. Instrum.* **73**, 2643 (2002).
21. R. Bashir, A. Gupta, G. W. Neudeck, M. McElfresh, R. Gomez, *J. Micromech. Microeng.* **10**, 483 (2000).
22. C. Liu, *Foundations of MEMS* (Pearson Prentice Hall, Upper Saddle River, NJ, 2005).
23. V. Dessard, B. Iniguez, S. Adriaensen, D. Flandre, *IEEE Trans. Electron Devices* **49**, 1289 (2002).
24. A. Blaum, O. Pilloud, G. Scalea, J. Victory, F. Sischka, in *Proceedings of the 2001 International Conference on Microelectronic Test Structures* (IEEE, Piscataway, NJ, 2001), pp. 125–130.
25. P. A. Rasmussen, J. Thaysen, O. Hansen, S. C. Eriksen, A. Boisen, *Ultramicroscopy* **97**, 371 (2003).

26. Supported by NSF Electrical and Communications System grant ECS-0330410 and Defense Advanced Research Projects Agency grant F30602-01-2-0540. This work made use of the Microfabrication Applications Laboratory at the University of Illinois, Chicago, the Center for Nanophase Materials Science at Oak Ridge National Laboratory, and the NU*ANCE* center facilities at Northwestern University. We thank R. Lajos, H. Zeng, and A. Feinerman for process assistance and support; T. Thundat, D. Ramaya, K. Hansen, and I. Lee for assistance in immobilization of antibodies; and A. Srivastava for assistance in noise measurements.

Supporting Online Material

www.sciencemag.org/cgi/content/full/1122588/DC1
Materials and Methods
References

14 November 2005; accepted 20 January 2006
Published online 2 February 2006;
10.1126/science.1122588
Include this information when citing this paper.

Broadband Cavity Ringdown Spectroscopy for Sensitive and Rapid Molecular Detection

Michael J. Thorpe, Kevin D. Moll, R. Jason Jones, Benjamin Safdi, Jun Ye*

We demonstrate highly efficient cavity ringdown spectroscopy in which a broad-bandwidth optical frequency comb is coherently coupled to a high-finesse optical cavity that acts as the sample chamber. 125,000 optical comb components, each coupled into a specific longitudinal cavity mode, undergo ringdown decays when the cavity input is shut off. Sensitive intracavity absorption information is simultaneously available across 100 nanometers in the visible and near-infrared spectral regions. Real-time, quantitative measurements were made of the trace presence, the transition strengths and linewidths, and the population redistributions due to collisions and the temperature changes for molecules such as C_2H_2, O_2, H_2O, and NH_3.

The real-time detection of trace amounts of molecular species is needed for applications that range from detection of explosives or biologically hazardous materials to analysis of a patient's breath to monitor diseases such as renal failure (*1*) and cystic fibrosis (*2*). Spectroscopic systems capable of making the next generation of atomic and molecular measurements will require the following: (i) a large spectral bandwidth, allowing for the observation of the global energy level structure of many different atomic and molecular species; (ii) high spectral resolution for the identification and quantitative analysis of individual spectral features; (iii) high sensitivity for the detection of trace amounts of atoms or molecules and for the recovery of weak spectral features; and (iv) a fast spectral acquisition time, which takes advantage of high sensitivity, for the study of dynamics.

JILA, National Institute of Standards and Technology (NIST) and University of Colorado, and Department of Physics, University of Colorado, Boulder, CO 80309-0440, USA.

*To whom correspondence should be addressed. E-mail: ye@jila.colorado.edu

Unfortunately, the characteristics of a good spectroscopic system are often in competition with each other. For example, designing a system with a large spectral bandwidth and high resolution (or high sensitivity) requires some way of selecting a narrow spectral band from a broad-spectrum source. Thus, modern spectroscopic methods, which are designed to meet two or three of the desired system characteristics with excellent performance, will function poorly in the remaining areas. Single-pass absorption techniques, such as Fourier transform infrared (FTIR) (*3*) and wavelength agile methods (*4*), do an excellent job of providing large bandwidths (up to several hundreds of nanometers) and achieve remarkably fast acquisition times by recording entire spectra in microseconds. But these techniques offer sensitivities that are many orders of magnitude too low for applications involving trace detection or observation of weak spectral features. Both of these techniques can achieve high resolution but at the cost of prolonged spectral acquisition times or reduced spectral bandwidths.

Cavity-enhanced techniques, such as noise-immune, cavity-enhanced, optical heterodyne molecular spectroscopy (NICE-OHMS) (*5*, *6*) and cavity ringdown spectroscopy (CRDS) (*7*), offer incredibly high sensitivities (10^{-10} and beyond) at 1-s averaging time, and they can provide high resolution; however, they are generally limited to small spectral bandwidths (only a few nanometers). Newer approaches to cavity-enhanced spectroscopy have been directed at increasing the spectral bandwidth and reducing the acquisition time (*8*–*11*). Such efforts have demonstrated large bandwidths of up to 50 nm with an acquisition time of 2 s (*10*) and fast acquisition times of 1 ms for a bandwidth of 0.5 nm (*11*). However, these methods have yet to demonstrate tens of nanometers of spectral bandwidth at millisecond acquisition times.

The broadband CRDS reported here addresses all of the mentioned system characteristics by efficiently coupling a broadband frequency comb into a high-finesse optical cavity to create the simultaneous ringdown decay of 125,000 individual cavity modes. We report a spectral bandwidth of 100 nm that is limited only by the bandwidth of a mode-locked femtosecond laser. A spectral resolution of 0.8 cm^{-1} was achieved, which can extract linewidths as narrow as 0.01 cm^{-1} (0.3 GHz) via measured pressure broadening of the spectral width of the gas target. An integrated absorption sensitivity of 1×10^{-8} at 1 s was achieved, and an acquisition time of 1.4 ms was realized for a spectral window of more than 15 nm. In principle, this acquisition time is limited only by the actual cavity ringdown time (several microseconds). We present measurements of several atomic and molecular species (Ar, C_2H_2, O_2, H_2O, and NH_3), revealing quantitative information about the gas concentrations, linewidths, collision rates, temperatures, and plasma dynamics.

Broadband CRDS differs from previously demonstrated CRDS methods in how the broadband frequency comb is coupled to the ringdown cavity and the way in which broadband ringdown events are detected. In general, CRDS is performed by overlapping the laser frequency to that of a cavity resonance, allowing light to couple into the cavity, with the resulting ringdown curve providing absorption information at the laser wavelength. In the broadband comb case, we simultaneously couple 125,000 comb components to their respective longitudinal cavity modes and subsequently provide separate detections of ringdown waveforms available from many parallel channels in a single transmitted beam.

In principle, the frequency comb and the cavity are a natural match. The regularly spaced resonant frequency structure of the comb provides the potential for coupling the entire incident power into the cavity over a large spectral bandwidth. In practice, such coupling is difficult to achieve. The frequency structure of the comb is given by the relation $\nu_n = nf_{rep} + f_o$, where the integer n refers to the nth mode of the comb and f_{rep} and f_o refer to the repetition frequency and the carrier-offset frequency, respectively (*12*). To match this set of frequencies to a specific, regularly spaced set of cavity modes, both f_{rep} and f_o must be independently controlled (*13*). For the titanium-doped sapphire (Ti:sapphire) oscillator we used, such control was achieved with several piezo-electric (PZT) and picomotor actuators that adjusted the length and dispersion of the laser cavity. f_{rep} was controlled by adjusting the cavity length by using a combination of a picomotor for coarse adjustments and a PZT for fine adjustments. This combination can precisely adjust f_{rep} by as much as 4 MHz. We controlled f_o by tilting the high-reflecting mirror in the dispersive arm of the Ti:sapphire laser (*14*). This mirror is mounted on two PZTs that are actuated simultaneously to rotate the mirror by a fraction of a degree ($\pm 2 \times 10^{-4}$). Rotating this mirror causes a differential change in the phase and group velocities of the light inside of the laser cavity, which can tune the value of f_o across its entire range from zero to f_{rep}. When the comb frequencies are matched to the cavity modes, successive laser pulses add coherently inside of the cavity, which enhances intracavity intensities and ringdown signals.

Independent control of both degrees of freedom of the comb is only half of the solution to the problem of coupling the comb to the cavity over a large spectral bandwidth. Dispersion in an optical cavity causes the cavity modes to be spaced nonuniformly, producing a cavity resonant frequency structure that the comb cannot match rigorously. All of the optical elements, including the intracavity gases under investigation, have dispersive properties that tend to make the cavity mode spacing nonuniform. Thus, we needed to construct a ringdown cavity that has the appropriate dispersion properties by using low-dispersion, broadband mirrors, and, depending on the gas pressure under investigation, a negative-dispersion mirror to compensate for the positive material dispersion introduced by the gas (*15*). The high cavity finesse for enhanced detection sensitivities must be balanced with usable spectral bandwidth that can be coupled into the cavity for a given property of mirror dispersion. Higher reflectivity mirrors can provide a longer ringdown signal that leads to more sensitive detection, but they also reduce the cavity linewidth, such that a smaller amount of uncompensated dispersion will limit the bandwidth of the comb that can

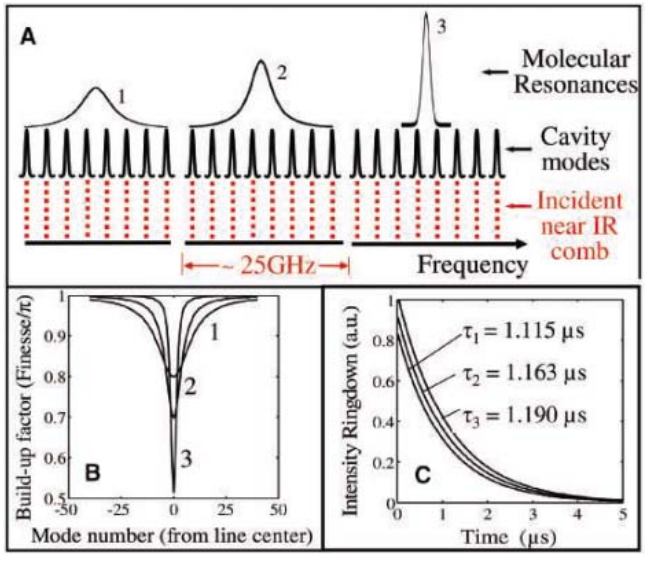

Fig. 1. (**A**) A frequency-domain schematic of the interaction between the femtosecond laser modes, the cavity modes, and the molecular resonances. The set of laser/cavity modes associated with each molecular resonance represents the detection window of 25 GHz set by the monochromator resolution. Each detection window contains roughly 60 cavity modes that ring down simultaneously onto a single detector. (**B**) The calculated buildup of individual cavity modes for three different molecular resonances shown in (A). The buildup is normalized against F/π, the maximum cavity buildup. (**C**) The calculated ringdown signals for the buildup profiles in (B) show that broader absorption peaks result in overall less buildup and shorter ringdown times. a.u., arbitrary units.

be coupled into the cavity. We used mirrors with reflectivity >0.999 between 790 and 850 nm that maintained the cavity dispersion at <10 fs², which allowed for the simultaneous coupling of the comb components into the cavity over this entire wavelength range. Outside of this wavelength range, the nonuniform structure of the cavity modes limits the single-shot detection bandwidth, although it never falls below 15 nm over the entire laser spectrum.

For detection, the resolving power of current dispersive systems—such as a grating monochromator—is not high enough to resolve individual modes of the frequency comb. Each detector element is actually recording the combined ringdown of several cavity modes. The time-varying intensity of the combined ringdown signal is a sum of individual cavity mode ringdown signals incident on a single detector element, $I_{\text{combined}}(t) = \sum_i I_i e^{-\kappa_i t}$. Here I_i and κ_i are the intracavity built-up intensity and the inverse decay time for the ith cavity mode, respectively, I_{combined} is the signal recorded by the detector, and t is time. For the ¼-m monochromator we used, each detector element captured ~60 comb modes, which corresponds to a resolution of 25 GHz. This combination of many ringdown decay signals onto a single detector can be exploited to extract information about the line shape of molecular resonances from the recorded decay time. A simulation of how the ringdown time recorded by a detector element changes for three different molecular resonance line shapes, all with the same absorption strength, is shown in Fig. 1. A detailed model of the ringdown system was created that included cavity buildup affected by the intracavity absorption, ringdown time, the line shape and transition strength of the molecular resonance, and filtering effects of the monochromator.

By using this model, we calculated and compared the ringdown signal due to a molecular resonance of fixed transition strength and three different Lorentzian linewidths (Fig. 1A). Each of the three graphical windows represents a single detector element containing 60 comb modes and a single molecular resonance. The three molecular resonances differ only by the amount of homogeneous broadening included in their respective Voigt line shapes. The total area under each of these resonances is fixed, corresponding to constant absorption strength. The calculated buildup of intracavity light intensity versus cavity mode for each molecular resonance (Fig. 1B) assumes perfect coupling of the comb modes to their respective cavity modes in the absence of absorption.

These simulations show that the broad resonance 1 results in less intracavity buildup intensity and a faster ringdown time, whereas the narrow resonance 3 yields more buildup and a longer ringdown time (Fig. 1C). This effect depends on the number of cavity modes that interact with the molecular absorption and the strength of the interaction. For resonance 3, only a few cavity modes interact with a strong molecular absorption, causing these modes to build up much less and ring down much faster than the majority of other modes inside the detector window. Hence, the contribution of the interacting modes to the overall ringdown signal is small in amplitude and decays away quickly relative to the noninteracting modes. In contrast, resonance 1 allows many modes to interact with the same molecular absorption feature. Here the buildup and ringdown of the interacting modes is not diminished as much relative to the noninteracting modes. Thus, a large contribution to the overall ringdown signal was made by modes that interacted with the molecular absorption.

This type of analysis allows for the determination of the linewidth of a resonance with a resolution much higher than the actual resolving power of the spectrometer. This same analysis can be used to determine the transition strength of molecular transitions by varying the concentration of the gas sample. Finally, if both the transition strength and linewidth for a particular resonance are unknown, they can be determined by using this method of studying the ringdown signal under various target gas concentrations and buffer gas pressures.

For the experimental setup, we used a mode-locked Ti:sapphire laser that generates a train of ~10-fs pulses with a repetition frequency (f_{rep}) of 380 MHz and an average power of 300 mW. This femtosecond optical frequency comb was

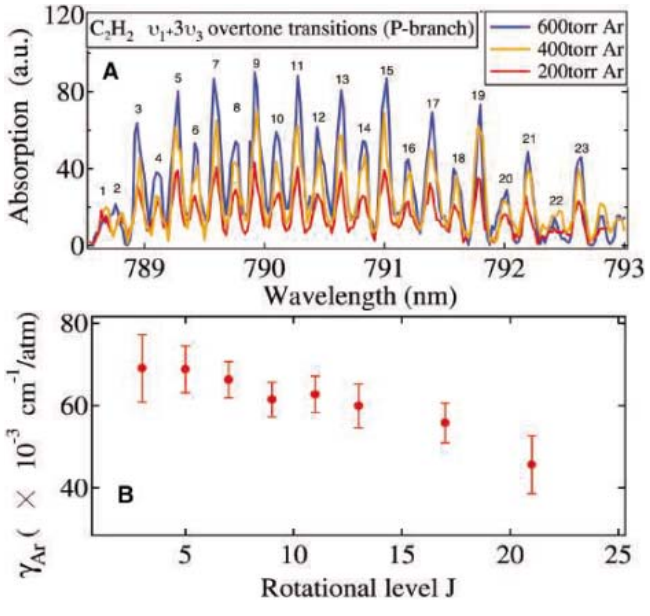

Fig. 2. (**A**) An average of 1000 scans of the P-branch spectrum of the $\upsilon_1 + 3\upsilon_3$ overtone band of C_2H_2. The rotational quantum number for the ground state of each transition is indicated above the spectral peak. The three traces show the change in spectral intensity under a fixed C_2H_2 pressure and three different argon pressures. (**B**) The measured half width at half maximum pressure broadening coefficients (cm^{-1}/atm) for several rotational lines show a decreasing collision rate with increasing rotational quantum number J. Error bars indicate the uncertainty in line shape fit and gas pressures.

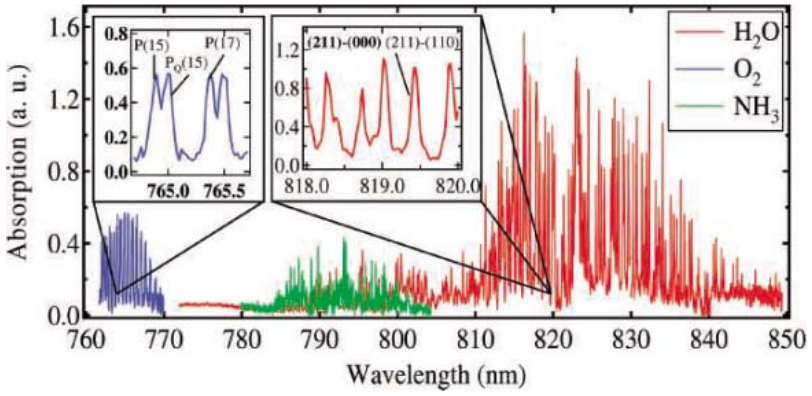

Fig. 3. The overtone spectrum of H_2O (red), the P-branch of the (0,0) vibrational transition of the $^{X3}\Sigma_g^- \rightarrow {}^{b1}\Sigma_g^+$ electronic transition in O_2 (blue), and the overtone spectrum of NH_3 near 790 nm (green) demonstrate the broadband, high-resolution, and high-sensitivity capabilities of this spectroscopic technique. For each molecule, 1000 spectral scans were averaged to produce the traces shown. The inset graphs show that the individual rotational lines of each spectrum have been resolved, revealing the characteristic doublet structure of the O_2 rotational spectrum and the irregular structure of the H_2O rovibrational spectrum. Three of the P-branch lines of O_2 and one H_2O line are labeled. For the H_2O line, the bold text labels the excited and ground vibrational states, and the normal text labels the excited and ground rotational states, respectively.

passed through an acousto-optical modulator (AOM), and the first order diffraction from the AOM (~150 mW) was coupled into a high finesse (F = 4500) optical cavity where the ringdown spectroscopy was performed (*16*). The free spectral range (FSR) of the cavity was 380 MHz, which matches that of the optical comb. With the AOM switched on and the comb components tuned to resonate with respective cavity modes, thousands of femtosecond pulses coherently add inside of the cavity. When the light inside of the cavity reached a preset intensity, the AOM was switched off and the intensity in each cavity mode began to decay (ring down). Light transmitted from the cavity (>50% of the total incident power) was passed through a ¼-m monochromator with a spectral resolution of 25 GHz. The detection of ringdown events was performed by a detector placed at the monochromator output image plane. In cases where fast, broadband spectral acquisition was desirable, a streak camera detection scheme was used (*17*). A scanning mirror was placed near the output image plane of the monochromator and was used to deflect the beam in the vertical direction. Spectrally dispersed wavelengths were recorded along the horizontal rows of pixels, whereas the ringdown waveform in the time domain was recorded on the vertical columns of pixels. The scanning mirror was operated at 355 Hz, allowing for the acquisition of a ringdown spectrum every 1.4 ms. The charge-coupled device (CCD) had 340 pixels in the horizontal dimension, allowing for a single-shot acquisition of 15 nm of spectrum at 25-GHz resolution.

The first molecular sample we studied with this system was acetylene (C_2H_2). The linear rotor structure of C_2H_2 results in a relatively simple spectrum (Fig. 2A). The transitions in the $\upsilon_1 + 3\upsilon_3$ overtone band originate from rotational levels in the vibrational ground state and are excited to the $\upsilon_1 = 1$, $\upsilon_3 = 3$ overtone band and $\Delta J = -1$ states (P-branch). The relative strengths of these transitions are described by a Boltzmann distribution $S_J \propto Jg_i e^{-E_J/k_BT}$, where J is the rotational quantum number, g_i is the nuclear spin degeneracy, E_J is the energy of the Jth rotational level in the vibrational ground state, and k_BT indicates the thermal energy of the gas (*18*). The nuclear spin dependence arises from the fermionic nature of C_2H_2. As a result, symmetric spin states must be paired with antisymmetric rotational states and vice versa. Symmetric (ortho) spin states outnumber the antisymmetric spin states (para) by a ratio of 3:1, and the relative strengths of adjacent rotational transitions are similarly weighted.

A fixed C_2H_2 pressure (2 torr) at fixed temperature (295 K) was maintained inside the ringdown cavity, and spectra were recorded while the pressure of an inert buffer gas (argon) was varied between 200 and 600 torr. Collisions between argon and C_2H_2 increased the Lorentzian contribution to the Voigt line shape of the C_2H_2 resonances, and this Lorentzian broadening of the C_2H_2 resonances was detected as a decrease in the cavity ringdown time that results from the larger number of comb modes interacting with the molecular absorption (Fig. 2A). Changes in the Lorentzian linewidth as small as 200 MHz can be detected in this way, providing resolution that is two orders of magnitude better than that of the monochromator. The pressure broadening rate of the Lorentzian linewidth was linear in pressure. The half width at half maximum pressure broadening coefficients were plotted as a function of rotational level J (Fig. 2B). The measured pressure broadening coefficients for the P-branch of the $\upsilon_1 + 3\upsilon_3$ overtone of C_2H_2 are in good agreement with measurements by Herregodts *et al*. (*19*), which used continuous wave (CW) absorption techniques that required much more challenging frequency-referencing methods to achieve a similar level of precision.

The second molecule we examined was water (H_2O). Between 780 and 850 nm, H_2O has an enormous number of transitions corresponding to several vibrational modes and hundreds of rotational levels. Because of its complicated asymmetric top structure, the H_2O spectrum has a highly irregular structure. However, this large range of transition frequencies makes it an ideal candidate to demonstrate the broadband and yet high-resolution characteristics of this method. The H_2O spectrum was measured from 100 mtorr to 20 torr (relative humidities ranging from 0.5 to 90%). Both absolute pressure and partial pressure (mixed with argon) measurements were performed within this pressure range. The H_2O overtone spectrum between 770 and 850 nm is shown in Fig. 3 for 10 torr of H_2O and 600 torr of argon buffer gas. The inset identifies the rovibrational transition: (000) to (211) in vibrational quantum numbers (ν_1, ν_2, ν_3) and (110) to (211) in rotational quantum numbers (J, k_a, k_c) (*20*).

To demonstrate fully the broadband nature of this system using the entire spectral bandwidth of the laser, the spectrum of an electric dipole forbidden electronic transition in $O_2({}^{X3}\Sigma_g^- \rightarrow {}^{b1}\Sigma_g^+)$, where X indicates the electronic ground state, g (gerade) indicates even symmetry, and b indicates the excited electronic state. Overtone transitions of NH_3 were also detected, and the rotational lines were identified. For the O_2 measurement, the cavity was filled with 600 torr of air corresponding to a pressure of 124.8 torr of O_2. For the NH_3 data, a partial pressure of 3 torr was used. Together, the H_2O, NH_3, and O_2 spectra presented in Fig. 3 demonstrate nearly the entire 100-nm spectral width that can be probed simultaneously with the current frequency comb–cavity system.

The final two measurements presented here aim to demonstrate the fast spectral acquisition time of this system. First, a single-shot measurement of the H_2O spectrum was used to demonstrate the current limit on the spectral acquisition

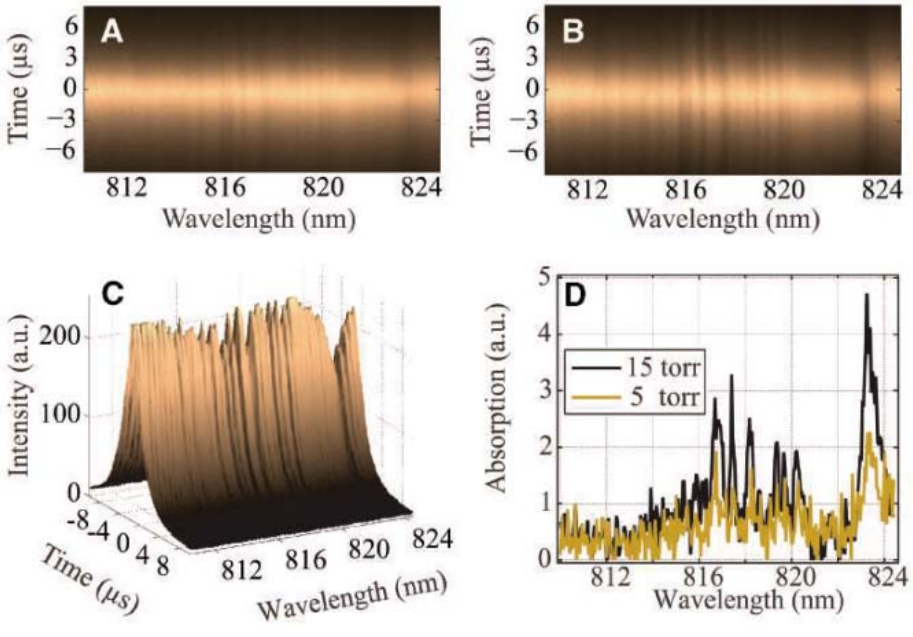

Fig. 4. Fast spectral acquisition provided by broadband CRDS. A portion of the H_2O overtone spectrum near 820 nm recorded with (**A**) 5 torr and (**B**) 15 torr of H_2O, containing 15 nm of spectral information, was acquired by the camera in 30 μs and transferred to the computer. For these plots, t = 0 corresponds to the time when the AOM is shut off. For $t < 0$, the cavity is building up, and for $t > 0$ the cavity is ringing down. (**C**) A surface plot of the 15-torr image shows a reduction in cavity buildup and more rapid cavity decay in spectral regions corresponding to H_2O absorption. (**D**) Decay constants extracted from the 5- and 15-torr images reveal the H_2O absorption spectrum.

time. A second measurement was performed on discharged argon to demonstrate the fundamental limitation to the spectral acquisition time.

The H_2O measurement was performed by recording single ringdown events without averaging. False-color CCD images of two of these single-shot ringdown events were recorded (Fig. 4, A and B) along with the processed data following the procedure described in (*16*). The surface plot (Fig. 4C) shows that high resolution and a broad detection bandwidth were achieved in real time. The noise associated with this detection scheme allows for the detection of changes in integrated absorption (αL, where α is the absorption per unit length and L is the cavity length) of 2.5×10^{-5} using an integration time constant of 0.15 μs per CCD pixel. This corresponds to a detection sensitivity of 1×10^{-8} integrated absorption at 1-s averaging time. The 1.4-ms acquisition time is currently limited by the speed of the optical scanner. The fundamental time limitation for the acquisition of a ringdown spectrum is the cavity lifetime, which is on the order of a few microseconds.

The second real-time measurement, which was performed on a decaying argon plasma, demonstrated a measurement time scale approaching the cavity decay limit. A radio frequency (RF) discharge was used to create argon plasma inside of the ringdown cavity (*21*). The RF source driving the plasma was rapidly switched, and a transition at 811.53 nm (Fig. 5, inset), originating from an argon metastable state $3s^2 3p^5 \left(^2P^0_{3/2}\right)4s \rightarrow 3s^2 3p^5 \left(^2P^0_{3/2}\right)4p$, was studied. Here, the $3s^2 3p^5 \left(^2P^0_{3/2}\right)4s$ is a metastable state with a lifetime >1 s. However, at high temperatures inside the plasma, the metastable argon atoms decay via collisions with the walls of the optical cavity on the order of 10 μs.

When the RF discharge is turned off (at t = 0 μs in Fig. 5), the excited dipole-allowed transitions quickly decay, whereas the metastable atoms decay more slowly. Initially, we observed this effect when a high-pressure argon discharge (4 torr) was established inside the cavity and a collection lens and fast photodiode were placed along side the plasma. The RF discharge was turned off and the spectrally unresolved plasma decay was observed in fluorescence (Fig. 5, red trace), revealing a fast initial decay followed by the slower decay of the metastable states.

The argon plasma pressure was then decreased to 100 mtorr (below the detection capabilities of the fluorescence measurement), and a cavity-based measurement was performed. Because the 811.53-nm transition is strong, a simple cavity transmission measurement was used to measure the decay of the $3s^2 3p^5 \left(^2P^0_{3/2}\right)4s$ state inside of the cavity. The sensitivity of the ringdown cavity is such that 100 mtorr of discharged argon was sufficient to reduce the cavity buildup to 5% of the empty cavity value. The blue dots (Fig. 5) show the intracavity absorption in the presence of metastable argon at 811.53 nm for various times before and after the RF discharge was turned off. The agreement in decay times recorded by the photodiode and the cavity measurement confirms that the long-lived decay seen by the photodiode is indeed due to the decay of the metastable states. The decay time of the metastable state was around 10 μs, whereas the cavity buildup and ringdown times were on the order of 3 μs. This experiment demonstrates that as spectral acquisition times approach the fundamental cavity decay limit, measurements of this type will be performed in a single shot.

A number of improvements can still be implemented to push the system performance to the fundamental limits. With higher resolution detection and by using the latest mirror technology, detection sensitivities of 10^{-10} at 1 s can easily be achieved. The use of state-of-the-art mirrors that are more broadband and less dispersive also implies larger spectral bandwidths, up to several hundred nanometers. Mode-locked laser sources and detectors at spectrally important regions such as 1.5 μm are abundant. A larger (2 m) monochromator, although not an elegant solution, could bring the system resolution to a few gigahertz, and the comb structure would still allow for the investigation of linewidths on the 100s of MHz scale. A virtually-imaged phase array (VIPA) device (*16*) provides an even more attractive option (*22*). Achieving resolutions of <1 GHz, these devices are very close to resolving individual comb modes. Once single–comb mode resolution is realized, the resolution of the system will be limited by the laser or cavity linewidths, which can be made very narrow. Finally, the use of diode array detection eliminates the need for fast scanning optics and data transfer, and it allows acquisition times to approach the fundamental cavity decay limit for the entire spectral bandwidth.

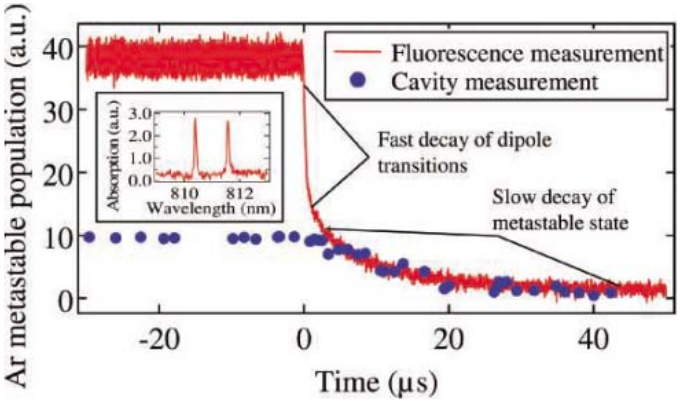

Fig. 5. Decay of hot metastable argon atoms inside of the ringdown cavity is measured by a high–plasma pressure (4 torr) fluorescence measurement and a low-pressure (100 mtorr) cavity transmission measurement. The cavity measurement has been scaled to overlap the fluorescence measurement to highlight the agreement in decay time. The decay time for the hot metastable argon is measured to be 10 μs by both methods. This measurement demonstrates that when the spectral acquisition time of CRDS is reduced to its fundamental limit, measurements such as the hot argon metastable decay will be made with high sensitivity and in a single shot.

References and Notes

1. L. R. Narasimhan, W. Goodman, C. K. N. Patel, *Proc. Natl. Acad. Sci. U.S.A.* **98**, 4617 (2001).
2. S. A. Kharitonov, P. J. Barnes, *Am. J. Respir. Crit. Care Med.* **163**, 1693 (2001).
3. F. Keilmann, C. Gohle, R. Holzwarth, *Opt. Lett.* **29**, 1542 (2004).
4. S. T. Sanders *et al.*, *Opt. Photonics News* **16**, 36 (2005).
5. J. Ye, L. S. Ma, J. L. Hall, *Opt. Lett.* **21**, 1000 (1996).
6. J. Ye, L. S. Ma, J. L. Hall, *J. Opt. Soc. Am. B* **15**, 6 (1998).
7. J. Ye, J. L. Hall, *Phys. Rev. A.* **61**, 061802 (2000).
8. T. Gherman, D. Romanini, *Opt. Express* **10**, 1033 (2002).
9. E. R. Crosson *et al.*, *Rev. Sci. Instrum.* **70**, 4 (1999).
10. Y. He, B. J. Orr, *Appl. Phys. B* **79**, 941 (2004).
11. I. Debecker, A. K. Mohamed, D. Romanini, *Opt. Express* **13**, 2906 (2005).
12. S. T. Cundiff, J. Ye, *Rev. Mod. Phys.* **75**, 325 (2003).
13. R. J. Jones, I. Thomann, J. Ye, *Phys. Rev. A.* **69**, 051803 (2004).
14. J. Reichert, R. Holzwarth, T. Udem, T. W. Hänsch, *Opt. Commun.* **172**, 59 (1999).
15. M. J. Thorpe, R. J. Jones, K. D. Moll, J. Ye, R. Lalezari, *Opt. Express* **13**, 882 (2005).
16. Materials and methods are available as supporting material on *Science* Online.
17. J. J. Scherer *et al.*, *Appl. Opt.* **40**, 6725 (2001).
18. J. Ye, thesis, University of Colorado (1997).
19. F. Herregodts, D. Hurtmans, J. Vander Auwera, M. Herman, *Chem. Phys. Lett.* **316**, 460 (2000).
20. High-resolution transmission (HITRAN) molecular database, 2005.
21. C. I. Sukenik, H. C. Busch, *Rev. Sci. Instrum.* **73**, 493 (2001).
22. A. Vega, A. M. Weiner, C. Lin, *Appl. Opt.* **42**, 4152 (2003).

23. We thank E. Hudson for technical discussions and S. Cundiff, H. Lewandowski, and R. McLeod for equipment loans. The research work at JILA is supported by Air Force Office of Scientific Research, the Office of Naval Research, NASA, NIST, and NSF. M.J.T. thanks NSF–Integrative Graduate Education and Research Traineeship Program and the University of Colorado Optical Science and Engineering Program for financial support. J.Y. is a member of the NIST Quantum Physics Division.

Supporting Online Material

www.sciencemag.org/cgi/content/full/311/5767/1595/DC1
Materials and Methods
Fig. S1
References

15 December 2005; accepted 8 February 2006
10.1126/science.1123921

Probing Gene Expression in Live Cells, One Protein Molecule at a Time

Ji Yu,[1*] Jie Xiao,[1*] Xiaojia Ren,[1] Kaiqin Lao,[2] X. Sunney Xie[1]†

We directly observed real-time production of single protein molecules in individual *Escherichia coli* cells. A fusion protein of a fast-maturing yellow fluorescent protein (YFP) and a membrane-targeting peptide was expressed under a repressed condition. The membrane-localized YFP can be detected with single-molecule sensitivity. We found that the protein molecules are produced in bursts, with each burst originating from a stochastically transcribed single messenger RNA molecule, and that protein copy numbers in the bursts follow a geometric distribution. The quantitative study of low-level gene expression demonstrates the potential of single-molecule experiments in elucidating the workings of fundamental biological processes in living cells.

The central dogma of molecular biology states that DNA is transcribed into mRNA, which is then translated into protein. Ever since the pioneering work on the *lac* operon (*1*), our knowledge of gene expression has come primarily from genetic and biochemical studies (*2*–*4*) conducted with large populations of cells and molecules. Recently, many in vitro single-molecule experiments have probed real-time dynamics and yielded valuable mechanistic insights into macromolecules (*5*–*8*), including transcriptional (*9*) and translational (*10*) machineries. In order to understand the workings of these machineries in their physiological contexts, we set out to probe gene expression at the single-molecule level by real-time monitoring of protein production in live cells.

Gene expression is often stochastic (*11*–*14*), because most genes exist at single or low copy numbers in a cell. Some genes are expressed at high levels and others at low levels. The mRNA expression can now be tracked in a single cell with single-molecule sensitivity (*15*, *16*). The protein expression has been traditionally characterized by averages of cell populations, in which stochasticity is masked. More information is available from both the distribution of expression levels among a cell population (*17*–*19*) and the temporal evolution of a single cell by using fluorescent reporters (*20*). However, these studies have been restricted to high expression levels because of the low sensitivity for protein detection, yet many important proteins are produced at small copy numbers (*21*, *22*). Here, we demonstrate probing protein expression in individual *Escherichia coli* cells under the control of a repressed *lac* promotor, one molecule at a time (*23*).

The most popular reporters for monitoring gene expression in live cells are green fluorescent protein (GFP) and its derivatives, such as yellow fluorescent protein (YFP) (*24*–*26*). We use a YFP variant, Venus, as the reporter because of its short maturation time (*27*). However, it is difficult to image a single GFP or YFP molecule in cytoplasm, because its fluorescence signal spreads to the entire cytoplasm by fast diffusion during the image acquisition time and is overwhelmed by cellular autofluorescence. On the other hand, single YFP fusion protein molecules on cell membranes can be detected (*28*, *29*) because their diffusion is slowed. Therefore, we designed a fusion protein consisting of Venus and a membrane protein, Tsr, as the reporter for monitoring *lac* promoter activity. A well-studied methylation-dependent chemotaxis receptor protein (MCP) (*30*), Tsr contains two transmembrane domains and is fused to the N terminus of Venus.

We constructed an *E. coli* strain SX4 in which a single copy of the chimeric gene *tsr-venus* was incorporated into the *E. coli* chromosome, replacing the native *lac*Z gene. The endogenous *tsr* gene of *E. coli* was left intact. Because the *tsr* gene is highly expressed (*30*), a small amount of exogenous Tsr-Venus poses minimal perturbation to cells' normal functions. Western assay of induced SX4 cells showed the presence of Venus only in the membrane fraction and not in the cytoplasmic fraction, suggesting efficient membrane localization of Tsr-Venus. We also compared the levels of induced expression of Tsr-Venus and Venus in two strains, both under the control of the *lac* promoter [Supporting Online Material (SOM) Text and fig. S1]. No notable difference was observed, indicating that the introduction of the *tsr* sequence does not change the yield of Venus production, which is not the case for many other membrane-targeting sequences that we tested.

We first show the ability to detect single Tsr-Venus fluorescent protein molecules expressed in SX4 cells (Fig. 1). Figure 1A shows two diffraction-limited fluorescent spots [full width at half maximum (FWHM) ~ 300 nm] in the left cell. A line cross section of the fluorescence image along the cells' long axes shows the signal distinctly above the cells' autofluorescence background (Fig. 1C). We attribute each fluorescent peak to an individual Tsr-Venus molecule on the basis of abrupt disappearance of the signal upon photobleaching, which is characteristic of single molecules. Figure 1D shows such a photobleaching time trace. Had the signal arisen from multiple molecules, its disappearance would be in multiple steps. In addition, the fluorescence intensity of each peak is consistent with in vitro measurements of purified single Venus molecules (fig. S2).

A sketch of our live-cell experiment is shown in Fig. 2. Upon an infrequent and spontaneous

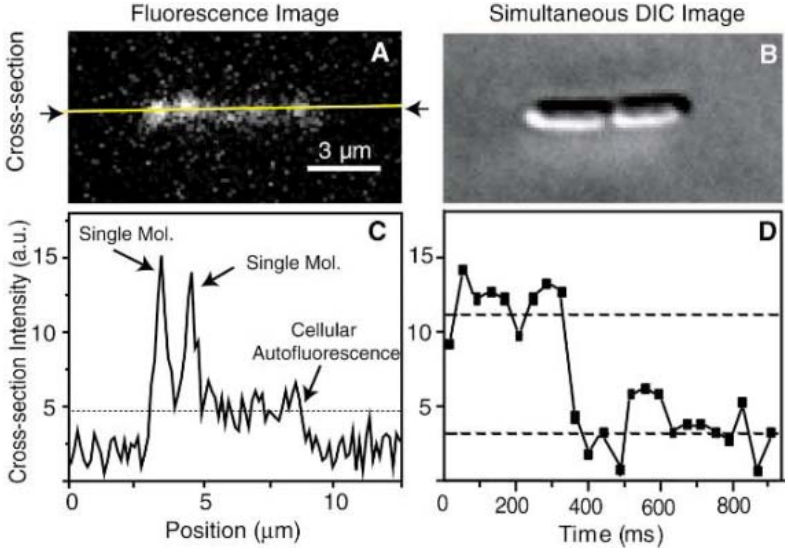

Fig. 1. Single-molecule detection of a fluorescent fusion protein, Tsr-Venus, in live *E. coli* cells. (**A**) Fluorescence and (**B**) DIC images of two *E. coli* cells (strain SX4) expressing Tsr-Venus. Two single fusion protein molecules were detected as diffraction-limited fluorescent spots (FWHM at ~300 nm) in the left cell. The fluorescence image is taken with 514-nm laser excitation and a 100-ms exposure time at 0.3 kW/cm². (**C**) Line cross section of the fluorescence signal along long axes of the two *E. coli* cells. a.u., arbitrary units. (**D**) Fluorescence time trace of a single Tsr-Venus molecule in an *E. coli* cell, showing abrupt photobleaching (40-ms exposure at 0.5 kW/cm²).

[1]Department of Chemistry and Chemical Biology, Harvard University, Cambridge, MA 02138, USA. [2]Applied Biosystems, Foster City, CA 94404, USA.

*These authors contributed equally to this work.
†To whom correspondence should be addressed. E-mail: xie@chemistry.harvard.edu

dissociation event of the repressor from the operator region of DNA, transcription by RNA polymerase is initiated, generating one mRNA molecule. A few ribosome molecules bind to the mRNA, producing a burst of fusion protein molecules. These molecules can be detected after the completion of their assembly process, including protein folding, incorporation onto the inner cell membrane, and maturation of the Venus fluorophore. Meanwhile, the repressor quickly rebinds to the operator under the highly repressing condition until the next event of protein production.

An epifluorescence microscope and a charge-coupled device (CCD) camera were used to image Venus with 514-nm laser excitation, while differential interference contrast (DIC) images were taken simultaneously to record the cell contours during growth. To count the fusion protein molecules as they were continuously generated, we photobleached the Venus fluorophores after their detection. Specifically, we applied a 1200-ms laser exposure every 3 min. The laser power used was 0.3 kW/cm^2, at which the sample photobleaching time constant is ~250 ms. Fluorescence images were recorded only in the first 100 ms, during which photobleaching is minimal, and were discarded in the following 1100 ms in order to avoid variation in the integrated signal and reduction of the signal-to-background ratio due to photobleaching. The 3-min dwell time, which defines the temporal resolution, was chosen to avoid photodamage to the cells. Cells grown under such laser illumination in a temperature-controlled sample chamber have an average cell division time of τ_{cell} = 55 min, the same τ_{cell} as in shaking M9 liquid culture without laser illumination. In each image, one cell usually produces no more than five fluorescent protein molecules, which can be spatially resolved. In principle, higher expression levels can be quantified with integrated fluorescence signals.

The activity of the *lac* promoter in the SX4 strain under the highly repressing condition was monitored for cells immobilized by an agarose gel pad of M9 media maintained at 37°C through several cell cycles, and time-lapse movies were recorded (movies S1 and S2). A sequence of images from one of them is shown in Fig. 3A. In each fluorescence image, the fluorescent spots correspond to newly synthesized fluorescent molecules during the last 3 min. Although Tsr is known to cluster at one of the cell poles (SOM Text and fig. S6), we found that Tsr-Venus protein molecules initially land on random positions in the membrane and migrate to and cluster at the cell poles at a longer time scale (SOM Text and fig. S6). Time traces of the fluorescent protein molecules along cell lineages were extracted from the time-lapse fluorescence-DIC movies (Fig. 3B). More than 60 time traces have been collected for statistical analyses.

Several qualitative features are evident from these time traces. First, protein molecules are generated in bursts. Second, the number of protein molecules in each burst varies. Third, the bursts exhibit particular temporal spreads. Analysis of the data allows us to address the following four questions: Do these gene expression bursts occur randomly in time? How many mRNA molecules are responsible for each gene expression burst under the repressed condition? What is the distribution of the number of protein molecules in each burst? And what is the origin of the temporal spread of the individual bursts?

To address the first question, we show (Fig. 4A) the distribution of the number of gene expression bursts per cell cycle for all cells. The histogram is well fit with a Poisson distribution, which suggests that gene expression bursts occur randomly and are uncorrelated in time. We also observed a weak cell cycle dependence of the burst frequency (fig. S3), which might arise from an increase of gene copy number associated with DNA replication during cell growth and does not change the Poissonian distribution. The average number of bursts is n_{burst} = 1.2 per cell cycle, yielding an average time of 46 min between two adjacent bursts. This time is comparable to in vitro dissociation times of *lac* repressor from *lac* operator O_1 (20 to 50 min) (*31*, *32*); albeit the dissociation time in live cells can be different, and each repressor dissociation event may not lead to successful transcription because of either temporary unavailability of RNA polymerase or failed transcription.

In order to answer whether the bursts arise from one copy or multiple copies of mRNA, we determined the average number of mRNA molecules per burst (m) according to $m = n_{mRNA}\tau_{cell}/(n_{burst}\tau_{mRNA})$, where n_{mRNA} is the steady-state abundance of *tsr-venus* mRNA molecules averaged over a cell population, τ_{cell} is the average cell division time, n_{burst} is the average number of expression bursts per cell division cycle, and τ_{mRNA} is the cellular lifetime of the *tsr-venus* mRNA. By using real-time reverse transcription polymerase chain reaction (RT-PCR), we obtained n_{mRNA} = 0.037 ± 0.013 for SX4 cells (table S1 and fig. S5). We also measured the cellular lifetime of *tsr-venus* mRNA to be τ_{mRNA} = 1.5 ± 0.2 min (fig. S4) by a real-time RT-PCR assay after a pulse induction of the mRNA production. It follows that m = 1.14 ± 0.42 (a 95% confidence interval; see SOM Text for more details). We thus conclude that under the repressed condition each gene expression burst results from one mRNA molecule, implying that Lac repressor quickly rebinds the exposed operator region of DNA, allowing transcription initiation of one mRNA molecule.

Next, we show the histogram of the number of protein molecules (n) produced per mRNA molecule (Fig. 4B). The distribution fits well with a single exponential decay, which is termed the geometric distribution for integer n. This distribution arises from the stochastic cellular lifetime of an mRNA molecule with mean τ_{mRNA} = 1.5 min (fig. S4) due to degradation of mRNA by ribonuclease (RNase) E, which competes with ribosomes for mRNA binding (*33*). It was shown theoretically that the probability of generating n protein molecules from one mRNA follows a geometric distribution (*11*, *12*, *34*):

$$P(n) = \rho^n(1 - \rho) \qquad (1)$$

where ρ is the probability of the ribosome binding and 1 – ρ is the probability of RNase E binding to the overlapping site on mRNA (*33*). We proved that this model is consistent with our single-molecule measurement. Data fitting of Fig. 4B to Eq. 1 yields ρ = 0.8 ± 0.1 and an average of 4.2 ± 0.5 molecules produced per burst. This number multiplied by the number of bursts per cell cycle (1.2) results in a steady-state protein abundance of 5.0 ± 0.8 molecules per cell in a cell population. Consistently, we ex-

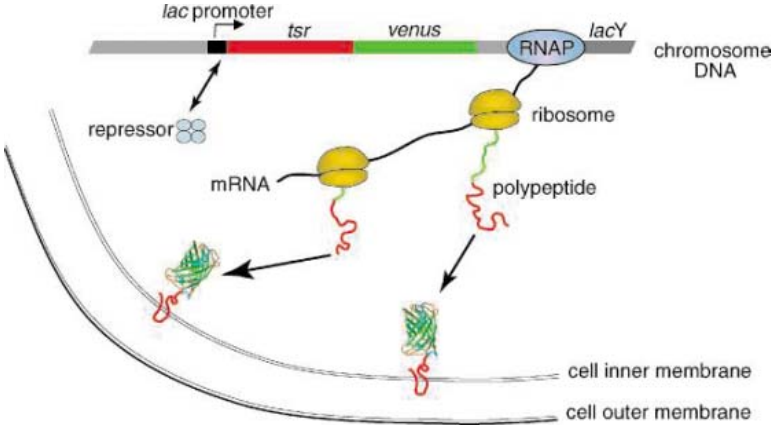

Fig. 2. Experimental design for live-cell observations of gene expression. Tsr-Venus is expressed under the control of *lac* repressor, which binds tightly to the *lac* operator on DNA. Transcription of one mRNA by an RNA polymerase results from an infrequent and transient dissociation event of repressor from DNA. Multiple copies of protein molecules are translated from the mRNA by ribosomes. Upon being assembled into *E. coli*'s inner membrane, Tsr-Venus protein molecules can be detected individually by a fluorescence microscope.

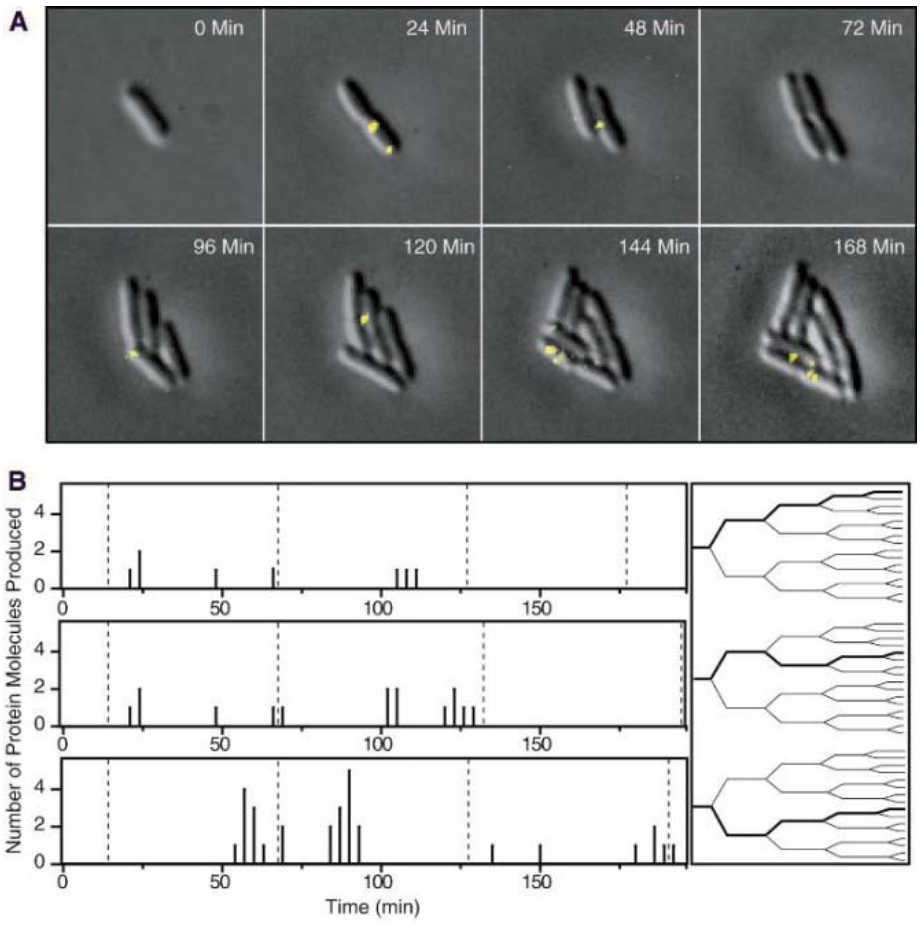

Fig. 3. Real-time monitoring of the expression of *tsr-venus* under the control of repressed *lac* promoter. (**A**) Sequence of fluorescent images (yellow) overlaid with simultaneous DIC images (gray) of *E. coli* cells expressing Tsr-Venus on agarose gel pad of M9 medium. The cell cycle is 55 ± 10 min in a temperature-controlled chamber on a microscope stage. The eight frames are from time-lapse fluorescence movie S1 taken over 195 min with 100-ms laser exposures (0.3 kW/cm^2) every 3 min. An 1100-ms exposure is applied after each image collection to photobleach the Venus fluorophores. (**B**) Time traces of the expression of Tsr-Venus protein molecules (left) along three particular cell lineages (right) extracted from the time-lapse fluorescence-DIC movie of (A). The time resolution is 3 min. The vertical axis is the number of protein molecules newly synthesized during the last three minutes. The dotted lines mark the cell division times. The time traces show that protein production occurs in random bursts, within which variable numbers of protein molecules are generated. Each gene expression burst lasts ~3 to 15 min.

perimentally measured this abundance to be 4.1 ± 1.8 molecules per cell by counting the molecules in ~300 individual cells under the microscope at the same time.

Lastly, the temporal spread of the expression bursts can be characterized from the autocorrelation function of the fluctuation in protein expression, $C^{(2)}(\tau)$ (Fig. 4C), averaged from 30 different cell lineages from 15 different movies. The single exponential fit of $C^{(2)}(\tau)$ gives a decay time constant of 7.0 ± 2.5 min, corresponding to the average spread of the stochastic arrival times of fluorescent reporter proteins within a burst, despite the fact that the polypeptides are generated within the short lifetime of an mRNA (τ_{mRNA} = 1.5 min). We show (SOM Text) that, under the condition that there is one rate-limiting step for the posttranslation assembly of the fusion protein,

$$C^{(2)}(\tau) = \left(\frac{s\rho}{1-\rho}\right)^2\left[1 + \frac{\kappa}{s}\exp(-\kappa\tau)\right] \quad (2)$$

where s is the average rate of the expression burst and κ is the rate constant of Tsr-Venus assembly process, consisting of transcription, translation, folding, and chromophore maturation. The fitting of Fig. 4C with Eq. 2 gives $s = (29 \pm 8\ \text{min})^{-1}$, in agreement with the average number of expression bursts per cell cycle of 1.2 ± 0.3 (Fig. 4A); $\rho = 0.7 \pm 0.1$, consistent with the value of 0.8 ± 0.1 determined from Fig. 4B; and $1/\kappa = 7.0 \pm 2.5$ min, corresponding to the rate-limiting step of the protein assembly process. Considering the fast transcription (~45 bases/s) and translation (~15 residues/s) rates, we tentatively assign $1/\kappa$ to the fluorophore maturation process (SOM Text). Although we can only spatially resolve a few molecules within an *E. coli* cell because of the diffraction limit, the long spread of the stochastic arrival times of Venus allows many more protein molecules per expression burst to be counted in several consecutive images.

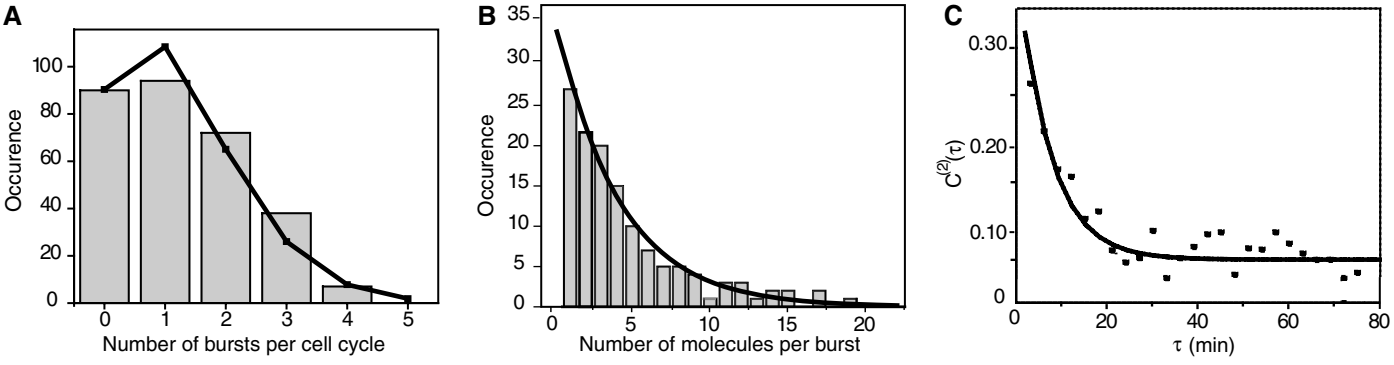

Fig. 4. Statistical analyses of the protein production time traces. (**A**) Histogram (gray bars) of the number of expression events per cell cycle. The data fit well to a Poisson distribution (solid line) with an average of 1.2 gene expression burst per cell cycle. (**B**) Distribution of the number of fluorescent protein molecules detected in each gene expression burst, which follows a geometric distribution (solid line), giving a probability of ribosome binding of 0.81 ± 0.05 and an average number of molecules per burst of 4.2. (**C**) Autocorrelation function of the protein production time traces calculated according to Eq. S9. The result is averaged from 30 individual cell lineages because of the insufficient statistics of a single time trace. The fitting to Eq. 2 (solid line) gives $1/\kappa = 7.0 \pm 2.5$ min, which is attributed to posttranslational assembly of the fluorescent fusion protein.

Gene expression, central to life processes, is intrinsically a stochastic process involving low copy number of biomolecules. Our real-time assay allows probing of low copy number proteins in single live cells not accessible by current technologies. This approach, together with other emerging single-molecule techniques (*35*), will yield further insight into not only gene expression but also other fundamental biological processes.

References and Notes

1. F. Jacob, J. Monod, *Cold Spring Harbor Symp. Quant. Biol.* **26**, 193 (1961).
2. J. Beckwith, *Science* **156**, 597 (1967).
3. W. Gilbert, B. Muller-Hill, *Proc. Natl. Acad. Sci. U.S.A.* **58**, 2415 (1967).
4. M. Ptashne, A. Gann, *Genes and Signals* (Cold Spring Harbor Laboratory Press, Cold Spring Harbor, NY, 2002).
5. X. S. Xie, H. P. Lu, *J. Biol. Chem.* **274**, 15967 (1999).
6. C. Bustamante, Z. Bryant, S. Smith, *Nature* **421**, 423 (2003).
7. A. Ishijima, T. Yanagida, *Trends Biochem. Sci.* **26**, 438 (2001).
8. S. Weiss, *Science* **283**, 1676 (1999).
9. M. D. Wang *et al.*, *Science* **282**, 902 (1998).
10. S. Blanchard, R. Gonzalez, H. Kim, S. Chu, J. Puglisi, *Nat. Struct. Mol. Biol.* **11**, 1008 (2004).
11. O. Berg, *J. Theor. Biol.* **71**, 587 (1978).
12. D. Rigney, *J. Theor. Biol.* **79**, 247 (1979).
13. J. Paulsson, *Nature* **427**, 415 (2004).
14. J. Paulsson, *Phys. Life Rev.* **2**, 157 (2005).
15. Y. Shav-Tal *et al.*, *Science* **304**, 1797 (2004).
16. I. Golding, E. Cox, *Proc. Natl. Acad. Sci. U.S.A.* **101**, 11310 (2004).
17. N. Barkai, S. Leibler, *Nature* **403**, 267 (2000).
18. E. M. Ozbudak, M. Thattai, I. Kurtser, A. D. Grossman, A. van Oudenaarden, *Nat. Genet.* **31**, 69 (2002).
19. M. B. Elowitz, A. J. Levine, E. D. Siggia, P. S. Swain, *Science* **297**, 1183 (2002).
20. N. Rosenfeld, J. W. Young, U. Alon, P. S. Swain, M. B. Elowitz, *Science* **307**, 1962 (2005).
21. S. Ghaemmaghami *et al.*, *Nature* **425**, 737 (2003).
22. P. Guptasarma, *Bioessays* **17**, 987 (1995).
23. Materials and methods are available as supporting material on *Science* Online.
24. R. J. Bongaerts, I. Hautefort, J. M. Sidebotham, J. C. Hinton, *Methods Enzymol.* **358**, 43 (2002).
25. R. Y. Tsien, *Annu. Rev. Biochem.* **67**, 509 (1998).
26. M. Chalfie, Y. Tu, G. Euskirchen, W. W. Ward, D. C. Prasher, *Science* **263**, 802 (1994).
27. T. Nagai *et al.*, *Nat. Biotechnol.* **20**, 87 (2002).
28. P. H. Lommerse *et al.*, *Biophys. J.* **86**, 609 (2004).
29. J. Deich, E. M. Judd, H. H. McAdams, W. E. Moerner, *Proc. Natl. Acad. Sci. U.S.A.* **101**, 15921 (2004).
30. S. L. Mowbray, M. O. J. Sandgren, *J. Struct. Biol.* **124**, 257 (1998).
31. K. Bondeson, A. Frostellkarlsson, L. Fagerstam, G. Magnusson, *Anal. Biochem.* **214**, 245 (1993).
32. W. Hsieh, P. Whitson, K. Matthews, R. Wells, *J. Biol. Chem.* **262**, 14583 (1987).
33. O. Yarchuk, N. Jacques, J. Guillerez, M. Dreyfus, *J. Mol. Biol.* **226**, 581 (1992).
34. H. H. McAdams, A. Arkin, *Proc. Natl. Acad. Sci. U.S.A.* **94**, 814 (1997).
35. L. Cai, N. Friedman, X. S. Xie, *Nature* **440**, 358 (2006).

36. We thank P. Choi, L. Cai, N. Friedman, J. Elf, L. Xun, and R. Losick for helpful discussions and critical reading of the manuscript, J. Hearn for technical assistance, and A. Miyawaki (RIKEN) for the generous gift of the *venus* gene. This work was supported by NIH Director's Pioneer Award program, a NIH R21 grant, and in part by U.S. Department of Energy, Office of Science, and Applied Biosystems' Exploratory Fund. J.Y. acknowledges a Genome-Related Research Award from Merck.

Supporting Online Material

www.sciencemag.org/cgi/content/full/311/5767/1600/DC1
Materials and Methods
SOM Text
Figs. S1 to S6
Table S1
References
Movies S1 and S2

1 September 2005; accepted 7 February 2006
10.1126/science.1119623

Late Colonization of Easter Island

Terry L. Hunt[1]* and Carl P. Lipo[2]

Easter Island (Rapa Nui) provides a model of human-induced environmental degradation. A reliable chronology is central to understanding the cultural, ecological, and demographic processes involved. Radiocarbon dates for the earliest stratigraphic layers at Anakena, Easter Island, and analysis of previous radiocarbon dates imply that the island was colonized late, about 1200 A.D. Substantial ecological impacts and major cultural investments in monumental architecture and statuary thus began soon after initial settlement.

With an empty landscape containing gigantic statues and other cultural achievements, Easter Island, or Rapa Nui, symbolizes an isolated civilization that once flourished but suffered ecological catastrophe. Central to understanding the cultural, ecological, and demographic processes that shaped Rapa Nui's prehistory is the establishment of a reliable chronology for the island. Here, we provide radiocarbon dates from deposits likely to represent the earliest occupation on the island and evaluate previous ^{14}C dates to show that Rapa Nui's prehistoric chronology is later than has been commonly assumed.

Early Polynesians colonized Fiji, Tonga, and Samoa in the central South Pacific about 2800 years ago. Accumulating evidence shows that continued expansion from Samoa-Tonga into eastern Polynesia (e.g., Cooks, Societies, Marquesas, and Hawaii) did not occur until after 800 A.D., although notably longer chronologies have been suggested and debated (*1*–*3*). Many eastern Polynesian sites once considered centuries older have been shown to be consistently younger (*4*, *5*). For example, it is now thought that New Zealand was colonized after 1200 A.D., about 400 years after the date that has long been assumed (*6*). This date has been confirmed by radiocarbon dating of seeds gnawed by the Polynesian rat (*Rattus exulans*) (*7*), clear evidence of human presence because rats are commensal species.

Smith (*8*) obtained initial radiocarbon dates from Rapa Nui with the Norwegian expedition of Heyerdahl in the 1950s. His suite of 19 radiocarbon dates included one from a burn horizon at Poike Ditch of 400 A.D. [1570 ± 80 years before the present (yr B.P.), 384 to 664 calibrated (cal) A.D.]. Subsequent researchers cited the

Table 1. Radiocarbon dates from recent excavations at the Anakena Dune site.

Sample Beta-	Material/layer	Radiocarbon age (yr B.P.)	$^{13}C/^{12}C$	Conventional C^{14} age (yr B.P.)	2σ calibration (cal A.D.) (*19*, *20*)	Probability
196711	Charcoal/Unit 1 Layer 8	660 ± 40	−24.9	660 ± 40	1294–1403	1.00
196712	Charcoal/Unit 1 Layer 5	690 ± 60	−25.6	680 ± 60	1274–1414	1.00
196713	Charcoal/Unit 1 Layer 8	670 ± 40	−24.8	670 ± 60	1291–1400	1.00
196714	Charcoal/Unit 1 Layer 9	600 ± 60	−26.0	590 ± 60	1300–1368	0.369341
					1373–1450	0.630659
196715	Charcoal/Unit 1 Layer 11	670 ± 40	−22.5	710 ± 40	1279–1391	1.00
196716	Charcoal/Unit 1 Layer 12	720 ± 60	−24.7	720 ± 60	1229–1251	0.046194
					1260–1400	0.953806
209903	Charcoal/Unit 5 Base	870 ± 80	−23.8	870 ± 80	1029–1300	0.996544
					1368–1372	0.003456
209904	Charcoal/Unit 5 Base	870 ± 40	−23.8	870 ± 40	1055–1058	0.003916
					1151–1278	0.996084

[1]Department of Anthropology, University of Hawai'i Manoa, 2424 Maile Way, Honolulu, HI 96822, USA. [2]Department of Anthropology and Institute for Integrated Research in Materials, Environments, and Society, California State University Long Beach, 1250 Bellflower Boulevard, Long Beach, CA 90840, USA.

*To whom correspondence should be addressed. E-mail: thunt@hawaii.edu

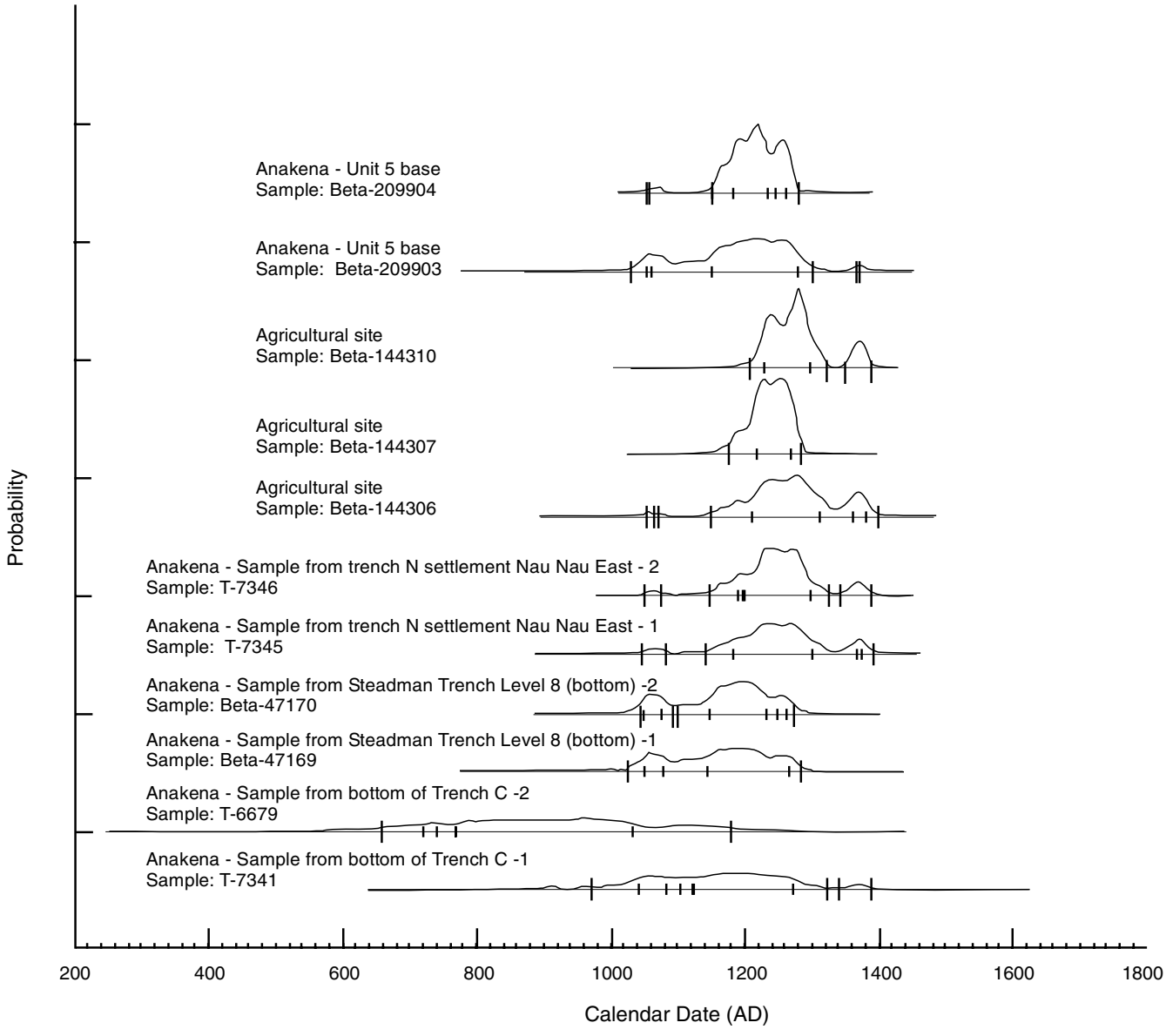

Fig. 1. Probability distributions for 11 calibrated pre-750 yr B.P. dates that meet "chronometric hygiene" criteria from Rapa Nui; included are two new dates on wood charcoal from the base of recent excavations at the Anakena Dune site.

early date as consistent with models for historical linguistics in Polynesia (*9*, *10*). Three dates on lake core sequences also provided, it seemed, evidence for an early colonization. The earliest signs of abrupt and massive vegetation change appeared to occur about 750 A.D. (*11*), suggesting the arrival of the first Polynesians. This long chronology has formed the basis of many accounts of the region's prehistory (*12*).

Recent studies have highlighted sources of error that may render radiocarbon chronologies from both archaeology and paleoenvironmental work erroneously old (*3*). Indeed, a recent analysis has shown the anomalous dating of bulk sediment samples from the lake cores of Rapa Nui (*13*). The lake core sediment dates reflect the continuous deposition of both old and young organic components, resulting in dates that are too old by hundreds of years (*14*). This makes the present radiocarbon dates of bulk sediment from lake cores problematic, at least in terms of generating high-resolution paleoenvironmental reconstruction for Rapa Nui.

Recently questions have arisen about the long chronology. In an analysis compiling over 120 radiocarbon dates for the island, Martinsson-Wallin and Crockford (*15*) (table S1) rejected the early Poike date and questioned the validity of dates from 400 to 800 A.D. These authors concluded that dates before 800 A.D. were unreliable, but they accepted radiocarbon ages from 800 to 1200 A.D. and concluded that colonization dated to the beginning of that period (*15*).

Over the past two field seasons (2004 and 2005) on Rapa Nui, we excavated primary, in situ, and deeply stratified archaeological deposits at Anakena (figs. S1 to S6). Anakena is the island's only sand dune and provides a stratified context of archaeological materials with superb preservation. In 2004 and 2005, we excavated an area of 14 m^2 containing 12 distinctive strata to a depth of more than 345 cm below surface (figs. S2 to S6 and table S2). The basal layer of these strata was clay substrate with an in situ primeval soil (paleosol) containing artifacts, charcoal, faunal remains (including *R. exulans*, introduced by Polynesians), and the distinctive tubular root molds of the giant, extinct *Jubaea* palm (also designated *Paschalococos disperta*). Below this horizon, the remaining stratum of clay was entirely devoid of cultural materials. Thus, the basal cultural layer preserves evidence of the initial human occupation at Anakena and, given the environmental context, probably the primary occupation for the island (*15*, *16*).

Our excavations yielded faunal remains in quantities and composition comparable to the

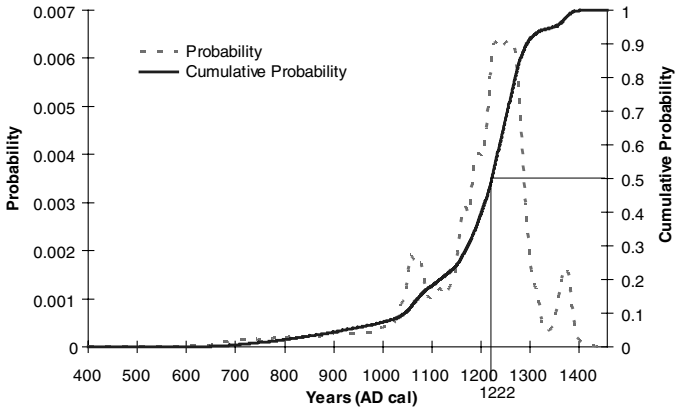

Fig. 2. Aggregate (dashed line) and cumulative (solid line) probabilities for 11 calibrated pre-750 yr B.P. dates from Rapa Nui using CALIB 5.0 (*19*) and the southern hemisphere calibration curve, SHCal04 (*20*). The aggregate is the sum of probabilities at any particular point in time. The cumulative probability represents increasing confidence of dating the colonization event in the radiocarbon data set. A confidence of 0.50 is reached at 1222 cal A.D., suggesting colonization by this time. The tail permits earlier settlement (e.g., 1050 to 1150 A.D.), but the probability is very low based on the current radiocarbon record.

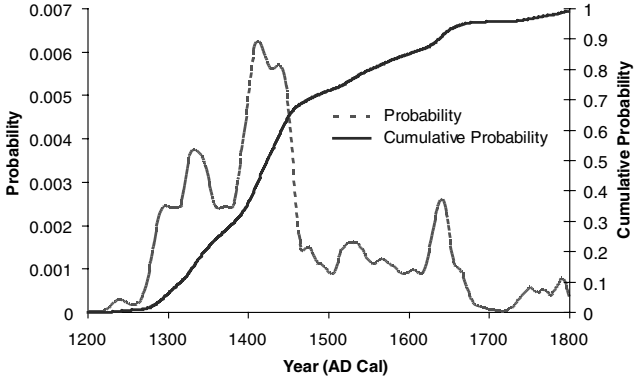

Fig. 3. Aggregate (dashed line) and cumulative (solid line) probabilities for 41 calibrated radiocarbon dates associated with extinct *Jubaea* palm remains and/or truncated primeval soils indicating human induced erosion. Note the post-1200 A.D. ranges for all dates and the steep rise after 1300 cal A.D. We compiled these dates from island-wide paleoenvironmental research reported by Mann *et al.* (*23*) and Mieth and Bork (*24*).

well-known early assemblage excavated by Steadman *et al*. (*16*) at Anakena, where they reported 7311 specimens comprising (i) dolphin, (ii) rat, (iii) fish, (iv) bird, (v) pinniped, and (vi) human, in order of abundance. We recovered 6533 identifiable bones in which the *R. exulans* ranks first in quantity, followed by (ii) fish, (iii) sea mammals, (iv) bird, (v) human, (vi) "medium mammal" (i.e., likely sea mammal bone fragments and possible pinniped remains), and (vii) sea turtle. Both of the collections are notably different than later faunal assemblages from Rapa Nui that generally lack marine mammal resources.

To establish a chronology for the Anakena Dune strata, we obtained eight radiocarbon dates on wood charcoal samples (Table 1). We selected small wood charcoal specimens (i.e., from short-lived taxa) acquired from the same stratum or from directly superimposed strata. Pairing samples from stratigraphic contexts in this way allows for replication in radiocarbon assays. These radiocarbon results are consistent with stratigraphic superposition; they overlap in age at two standard deviations and document human occupation beginning about 1200 cal A.D. These late dates from Anakena led us to question the longer chronologies widely accepted for Rapa Nui.

Following primary criteria from the protocol established by Spriggs and Anderson (*4*, *6*) and further developed among radiocarbon specialists (*17*), we compiled 45 published radiocarbon dates reported as older than 750 yr B.P. (uncalibrated radiocarbon years) for Rapa Nui (table S1). This age approximates the earliest radiocarbon values from our recent excavations at Anakena, but use of this younger age allows us to consider a large pool of radiocarbon results. By using the general approach of Spriggs and Anderson (*4*), we rejected dates on only three criteria: (i) those measured on unacceptable materials such as marine materials or terrestrial animal bone, which can be grossly affected by incorporation of old carbon from the marine reservoir effect and can have variable or poorly known correction procedures (*3*, *4*, *18*); (ii) samples of mixed isotopic fractionation (e.g., mixed charcoal and soil); and (iii) single radiocarbon dates not replicated with overlap at two standard deviations from the same archaeological context, albeit here broadly defined by stratum or adjacent strata. We used fewer criteria than Spriggs and Anderson (*4*), making our sample of dates more inclusive but more vulnerable to the acceptance of dates that are erroneously old. Applying these criteria, we have a sample of 11 radiocarbon dates of 750 yr B.P. or older: eight from excavations at Anakena, including our own, and three dates from "agricultural features" (*15*) (Fig. 1 and table S1). The calibrated probability distributions of these radiocarbon ranges (*19*, *20*) center around 1200 cal A.D. and all overlap at two standard deviations, with only a single determination (T-6679) yielding a long, flat calibrated range of low probabilities from 657 to 1180 cal A.D. (2σ).

The assemblage of 11 calibrated dates are age probabilities that, when aggregated, estimate a cumulative probability for the target event of the first human colonization of Rapa Nui (Fig. 2). The distribution shows that a 0.50 confidence, a better than chance estimation, is not reached until 1222 cal A.D. for the date of initial occupation of Rapa Nui. The error terms of these radiocarbon estimates permit earlier settlement; however, the chance in probability terms remains low. For example, the available dates show that a settlement event by 1050 A.D. has an aggregate probability of 0.0017 and a cumulative probability of only 0.24, i.e., possible, but less likely in the overall distribution. Additional radiocarbon dates will likely change the probability distribution and could reveal colonization of Rapa Nui sometime slightly earlier than 1200 A.D. (e.g., circa 1050 to 1150 A.D.).

These dates postdate by 700 to 800 (*12*) or at least 300 to 400 (*15*) years from the widely accepted human chronologies for Easter Island. Yet, a date of about 1200 A.D. for the colonization of Rapa Nui fits well with the evidence that has emerged for colonization from elsewhere in the southeastern Pacific (*4*, *5*), including remote islands such as Mangareva (*21*).

A late chronology challenges our understanding of the dramatic environmental changes that occurred on the island, highlighted by deforestation and concomitant erosion of primeval soils. We anticipate that given the effects of colonization, including introduction of the Polynesian rat, evidence of ecological change such as deforestation will closely mark the time of Polynesian arrival (*22*). Forty-one radiocarbon dates directly associated with deforestation from multiple sites around the island (*23*, *24*) (table S3) all fall after 1200 A.D., and most cluster after 1300 A.D. (Fig. 3). The long chronology (*23*, *24*) requires that Polynesian settlers had virtually no impact on the island's ecology and maintained an exceptionally low population growth rate for several centuries until a point of abrupt, dramatic human impacts. However, Polynesian "supertramp" populations expanded their numbers over the vast Pacific in a remarkably short time (*25*). Indeed, rapid population growth would be critical to successful colonization of remote islands. With even small numbers of initial colonizers (e.g., 50) at 3.0% growth rate (*26*), populations would rise dramatically and reach more than 2000 (a density of over 10 people per square kilometer on Rapa Nui) in just over 100 years.

Our analysis and dates for Rapa Nui imply that colonists arrived around 1200 A.D. The founding Polynesian population then grew rap-

idly, had immediate, major, and visible impacts on the island's biota and physical landscape, and began investing in monumental architecture and statuary within the first century or two of settlement. Although still poorly dated, monumental architecture and statuary are known from islands, such as the Societies, Marquesas, and Austral Islands, from perhaps as early as 1200 A.D. Nearly immediate building of monuments, carving giant statues, and transporting them to every corner of the island may have been cultural investments, homologous to forms elsewhere in eastern Polynesia, that mediated against overpopulation and resource shortfalls in an unpredictable environment. Such a model would help to explain the success of ancient Polynesians on tiny, remote Rapa Nui (*27*). Demographic and cultural collapse resulted from European contact beginning in 1722 A.D. with the devastating consequences of newly introduced Old World diseases to a nonimmune Polynesian population (*28*, *29*).

References and Notes

1. P. V. Kirch, J. Ellison, *Antiquity* **68**, 310 (1994).
2. A. Anderson, *Antiquity* **68**, 845 (1994).
3. A. Anderson, *J. Polynesian Soc.* **104**, 110 (1995).
4. M. Spriggs, A. Anderson, *Antiquity* **67**, 200 (1993).
5. A. Anderson, Y. Sinoto, *Asian Perspect.* **41**, 242 (2002).
6. A. Anderson, *Antiquity* **65**, 767 (1991).
7. J. Wilmshurst, T. Higham, *Holocene* **14**, 801 (2004).
8. C. Smith, in *The Archaeology of Easter Island, Vol. 1*, T. Heyerdahl, E. Ferdon, Eds. (Monographs of the School of American Research and the Museum of New Mexico, Santa Fe, NM, 1961), pp. 393–396.
9. R. Green, *J. Polynesian Soc.* **75**, 6 (1966).
10. W. Ayres, *J. Polynesian Soc.* **80**, 497 (1971).
11. J. Flenley, in *Easter Island Studies: Contributions to the History of Rapanui in Memory of William T. Mulloy*, S. R. Fischer, Ed. (Oxford Books, Oxford, 1993), pp. 27–45.
12. P. Kirch, *On the Road of the Winds: An Archaeological History of the Pacific Islands Before European Contact* (Univ. California Press, Berkeley, CA, 2000).
13. K. Butler, C. Prior, J. Flenley, *Radiocarbon* **46**, 395 (2004).
14. McGlone and Wilmshurst (*30*) document a similar problem in radiocarbon dating the inception of continuous deforestation in New Zealand. Lake and swamp cores susceptible to in-washing of old carbons yielded dates hundreds of years older than deforestation events recorded in ombrogenous peat bog strata.
15. H. Martinsson-Wallin, S. Crockford, *Asian Perspect.* **40**, 244 (2002).
16. D. Steadman, P. Vargas Casanova, C. Cristino Ferrando, *Asian Perspect.* **33**, 79 (1994).
17. T. F. G. Higham, A. G. Hogg, *Radiocarbon* **39**, 149 (1997).
18. Beck *et al.* (*31*) established a shallow-water marine reservoir correction for Rapa Nui. In the same study they report radiocarbon dating of 27 abraded coral artifacts, many identified as statue eye fragments. As listed in table S1, 15 of these dates on coral artifacts are greater than 750 yr B.P. For our analysis, we reject these dates. As Beck *et al.* correctly point out, the coral may have been collected live, or perhaps more likely given ease of access to beach cobbles, used long after the death of the coral. Beck *et al.* also warn that living coral is comprised of significantly older interior parts. We take these caveats to mean that there is no warrant to treat the death of coral and its use in artifacts as an event known to be contemporaneous or necessarily closely related in time. Indeed, the coral death ages will be systematically older than the manufacture events, but by unknowable amounts.
19. M. Stuiver, P. J. Reimer, R. W. Reimer, CALIB 5.0 (http://calib.qub.ac.uk/calib/).
20. F. G. McCormac *et al.*, *Radiocarbon* **46**, 1087 (2004).
21. P. Kirch, E. Conte, in *Archaeological Investigations in the Mangareva Islands (Gambier Archipelago), French Polynesia*, E. Conte, P. Kirch, Eds. (Archaeological Research Facility, University of California, Berkeley, 2004), pp. 149–159.
22. J. S. Athens, H. D. Tuggle, J. V. Ward, D. J. Welch, *Archaeol. Oceania* **37**, 57 (2002).
23. D. Mann *et al.*, in *Easter Island: Scientific Exploration into the World's Environmental Problems in Microcosm*, J. Loret, J. Tanacredi, Eds. (Kluwer Academic, New York, 2003), pp. 133–153.
24. A. Mieth, H.-R. Bork, *Easter Island-Rapa Nui: Scientific Pathways to Secrets of the Past* (Man and Environment I, University of Kiel, Kiel, Germany, 2004).
25. J. Diamond, W. Keegan, *Nature* **311**, 704 (1984).
26. J. Birdsell, *Cold Spring Harbor Symp. Quant. Biol.* **22**, 47 (1957).
27. T. Hunt, C. P. Lipo, in *Pacific 2000: Proceedings of the Fifth International Conference on Easter Island and the Pacific*, C. Stevenson, G. Lee, F. Morin, Eds. (Easter Island Foundation, Los Osos, USA, 2001), pp. 103–115.
28. P. Rainbird, *World Archaeol.* **33**, 436 (2002).
29. B. Peiser, *Energy Environ.* **16**, 513 (2005).
30. M. S. McGlone, J. M. Wilmshurst, *Quaternary Int.* **59**, 5 (1999).
31. J. W. Beck, L. Hewitt, G. S. Burr, J. Loret, F. Torres Hochstetter, in *Easter Island: Scientific Exploration into the World's Environmental Problems in Microcosm*, J. Loret, J. Tanacredi, Eds. (Kluwer Academic, New York, 2003), pp. 93–111.

Supporting Online Material

www.sciencemag.org/cgi/content/full/1121879/DC1
SOM Text
Figs. S1 to S6
Tables S1 to S3
References and Notes

26 October 2005; accepted 21 February 2006
Published online 9 March 2006;
10.1126/science.1121879
Include this information when citing this paper.

Reward Timing in the Primary Visual Cortex

Marshall G. Shuler and Mark F. Bear*

We discovered that when adult rats experience an association between visual stimuli and subsequent rewards, the responses of a substantial fraction of neurons in the primary visual cortex evolve from those that relate solely to the physical attributes of the stimuli to those that accurately predict the timing of reward. In addition to revealing a remarkable type of response plasticity in adult V1, these data demonstrate that reward-timing activity—a "higher" brain function—can occur very early in sensory-processing paths. These findings challenge the traditional interpretation of activity in the primary visual cortex.

Primary visual cortex (V1) is the most peripheral station in the ascending visual pathway where information from the two eyes is combined, and specific features of visual stimuli, such as orientation and direction of movement, are represented by neural activity (*1*, *2*). It has long been held that, although the quality of sensory experience is used to fine-tune visual response properties during a critical period of early postnatal life, plasticity of visual responses in adults is sharply limited so as to ensure that sensory processing is reliable and reproducible. Only after the initial processing in V1 are subsequent brain regions thought to be engaged to elaborate on the significance of visual input, holding it in working memory (*3*–*8*), attributing behavioral and predictive value (*9*–*12*), and ultimately engendering appropriate behaviors.

The view of adult primary visual cortex as an immutable feature detector has undergone revision in recent years. It is now understood that deprivation and selective visual experience continue to alter cortical responsiveness in adulthood (*13*, *14*) and that V1 activity can be rapidly modulated in various behavioral contexts (*15*–*18*). However, all these changes in activity can still be readily interpreted in the context of visual processing. Our experiments challenge current understanding of what activity in V1 represents.

Adult, Long-Evans rats were fitted with head-mounted goggles that delivered full-field retinal illumination for 0.4 s to either the right eye or the left eye (fig. S1a). Action potentials evoked in response to these stimuli were monitored with chronically implanted arrays of microelectrodes, subsequently confirmed by histology to have resided in the deep layers of primary visual cortex (fig. S2). Either left- or right-eye illumination was delivered when the rat neared a water tube. Left eye stimulation portended delivery of a drop of water after x licks on the water tube (fig. S1b), whereas right eye stimulation portended delivery of water after twice that number of licks, $2x$, (where x equaled 6 licks for three rats and 10 licks for two additional rats). Half of all the trials were unrewarded, so as to address whether changes in neural response were a result of reward delivery itself, or alternatively, reflected the formation of neural associations between stimuli and reward expectancy.

Howard Hughes Medical Institute, The Picower Institute for Learning and Memory, Department of Brain and Cognitive Sciences, Massachusetts Institute of Technology, Cambridge, MA 02139, USA.

*To whom correspondence should be addressed. E-mail: mbear@mit.edu

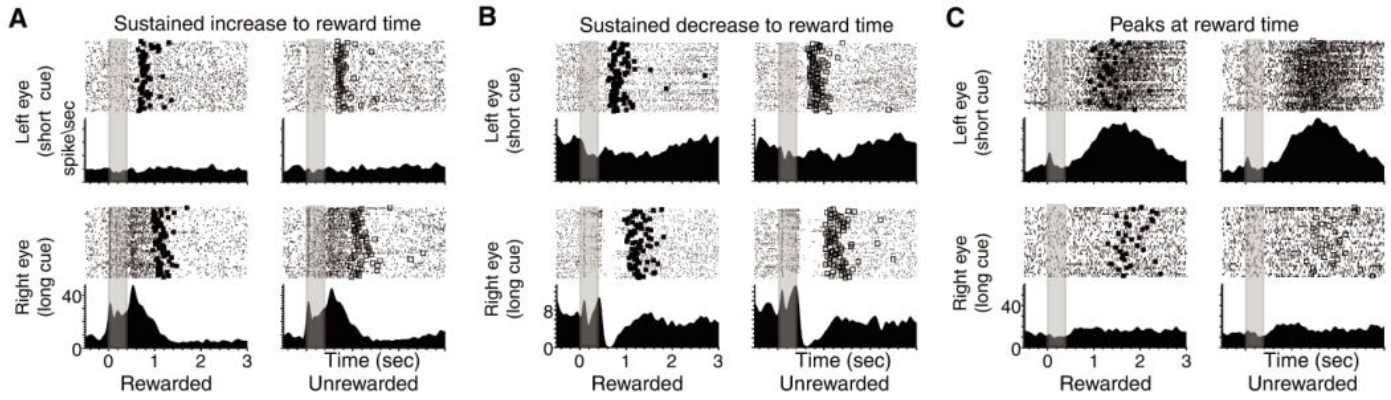

Fig. 1. Three forms of reward timing in V1. Three neurons with their peristimulus time histograms and raster plots for each of the four stimulus conditions are presented. Filled squares on raster plots indicate when reward was given on rewarded trials, whereas open squares indicate when reward would have been given if not an unrewarded trial. Shaded transparent box indicates time of stimulus. Note that reward-timing activity emerges in response to stimulation of only one eye: right eye (**A** and **B**); left eye (**C**).

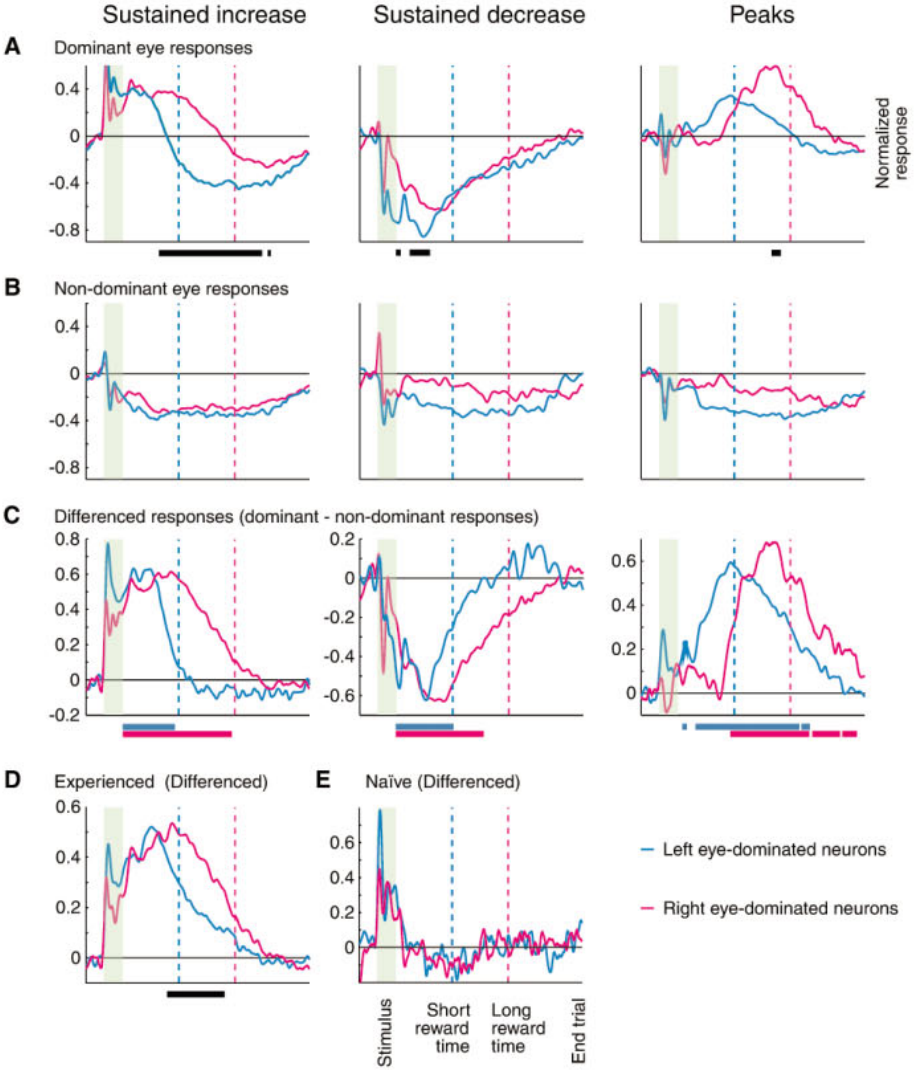

Fig. 2. Mean responses of neural subpopulations dominated by the left versus right eye. Time in reference to the events of the task is shown on the *x* axes. Dashed blue and pink vertical lines indicate mean short and long reward times, respectively. Normalized population responses are shown on the *y* axes. (**A**) Dominant eye responses for subpopulations dominated by the left (blue) and right eye (pink) for each of the three response classes. Black bar along *x* axes indicates time in which the responses of the subpopulations dominated by the left and right eye significantly differ ($P < 0.05$). (**B**) Mean responses evoked by neurons' nondominant eye do not significantly differ at any poststimulus moment for subpopulations dominated by the left or right eye. (**C**) Subtracting each neuron's dominant (A) by nondominant (B) response yields the differenced responses for each eye-dominated subpopulation, the mean of which is shown in (C) for each of the three response classes. Intervals significantly different from zero (99% confidence interval) are shown as bars below the *x* axis. (**D**) Mean response of all reward-timing neurons from experienced animals. Black bar along *x* axis indicates time in which differenced responses dominated by the left and right eye significantly differ ($P < 0.05$). (**E**) Left eye–dominated and right eye–dominated differenced responses from naïve animals do not significantly differ at any poststimulus moment.

Responses of V1 neurons in animals inexperienced with the task related to the physical attributes of the visual stimuli, such as the onset, offset, duration, and the eye of origin [$n = 5$ animals, 65 neurons (fig. S3)]. However, over the course of three to seven sessions performing the task, a significant proportion of neurons began to express activity in response to one of the two visual cues that was clearly correlated with the reward time associated with that visual cue (Fig. 1, A to C). This poststimulus response relating to expected reward time appeared to occur only to stimulation of one of the two eyes, even in neurons with binocular short-latency visual responses (confirmed quantitatively below).

In experienced animals (after reward-timing activity was first detected), 43% of the recorded neurons (130 out of 300) showed reward timing. Of these, 50% (65 out of 130) showed a sustained increase in response until the reward was expected, 22% (29 out of 130) showed a sustained decrease in response until the reward was expected, and 28% (36 out of 130) showed responses that peaked at reward time (Fig. 1, A to C). The emergence of apparent timing activity was not related to the delivery of the reward per se, because rewarded and unrewarded trials evoked responses that were indistinguishable from each other. Instead, poststimulus activity appeared to be related to reward-time prediction, as it occurred reliably during the unrewarded trials.

We wished to assess at the population level our qualitative observation that neurons with significant poststimulus modulation related reward expectancy. Because poststimulus activity appeared to be triggered in any given neuron by stimulation of only one eye, the initial step in our analysis was to determine quantitatively for each neuron which eye was dominant and which eye was nondominant for poststimulus modulation (*19*). Applying our algorithm, we found that 60% (78 out of 130) of neurons with reward timing were left eye–dominated and 40% (52 out of 130) were right eye–dominated. By assessing poststimulus eye dominance, we could then test the working hypothesis that neurons dominated by the left or right eye express different reward-time expectancies.

To address this question, we pooled neuronal responses across all animals and recording sessions by normalizing activity to its maximal extent from baseline and by normalizing the time to that which elapsed between events within each session (stimulus offset, mean short reward time, mean long reward time, and trial end). This normalization procedure allowed us to average the activity modulation in the task across all 130 neurons to yield population responses evoked by neurons' dominant (Fig. 2A) and nondominant eye (Fig. 2B). Neural subpopulations dominated by the left and right eyes differed significantly in their poststimulus modulation to dominant-eye stimulation (Fig. 2A), consistent with the interpretation that the different populations relate the different reward times. In the same neurons, analysis of evoked activity to the nondominant eye showed no such difference in time course between the left and right eye subpopulations, consistent with our impression that reward-timing activity was driven only by the dominant eye (Fig. 2B).

If both eyes evoke responses that report the properties of the stimulus, but only one eye evokes poststimulus reward-timing activity, then the activity unique to timing can be revealed by taking the interocular difference of responses to the dominant and nondominant eye for each neuron. This analysis reveals an even stronger relation between neural activity and reward times (Fig. 2C). For left eye–dominated and right eye–dominated neurons classified as "sustained increase" or "sustained decrease," the moment in which the "differenced" interocular mean responses are no longer distinguishable from zero (<99% confidence level) corresponds well to their respective reward times. Similarly, for "peak" neurons dominated by the left or the right eye, the moment in which the differenced interocular mean responses are maximally different from zero corresponds well to their respective cue-related reward times.

The population data can also be analyzed without dividing cells into response categories, and because response categories do not preexist when animals are relatively inexperienced in the task, this method provides a means of fairly comparing naïve and experienced responses (*19*). This analysis revealed in experienced animals a statistically significant difference in the time course of poststimulus modulation between left eye–dominated and right eye–dominated neurons that closely matched the difference in short and long reward times, respectively (Fig. 2D). Using the same analysis, neurons recorded from animals in the naïve state (before exhibiting reward timing) revealed no such difference (Fig. 2E). Therefore, after animals gained experience in the task, two functional groups of neurons emerged: one group that signals expectancy to the short reward time evoked by stimulation of the left eye, and the other group that signals expectancy to the long reward time, evoked by stimulation of the right eye.

How accurately do individual neural responses relate the visual cues to their appropriately associated reward time? To quantify this question, a moment of poststimulus time was credited as being the neuron's report of reward expectancy (fig. S4), which we designated the "neural reward moment" (NRM) (*19*). The NRMs for left eye– and right eye–dominated neurons across the entire population were then

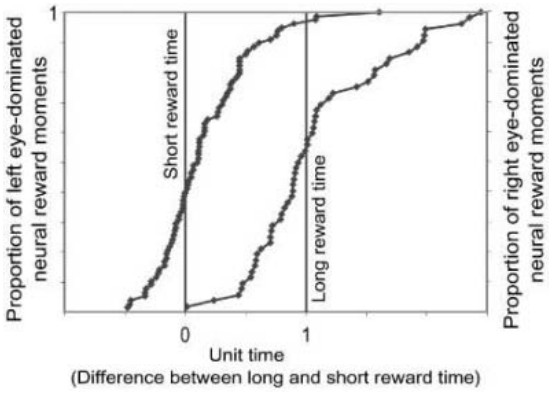

Fig. 3. Cue-evoked neural timing of short and long reward expectancy. Cumulative histograms of neural reward moments for neural subpopulations dominated by the left (leftmost curve) or right (rightmost curve) eye are shown and differ significantly (Kolmogorov-Smirnov test, $P < 0.001$). The proportion of time between the short and long reward times is shown on the *x* axis.

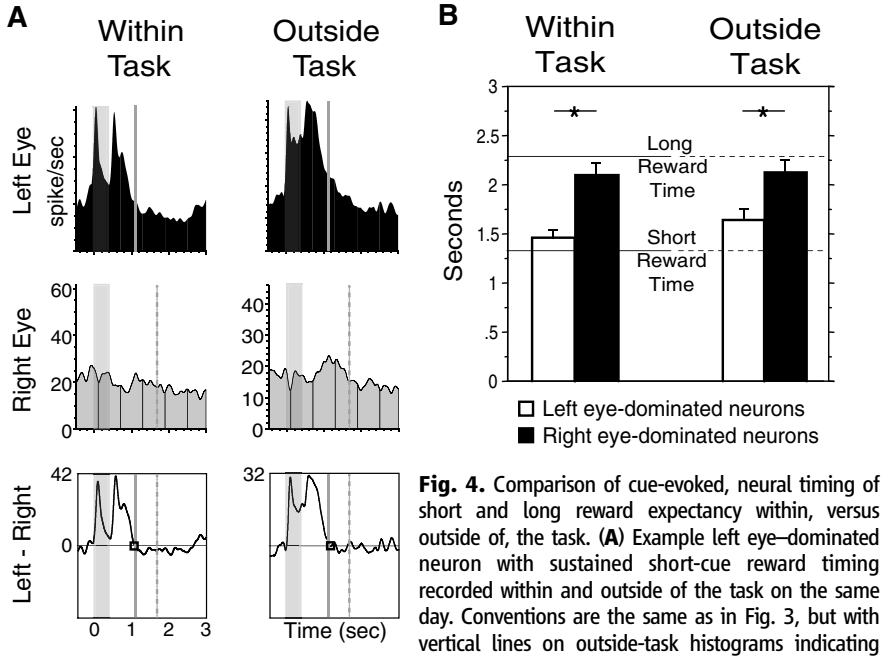

Fig. 4. Comparison of cue-evoked, neural timing of short and long reward expectancy within, versus outside of, the task. (**A**) Example left eye–dominated neuron with sustained short-cue reward timing recorded within and outside of the task on the same day. Conventions are the same as in Fig. 3, but with vertical lines on outside-task histograms indicating within-task reward times, for comparison. Shading indicates stimulus time. (**B**) NRMs (means ± SEM) within, versus outside of, the task for neural subpopulations dominated by the left or right eye. Barred asterisks indicate significance between mean short- and long-cued NRMs (*t* test; $P < 0.05$).

compared with the actual short and long reward times of the recording sessions, respectively (Fig. 3). Across recordings in experienced animals, the time (mean ± SEM) to the short reward was 1191 ± 35 ms; the mean left eye–dominated NRM was 1278 ± 42 ms. The time to the long reward was 1814 ± 84 ms; the mean right eye–dominated NRM was 1883 ± 116 ms. Therefore, on average, individual neurons predict reward time quite accurately.

The experience of pairing visual stimuli with delayed reward clearly alters the responses of V1 neurons to these visual cues while animals are performing the task. We next asked whether reward-timing activity would continue to be evoked by the same visual cues when the animals were not performing the task. After "within-task" recording sessions, access to the nose-poke/lick tube was obstructed, and the left and right eyes were stimulated pseudorandomly on a fixed 6-s interval until 180 presentations were reached for each stimulus, constituting "outside-task" sessions. By recording from the same neurons on a given day, we found that, of neurons expressing reward-timing activity within the task (47 out of 93; 51%), 66% (31 out of 47) continued to express apparent reward-timing activity to the visual stimuli when presented outside of the task (Fig. 4A). For these neurons, the accuracy with which they continued to "predict" the short and long reward times could be compared with their performance inside the task (Fig. 4B). Although neural timing of reward outside the task was degraded, left eye– and right eye–dominated neurons continued to have mean NRMs that were significantly different from each other ($P < 0.05$), relating to the appropriate reward times. This result indicates that pairing visual cues to delayed rewards within the task creates a lasting alteration in the manner in which the visual cortex responds to those cues when observed in other contexts. We hasten to add, however, that, although our data show that V1 responses evolve to accurately predict reward timing, further study is required to assess whether and how such information is used by the animal to guide behavior.

Such timing activity has been reported previously in higher cortical areas (*20*–*22*) and in associated subcortical structures (*23*–*25*), but never before in primary sensory cortex. The current findings imply that V1 neurons, at least in rats, do not function as simple feature detectors (*26*). Because reward-timing activity can persist long after the visual stimulus has disappeared, it no longer faithfully reports retinal illumination, but rather what retinal illumination portends. As reward timing is shown to be eye-specific, activating different subpopulations of neurons, general brain arousal/attention cannot explain this activity. Further, because these altered responses persist outside the task, emergent reward-timing activity can be independent of both context and behavior.

The mechanism for this remarkable plasticity in V1 remains to be determined. Subthreshold responses to stimulation of visual cortex, likely reflecting weak recurrent connections, can persist for seconds (*27*). Our findings could be explained if a modulatory input that signifies delivery of reward (possibly dopamine) causes a persistent potentiation or unmasking of recently active connections.

References and Notes

1. D. Hubel, T. Wiesel, *J. Physiol.* **150**, 91 (1959).
2. D. Hubel, T. Wiesel, *J. Physiol.* **160**, 106 (1962).
3. J. M. Fuster, G. E. Alexander, *Science* **173**, 652 (1971).
4. J. M. Fuster, *J. Neurophysiol.* **36**, 61 (1973).
5. E. K. Miller, C. A. Erickson, R. Desimone, *J. Neurosci.* **16**, 5154 (1996).
6. Y. Miyashita, H. S. Chang, *Nature* **331**, 68 (1988).
7. P. S. Goldman-Rakic, *Neuron* **14**, 477 (1995).
8. R. Desimone, *Proc. Natl. Acad. Sci. U.S.A.* **93**, 13494 (1996).
9. E. T. Rolls, *Cereb. Cortex* **10**, 284 (2000).
10. E. A. Gaffan, D. Gaffan, S. Harrison, *J. Neurosci.* **8**, 3144 (1988).
11. Z. Liu, E. A. Murray, B. J. Richmond, *Nat. Neurosci.* **3**, 1307 (2000).
12. M. R. Roesch, C. R. Olson, *J. Neurophysiol.* **90**, 1766 (2003).
13. Y. Tagawa, P. O. Kanold, M. Majdan, C. J. Schatz, *Nat. Neurosci.* **8**, 380 (2005).
14. N. B. Sawtell *et al.*, *Neuron* **38**, 977 (2003).
15. M. Ito, C. D. Gilbert, *Neuron* **22**, 593 (1999).
16. C. Gilbert, M. Ito, M. Kapadia, G. Westheimer, *Vision Res.* **40**, 1217 (2000).
17. H. Supèr, H. Spekreijse, V. A. Lamme, *Science* **293**, 120 (2001).
18. R. F. Salazar, P. Konig, C. Kayser, *Eur. J. Neurosci.* **20**, 1391 (2004).
19. Materials and Methods are available as supporting material on *Science* Online.
20. M. Leon, M. N. Shadlen, *Neuron* **38**, 317 (2003).
21. A. V. Egorov, B. N. Hamam, E. Fransen, M. E. Hasselmo, A. A. Alonso, *Nature* **420**, 173 (2002).
22. J. M. Fuster, J. P. Jervey, *Science* **212**, 952 (1981).
23. Y. Komura *et al.*, *Nature* **412**, 546 (2001).
24. W. Schultz, P. Dayan, P. R. Montague, *Science* **275**, 1593 (1997).
25. Y. Watanabe, S. Funahashi, *J. Neurophysiol.* **92**, 1738 (2004).
26. D. Purves, R. B. Lotto, S. M. Williams, S. Nundy, Z. Yang, *Philos. Trans. R. Soc. London B Biol. Sci.* **356**, 285 (2001).
27. M. V. Sanchez-Vives, D. A. McCormick, *Nat. Neurosci.* **3**, 1027 (2000).

28. This work was supported by the Howard Hughes Medical Institute. We thank R. Crozier, D. Foster, A. Heynen, M. Jones, D. Katz, J. Morgan, M. Linden, B. Rubin, and H. Shouval.

Supporting Online Material

www.sciencemag.org/cgi/content/full/311/5767/1606/DC1
Materials and Methods
SOM Text
Figs. S1 to S4
References and Notes

6 December 2005; accepted 13 February 2006
10.1126/science.1123513

αE-Catenin Controls Cerebral Cortical Size by Regulating the Hedgehog Signaling Pathway

Wen-Hui Lien,[1,2]* Olga Klezovitch,[1]* Tania E. Fernandez,[1] Jeff Delrow,[3] Valeri Vasioukhin[1]†

During development, cells monitor and adjust their rates of accumulation to produce organs of predetermined size. We show here that central nervous system–specific deletion of the essential adherens junction gene, *αE-catenin,* causes abnormal activation of the hedgehog pathway, resulting in shortening of the cell cycle, decreased apoptosis, and cortical hyperplasia. We propose that αE-catenin connects cell-density–dependent adherens junctions with the developmental hedgehog pathway and that this connection may provide a negative feedback loop controlling the size of developing cerebral cortex.

During brain development, proliferation of neural progenitor cells is tightly controlled to produce the organ of predetermined size. We hypothesized that cell-cell adhesion structures may be involved in this function, because they can provide cells with information concerning the density of their cellular neighborhood. Intercellular adhesion in neural progenitors is mediated primarily by adherens junctions, which contain cadherins, β-catenins and α-catenins (*1*). We found that progenitors express αE (epithelial)–catenin, while differentiated neurons express αN (neural)–catenin (fig. S1, A to D). Because α-catenin is critical for the formation of adherens junctions (*2*, *3*), we decided to determine the role of these adhesion structures in neural progenitor cells by generating mice with central nervous system (CNS)–specific deletion of *αE-catenin*. Mice with a conditional *αE-catenin* allele (*αE-catenin*$^{loxP/loxP}$) (*4*) were crossed with mice carrying nestin-promoter–driven Cre recombinase (*Nestin-Cre*$^{+/-}$), which

[1]Division of Human Biology, Fred Hutchinson Cancer Research Center, Seattle, WA 98109, USA. [2]Molecular and Cellular Biology Program, University of Washington, Seattle, WA 98195, USA. [3]Genomics Resource, Fred Hutchinson Cancer Research Center, Seattle, WA 98109, USA.

*These authors contributed equally to this work.
†To whom correspondence should be addressed. E-mail: vvasiouk@fhcrc.org

is expressed in CNS stem/neural progenitors starting at embryonic day 10.5 (E10.5) (fig. S1E) (*5*). The resulting *αE-catenin$^{loxP/loxP}$/Nestin-Cre$^{+/-}$* animals displayed loss of αE-catenin in neural progenitor cells (fig. S1F).

Although no phenotype was observed in heterozygous *αE-catenin$^{loxP/+}$/Nestin-Cre$^{+/-}$* mice, the knockout *αE-catenin$^{loxP/loxP}$/Nestin-Cre$^{+/-}$* mice were born with bodies similar to their littermates, but with enlarged heads (fig. S2A). After birth, the heads of these animals continued to grow, but their bodies were developmentally retarded, generating abnormal large-headed pups that failed to thrive and died between 2 and 3 weeks of age (fig. S2B). Counting brain cell numbers at different points of embryonic development revealed massive hyperplasia in the mutant brains, with twice as many total brain cells by the time of birth (fig. S2C). Although no differences were found at E12.5, mutant brains displayed a 40% increase in total cell numbers only 1 day later at E13.5. In addition to an increase in brain cell numbers, the mutant animals displayed increases in brain weights and brain-to-body-weight ratios (fig. S2, D and E). Histologic analysis of *αE-catenin$^{loxP/loxP}$/Nestin-Cre$^{+/-}$* animals revealed severe dysplasia and hyperplasia in the mutant brains (Fig. 1). *αE-catenin$^{-/-}$* ventricular zone cells were dispersed throughout the developing brains, forming invasive tumor–like masses that displayed widespread pseudopalisading and the formation of rosettes (Fig. 1F′) similar to Homer-Wright rosettes in human medulloblastoma, neuroblastoma, retinoblastoma, pineoblastoma, neurocytoma, and pineocytoma tumors (*6*–*8*). Although E12.5 *αE-catenin$^{-/-}$* cortices already showed some disorganization (Fig. 1B′), the general appearance of the brain was similar between the wild-type and *αE-catenin$^{-/-}$* embryos (Fig. 1, A and A′). In contrast, the E13.5 mutants exhibited a prominent increase in the thickness and size of the cerebral cortex (Fig. 1, C and C′). Massive expansion of dysplastic cortical progenitor cells continued later in development, causing a posterior and ventral shift in localization of the lateral ventricle (Fig. 1, D to E′, and fig. S3).

We next analyzed the mechanisms responsible for dysplasia in *αE-catenin$^{-/-}$* brains. Ventricular zone progenitors are bipolar, with one extension reaching the ventricular surface and another process reaching in the opposite direction (fig. S4A). These cells form a prominent cell-cell adhesion structure at the ventricular interface called an apical-junctional complex. Staining with cell adhesion and cell polarity markers showed disruption of apical-junctional complexes and loss of cell polarity in *αE-catenin$^{-/-}$* neural progenitor cells (Fig. 2 and fig. S4). Electron microscopic analyses of *αE-catenin$^{-/-}$* brains revealed progenitors that were nonpolarized, round, and loosely connected to each other and that lacked apical-junctional complexes (Fig. 2, G and H). Perhaps because of residual amounts of *αN-catenin* present in the progenitor cells, small fragments of *αE-catenin$^{-/-}$* neuroepithelium were still capable of maintaining cell polarity, but they were often engulfed by protruding nonpolarized cells, folded back on themselves, and internalized to form rosettes (Fig. 2, D to F and I, and fig. S4, B and D). We concluded that loss of apical-junctional complexes and subsequent loss of cell polarity may represent the mechanism responsible for dysplasia in *αE-catenin$^{-/-}$* brains.

We next analyzed the mechanisms responsible for hyperplasia in *αE-catenin$^{-/-}$* brains. Failure of cell cycle withdrawal is responsible for hyperplasia in brains with hyperactive

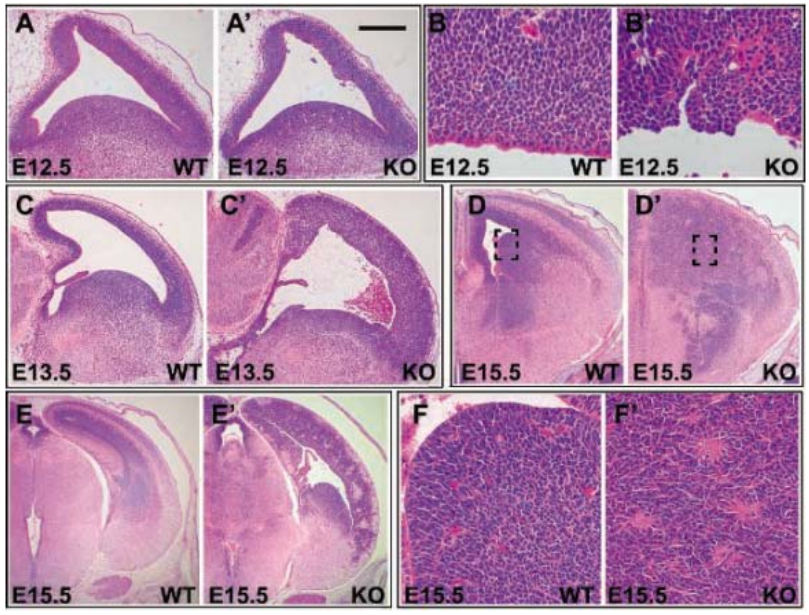

Fig. 1. Severe dysplasia and hyperplasia in *αE-catenin$^{-/-}$* brain. Histologic appearance of brains from wild-type (WT) and *αE-catenin$^{LoxP/LoxP}$/Nestin-Cre$^{+/-}$* (KO) mice. Sagittal sections through developing telencephalon from wild-type (**A** and **C**) and *αE-catenin$^{-/-}$* (**A′** and **C′**) brains of E12.5 [(A) and (A′)] and E13.5 [(C) and (C′)] embryos. Ventricular zone of the cerebral cortex from the E12.5 wild-type (**B**) and *αE-catenin$^{-/-}$* (**B′**) brains. Coronal sections from the E15.5 wild-type (**D** to **F**) and *αE-catenin$^{-/-}$* (**D′** to **F′**) brains. Areas in dashed squares in (D) and (D′) are shown at higher magnification in (F) and (F′). Scale bar in (A′) represents 0.27 mm in (A) and (A′), 40 μm in (B) and (B′), 0.36 mm in (C) and (C′), 0.42 mm in (D) and (D′), 0.54 mm in (E) and (E′), and 50 μm in (F) and (F′).

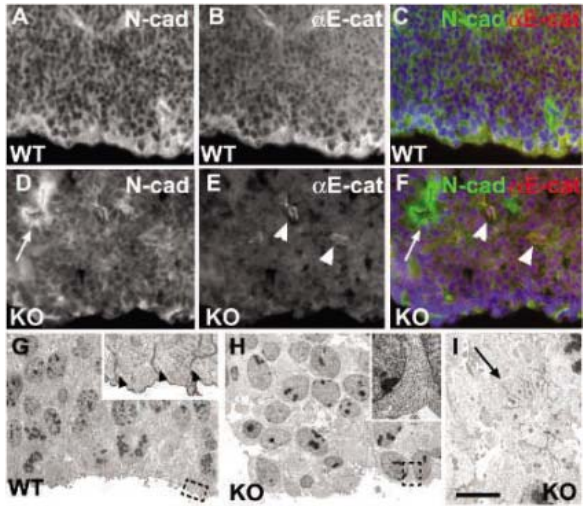

Fig. 2. Loss of cell polarity and disruption of apical-junctional complex in *αE-catenin$^{-/-}$* neural progenitor cells. (**A** to **F**) Disruption of apical adherens junctions in *αE-catenin$^{-/-}$* neural progenitors. Staining with antibody to N-cadherin [(A) and (D); green in (C) and F)] and antibody to αE-catenin [(B) and (E); red in (C) and F)]. (**G** to **I**) Electron microscopy analysis of cortical neural progenitor cells of E12.5 wild-type (G) and *αE-catenin$^{-/-}$* [(H) and (I)] embryos. Areas in dashed squares in (G) and (H) are magnified in insets. Arrowheads in inset to (G) denote apical-junctional complexes. Arrows indicate internalization of polarized neuroepithelium and formation of rosettelike structures maintaining apical-junctional complexes. Arrowheads in (E) and (F) denote blood vessels not targeted by Nestin-Cre. Scale bar in (I) represents 30 μm in (A) to (F), 10 μm in (G) and (H), 4 μm in (I), and 1.8 μm in insets to (G) and (H).

β-catenin pathways (*9*). To analyze cell cycle withdrawal in *αE-catenin*$^{-/-}$ brains, we counted the proportion of cells that had exited the cell cycle 24 hours after labeling with 5-bromo-2′-deoxyuridine (BrdU) (Fig. 3, B and B′). We concentrated on E13.5 mutants, because we observed the most rapid increase in total brain cell numbers during the E12.5 to E13.5 interval of development. We found no significant differences in cell cycle withdrawal between the wild-type and mutant cells (Fig. 3C). To determine whether differentiation was affected in *αE-catenin*$^{-/-}$ brains, we used antibodies to β-tubulin III and nestin—neuronal and progenitor cell markers, respectively (fig. S5, A to B′). Although there were no differences in appearance of E12.5 wild-type and mutant cortices (fig. S5, A and A′), E13.5 *αE-catenin*$^{-/-}$ cortices were disorganized and thickened, with neurons present not only in the cortical plate but also elsewhere throughout the cortex (fig. S5, B and B′). Nevertheless, the overall ratio between differentiated and nondifferentiated cells remained unchanged (fig. S5C). Moreover, Western blot analyses of total brain proteins with cell type–specific antibodies did not reveal consistent differences between the wild-type and *αE-catenin*$^{-/-}$ brains (fig. S5D). In addition, we found no differences between the wild-type and *αE-catenin*$^{-/-}$ brains in the position and numbers of Cajal-Retzius neurons located at the surface of cerebral cortex (fig. S6). We concluded that, despite the loss of progenitor cell polarity, the general program governing differentiation is not affected in *αE-catenin*$^{-/-}$ brains.

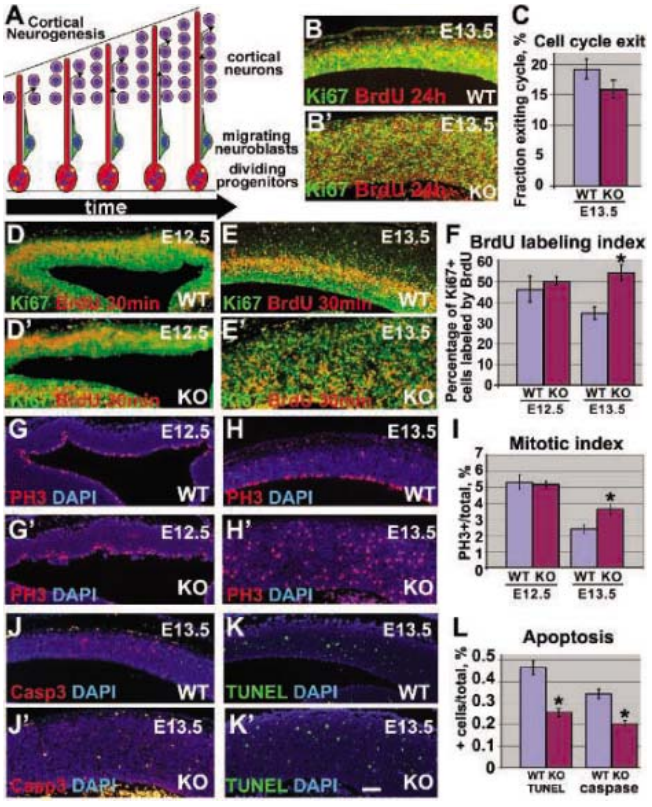

Fig. 3. Shortening of cell cycle and decreased apoptosis in *αE-catenin*$^{-/-}$ cerebral cortices. (**A**) Model of cortical neurogenesis. (**B** and **B′**) Minor changes in cell cycle withdrawal in *αE-catenin*$^{-/-}$ cortices. Pregnant females were injected with BrdU 24 hours before being sacrificed. Cells reentering the cell cycle are BrdU^{+}/Ki67^{+}, whereas cells withdrawn from the cell cycle are BrdU^{+}/Ki67^{-}. (**C**) Quantitation of experiments shown in (B) and (B′). Cell cycle exit is determined as a ratio of cells that exited the cell cycle (BrdU^{+}/Ki67^{-}) to all cells that incorporated BrdU. $n = 3$; (**D** to **E′**) Decrease in cell cycle length in *αE-catenin*$^{-/-}$ progenitors. A higher percentage of *αE-catenin*$^{-/-}$ progenitor cells (Ki67^{+}) are labeled with BrdU after a 30-min pulse. (**F**) Quantitation of experiments shown in (D) to (E′). BrdU labeling index is the percentage of Ki67^{+} cells that incorporated BrdU. $n = 3$; $^{*}P < 0.001$. (**G** to **H′**) Immunostaining of cortical sections from wild-type and *αE-catenin*$^{-/-}$ brains with antibodies to phosphohistone 3 (red) reveals an increase in mitotic cells in E13.5 mutants. DNA was counterstained by 4′,6′-diamidino-2-phenylindole (blue). (**I**) Quantitation of the experiments shown in (G) to (H′). Mitotic index is a ratio of mitotic cells to the total brain cell number. $n = 3$; $^{*}P < 0.001$. (**J** to **K′**) Decrease in apoptosis in *αE-catenin*$^{-/-}$ cortices. Apoptotic cells in the wild-type [(J) and (K)] and mutant [(J′) and K′)] brains were detected by staining with anti-body to cleaved caspase 3 (Casp3) and terminal deoxynucleotidyl transferase–mediated deoxyuridine triphosphate nick end labeling (TUNEL). (**L**) Quantitation of experiments shown in (J) and (K′). Ratios of Casp3^{+} or TUNEL^{+} cells to total cell numbers are shown. $n = 3$; $^{*}P < 0.001$. Scale bar in (K′) represents 100 μm in all cortical sections.

To analyze whether loss of αE-catenin led to changes in proliferation, we studied neural progenitor cell cycle length and number of cells in mitosis. To measure cell cycle length, we counted the proportion of neural progenitor cells labeled by a pulse of BrdU (*9*) (Fig. 3, D to E′). We found significant shortening of the cell cycle in E13.5 *αE-catenin*$^{-/-}$ progenitor cells (Fig. 3F). In addition, E13.5 mutant brains displayed a 40% increase in the number of mitotic cells (Fig. 3, G to I).

Apoptosis is also critical for regulation of total cell numbers in the developing brain (*10*). Counting of apoptotic cells revealed that apoptosis decreased by one-half in the *αE-catenin*$^{-/-}$ cortices (Fig. 3, J to L). We concluded that hyperplasia in the *αE-catenin*$^{-/-}$ brains was a combined outcome of the shortening of the cell cycle and the decreased apoptosis in neural progenitor cells.

To determine the molecular mechanisms responsible for hyperplasia in *αE-catenin*$^{-/-}$ brains, we used a microarray approach. Surprisingly, a genomewide analysis revealed few changes in gene expression (Table 1),

Table 1. Differentially expressed genes in E12.5 αE-catenin$^{-/-}$ brains. RNAs from *αE-catenin*$^{LoxP/+}$*/Nestin-Cre*$^{+/-}$ and *αE-catenin*$^{LoxP/LoxP}$*/Nestin-Cre*$^{+/-}$ brains were analyzed by Affymetrix expression arrays. Relative fold change is calculated with respect to heterozygous brains. Bayes.p is the *P* value obtained using the CyberT Bayesian statistical framework.

Name	Symbol	UG cluster	Relative fold change	Bayes.p
Up-regulated				
Fibroblast growth factor 15	Fgf15	Mm.3904	2.39	1.31×10^{-6}
GLI-Kruppel family member GLI	Gli1	Mm.336839	2.37	3.34×10^{-6}
RIKEN cDNA A830059I20 gene	A830059I20Rik	Mm.113787	1.98	5.86×10^{-7}
Expressed sequence AU040576	AU040576	Mm.26700	1.93	2.27×10^{-5}
High mobility group AT-hook 1	Hmga1	Mm.4438	1.59	1.60×10^{-5}
Down-regulated				
p53 binding protein 1	Trp53bp1	Mm.215389	−3.91	6.70×10^{-6}
RIKEN cDNA 2900097C17 gene	2900097C17Rik	Mm.349235	−2.63	5.41×10^{-6}
RIKEN cDNA A730017C20 gene	A730017C20Rik	Mm.209711	−1.92	2.55×10^{-7}

with only five transcripts up-regulated and three down-regulated in *αE-catenin*$^{-/-}$ brains. Interestingly, the two most up-regulated cDNAs, *Fgf15* and *Gli1*, represent well-known endogenous transcriptional targets of the hedgehog (Hh) pathway (*11*, *12*). We performed quantitative reverse transcription polymerase chain reaction (PCR) analysis of critical members and targets of the Hh pathway: *smoothened* (*Smo*), *patched1* (*Ptch*), *sonic hedgehog* (*Shh*), *indian hedgehog* (*Ihh*), *desert hedgehog* (*Dhh*), *Rab23*, *Gli1*, *Gli2*, *Gli3*, and *Fgf15*. We found that the expression of *Gli1*, *Fgf15*, and *Smo* was significantly up-regulated in *αE-catenin*$^{-/-}$ brains (Fig. 4A). To determine the compartment of the developing brain displaying up-regulation of Hh signaling, we performed in situ hybridizations with *Gli1*, *Fgf15*, and *Smo* probes (Fig. 4, B to D′). We found that *Gli1* and *Fgf15* transcripts are up-regulated in the progenitor cell domain of *αE-catenin*$^{-/-}$ cerebral cortex, the area most severely affected by hyperplasia in *αE-catenin*$^{-/-}$ brains (Fig. 1C′).

Up-regulation of endogenous targets of the Hh signaling pathway suggests activation of this pathway in developing cortices of the *αE-catenin*$^{loxP/loxP}$*/Nestin-Cre*$^{+/-}$ mice. Although the exact mechanism responsible for αE-catenin–mediated regulation of *Gli1* and *Fgf15* is presently unknown, an increase in expression of the activator of the Hh signaling *Smo* is likely to play a causal role in abnormal activation of the Hh pathway in *αE-catenin*$^{-/-}$ brains. Indeed, *Smo* up-regulation is responsible for activation of Hh signaling in cancer cell lines, and it may be a focal point of regulation of the pathway in tissue regeneration and cancer (*13*).

The Hh pathway plays a critical role in mammalian CNS development and brain cancer (*14*). Sonic hedgehog stimulates proliferation of progenitor cells in the developing cerebral cortex (*15*, *16*). In addition, Hh signaling promotes survival and blocks apoptosis of neuroepithelial cells (*17*). Therefore, abnormal activation of the Hh pathway may be responsible for cortical hyperplasia in *αE-catenin*$^{-/-}$ brains. To determine whether this is indeed the case, we used cyclopamine, a specific inhibitor of Smoothened (*18*), which can block the Hh pathway in vivo (*19*). We found that a single injection of cyclopamine at E12.5 (immediately before the onset of hyperplasia) did not interfere with depletion of αE-catenin (fig. S7) but eliminated the differences in total cell numbers between the E13.75 wild-type and *αE-catenin*$^{-/-}$ brains (Fig. 4E). Injections of decreasing amounts of cyclopamine produced intermediate phenotypes demonstrating dose dependence between the inhibitor and hyperplasia (fig. S8). As expected, inhibition of Hh did not rescue cortical disorganization, which results from the disruption of adherens junctions in *αE-catenin*$^{-/-}$ brains (fig. S9). Analyses of the cell cycle length and apoptosis showed rescue of the cell cycle and apoptosis abnormalities in cyclopamine-treated *αE-catenin*$^{-/-}$ brains (Fig. 4E and fig. S9, C to H′). As expected, cyclopamine injection led to a decrease in expression of the Hh pathway transcriptional targets *Gli1* and *Fgf15* (fig. S10). We concluded that abnormal activation of the Hh pathway was responsible for shortening of the cell cycle, decreased apoptosis, and subsequent hyperplasia in *αE-catenin*$^{-/-}$ cerebral cortices.

Our findings allow us to propose a model of a negative feedback loop that regulates the rates of cell proliferation to control the size of the cerebral cortex (fig. S11). In this "crowd control" model, the increase in cell density, which is sensed by an increase in the per cell area occupied by adherens junctions (fig. S11A), is translated into down-regulation of Hh signaling and subsequent decrease in cell proliferation (fig. S11B). The abnormal decrease in cell density, which is measured by destabilization and paucity of adherens junctions, is translated into activation of the Hh pathway and subsequent acceleration of cell proliferation until the normal cell density is achieved. Therefore, the density of cellular crowding ultimately regulates the rates of cell accumulation during normal development. Solid tumors may escape "crowd control" of cell proliferation by destabilizing the adherens junctions, one of the frequent events reported in human cancers (*20*).

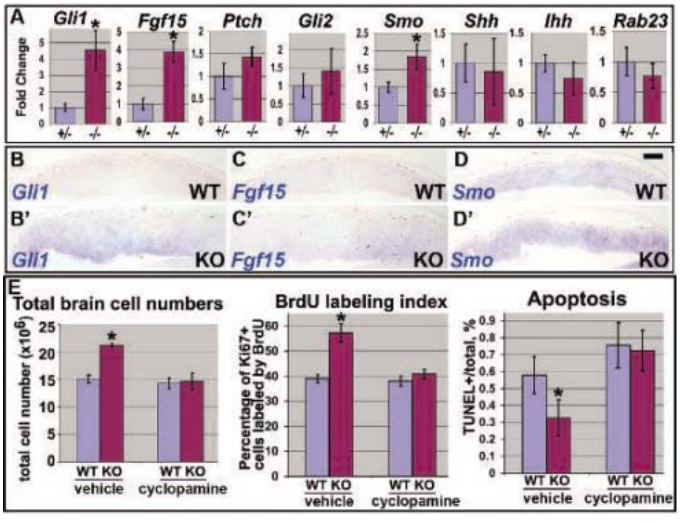

Fig. 4. Activation of the Hh pathway is responsible for shortening of the cell cycle, decreased apoptosis, and subsequent hyperplasia in *αE-catenin*$^{-/-}$ cerebral cortices. (**A**) Quantitative real-time PCR (QPCR) analysis of Hh pathway transcripts in E12.5 heterozygous and mutant brains. The levels of expression are shown in arbitrary units, with mean heterozygous levels adjusted to 1. Data represent mean ± SD. $n \geq 4$; *$P < 0.002$. (**B** to **D′**) Cortical sections from E12.5 wild-type and αE-catenin$^{-/-}$ embryos were analyzed by in situ hybridization with *Gli1*, *Fgf15*, and *Smo* probes. Scale bar in (D) represents 200 μm. (**E**) Inhibition of the Hh pathway by cyclopamine eliminates the differences in total cell numbers, cell cycle length, and apoptosis between the wild-type and *αE-catenin*$^{-/-}$ brains. Pregnant females were injected with 10 mg of cyclopamine per kg of body weight in 2-hydropropyl-β-cyclodextrin (vehicle) or vehicle alone at E12.5, and embryos were analyzed 30 hours later. Quantitation was performed as described in Fig. 3 and fig. S2. Data represent mean ± SD. $n \geq 3$; *$P < 0.001$.

References and Notes

1. A. Chenn, Y. A. Zhang, B. T. Chang, S. K. McConnell, *Mol. Cell. Neurosci.* **11**, 183 (1998).
2. S. Hirano, N. Kimoto, Y. Shimoyama, S. Hirohashi, M. Takeichi, *Cell* **70**, 293 (1992).
3. V. Vasioukhin, C. Bauer, M. Yin, E. Fuchs, *Cell* **100**, 209 (2000).
4. V. Vasioukhin, C. Bauer, L. Degenstein, B. Wise, E. Fuchs, *Cell* **104**, 605 (2001).
5. D. Graus-Porta *et al.*, *Neuron* **31**, 367 (2001).
6. O. P. Sangueza, P. Sangueza, L. R. Valda, C. K. Meshul, L. Requena, *J. Am. Acad. Dermatol.* **31**, 356 (1994).
7. D. I. Graham, P. L. Lantos, *Greenfield's Neuropathology* (Arnold, New York, NY, 2002).
8. P. C. Burger, Scheithauer, *Atlas of Tumor Pathology. Tumors of the Central Nervous System* (Armed Forces Institute of Pathology, Washington, DC, 1994).
9. A. Chenn, C. A. Walsh, *Science* **297**, 365 (2002).
10. V. Depaepe *et al.*, *Nature* **435**, 1244 (2005).
11. M. Ishibashi, A. P. McMahon, *Development* **129**, 4807 (2002).
12. H. Saitsu *et al.*, *Dev. Dyn.* **232**, 282 (2005).
13. S. S. Karhadkar *et al.*, *Nature* **431**, 707 (2004).
14. A. Ruiz i Altaba, V. Palma, N. Dahmane, *Nat. Rev. Neurosci.* **3**, 24 (2002).
15. N. Dahmane *et al.*, *Development* **128**, 5201 (2001).
16. V. Palma, A. Ruiz i Altaba, *Development* **131**, 337 (2004).
17. C. Thibert *et al.*, *Science* **301**, 843 (2003).
18. J. K. Chen, J. Taipale, M. K. Cooper, P. A. Beachy, *Genes Dev.* **16**, 2743 (2002).
19. D. M. Berman *et al.*, *Science* **297**, 1559 (2002).
20. U. Cavallaro, G. Christofori, *Nat. Rev. Cancer* **4**, 118 (2004).

21. We thank P. Soriano, S. Parkhurst, S. Tapscott, D. Gottschling, B. Edgar, and all members of the Vasioukhin laboratory for advice and encouragement; A. Nagafuchi, S. Tsukita, and the Developmental Studies Hybridoma Bank for the generous gift of antibodies; and L. Cherepoff, F. Remington, M. Null, and B. Helbing for help with histology, electron microscopy, genotyping, and manuscript preparation, respectively. This work was supported by National Cancer Institute grant R01 CA098161.

Supporting Online Material

www.sciencemag.org/cgi/content/full/311/5767/1609/DC1
Materials and Methods
Figs. S1 to S11
References

17 October 2005; accepted 31 January 2006
10.1126/science.1121449

State-Dependent Learned Valuation Drives Choice in an Invertebrate

Lorena Pompilio,* Alex Kacelnik,† Spencer T. Behmer‡

Humans and other vertebrates occasionally show a preference for items remembered to be costly or experienced when the subject was in a poor condition (this is known as a sunk-costs fallacy or state-dependent valuation). Whether these mechanisms shared across vertebrates are the result of convergence toward an adaptive solution or evolutionary relicts reflecting common ancestral traits is unknown. Here we show that state-dependent valuation also occurs in an invertebrate, the desert locust *Schistocerca gregaria* (Orthoptera: Acrididae). Given the latter's phylogenetic and neurobiological distance from those groups in which the phenomenon was already known, we suggest that state-dependent valuation mechanisms are probably ecologically rational solutions to widespread problems of choice.

Animal decision-making is often modeled using the assumption that choices are based on the fitness consequences that each choice yields. Fitness gains, in turn, depend on both the intrinsic properties of the options and the state of the subject at the time of the choice. Recently, however, studies in humans and other vertebrates (*1*, *2*) have shown that understanding the adaptive significance of learning mechanisms may be the key to progress in functional modeling of decision-making, because preferences more closely reflect the subject's state at the time of learning than at the time of choice. Classical learning models (*3*) do not address the subject's state, but recent treatments of evaluative incentive behavior do (*4*) and are compatible with the approach taken here.

A recent theoretical model linking learning to decision-making (*5*) proposes that anomalies of choice behavior in which past investments rather than expected returns dominate preference (examples include Sunk Costs, Work Ethics, and the Concorde Fallacy) result from a decelerated function of value (fitness or utility) versus objective payoff, combined with a mechanism of choice that is dependent on the remembered benefit previously yielded by each option (Fig. 1). Although some utility functions can be accelerated or sigmoid, because "desperados" in dire states would accrue less marginal gains from resources than would better-off individuals, most surviving organisms operate beyond this extreme zone, and hence the assumption of decelerated gains has very wide justification. In summary, if two sources (L and H) yielding the same objective payoff ($M_L = M_H$; M, magnitude) are systematically encountered when the individual is in different states (low or high reserves for L and H, respectively), then the source encountered when needs are greater (L) will yield larger value gains ($V_L > V_H$). According to the model, although gains depend jointly on payoff magnitude and present state, it is the remembered gains, rather than remembered payoff magnitudes or states, that drive future preferences.

The adaptive advantages of such a mechanism are not obvious because, at least under experimental conditions, they can produce irrational preferences: Starlings can prefer a more delayed over a more immediate reward even when having explicit knowledge of the delays involved (*6*), and rats can frantically operate a lever or chain that causes food or water rewards even when being neither hungry nor thirsty (*7*). Supporting evidence for incentive or state-dependent learning comes from the mammal and bird species that have been studied so far, but there is an open question as to whether this mechanism of learned value assignment was an early vertebrate acquisition or a wider phenomenon perhaps universally present because it confers selective advantages.

We tested whether such state-dependent valuation learning occurs in a grasshopper, an animal with a simpler nervous system (*8*) than that of the vertebrates in which these effects are known. Grasshoppers make particularly good test subjects for studying and modeling individual decision-making because they forage for themselves and are capable of learning (*9*, *10*). Additionally, much is known about how changes in their nutritional state affect their feeding behavior (*11*).

We manipulated nutritional state both at the time of learning and at the time of preference testing. We trained grasshoppers so that they encountered each of two options under different nutritional states: low (option L) and high (option H). Each option consisted of an odor (lemon grass or peppermint) paired during learning with a food item (a small piece of seedling wheat). Food items were of the same size and quality in both options, and each odor was always associated with the same state for each subject. Individuals received an equal number of reinforced trials with each option over a 3-day training regime (fig. S1). After training was completed, individual grasshoppers were presented with a choice between the two options. Half of the subjects had the test in the low state and the other half in the high state (*12*).

We considered four possible outcomes. The first of these, Magnitude Priority, states that if choices depend on the intrinsic properties of the options, no systematic preference will be observed between odors because the food items were identical. The second, Value Priority, states that if choices are controlled by past gains, preference should be for the option experienced in the low state during training,

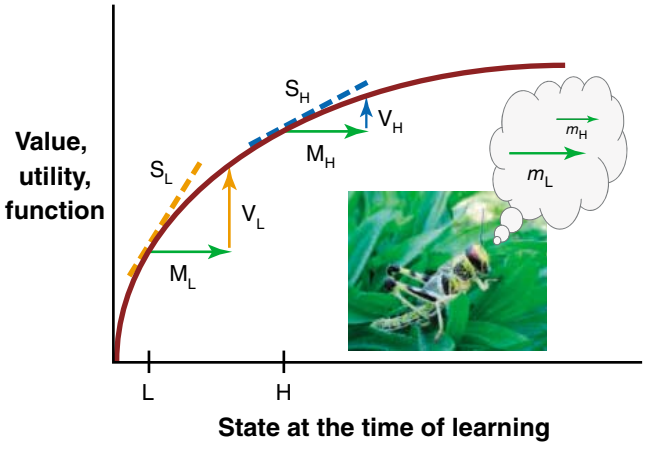

Fig. 1. Putative mechanisms of valuation learning as a function of a subject's state. The ordinate is a currency that is assumed to correlate to adaptive value, and the abscissa is a metric of objective state, here assumed to be the level of accumulated reserves. The plot illustrates consequences for a subject that encounters two food sources (L and H), each when the subject is in either of two states: low or high, respectively. The magnitudes of the outcomes are labeled M_L and M_H and are represented as arrows causing positive state displacements. The value (or benefit) of each outcome (V_L and V_H) is the vertical displacement that corresponds to each change in state. The first derivative (marginal rate) of the value-versus-state function at each initial state is indicated by the slopes of the tangents S_L and S_H. The inset shows that the subject's representation of the magnitude of rewards (m) may differ from the objective metrics of the outcomes (in the example, $M_L = M_H$ but $m_L > m_H$). Models of learning may use M, S, V, or m as being directly responsible for value assignment.

Department of Zoology, University of Oxford, South Parks Road, Oxford OX1 3PS, UK.

*Present address: Departamento de Ecología, Genética y Evolución, Facultad de Ciencias Exactas y Naturales, Universidad de Buenos Aires, Pabellon II Ciudad Universitaria, C1428EHA, Buenos Aires, Argentina.

†To whom correspondence should be addressed. E-mail: alex.kacelnik@zoo.ox.ac.uk

‡Present address: Department of Entomology, Texas A&M University, College Station, TX 77843–2475, USA.

regardless of state at the time of choice. The third, State Priority, stipulates that if options are valued by association with the desirability of the state they evoke, the option preferred should be that experienced in the high state during training, regardless of state during choice. The fourth, State-Option Association, stipulates that choice should favor the source met under the same state at the time of training. Thus, subjects may choose option L under state low and option H under state high.

A majority of the grasshoppers preferred option L (the stimulus to which the grasshoppers were trained when in a state of low reserves) regardless of their state at the time of testing (Fig. 2). Averaged across all test subjects, the mean preference (±SE) for option L was 0.71 ± 0.06. These results indicate a significant preference for option L ($t_{1,15} = 3.60$, $P < 0.01$; one sample t test against indifference). Preference was not affected by the state of the subject at the time of testing (Fig. 2) or by odor bias, and the state-by-odor interaction was not significant [analysis of variance (ANOVA): $F_{1,15} = 0.09$, $P > 0.77$; $F_{1,15} = 0.01$, $P > 0.92$; and $F_{1,15} = 0.01$, $P > 0.91$, respectively]. There also was no left arm–right arm positioning effect (paired-samples t test: $t_{1,15} = 0.17$, $P > 0.86$). Next, we considered whether the speed of learning during training, as measured by latencies to contact and eat the reward, might have anticipated the preference results. A repeated-measures ANOVA indicated that latencies to start eating decreased across the 3 days of training ($F_{2,15} = 15.00$, $P < 0.01$; fig. S2), but averaged over time, the latencies between the L and H options were similar ($F_{1,15} = 0.08$, $P > 0.78$), and no significant option-by-day interaction was observed ($F_{2,15} = 0.91$, $P > 0.42$). Finally, we considered the possibility that each grasshopper preferred the option for which it had a shorter latency during training (regardless of whether shorter latencies were exhibited for the L or H option) (*12*). We found, however, no association between latencies and choices (Pearson's correlation index, $r = 0.19$, $P = 0.48$).

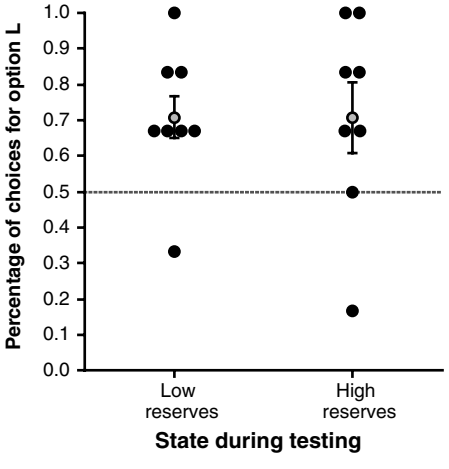

Fig. 2. Percentage of choices for option L exhibited by each subject under the two different states (low and high reserves) during testing. The figure shows individual data points (black circles) and means (±SE) (gray circles) with respect to indifference (dashed line). For both states, the percentage of choices for option L was significantly higher than indifference.

Our experiment supports the idea that in this insect, the benefit gained at the time of training affects later preference even when the magnitudes of the rewards are equal (namely, Value Priority). The Value Priority outcome can be mediated by two very different mechanisms that could be labeled Perception Distortion and Remembered Value. Perception Distortion states that the energetic state at the time of training influences the distal mechanisms of perception, so that the memory of the properties of the options is altered: Equal payoffs are perceived as being different (In Fig. 1, $m_L > m_H$). Under the Remembered Value mechanism, the memory for the magnitudes is accurate, but the animal attaches different subjective attractiveness to each option, depending on its state while learning. These considerations may apply to similar anomalies of decision-making in all animals, including humans.

In grasshoppers, there is evidence favoring the Perception Distortion mechanism, because preference for the option experienced when reserves are low could be explained by peripheral gustatory responses underlying feeding behavior. In these animals, as time since the last feed increases, nutrient levels in the hemolymph drop, and as a consequence, mouthpart taste receptors become increasingly sensitive to key depleted nutrients (*13*, *14*). This means that at a neurological level, a grasshopper with low reserves will receive greater feedback when it contacts a food item (*15*–*17*). Similarly, through digestive adaptations, individuals may extract more nutrients from identical food items when in greater need (*18*), and later choices may be governed by the memory of the postabsorptive gain (or the sensory adaptation consequent on the gains) and not of the objective features of the food items. The latter route for Perception Distortion could in theory also apply to vertebrates, but the available evidence does not point in this direction, at least for starlings. In their case, peripheral adjustments leading to either distorted representations or distorted perceptions due to rapid absorptive adaptations are both unlikely. This is because in learned valuation effects, starlings' preference between equally delayed rewards is not accompanied by alterations in the pecking rate (suggesting that neither the perception of the magnitude of the reward nor timing was altered) (*1*, *5*, *6*).

Thus, although similar behavioral outcomes are observed in starlings and grasshoppers, it is possible that different underlying mechanisms drive state-dependent learned valuation in each species. This difference supports the view that state-dependent learned valuation has intrinsic, although not yet identified, adaptive advantages and has probably emerged and persisted in distant species via convergent evolution.

State-dependent valuation may be computationally more efficient than remembering the attributes of each option and weighing them against current nutritional state. This may reduce errors and help when decisions need to be made quickly and where neural constraints limit the amount of information that can be processed (*19*, *20*). State-dependent valuation can cause suboptimal choices if there is a difference between the choice circumstances and the circumstances for learning about each option, as in our experiment. In particular, for there to be a cost, there must be a correlation between state and the probability of encounter with each option when options are met singly. This would occur because when these options are met simultaneously and a choice takes place, information about past gains could be misleading. Outside these probably rare circumstances, the mechanisms do not favor suboptimal alternatives (*21*). It could be argued that even if state-dependent valuation causes frequent and costly suboptimal choices in nature, it may persist because of neural or psychological constraints or because the cost associated with the development of a different mechanism is higher than the cost of using such a metric. The latter possibility cannot be discarded, but we do not favor it as a working hypothesis.

Ultimately, it would be ideal to measure the prevalence of different learning and choice circumstances in natural environments, but until that becomes possible, progress can be made by modeling the theoretical ecological worlds under which state-dependent valuation would be evolutionarily stable when used in competition with animals that form preferences based on the absolute properties of their options.

References and Notes

1. B. Marsh, C. Schuck-Paim, A. Kacelnik, *Behav. Ecol.* **15**, 396 (2004).
2. T. S. Clement, J. R. Feltus, D. H. Kaiser, T. R. Zentall, *Psychon. Bull. Rev.* **7**, 100 (2000).
3. R. A. Rescorla, A. R. Wagner, in *Classical Conditioning II: Current Research and Theory*, A. H. Black, W. F. Prokasy, Eds. (Appleton-Century-Crofts, New York, 1972), pp. 64–99.
4. B. W. Balleine, in *The Behavior of the Laboratory Rats: A Handbook with Tests*, I. Q. W. Kolb, Ed. (Oxford Univ. Press, Oxford, 2006), pp. 436–446.
5. A. Kacelnik, B. Marsh, *Anim. Behav.* **63**, 245 (2002).
6. L. Pompilio, A. Kacelnik, *Anim. Behav.* **70**, 571 (2005).
7. A. Dickinson, B. W. Balleine, in *Steven's Handbook of Experimental Psychology*, vol. 3, *Learning, Motivation and Emotion*, ed. 3, H. Pashler, R. Gallistel, Eds. (Wiley, New York, 2002), pp. 497–533.
8. M. Burrows, *The Neurobiology of an Insect Brain* (Oxford Univ. Press, Oxford, 1996).
9. R. Dukas, E. A. Bernays, *Proc. Natl. Acad. Sci. U.S.A.* **97**, 2637 (2000).
10. S. T. Behmer, C. E. Belt, M. S. Shapiro, *J. Exp. Biol.* **208**, 3463 (2005).
11. S. J. Simpson, D. Raubenheimer, *Adv. Study Behav.* **29**, 1 (2000).
12. Materials and methods are available as supporting material on *Science* Online.
13. S. J. Simpson, M. S. J. Simmonds, W. M. Blaney, S. James, *Appetite* **17**, 141 (1991).

14. S. J. Simpson, C. L. Simpson, *J. Exp. Biol.* **168**, 269 (1992).
15. J. D. Abisgold, S. J. Simpson, *J. Exp. Biol.* **135**, 215 (1988).
16. C. L. Simpson, S. Chyb, S. J. Simpson, *Entomol. Exp. Appl.* **56**, 259 (1990).
17. R. F. Chapman, *Annu. Rev. Entomol.* **48**, 455 (2003).
18. R. M. Sibly, in *Physiological Ecology: An Evolutionary Approach to Resource Use*, T. C. P. Calow, Ed. (Blackwell, Oxford, 1981), pp. 109–139.
19. L. A. Real, *Am. Nat.* **140**, S108 (1992).
20. E. A. Bernays, *Annu. Rev. Entomol.* **46**, 703 (2001).
21. G. Gigerenzer, *Behav. Brain Sci.* **27**, 336 (2004).
22. We thank C. Nadell and C. Spatola Rossi for help during data collection; C. Schuck-Paim and M. S. Shapiro for helpful discussion; and T. Dickinson, P. Harvey, T. Reil, O. Lewis, and two anonymous referees for valuable feedback on the manuscript.

Supporting Online Material
www.sciencemag.org/cgi/content/full/311/5767/1613/DC1
Materials and Methods
Figs. S1 and S2
References

15 December 2005; accepted 1 February 2006
10.1126/science.1123924

An Equivalence Principle for the Incorporation of Favorable Mutations in Asexual Populations

Matthew Hegreness,[1,2]* Noam Shoresh,[1]* Daniel Hartl,[2] Roy Kishony[1,3]†

Rapid evolution of asexual populations, such as that of cancer cells or of microorganisms developing drug resistance, can include the simultaneous spread of distinct beneficial mutations. We demonstrate that evolution in such cases is driven by the fitness effects and appearance times of only a small minority of favorable mutations. The complexity of the mutation-selection process is thereby greatly reduced, and much of the evolutionary dynamics can be encapsulated in two parameters—an effective selection coefficient and effective rate of beneficial mutations. We confirm this theoretical finding and estimate the effective parameters for evolving populations of fluorescently labeled *Escherichia coli*. The effective parameters constitute a simple description and provide a natural standard for comparing adaptation between species and across environments.

Spontaneous beneficial mutations are the fuel for adaptation, the source of evolutionary novelty, and one of the least understood aspects of biology. Although adaptation is everywhere—cancer invading tissues, bacteria escaping drugs, viruses switching from livestock to humans—beneficial mutations are notoriously difficult to study (*1*, *2*). Theoretical and experimental advances have been made in recent years by focusing on the distribution of fitness effects of spontaneous beneficial mutations (*3*–*8*). Mapping the options for improvement available to single organisms, however, is insufficient for understanding the adaptive course of an entire population, especially in asexual populations of microorganisms or cancer cells where multiple mutations often spread simultaneously (*9*–*16*). Here, we use modeling and experimental results to show that the seeming additional complication of having multiple lineages competing within a population leads in fact to a drastic simplification: Regardless of the distribution of mutational effects available to individuals, a population's adaptive dynamics can be approximated by an equivalent model in which all favorable mutations confer the same fitness advantage, which we call the effective selection coefficient. We provide experimental estimates of the effective selection coefficient and the corresponding effective rate of beneficial mutations for laboratory populations of *Escherichia coli*, and we demonstrate the predictive power of these effective parameters.

First, we use numerical simulations to demonstrate the simplification that emerges in a population large enough and a mutation rate high enough that clonal interference (*17*–*19*)—competition among lineages carrying favorable mutations—is common. In an evolving population, most beneficial mutations are rapidly lost to random genetic drift (*20*, *21*). Of the remaining mutant lineages, some increase in frequency slightly, only to decline as more fit lineages appear and expand in the population (*10*, *16*, *17*, *22*). The evolutionary path taken by the population as a whole is determined by successful mutations that escape stochastic loss and whose frequencies rise above some minimal level. Using a population genetics model that includes mutation, selection, drift, as well as clonal interference (*23*), we explore the distribution of these successful mutations for several underlying distributions of beneficial mutations (Fig. 1), including an exponential distribution as suggested by Gillespie's (*8*) and Orr's (*3*) use of extreme value theory.

The salient feature of Fig. 1 is that very dissimilar underlying distributions—exponential, uniform, lognormal, even an arbitrary distribution—all yield a similar distribution of successful mutations (*24*). Moreover, the distribution of successful mutations has a simple form, peaked around a single value. This fitness value is typical of those mutations whose effects are not so small that they are lost through competition with more fit lineages, but are also not so large that they are impossibly rare. The unimodal shape motivates the hypothesis that an equivalent model that allows mutations with only a single selective value might approximate the behavior of the entire distribution of beneficial mutations.

We investigate whether the adaptive dynamics observed in evolving *E. coli* populations can be reproduced by an equivalent model with only a single value, a Dirac delta function of mutational effects. We rely on a classic strategy for characterizing beneficial mutations in coevolving subpopulations that differ initially only by selectively neutral marker. The spread of mutations is monitored through changes in the marker ratio (*22*, *25*–*29*). Our experimental technique uses constitutively expressed variants of GFP (green fluorescent protein)—YFP (yellow fluorescent protein) and CFP (cyan fluorescent protein)—as neutral markers. All experimental populations start with equal numbers of YFP and CFP *E. coli* cells (N_Y and N_C) and evolve for 300 generations through serial transfers while adapting to glucose minimal medium.

The expected behavior of the marker-ratio trajectories depends upon the rate at which beneficial mutations appear in a population. When beneficial mutations are rare, mutant lineages arise and fix one at a time (*8*, *17*). The spread of each individual mutant lineage shows as a line of

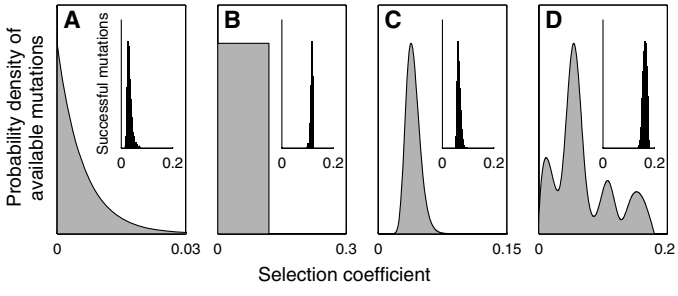

Fig. 1. Successful mutations cluster around a single value, irrespective of the shape of the underlying mutational distribution. Probability density of four underlying distributions: (**A**) exponential; (**B**) uniform; (**C**) lognormal; (**D**) arbitrary. (Insets) The corresponding distributions of successful mutations, defined here as those whose lineages constitute at least 10% of the population at any time before the ancestral genotype diminishes to less than 1%. All simulations were done with beneficial mutation rate of $\mu_b = 10^{-5}$ and population size $N = 2 \times 10^6$ and were replicated 1000 times (*23*).

[1]Bauer Center for Genomics Research, Harvard University, Cambridge, MA 02138, USA. [2]Department of Organismic and Evolutionary Biology, Harvard University, Cambridge, MA 02138, USA. [3]Department of Systems Biology, Harvard Medical School, Boston, MA 02115, USA.

*These authors contributed equally to this work.
†To whom correspondence should be addressed. E-mail: roy_kishony@hms.harvard.edu

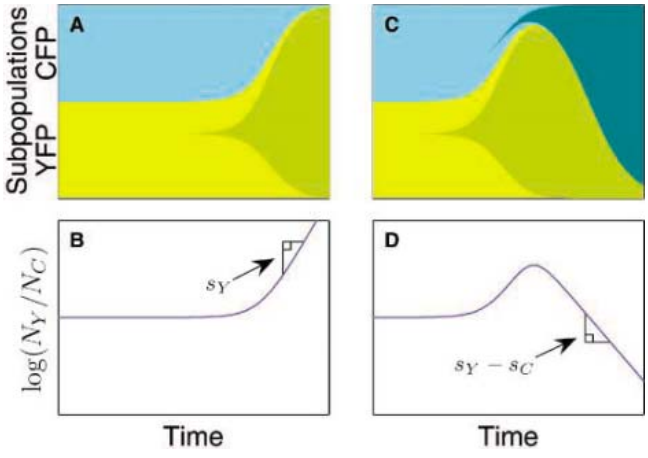

Fig. 2. The evolutionary spread of beneficial mutations. (**A**) A mutation (dark yellow) that occurs in a YFP-labeled cell takes over a mixed population of YFP and CFP cells. (**B**) The observed N_Y/N_C ratio in the population from (A); the mutant's selection coefficient, s_Y, can be obtained from the slope at late times. (**C**) A beneficial mutation in YFP competing with a beneficial mutation in CFP that occurs later but has a stronger selective advantage, s_C. (**D**) N_Y/N_C in the population from (C); the slope $d\log_2(N_Y/N_C)/dt$ at late times is equal to $s_Y - s_C$.

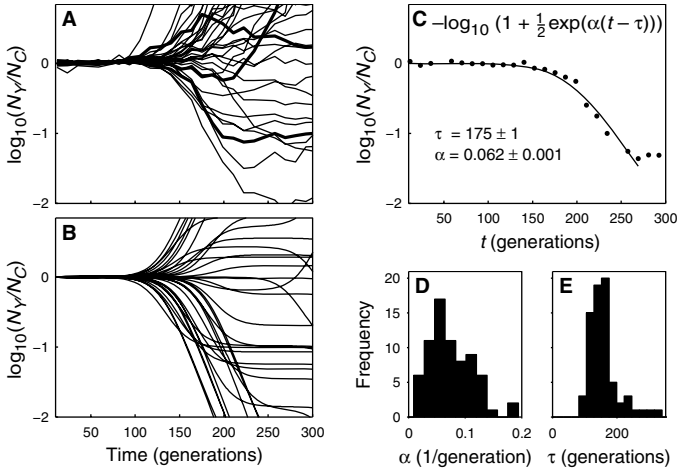

Fig. 3. Empirical and numerical marker-ratio data and trajectory parameterization. (**A**) Ratio of YFP to CFP cells of *E. coli* monitored for 300 generations (for clarity, 36 of 72 populations are shown and the rest are presented in fig. S2). The plateaus and reversals (see examples in bold) reveal the simultaneous spread of distinct beneficial mutations. The asymmetry in the vertical axis reflects the asymmetry in the dynamic range due to the fluorescence properties of YFP and CFP. (**B**) Ratios based on simulations using the Dirac delta function with a beneficial mutation rate $\mu_e = 10^{-6.7}$ and a selection coefficient $s_e = 0.054$ (values obtained from region of agreement in Fig. 4). (**C**) α and τ are defined by the function shown. The data, the best fit curve, and the corresponding values for α and τ are shown from one experimental population. (**D** and **E**) Histograms of estimated values of α and τ for each of the 72 experimental populations (for the correlation between α and τ see fig. S5).

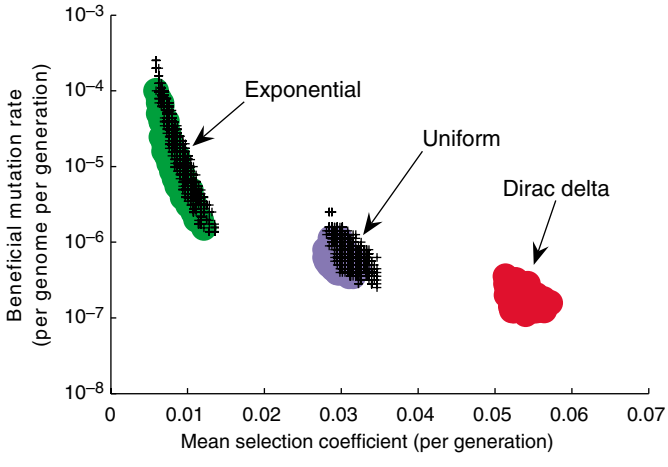

Fig. 4. Estimation of the effective parameters and demonstration that their predictive power is robust to the underlying distribution. Filled regions represent agreement (at 95% confidence level) between empirical data and model simulations, based on comparison of marker-ratio trajectories; shown in red is the region of agreement for the Dirac delta function, which provides an estimate of the effective parameters; also shown are the regions of agreement for exponential (green) and uniform (blue) underlying distributions. Crosshatched areas are the regions where calculations of $\langle f_{max} \rangle$ and $\langle s_{suc} \rangle$ from the exponential and uniform distributions agree with predictions of these quantities derived from the effective parameters.

constant nonzero slope when the logarithm of the marker ratio is plotted against time (Fig. 2A), where the slope is equal to the selection coefficient of the expanding lineage (*27*). When the mutation rate in asexual populations is high, however, beneficial mutations arise in both subpopulations and compete (Fig. 2B).

Results of the adaptation experiments are shown in Fig. 3A. As expected, the curves of the logarithm of the ratio of N_Y to N_C are initially flat, reflecting the equal initial fitness of the ancestral YFP and CFP cells. Beneficial mutations cause the marker ratio to deviate from its starting value after ~100 generations. The plateaus and reversals of the slopes that often appear after these initial deviations reveal the simultaneous spread of multiple beneficial mutations (additional evidence for the presence of clonal interference is shown in figs. S3 and S4). Concentrating on the initial phase of the experiment, we extract the time, τ, when significant deviation from a flat line first occurs, and the slope, α, of that deviation (Fig. 3C). We extract these for all 72 marker-ratio trajectories, obtaining empirical samples of α and τ (Fig. 3, D and E).

Results from the evolving *E. coli* populations are compared to simulations results produced with a theoretical model. The model tracks two coevolving subpopulations ("cyan" and "yellow") and accounts for the fluctuating population size due to serial dilution, selection, and random drift (*23*). An input to the model is a distribution from which the selection coefficients of beneficial mutations are drawn.

To test whether mutations of a single effect can generate variable adaptive dynamics compatible with the empirical data, we use a Dirac delta function as the equivalent underlying distribution of beneficial mutations. We also explore two other one-parameter distribution families—uniform and exponential (to facilitate comparison, distributions with more than one parameter, including the log-normal distribution from Fig. 1, are excluded from this analysis, though the conclusions that follow apply to these as well). Given a mutational distribution, the model has only two free parameters: the beneficial mutation rate and the mean of the distribution. For each distribution, for each point in parameter space, many realizations of the model are simulated (see example in Fig. 3B), generating theoretical predictions in the form of numerical samples of α and τ. These numerical samples, produced with the model, are then compared to the corresponding empirical ones from the *E. coli* experiments (using a Kolmogorov-Smirnov test). The filled areas in Fig. 4 indicate the region of agreement between the model and the empirical data for each of the underlying distributions of beneficial mutations.

The agreement with the Dirac delta function demonstrates that beneficial mutations of a single magnitude can indeed give rise to the rich adaptive behavior observed in the experiment. In particular, the differences in the timings of the mutations are a sufficient source for the variabil-

ity in the marker-ratio data. The effective parameters of the bacterial populations are estimated from the delta function's region of agreement: the effective selection coefficient $s_e = 0.054 \pm 0.003$ and the effective rate $\mu_e = 10^{-6.7 \pm 0.2}$ mutations per genome per generation.

The consistency of more than one underlying distribution with the data reinforces the point illustrated in Fig. 1: Adaptive dynamics are largely determined by a few broad properties of the distribution, encapsulated by the effective parameters, and not by its exact shape. The regions of agreement, obtained by comparing marker-ratio trajectories, are thus interpreted as reducing to the same effective parameters.

The equivalent model (defined by the effective parameters) predicts other measures of adaptation not trivially related to the marker-ratio data. Using simulations, we examine two quantities: $\langle f_{max} \rangle$, the degree of polymorphism, as measured by the average (over repeated simulations) of the frequency of the most common beneficial mutation when the ancestral strain goes extinct (reduces to 1% of the population); and $\langle s_{suc} \rangle$, the mean effect of successful mutations, that is, the average fitness of all mutant lineages that ever reach more than 10% frequency by this time. Predictions of these quantities based on the effective parameters are obtained through model simulations with the Dirac delta function. Regions where calculations of $\langle f_{max} \rangle$ and $\langle s_{suc} \rangle$ from the exponential and uniform distributions agree with these predictions are shown as the crosshatched areas in Fig. 4. The striking overlap of the new regions with the regions estimated from the marker-ratio data highlights the diversity of features captured by the effective parameters. Comparing the Dirac delta function with a more complicated underlying distribution, we see that if the distributions agree in their predictions for one aspect of adaptation (marker-ratio trajectories), they will also agree in other aspects ($\langle f_{max} \rangle$ and $\langle s_{suc} \rangle$). In accordance with the idea of an equivalent model, these results suggest that the predictive potential of the effective parameters is independent of the actual underlying mutational distribution.

When multiple beneficial mutations spread simultaneously in asexual populations, adaptive dynamics can be reasonably described by an equivalent model in which all favorable mutations confer the same selection advantage. The scope of this simple approximation, namely, the breadth of observables it captures and the limits at which it breaks down, is the subject of future research. Like a local adaptive landscape, the effective selection coefficient and the effective rate of beneficial mutations characterize the dynamics of a population at a specific point in its evolution. An entire adaptive trajectory might be represented by tracking changes in the effective parameters. Compared to high-dimensional fitness landscapes, effective parameters constitute a major simplification and can serve as mileposts along the adaptive walk.

References and Notes

1. J. J. Bull, S. P. Otto, *Nat. Genet.* **37**, 342 (2005).
2. H. A. Orr, *Evolution* **52**, 935 (1998).
3. H. A. Orr, *Genetics* **163**, 1519 (2003).
4. D. R. Rokyta, P. Joyce, S. B. Caudle, H. A. Wichman, *Nat. Genet.* **37**, 441 (2005).
5. R. Sanjuan, A. Moya, S. F. Elena, *Proc. Natl. Acad. Sci. U.S.A.* **101**, 8396 (2004).
6. M. A. DePristo, D. M. Weinreich, D. L. Hartl, *Nat. Rev. Genet.* **6**, 678 (2005).
7. M. Lunzer, S. P. Miller, R. Felsheim, A. M. Dean, *Science* **310**, 499 (2005).
8. J. H. Gillespie, *The Causes of Molecular Evolution* (Oxford Univ. Press, New York, 1991).
9. R. E. Lenski, M. R. Rose, S. C. Simpson, S. C. Tadler, *Am. Nat.* **138**, 1315 (1991).
10. R. Miralles, P. J. Gerrish, A. Moya, S. F. Elena, *Science* **285**, 1745 (1999).
11. J. A. G. M. de Visser, C. W. Zeyl, P. J. Gerrish, J. L. Blanchard, R. E. Lenski, *Science* **283**, 404 (1999).
12. N. Colegrave, *Nature* **420**, 664 (2002).
13. A. Moya, E. C. Holmes, F. Gonzalez-Candelas, *Nat. Rev. Microbiol.* **2**, 279 (2004).
14. G. H. Heppner, *Cancer Res.* **44**, 2259 (1984).
15. M. R. Novelli *et al.*, *Science* **272**, 1187 (1996).
16. J. Kim, L. R. Ginzburg, D. E. Dykhuizen, in *Assessing Ecological Risks of Biotechnology*, L. R. Ginzburg, Ed. (Butterworth-Heinemann, Boston, 1991), pp. 193–214.
17. P. J. Gerrish, R. E. Lenski, *Genetica* **102-103**, 127 (1998).
18. H. J. Muller, *Am. Nat.* **66**, 118 (1932).
19. J. F. Crow, M. Kimura, *Am. Nat.* **99**, 439 (1965).
20. M. Kimura, *The Neutral Theory of Molecular Evolution* (Cambridge Univ. Press, New York, 1983).
21. J. Haldane, *Proc. Cambridge Philos. Soc.* **23**, 838 (1927).
22. D. E. Rozen, J. de Visser, P. J. Gerrish, *Curr. Biol.* **12**, 1040 (2002).
23. Materials and methods are available as supporting material on *Science* Online.
24. A similar observation was made by Gerrish and Lenski in (*17*) concerning the probability of transiently polymorphic beneficial mutations.
25. K. C. Atwood, L. K. Schneider, F. J. Ryan, *Proc. Natl. Acad. Sci. U.S.A.* **37**, 146 (1951).
26. D. L. Hartl, D. E. Dykhuizen, *Proc. Natl. Acad. Sci. U.S.A.* **78**, 6344 (1981).
27. L. Chao, E. C. Cox, *Evolution* **37**, 125 (1983).
28. M. M. Zambrano, D. A. Siegele, M. Almiron, A. Tormo, R. Kolter, *Science* **259**, 1757 (1993).
29. M. Imhof, C. Schlotterer, *Proc. Natl. Acad. Sci. U.S.A.* **98**, 1113 (2001).

30. We thank D. Huse for theoretical advice regarding the model; M. Elowitz for strains and suggestions; N. Barkai and R. Lenski for important comments; and U. Alon, D. Damian, A. DeLuna, M. Depristo, M. Desai, D. Fisher, L. Garwin, A. Murray, V. Savage, K. Vestigian, and D. Weinreich for discussions and comments on the manuscript. This work was supported by the Bauer Center for Genomics Research and by grants from the NSF and the Ellison Medical Foundation. M.H. dedicates this work to the memory of his mother, Kari Hegreness.

Supporting Online Material

www.sciencemag.org/cgi/content/full/311/5767/1615/DC1
Materials and Methods
SOM Text
Figs. S1 to S5
References

10 November 2005; accepted 9 February 2006
10.1126/science.1122469

Parietal-Eye Phototransduction Components and Their Potential Evolutionary Implications

Chih-Ying Su,[1]*† Dong-Gen Luo,[1] Akihisa Terakita,[2] Yoshinori Shichida,[2] Hsi-Wen Liao,[1] Manija A. Kazmi,[3] Thomas P. Sakmar,[3] King-Wai Yau[1]*

The parietal-eye photoreceptor is unique because it has two antagonistic light signaling pathways in the same cell—a hyperpolarizing pathway maximally sensitive to blue light and a depolarizing pathway maximally sensitive to green light. Here, we report the molecular components of these two pathways. We found two opsins in the same cell: the blue-sensitive pinopsin and a previously unidentified green-sensitive opsin, which we name parietopsin. Signaling components included gustducin-α and $G\alpha_o$, but not rod or cone transducin-α. Single-cell recordings demonstrated that G_o mediates the depolarizing response. Gustducin-α resembles transducin-α functionally and likely mediates the hyperpolarizing response. The parietopsin-G_o signaling pair provides clues about how rod and cone phototransduction might have evolved.

Lizards and some other lower vertebrates have a third eye (parietal eye) (*1*) in addition to the two lateral eyes. This eye may mediate the global detection of dawn and dusk (*1*, *2*) instead of conventional image-forming vision. The parietal-eye photoreceptors resemble rods and cones in morphology, but they show chromatic antagonism (a unique feature among all known photoreceptors) consisting of a hyperpolarizing light response most sensitive to blue light and a depolarizing light response most sensitive to green light (*2*). The hyperpolarizing response is produced, as in rods and cones, by the activation of a guanosine 3′,5′–cyclic monophosphate (cGMP)–phosphodiesterase that lowers the cGMP concentration and closes cyclic nucleotide-gated

[1]Department of Neuroscience, Johns Hopkins University School of Medicine, Baltimore, MD 21205, USA. [2]Department of Biophysics, Graduate School of Science, Kyoto University and Core Research for Evolutional Science and Technology, Japan Science and Technology Agency, Kyoto 606-8502, Japan. [3]Laboratory of Molecular Biology and Biochemistry, Rockefeller University, 1230 York Avenue, New York, NY 10021, USA.

*To whom correspondence should be addressed. E-mail: chih-ying.su@yale.edu (C.-Y.S.); kwyau@mail.jhmi.edu (K.-W.Y.)
†Present address: Department of Molecular, Cellular, and Developmental Biology, Yale University, New Haven, CT 06520, USA.

(CNG) channels (*3*, *4*). The depolarizing response, on the other hand, is produced by the inhibition of the same phosphodiesterase, elevating cGMP and opening CNG channels (*3*, *4*). We cloned the molecular components underlying this antagonism.

By screening a parietal-eye cDNA library from the side-blotched lizard (*Uta stansburiana*) for vertebrate opsins (*5*), we found pinopsin, a blue-sensitive pigment first identified in chicken pinealocytes (*6*, *7*). In addition, we found a previously unidentified opsin, which we named parietopsin (fig. S1). We also found orthologs of parietopsin in fish and frog DNA databases. The conserved glutamate constituting the counterion for the protonated Schiff-base in typical opsins is replaced in parietopsin by glutamine (Gln^{103}), indicating that parietopsin uses another conserved glutamate (probably Glu^{171}) as the counterion (*8*). This feature appears to be a characteristic of evolutionarily ancient vertebrate opsins (*8*). In pairwise alignments, parietopsin showed the highest degree of identity (~40%) to parapinopsin, an ancient opsin identified in the fish parapineal organ (*9*) (table S1). However, a phylogenetic analysis including lizard parietopsin and its orthologs demonstrated that parietopsins defined a distinct opsin subfamily (Fig. 1A). When expressed in human embryonic kidney (HEK) 293 cells, parietopsin had a λ_{max} at 522 nm (Fig. 1B), indicating that it is a green-sensitive pigment.

For comparison, we also identified five lateral-eye (i.e., rod and cone) opsins in the same lizard (*5*). Polymerase chain reaction (PCR) analyses indicated that the lateral and parietal eyes expressed nonoverlapping sets of opsins [fig. S2 and supporting online material (SOM) text]. In rod and cone opsins, the second and third cyto-

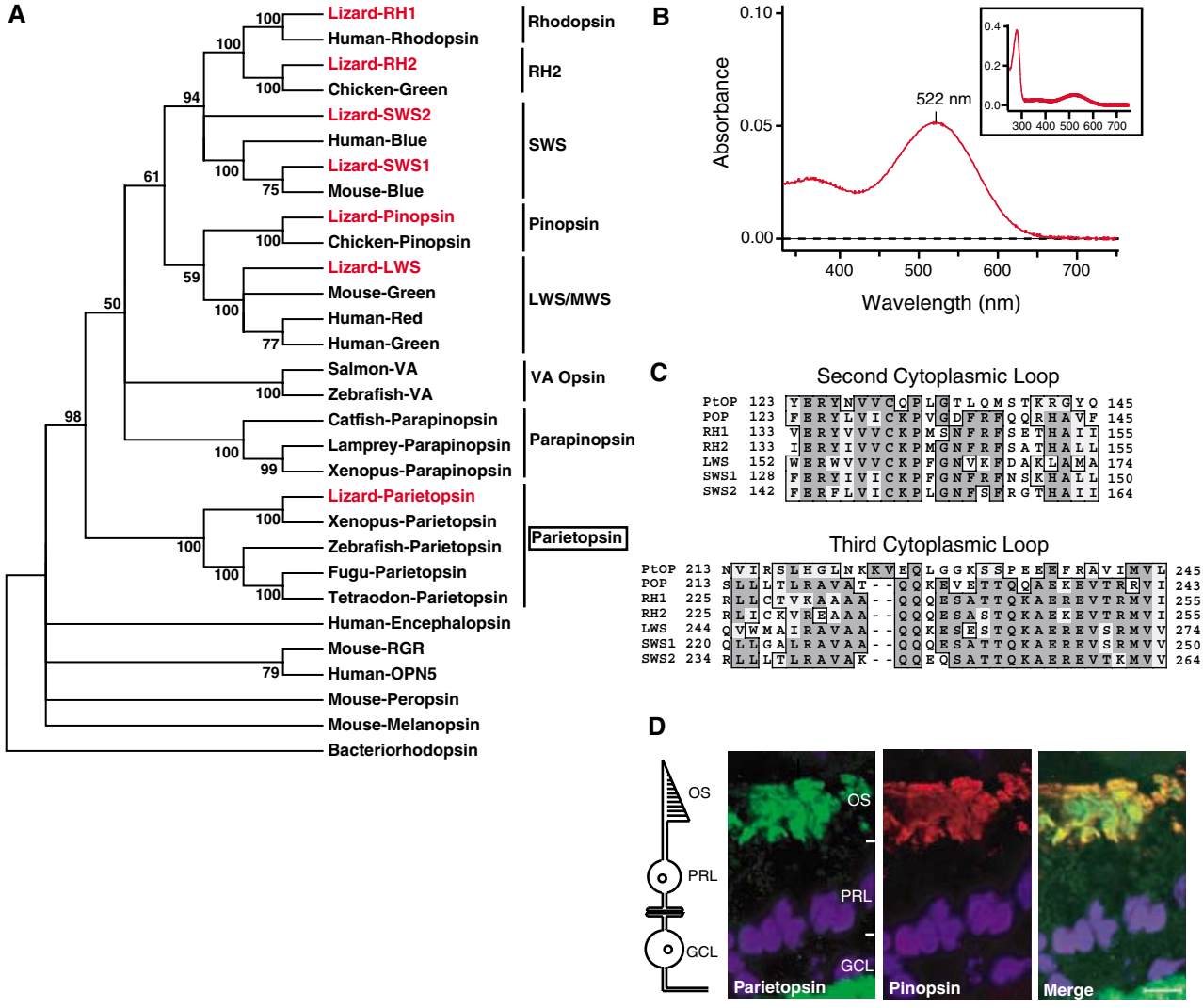

Fig. 1. Parietal-eye opsins. (**A**) Phylogenetic analysis of parietopsin and other vertebrate opsins. The tree was constructed by the Neighbor-Joining algorithm with bacteriorhodopsin as an outgroup (*5*). Bootstrap probability (%), which is a statistical evaluation of the robustness of the grouping, is shown when ≥50. Parietopsins defined a distinct opsin subfamily with a very strong bootstrap support (100%). Opsins identified in this study are shown in red. RH, rhodopsin; SWS, short wavelength–sensitive opsin; LWS, long wavelength–sensitive opsin; MWS, medium wavelength–sensitive opsin; VA, vertebrate ancient opsin; RGR, retinal pigment epithelium G protein–coupled receptor; OPN5, neuropsin. (**B**) Absorption spectrum of purified lizard parietopsin expressed in HEK293 cells. It showed a λ_{max} at 522 nm at pH 6.5 with 11-*cis*-retinal as chromophore, in darkness (*5*) (SOM text). (Inset) The full dark spectrum of parietopsin. The ratio of the protein absorbance at 280 nm to the λ_{max} of parietopsin is 7.4. (**C**) Sequence alignments of the second and third cytoplasmic loops of the lizard opsins identified in this study. Identical and similar residues are shaded in dark and light gray, respectively. PtOP, parietopsin; POP, pinopsin. (**D**) Confocal images of parietal-eye sections double-stained with antibodies against parietopsin (green) and pinopsin (red). Nuclei were counterstained with 4′,6′-diamidino-2-phenylindole (DAPI) in blue. The staining of parietopsin antiserum beneath the ganglion cell layer (GCL) was nonspecific because it was also seen with the preimmune serum. The merged image (right) shows that parietopsin and pinopsin colocalized in the outer segments of the photoreceptors. Scale bar, 5 μm. OS, outer segment; PRL, photoreceptor layer.

plasmic loops are highly conserved, reflecting their importance in specific interactions with the downstream G protein, transducin (*10*). Pinopsin, but not parietopsin, shared these homologous sequences (Fig. 1C). Double immunolabeling with specific antibodies showed that pinopsin and parietopsin colocalized in the same photoreceptor outer segment, where phototransduction takes place (Fig. 1D; see also fig. S3 for antibody specificities). Thus, pinopsin and parietopsin appear to drive the hyperpolarizing and depolarizing responses, respectively.

In the chicken, pinopsin colocalizes with rod transducin-α in pinealocytes (*11*) and activates it in the light (*11*, *12*), suggesting that the two are functionally coupled in these cells. However, we did not find rod or cone transducin-α in the parietal-eye cDNA library (although we did find them in the lateral-eye cDNA library). Instead, we found gustducin-α, the G protein mediating bitter and sweet transductions in taste buds (*13*, *14*). Sequence alignments of the lizard gustducin-α and rod and cone transducin-α proteins showed 80% identities among all three (fig. S4); the degrees of sequence identities are similar in the rat (*13*). With reverse transcription (RT)–PCR, we confirmed the same gustducin sequence in lizard tongue. RT-PCR also showed that the gustducin-α message was absent in the lateral eyes, and the rod and cone transducin-α messages were absent in the parietal eye (*15*), confirmed by immunocytochemistry with antibodies against the cloned gustducin-α and cone transducin-α, respectively (Fig. 2, A and B).

We also found $G\alpha_o$ in the parietal-eye cDNA library. A polyclonal antibody (K-20, Santa Cruz Biotechnology) that recognized $G\alpha_o$ in lizard lateral-eye ON-bipolar cells (*16*) (positive control; fig. S5) but did not cross-react with transducin-α in rods or cones also labeled the parietal-eye photoreceptors. Double-immunolabeling with K-20 and a monoclonal antibody that recognizes lizard gustducin-α (TF15, CytoSignal; Fig. 2A) confirmed the colocalization of gustducin-α and $G\alpha_o$ in the same photoreceptor outer segment (Fig. 2C).

The similarities in structure and function between gustducin-α and transducin-α (*13*, *17*, *18*), together with the similarity between pinopsin and rod and cone opsins, suggest that pinopsin couples to gustducin to produce the hyperpolarizing light response. If so, parietopsin likely couples to G_o to produce the depolarizing light response. For functional verification, we did whole-cell recordings from isolated parietal-eye photoreceptors. At a holding potential of –45 mV [near the membrane potential in darkness (*2*)], cGMP in the whole-cell pipette induced an inward current in darkness by opening CNG channels (*3*, *4*). The 100 μM cGMP induced a much smaller current (36 ± 5 pA, mean ± SEM, $n = 27$) than the 150 μM cGMP (118 ± 28 pA, $n = 6$) (Fig. 3A, top and bottom), indicating that the current induced by 100 μM cGMP was far from saturated, attributable to high endogenous phosphodiesterase activity (*4*). With 100 μM cGMP, a white flash elicited a biphasic response consisting of an outward current followed by an inward current (Fig. 3B, top left). A green (520-nm) flash, however, elicited only an inward current, and a blue (480-nm) flash elicited only an outward current (Fig. 3B, middle and bottom left), corresponding to a membrane depolarization and hyperpolarization, respectively, under current clamp (*2*). When the pipette also contained 20 μM mastoparan, a peptide that activates G_o but has little effect on transducin (*19*), the inward current induced by 100 μM cGMP increased to 92 ± 16 pA ($n = 18$) (Fig. 3A, middle and bottom). Also, a white flash in this case elicited only an outward current (Fig. 3B, top right). Correspondingly, a green flash elicited no response, whereas a blue flash still elicited an outward current (Fig. 3B, middle and bottom right). Finally, the inactive mastoparan analog

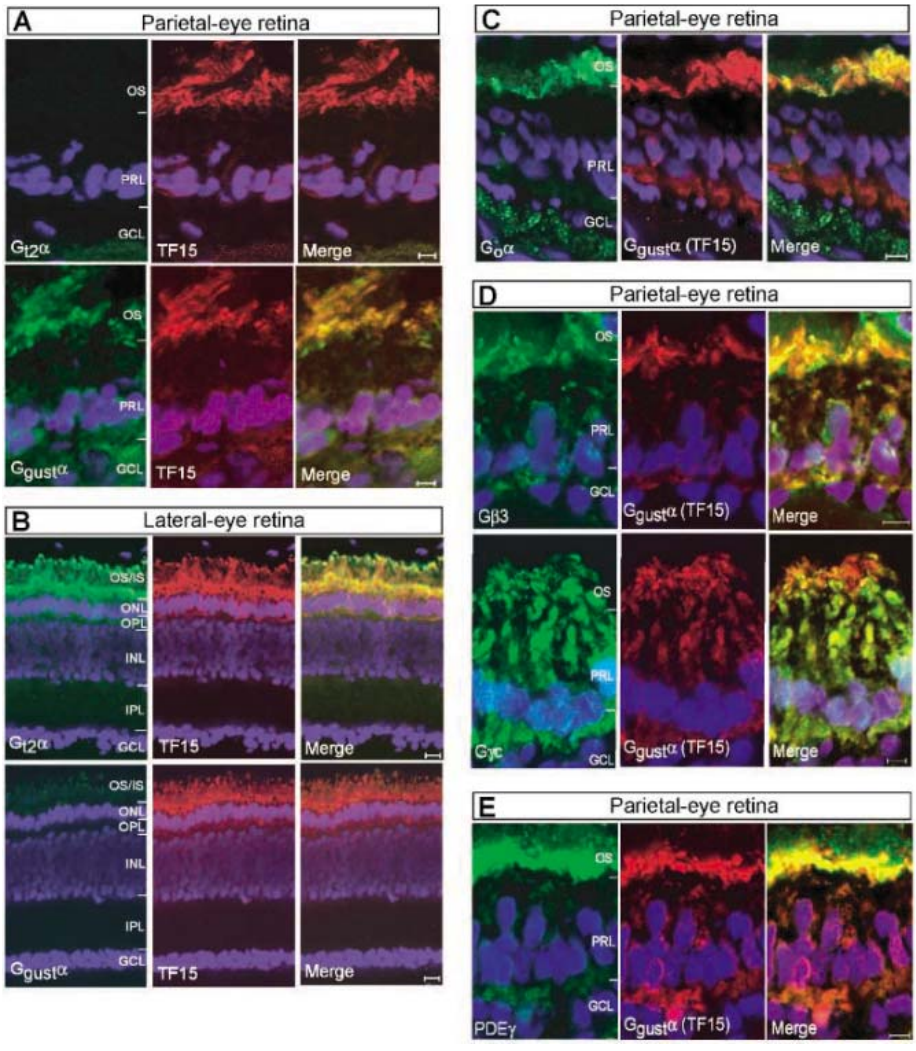

Fig. 2. G proteins and other phototransduction components. (**A** to **B**) Immunocytochemistry of parietal-eye retina and lateral-eye retina with the use of specific antibodies against cone transducin-α ($G_{t2}\alpha$) and gustducin-α ($G_{gust}\alpha$). Parietal-eye photoreceptors expressed $G_{gust}\alpha$ but not $G_{t2}\alpha$. Conversely, $G_{t2}\alpha$, but not $G_{gust}\alpha$, was expressed in the lateral eyes. Most lateral-eye photoreceptors were labeled by the $G_{t2}\alpha$ antibody because the retina of the side-blotched lizard is cone dominant. A monoclonal antibody, TF15, that recognizes both $G_{gust}\alpha$ and $G_{t1}\alpha/G_{t2}\alpha$ was used as a positive control. Merged images show that TF15 labeled $G_{gust}\alpha$ in the parietal eye and $G_{t1}\alpha/G_{t2}\alpha$ in the lateral eye. (**C** to **E**) Double-immunostaining of parietal-eye sections. $G_{gust}\alpha$ was labeled by TF15, as shown in (A). (C) $G\alpha_o$ labeling in the outer segments overlapped with $G_{gust}\alpha$. Likewise, Gβ3 and Gγc (D), as well as PDEγ (E), also colocalized with $G_{gust}\alpha$ in the parietal-eye photoreceptors. Gβ3 and Gγc, similar to $G_{gust}\alpha$, were expressed throughout the photoreceptor, whereas PDEγ labeling was found mainly in the outer segment. The specificities of the Gβ3 and Gγc antibodies we used were verified in the lateral-eye retina, where their labelings colocalized with that of cone transducin-α in most photoreceptors (*15*). OS/IS, outer segment/inner segment; ONL, outer nuclear layer; OPL, outer plexiform layer; INL, inner nuclear layer; IPL, inner plexiform layer; GCL, ganglion cell layer; PRL, photoreceptor layer. Scale bars, 5 μm [(A) and (C) to (E)] and 10 μm (B).

Mas-17 (*20*) affected neither the cGMP-induced current in darkness (Fig. 3A, bottom) nor the light responses (*15*). These results suggest that G_o inhibits the phosphodiesterase to produce the depolarizing light response (*4*), so that its activation by mastoparan in our experiments increased the cGMP-induced inward current in darkness and occluded the depolarizing light response. Collectively, a white flash–induced response showed an outward-current component in 14 out of 25 cells without mastoparan [the hyperpolarizing pathway is less sensitive to light (*2*)] and still showed the outward-current component in all of 13 cells with mastoparan. Thus, the effect of mastoparan was quite specific. The inhibition of the phosphodiesterase by G_o could be direct or indirect (SOM text).

By immunocytochemistry, we also found in the parietal-eye photoreceptor Gβ3 and Gγc (i.e., cone transducin-βγ) (*21*, *22*), but not Gβ1 and Gγ1 (rod transducin-βγ), despite their positive labelings in the lateral eyes. The labeling of Gβ3 and Gγc colocalized with that of gustducin-α (Fig. 2D). Further cDNA library screenings identified the catalytic subunit (PDEα′) and the inhibitory subunit (PDEγ) of the cone cGMP phosphodiesterase (*23*), which also colocalized with gustducin-α in the outer segment of the parietal-eye photoreceptor (Fig. 2E). Finally, in the parietal eye, we found clones for the rod CNG channel α subunit (CNGA1) and the guanosine triphosphatase (GTPase)–activating protein (GAP) complex (RGS9 and Gβ5L) common to rods and cones, proteins critical for response termination by promoting the GTPase activity of transducin (*24*). Previous electrical recordings also corroborate that the CNG channel on the parietal-eye photoreceptor is more similar to that of rods than that of cones (*3*).

The emerging picture is as follows (fig. S6): The hyperpolarizing light response is mediated by the blue-sensitive pinopsin, which activates a cGMP-phosphodiesterase by means of gustducin to lower cGMP concentration and close CNG channels. The depolarizing light response is mediated by the green-sensitive parietopsin, which inhibits the phosphodiesterase by means of G_o to elevate cGMP and open CNG channels. In conjunction with this chromatic antagonism, the parietal-eye photoreceptor synapses directly on ganglion cells (*1*). Thus, unlike in the lateral eyes where elaborate neuronal circuitry involving bipolar, horizontal, and amacrine cells performs substantial visual-signal processing (including chromatic antagonism), information processing in the primitive parietal eye takes place at least partly in the photoreceptors themselves, with the use of two pigments and two G proteins. Additionally, the molecular identities of the phototransduction components reported here may shed light on the evolutionary status of this photoreceptor. A clue comes from G_o, which also mediates phototransduction in the scallop hyperpolarizing photoreceptor (an invertebrate ciliary photoreceptor) (*25*) by coupling the visual pigment SCOP2 to the activation of a guanylate cyclase and leading to the opening of a cGMP-gated potassium channel (*25*, *26*). Similar to parietopsin, SCOP2 appears to be an ancient opsin that has diverged early in opsin evolution (*25*). Thus, a G_o-mediated phototransduction mechanism appears ancient. Moreover, although gustducin, transducin, and G_o all belong to the same G protein subfamily (G_i), G_o appears to be the most ancient because it is common to vertebrates and invertebrates. Accordingly, we propose the following evolutionary lineage of phototransduction mechanisms in ciliary photoreceptors, assuming that vertebrate and invertebrate (including the scallop ciliary photoreceptor) share one common precursor (*27*, *28*). A G_o-mediated phototransduction pathway might already be present in the ciliary photoreceptors of early coelomates, the last common ancestor of lizard (vertebrate) and scallop (mollusk), because both have this pathway. Later, the ancestral vertebrate photoreceptor acquired a second G protein, either gustducin or transducin, for chromatic antagonism and perhaps other purposes (SOM text). The parietal photoreceptor evolved subsequently and retained these ancestral features. The cones, rods, and light-sensitive pinealocytes [which are mechanistically identical to rods and cones in phototransduction (*29*, *30*)], on the other hand,

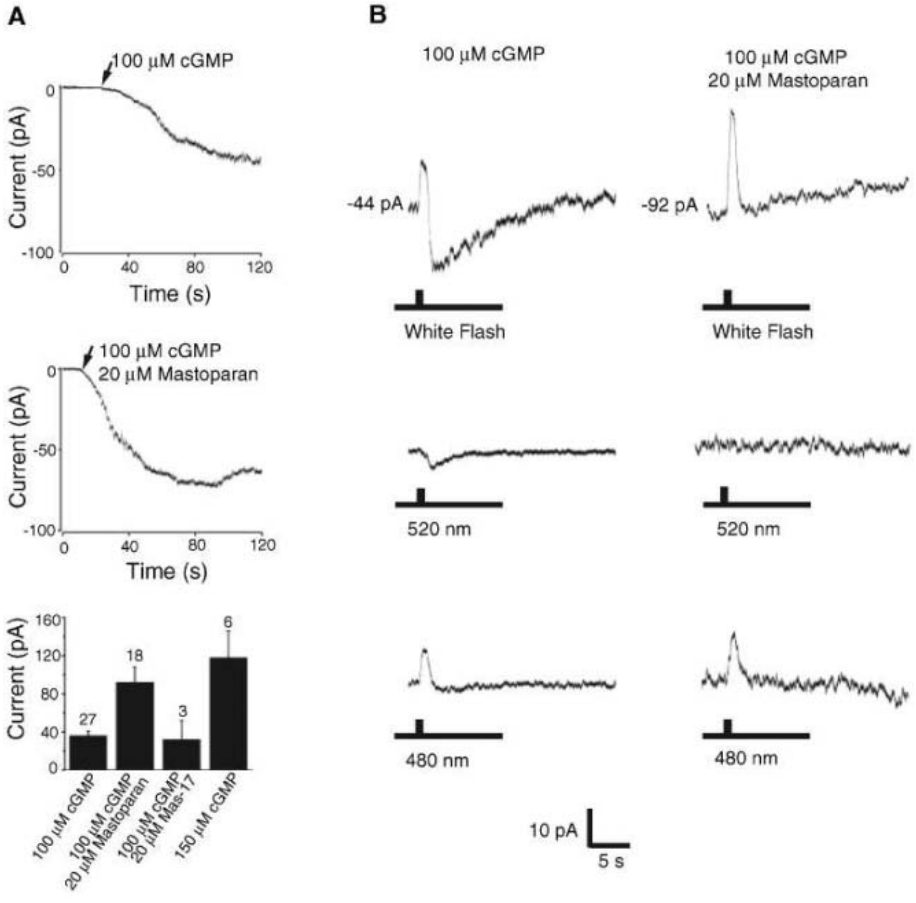

Fig. 3. Whole-cell recordings from isolated parietal-eye photoreceptors. (**A**) Inward current induced in darkness by 100-μM cGMP in the whole-cell pipette (membrane holding potential = –45 mV) in the absence (top) or presence (middle) of mastoparan, a G_o-activating peptide. The mastoparan concentration (20 μM) was empirically chosen in order to selectively activate G_o and at the same time to minimize nonspecific effects (*19*, *26*). The arrow indicates the time point at which whole-cell recording started. Collective results are shown at the bottom. Mas-17, an inactive form of mastoparan, was used as a negative control. (**B**) Light responses recorded after the cGMP-induced current reached steady state. (Left) Top, middle, and bottom panels are from the same cell. In the absence of mastoparan, the response to a white flash was biphasic (top), composed of a green-sensitive inward current and a blue-sensitive outward current, as revealed by the subsequent light responses at 520 nm (middle) and 480 nm (bottom). In the top panel, the cGMP-induced current before the flash was –44 pA. (Right) Similar experiment from another cell, but with mastoparan. In the presence of mastoparan, the response to a white flash showed only an outward-current component (top). A 520-nm flash produced no response (middle), whereas a 480-nm flash still produced an outward-current response (bottom) in this cell. In the top panel, the cGMP-induced current before the flash was –92 pA.

inherited only the gustducin/transducin-mediated pathway.

References and Notes

1. R. M. Eakin, *The Third Eye* (Univ. of California Press, Berkeley and Los Angeles, CA, 1973).
2. E. Solessio, G. A. Engbretson, *Nature* **364**, 442 (1993).
3. J. T. Finn, E. C. Solessio, K.-W. Yau, *Nature* **385**, 815 (1997).
4. W.-H. Xiong, E. C. Solessio, K.-W. Yau, *Nat. Neurosci.* **1**, 359 (1998).
5. Materials and methods are available as supporting material on *Science* Online.
6. T. Okano, T. Yoshizawa, Y. Fukada, *Nature* **372**, 94 (1994).
7. M. Max *et al.*, *Science* **267**, 1502 (1995).
8. A. Terakita *et al.*, *Nat. Struct. Mol. Biol.* **11**, 284 (2004).
9. S. Blackshaw, S. H. Snyder, *J. Neurosci.* **17**, 8083 (1997).
10. A. Terakita, T. Yamashita, N. Nimbari, D. Kojima, Y. Shichida, *J. Biol. Chem.* **277**, 40 (2002).
11. T. Kasahara, T. Okano, T. Yoshikawa, K. Yamazaki, Y. Fukada, *J. Neurochem.* **75**, 217 (2000).
12. M. Max, A. Surya, J. S. Takahashi, R. F. Margolskee, B. E. Knox, *J. Biol. Chem.* **273**, 26820 (1998).
13. S. K. McLaughlin, P. J. McKinnon, R. F. Margolskee, *Nature* **357**, 563 (1992).
14. G. T. Wong, K. S. Gannon, R. F. Margolskee, *Nature* **381**, 796 (1996).
15. C.-Y. Su *et al.*, data not shown.
16. N. Vardi, *J. Comp. Neurol.* **395**, 43 (1998).
17. M. A. Hoon, J. K. Northup, R. F. Margolskee, N. J. Ryba, *Biochem. J.* **309**, 629 (1995).
18. W. He *et al.*, *Chem. Senses* **27**, 719 (2002).
19. T. Higashijima, S. Uzu, T. Nakajima, E. M. Ross, *J. Biol. Chem.* **263**, 6491 (1988).
20. T. Higashijima, J. Burnier, E. M. Ross, *J. Biol. Chem.* **265**, 14176 (1990).
21. R. H. Lee, B. S. Lieberman, H. K. Yamane, D. Bok, B. K. Fung, *J. Biol. Chem.* **267**, 24776 (1992).
22. O. C. Ong *et al.*, *J. Biol. Chem.* **270**, 8495 (1995).
23. J. A. Beavo, *Physiol. Rev.* **75**, 725 (1995).
24. W. He *et al.*, *J. Biol. Chem.* **275**, 37093 (2000).
25. D. Kojima *et al.*, *J. Biol. Chem.* **272**, 22979 (1997).
26. M. P. Gomez, E. Nasi, *J. Neurosci.* **20**, 5254 (2000).
27. F. Pichaud, C. Desplan, *Curr. Opin. Genet. Dev.* **12**, 430 (2002).
28. D. Arendt, K. Tessmar-Raible, H. Snyman, A. W. Dorresteijn, J. Wittbrodt, *Science* **306**, 869 (2004).
29. G. A. Pu, J. E. Dowling, *J. Neurophysiol.* **46**, 1018 (1981).
30. S. Tamotsu, Y. Morita, *J. Comp. Physiol. [A]* **159**, 1 (1986).

31. We thank A. A. Lanahan for constructing the cDNA libraries; G. Engbretson for suggestions and initial help; J. Pevsner for help with phylogenetic analysis; R. H. Cote for the PDEγ antibody; W. J. De Grip for the CERN874 antibody; R. H. Lee for the Gβ1, Gβ3, and Gγc antibodies; A. Lesemann and R. R. Reed for the Gγ13 antibody; and R. S. Molday for the 1D4 and B630 antibodies. We also thank W.-H. Xiong, W. Luo, and J. Bradley for experimental help and V. Kefalov and N. Marsh-Armstrong for experiments expressing lizard pinopsin in transgenic *Xenopus*, which unfortunately were inconclusive. We thank S. Blackshaw, M. Do, J. Reisert, and V. Bhandawat for comments on the manuscript. This work was supported by EY06837 from the National Eye Institute (K.-W.Y.) and the Allene Reuss Memorial Trust (T.P.S.).

Supporting Online Material

www.sciencemag.org/cgi/content/full/311/5767/1617/DC1
Materials and Methods
SOM Text
Figs. S1 to S6
Tables S1 and S2
References

13 December 2005; accepted 3 February 2006
10.1126/science.1123802

A Protein Farnesyltransferase Inhibitor Ameliorates Disease in a Mouse Model of Progeria

Loren G. Fong,[1]* David Frost,[2] Margarita Meta,[3] Xin Qiao,[1] Shao H. Yang,[1] Catherine Coffinier,[1] Stephen G. Young[1]*

Progerias are rare genetic diseases characterized by premature aging. Several progeroid disorders are caused by mutations that lead to the accumulation of a lipid-modified (farnesylated) form of prelamin A, a protein that contributes to the structural scaffolding for the cell nucleus. In progeria, the accumulation of farnesyl–prelamin A disrupts this scaffolding, leading to misshapen nuclei. Previous studies have shown that farnesyltransferase inhibitors (FTIs) reverse this cellular abnormality. We tested the efficacy of an FTI (ABT-100) in *Zmpste24*-deficient mice, a mouse model of progeria. The FTI-treated mice exhibited improved body weight, grip strength, bone integrity, and percent survival at 20 weeks of age. These results suggest that FTIs may have beneficial effects in humans with progeria.

Hutchinson-Gilford progeria syndrome (HGPS) is a rare genetic disorder characterized by the precocious development of aging-like phenotypes (*1*, *2*). Children with HGPS exhibit retarded growth, osteoporosis, osteolytic lesions in bones, alopecia, loss of subcutaneous fat, and ultimately occlusive vascular disease, which generally leads to death by the teenage years (*1*, *2*). HGPS is caused by a *LMNA* mutation that leads to the production of a mutant prelamin A that cannot undergo the endoproteolytic processing step that yields mature lamin A (*3*). Lamin A is a key structural protein of the nuclear lamina, an intermediate filament meshwork that acts as a scaffold for the cell nucleus (*1*, *2*).

Prelamin A contains a *CaaX* motif that triggers the addition of a 15-carbon farnesyl lipid (a cholesterol biosynthetic intermediate) to a C-terminal cysteine (*2*, *4*). In normal cells, the farnesylation of prelamin A is thought to facilitate its targeting to the inner nuclear membrane, where it is cleaved by the zinc metalloproteinase ZMPSTE24 (*5*). ZMPSTE24 cleaves 15 amino acids from the C terminus of prelamin A that includes the farnesylcysteine, releasing mature lamin A. In HGPS, the mutant prelamin A cannot be processed by ZMPSTE24 and therefore retains its farnesyl lipid anchor; this mutant farnesylated protein is targeted to the nuclear rim, interferes with the integrity of the lamina, and causes misshapen cell nuclei (nuclei with blebs, folds, or wrinkles) (*3*). A more severe progeroid disorder, restrictive dermopathy, is caused by mutations leading to loss of ZMPSTE24 (*2*, *6*, *7*); partial loss of ZMPSTE24 can lead to mandibuloacral dysplasia, a progeroid disorder similar to HGPS (*8*, *9*). In ZMPSTE24-deficient cells, wild-type farnesyl–prelamin A accumulates along the nuclear envelope and likewise leads to misshapen cell nuclei (*6*, *7*, *10*).

When the farnesylation of prelamin A in HGPS cells and ZMPSTE24-deficient cells is blocked with a farnesyltransferase inhibitor (FTI), prelamin A does not accumulate at the nuclear rim and the percentage of cells with misshapen nuclei is reduced (*2*, *11*–*15*). These in vitro observations strongly suggest that the accumulation of farnesyl–prelamin A interferes with the scaffolding function of the nuclear

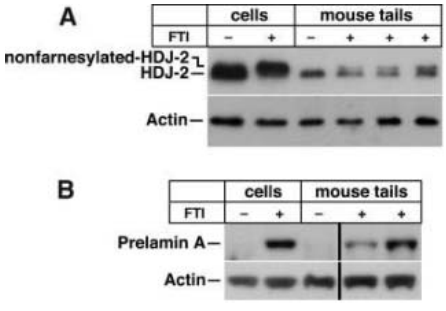

Fig. 1. Administration of an FTI in the drinking water of wild-type mice inhibits protein farnesylation in vivo. (**A**) Western blots of tail samples developed with a monoclonal antibody to HDJ-2, showing the appearance of nonfarnesylated HDJ-2 in mice treated with an FTI. Extracts of mouse embryonic fibroblasts grown in the presence and absence of an FTI (2.5 μM) were included as controls. (**B**) Western blot of tail extracts of wild-type mice with a prelamin A–specific antibody (*9*), showing the appearance of prelamin A in the setting of FTI treatment. Actin was measured as a control for sample loading.

[1]Department of Medicine/Division of Cardiology, David Geffen School of Medicine, University of California, Los Angeles, CA 90095, USA. [2]Abbott Laboratories, Abbott Park, IL 60064, USA. [3]Department of Radiology, University of California, San Francisco, CA 94107, USA.

*To whom correspondence should be addressed. E-mail: lfong@mednet.ucla.edu; sgyoung@mednet.ucla.edu

lamina. If the disrupted nuclear scaffolding were important to the pathogenesis of progeria, then FTIs might be expected to ameliorate disease symptoms in animal models of the disorder.

To explore this hypothesis, we treated *Zmpste24*-deficient mice (*Zmpste24*$^{-/-}$) with a potent FTI, ABT-100 (*16*, *17*). Like mice harboring a targeted HGPS mutation (*11*), *Zmpste24*$^{-/-}$ mice exhibit osteoporosis, osteolytic lesions in the ribs near the costovertebral joints, retarded growth after weaning, and a shorter life span (4 to 8 months, versus >24 months in wild-type mice) (*10*, *18*). The osteolytic lesions in the ribs lead to spontaneous rib fractures beginning at 3 months of age. The *Zmpste24*$^{-/-}$ mice also lose grip strength by 3 to 4 months of age, as judged by their inability to hang upside down from a grid (*10*, *18*).

The FTI (or vehicle alone) was orally administered to groups of male and female *Zmpste24*$^{-/-}$ mice (n = 7 to 9) and male and female littermate wild-type mice (n = 6 to 9) via the drinking water, beginning at 5 weeks of age (*17*). The plasma concentrations of ABT-100 were in the same range as those previously shown to be effective in inhibiting the growth of human tumor xenografts (*16*, *17*).

The FTI inhibited protein farnesylation in vivo, as judged by Western blots of HDJ-2, a biomarker of FTI activity (*17*, *19*, *20*). About 20 to 50% of the HDJ-2 in extracts of tail biopsies was nonfarnesylated (Fig. 1A). This level of nonfarnesylated HDJ-2 is similar to the levels attained in studies investigating the anticancer activity of other FTIs in mice (*21*–*23*). As expected, nonfarnesylated prelamin A was detected in the tail extracts from FTI-treated but not untreated wild-type mice (Fig. 1B) (*17*, *20*, *24*).

As in patients with HGPS (*1*, *2*), retarded growth is a key feature of the mice with progeria (*10*, *11*, *18*). We therefore monitored the effects of the FTI on body weight. In wild-type mice, FTI treatment reduced body weight in females (P = 0.022) and tended to reduce body weight in males (P = 0.077) relative to wild-type mice receiving the vehicle alone (Fig. 2). The reason for the reduced weight gain in the FTI-treated wild-type mice is not known, but it could be due to inhibition of protein farnesylation or to a toxic effect of the FTI. In contrast, FTI-treated *Zmpste24*$^{-/-}$ mice gained more weight than did the vehicle-treated *Zmpste24*$^{-/-}$ mice. This was true for both females (P < 0.0001) and males (P < 0.0001) (Fig. 2).

Zmpste24$^{-/-}$ mice normally lose the ability to hang upside down from a grid by 3 to 4 months of age (*10*, *18*). In this study, 100% of the female (7/7) and male (7/7) *Zmpste24*$^{-/-}$ mice receiving the vehicle exhibited abnormal grip strength by 16 weeks of age (Fig. 3, A and B). In contrast, only 28% of the female (2/7) and 33% of the male (2/6) mice treated with the FTI exhibited a grip abnormality (Fig. 3, A and

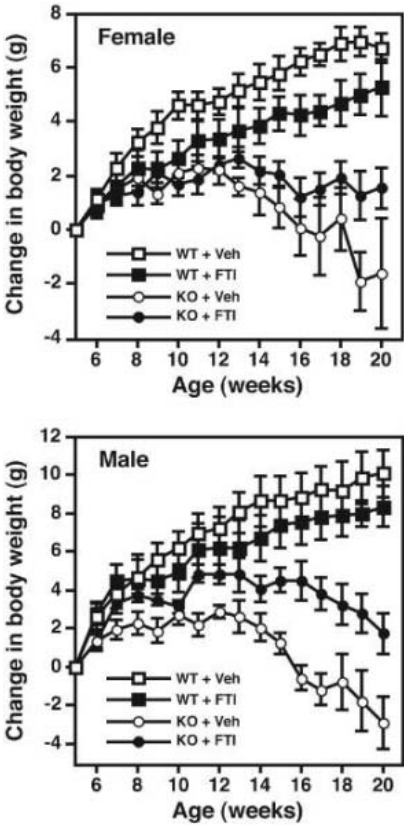

Fig. 2. Effect of FTI treatment on body weight. Wild-type (WT) and *Zmpste24*$^{-/-}$ (KO) mice were given FTI (solid symbols) or vehicle alone (open symbols) beginning at 5 weeks of age. Body weights were measured weekly; the mean change in body weight from baseline for females (upper panel) and males (lower panel) is shown. The body weight curves for the FTI-treated *Zmpste24*$^{-/-}$ mice were significantly different from those of the vehicle-treated *Zmpste24*$^{-/-}$ mice, both in males (P < 0.0001) and in females (P < 0.0001), as judged by repeated-measures analysis of variance. Numbers of mice for each group: female wild-type mice on vehicle, n = 9; female wild-type mice on ABT-100, n = 7; male wild-type mice on vehicle, n = 5; male wild-type mice on ABT-100, n = 4; female *Zmpste24*$^{-/-}$ mice on vehicle, n = 7; female *Zmpste24*$^{-/-}$ mice on ABT-100, n = 7; male *Zmpste24*$^{-/-}$ mice on vehicle, n = 7; male *Zmpste24*$^{-/-}$ mice on ABT-100, n = 6. Error bars: SEM.

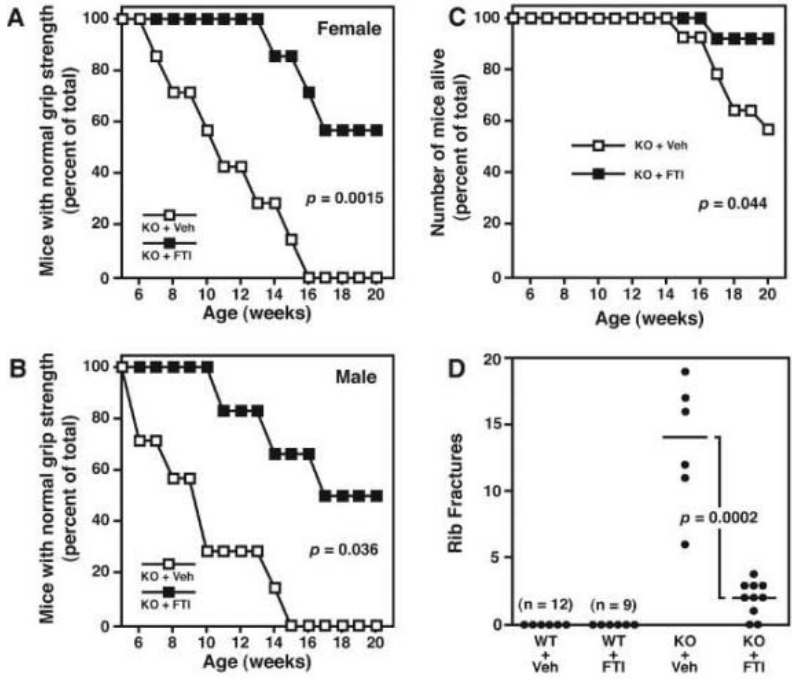

Fig. 3. FTI treatment improves grip strength, increases survival, and reduces the number of rib fractures in *Zmpste24*$^{-/-}$ mice. (**A** and **B**) Plots of grip strength in female and male mice over time. *Zmpste24*$^{-/-}$ mice were given vehicle alone (open symbols) or the FTI (solid symbols) starting at 5 weeks of age. The number of mice with a grip abnormality (inability to hang upside down from a grid for 60 s) was expressed as a percentage of the total number of mice in each group. On the basis of a log rank test, the FTI significantly improved grip strength in female (P = 0.0015) and male (P = 0.036) *Zmpste24*$^{-/-}$ mice. None of the wild-type mice developed a grip abnormality. (**C**) Survival of *Zmpste24*$^{-/-}$ mice on FTI versus vehicle alone. The number of surviving male and female mice was recorded weekly and is expressed as a percentage of the total number of mice. The significance of differences was determined with a log rank test. (**D**) Number of rib fractures in *Zmpste24*$^{-/-}$ mice on FTI versus vehicle alone. Wild-type and *Zmpste24*$^{-/-}$ mice were given vehicle alone or the FTI, starting at 5 weeks of age. At 20 weeks of age, the surviving mice were killed and the number of rib fractures was counted. The number of fractured ribs in the FTI-treated *Zmpste24*$^{-/-}$ mice was significantly lower than in the vehicle-treated *Zmpste24*$^{-/-}$ mice (P = 0.0002), as determined by the nonparametric Kruskal-Wallis test.

B). The delay in the appearance of the grip abnormality was significant in both females (P = 0.0015) and males (P = 0.036). Moreover, the mean length of time that the FTI-treated mice (n = 13) could hang on to the grid was longer than for the vehicle-treated *Zmpste24*$^{-/-}$ mice (n = 14) (37 s versus 5 s, $P < 0.0001$) (fig. S1).

Zmpste24$^{-/-}$ mice invariably develop osteolytic lesions and rib fractures by 3 to 4 months of age (*10*, *18*). Our goal was to score rib fractures in vehicle- and FTI-treated mice at a uniform time point. By 20 weeks of age, 6 of 14 vehicle-treated *Zmpste24*$^{-/-}$ mice had died, whereas only 1 of 13 FTI-treated mice had died (P = 0.0439) (Fig. 3C). At that time point, all of the surviving *Zmpste24*$^{-/-}$ mice were killed. The median number of rib fractures in the FTI-treated *Zmpste24*$^{-/-}$ mice was two, compared with 14 in the vehicle-treated mice. This difference was highly significant (P = 0.0002) (Fig. 3D). An improvement in bone was also apparent by computerized tomography scanning of the thoracic spine (fig. S2).

These studies show that an FTI ameliorates disease phenotypes in a mouse model of progeria, just as the FTI reduces the frequency of misshapen nuclei in progeria fibroblasts (*2*, *11*–*15*). However, our results do not formally prove that the improvement in disease phenotypes is a direct consequence of the improvement in nuclear morphology. Also, the disease phenotypes in the *Zmpste24*$^{-/-}$ mice were not completely eliminated by the FTI treatment. The FTI-treated *Zmpste24*$^{-/-}$ mice still had an abnormal growth curve relative to that of the wild-type mice; some treated mice still developed abnormal grip strength and a few mice ultimately developed several rib fractures. Additional studies will be required to determine whether a higher dose of an FTI and more complete inhibition of protein farnesylation could provide greater benefits. Different methods of drug delivery should also be tested. A study of much longer duration, involving a larger number of mice, is also needed to better define the impact of the FTI on survival.

The benefits of FTI treatment on disease phenotypes in mice with progeria are likely to fuel interest in testing FTIs in children with HGPS, which is uniformly fatal and for which no therapy exists. Two orally available FTIs, lonafarnib and tipifarnib, have already been extensively tested as antitumor agents in humans and are well tolerated in short-term studies (*21*, *25*). For treatment of children with progeria, it will be important to identify an FTI treatment program that is efficacious in blocking protein farnesylation, yet is well tolerated over the long term.

References and Notes

1. F. L. Debusk, B. Burke, C. L. Stewart, *J. Pediatr.* **80**, 697 (1972).
2. S. G. Young, L. G. Fong, S. Michaelis, *J. Lipid Res.* **46**, 2531 (2005).
3. M. Eriksson *et al.*, *Nature* **423**, 293 (2003).
4. F. Lin, H. J. Worman, *J. Biol. Chem.* **268**, 16321 (1993).
5. H. Hennekes, E. A. Nigg, *J. Cell Sci.* **107**, 1019 (1994).
6. C. L. Moulson *et al.*, *J. Invest. Dermatol.* **125**, 913 (2005).
7. C. L. Navarro *et al.*, *Hum. Mol. Genet.* **14**, 1503 (2005).
8. A. K. Agarwal, J.-P. Fryns, R. J. Auchus, A. Garg, *Hum. Mol. Genet.* **12**, 1995 (2003).
9. S. Shackleton *et al.*, *J. Med. Genet.* **42**, e36 (2005).
10. L. G. Fong *et al.*, *Proc. Natl. Acad. Sci. U.S.A.* **101**, 18111 (2004).
11. S. H. Yang *et al.*, *Proc. Natl. Acad. Sci. U.S.A.* **102**, 10291 (2005).
12. J. I. Toth *et al.*, *Proc. Natl. Acad. Sci. U.S.A.* **102**, 12873 (2005).
13. M. P. Mallampalli, G. Huyer, P. Bendale, M. H. Gelb, S. Michaelis, *Proc. Natl. Acad. Sci. U.S.A.* **102**, 14416 (2005).
14. B. C. Capell *et al.*, *Proc. Natl. Acad. Sci. U.S.A.* **102**, 12879 (2005).
15. M. W. Glynn, T. W. Glover, *Hum. Mol. Genet.* **14**, 2959 (2005).
16. D. Ferguson *et al.*, *Clin. Cancer Res.* **11**, 3045 (2005).
17. See supporting material on *Science* Online.
18. M. O. Bergo *et al.*, *Proc. Natl. Acad. Sci. U.S.A.* **99**, 13049 (2002).
19. E. Izbicka, D. Campos, G. Carrizales, A. Patnaik, *Anticancer Res.* **25**, 3215 (2005).
20. A. A. Adjei, J. N. Davis, C. Erlichman, P. A. Svingen, S. H. Kaufmann, *Clin. Cancer Res.* **6**, 2318 (2000).
21. M. Alsina *et al.*, *Blood* **103**, 3271 (2004).
22. G. K. Dy *et al.*, *Clin. Cancer Res.* **11**, 1877 (2005).
23. J. Sun *et al.*, *Cancer Res.* **63**, 8922 (2003).
24. A. A. Adjei *et al.*, *Clin. Cancer Res.* **9**, 2520 (2003).
25. E. S. Kim *et al.*, *Cancer* **104**, 561 (2005).

26. We thank K. Jarvis and J. Bauch for help with experiments on the pharmacokinetics and delivery of ABT-100 and B. Young for help with graphics. Supported by NIH grants AR050200 and HL76839 and grants from the Progeria Research Foundation.

Supporting Online Material

www.sciencemag.org/cgi/content/full/1124875/DC1
Materials and Methods
SOM Text
Figs. S1 and S2
References

11 January 2006; accepted 1 February 2006
Published online 16 February 2006;
10.1126/science.1124875
Include this information when citing this paper.

Programmable Controller

A multi-function temperature controller is available on PolyScience Circulators. Designed for heating and cooling applications requiring precise, multi-level temperature control, the Programmable Controller can be programmed with up to 10 different time and temperature profiles, each of which can have as many as 50 temperature steps and be repeated up to 99 times. For added versatility, the user can control programmed profiles using either temperature or time as the primary operational factor. The unit controls temperatures from as low as –40°C to as high as 200°C with ±0.25°C accuracy and ±0.01°C stability. Fluid temperature, setpoint, and other important operating parameters are displayed on a large graphics LCD.
PolyScience For information 800-229-7569 www.polyscience.com

Gram Positive DNA Purification

The MasterPure Gram Positive DNA Purification Kit provides all the reagents needed to purify DNA from gram positive bacteria. The DNA obtained is of high yield, of high molecular weight, and is ready for polymerase chain reaction (PCR). The method is scalable. The kit has been used successfully for a variety of different microbes, including *Streptococcus*, *Bacillus*, *Listeria*, and *Lactococcus*. The length of incubation time for release of DNA varies with the species, from 30 min to overnight. Genomic DNA purified using the kit can be used for fosmid library construction, PCR, restriction digests, and Southern blotting.
Epicentre Biotechnologies For information 800-284-8474 www.EpiBio.com

Microarray Sequences

The GeneChip Human Mitochondrial Resequencing Array 2.0 enables researchers to analyze the entire sequence of the mitochondrial genome in a single 48-hour experiment. The new microarray interrogates all 16,500 bases of the human mitochondrial genome with only three polymerase chain reactions, providing scientists with an efficient and cost-effective method for detecting variants associated with genetic disease, forensics, population studies, or stem cells.
Affymetrix For information 408-731-5791 www.affymetrix.com

Plasma Depletion Technology

The ProteoPrep 20 Plasma Immunodepletion Kit removes 99% of 20 high-abundant plasma proteins using a proprietary multivalent antibody affinity media in a convenient spin column format resulting in removal of 97% of the overall protein mass. The unique high-density antibody affinity media enhances the ability to visualize low abundance proteins in the plasma proteome using standard analysis technology. In addition, the multivalent antibody resin makes use of novel recombinant antibodies that allow for a significantly higher density of conjugation and hence, efficiency of depletion with minimal sample loss or dilution.
Sigma-Aldrich For information 314-286-7431 www.sigma-aldrich.com

Primary Cells

StemCell Technologies offers a wide range of primary cell products from human hematopoietic cell sources and more. Products include a variety of unprocessed and purified human blood and bone marrow cells, available fresh (in North America) or frozen, as well as cell lysates, RNA, and complementary DNA derived from these cells. Cells from hematopoietic sources include mononuclear cells, stem/progenitor cells, and purified lineage-committed cell types. Also available are stromal, endothelial, neural, and hepatic cells.
StemCell Technologies For information 800-667-0322 www.stemcell.com

Total RNA Isolation System

The LeukoLock Total RNA Isolation System makes use of leukocyte depletion filter technology to isolate leukocytes from whole blood. Ambion's RNAlater is used to stabilize the leukocyte RNA indefinitely. RNA is then isolated from the leukocytes through a magnetic bead-based process, producing RNA with low levels of globin messenger RNA for enhanced performance during expression profiling and other analytical procedures.
Ambion For information 512-651-0200 www.ambion.com

Molecular Imaging System

The Gel Logic 2200 Digital Imaging System, for in vitro imaging in life science research, handles a broad spectrum of advanced imaging needs. It features a cooled charge-coupled device camera and an integrated illumination cabinet to permit the sensitive detection of fluorescent, chemiluminescent, and chromogenic assays. The system includes a 2.2 million-pixel sensor, an f 1.2 lens, and 6× optical zoom to deliver accurate and sensitive 16-bit image capture for quantitative imaging of electrophoresis gels, blots, plates, and assays. Its versatile illumination cabinet offers customers a broad range of imaging capabilities, including applications that require broadband ultraviolet (UV) illumination, white light epi-illumination, and transillumination to image UV fluorescent dyes as well as chemiluminescence and colorimetric labels. The GL 2200 system also includes the leading edge Kodak Molecular Imaging Software, for quantitative image analysis, database, and overlay capabilities.
Eastman Kodak For information 877-747-4357 www.kodak.com/go/molecular

Newly offered instrumentation, apparatus, and laboratory materials of interest to researchers in all disciplines in academic, industrial, and government organizations are featured in this space. Emphasis is given to purpose, chief characteristics, and availability of products and materials. Endorsement by *Science* or AAAS of any products or materials mentioned is not implied. Additional information may be obtained from the manufacturer or supplier by visiting www.science.labvelocity.com on the Web, where you can request that the information be sent to you by e-mail, fax, mail, or telephone.

Need career insight?

Let the experts put you in the picture.
Visit www.ScienceCareers.org

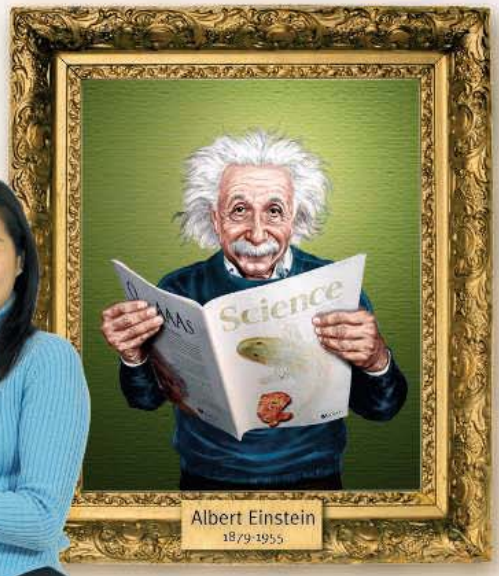

Your career is too important to leave to chance. So to find the right job or get career advice, turn to the experts. At ScienceCareers.org we know science. And we are committed to helping take your career forward. Our knowledge is firmly founded on the expertise of *Science*, the premier scientific journal, and the long experience of AAAS in advancing science around the world. Put yourself in the picture with the experts in science. Visit www.ScienceCareers.org.

ScienceCareers.org
We know science AAAS

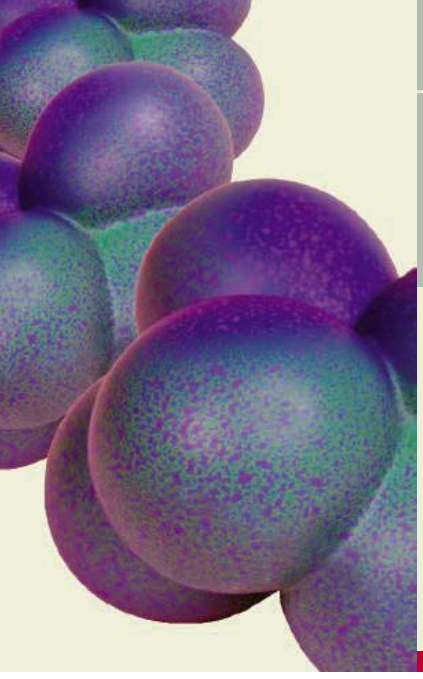

Life Science Technologies

Combinatorial and Computational Chemistry:

CREATING NEW THERAPEUTIC COMPOUNDS

Today's drug discovery relies heavily on numerical creations of compounds and models of them. These techniques help scientists design entirely new molecules or modify ones already in molecular libraries. The computed compounds often provide improved efficacy and safety profiles, and testing in silico often speeds up the process of drug development, including the regulatory phase. **by Mike May and Gary Heebner**

As the stakes grow ever higher in developing therapeutics, pharmaceutical and biotechnology companies continually enhance and improve every step between discovering and marketing a product. Today, many of those advances involve chemistry. "Chemistry plays a critical role from the start of lead discovery all the way through clinical development and beyond," says Eugene Vaisberg, chairman and chief executive officer of **ChemBridge Corporation** and its spinoff **ChemBridge Research Laboratories**. He adds, "The role of chemistry is fundamental and growing in importance. The historical reliance on compound libraries in pharmaceutical lead discovery and now by researchers doing chemical genetic studies has helped to influence some of the substantial recent advances in both the biology and chemistry of drug discovery."

Some of the most advanced areas of chemistry for drug discovery and development are combinatorial and computational chemistry. Kathleen Mensler, vice president of marketing and corporate development in discovery informatics at **Tripos**, says, "Combinatorial chemistry is the utilization of parallel synthesis techniques to increase the throughput of discovery, and computational chemistry supports key decisions in discovery, such as answering: Which compound should I make?" She adds, "Early combinatorial efforts showed that making lots of compounds, though, does not always get you to a drug faster. You need to make the right things. With a combination of computational chemistry and data from high throughput screening, we can zero in faster on good drug candidates."

The Power of Going Parallel

In the past, chemists often made one compound at a time. For example, they reacted compound A with compound B to give product AB, which was isolated after the reaction. In contrast, combinatorial chemistry can make every combination of compound A_1 to A_n with compound B_1 to B_n. In short, combinatorial chemistry provides a diversity of products that can be made separately or in mixtures, using either solid-phase or liquid-phase techniques. As a result, productivity increases dramatically.

That increase depends largely on automation. Manufacturers now offer semiautomated and fully automated systems for parallel chemical synthesis. The economy of such systems makes them available to industrial as well as academic research groups. A number of companies—including **Büchi Labortechnik**, **CEM Corporation**, **Genevac**, and **Zinsser Analytic**—offer systems and related products for parallel chemical synthesis and purification.

"In medicinal and combinatorial chemistry," says Gerhard Schoenenberger, business communication manager at Büchi Labortechnik, "about five years ago, the focus was more on library production, making a lot of compounds and then checking for activity or nonactivity." That often involved running a hundred or even a thousand reactions at once. But today's scientists now look in a new direction—one that usually only requires a dozen or fewer reactions running in parallel. "We are seeing more target-oriented designs," says Schoenenberger. He adds that this results in smaller instruments that are easy to use and offer individual solutions.

For example, Büchi's Syncore Reactor can run 24 or 96 samples for synthesis or analysis. Schoenenberger says, "This parallel reactor can be combined with parallel filtration to do both steps. It can also handle simple extractions, such as liquid-liquid extractions, all in the same instrument."

Analyzing the Results

Identifying the resulting compounds makes up a crucial aspect of combinatorial chemistry. The analytical methods used to characterize a library of chemical compounds depend on the nature of the compounds being synthesized. In so-called absolute characterization, Bob Collins, product manager at **Wyatt Technology**, **continued ›**

IN THIS ISSUE:

- Library production
- Parallel synthesis
- Light scattering
- Ion-trap mass spectrometry
- Custom libraries
- Cell-based screening
- Lead selection
- Informatics
- Lead optimization

Inclusion of companies in this article does not indicate endorsement by either AAAS or *Science*, nor is it meant to imply that their products or services are superior to those of other companies.

says, "We use the term absolute because the measured parameters are derived from first principles. All of our instruments are based on first principles—not using any relative standard or reference standard to a known molecular weight or size—because this provides more accurate results and a higher degree of confidence in the results, especially when comparing across different samples."

For characterization, Wyatt instruments use two different types of light scattering: multiangle light scattering, which shines laser light on macromolecules and then analyzes the scattered light as a function of concentration and angle; and dynamic light scattering, which analyzes scattered light as a function of time. The first can determine molecular weight and radius, and the second provides information about molecular movement, which is related to particle size.

These techniques can be applied to drug discovery in a variety of ways. For example, light scattering can reveal if compounds aggregate, proteins bind to a target enzyme, or that a drug nanoparticle is of an appropriate size. "In this way," says Collins, "light scattering can prescreen compounds or be used as a diagnostic. In addition, knowing the size and weight of, say, a drug delivered with nanoparticles can determine if the therapeutic could be taken up in biological organs."

In addition, Wyatt's DynaPro Plate Reader adds automation to characterizing compounds in 96-, 384-, or 1,536-well plates. Collins says, "This novel dynamic light scattering technology supports high throughput applications with low sample volumes and is fully automated."

Mass spectrometry (MS) can also analyze the results of combinatorial chemistry. Researchers can compare the data gathered from the end products with the properties of known molecules in a database and make an exact match or identification for an individual molecule. Companies that manufacture these instruments include **Applied Biosystems**, **Bruker**, **Thermo Electron**, and **Waters**.

Julian Phillips, product specialist at Thermo Electron, says, "It is important to characterize a library of compounds because you don't want to repeat analytical testing efforts. For example, if one structure is not bioactive, similar structures might also not be bioactive, and you might not want to make them." Phillips adds, "Similar compounds tend to display common characteristics, but this is not foolproof."

To characterize libraries, Thermo Electron instruments use ion-trap MS. Phillips says, "Our instruments provide routine and reliable analysis." He adds, "No matter which of our ion traps you use, the characteristic compound spectra are very similar, which allows fast, accurate library searching."

Ready-Made Libraries

Companies like ChemBridge, **ComGenex**, **Sigma-Aldrich**, and Tripos offer libraries of chemical compounds for drug discovery research. Some of these libraries are developed using combinatorial chemistry methods, while others are established with natural compounds that have been isolated from biological sources.

ChemBridge, for example, offers over 650,000 parallel-synthesized and handcrafted discrete small molecule compounds. Vaisberg says, "Scientists do not need many millions of easily produced marginal compounds. Instead, they need somewhat smaller numbers of compounds that are produced through more sophisticated techniques and of a higher quality." He adds, "Every major pharmaceutical company invests to create libraries of compounds, and the quality of those compounds is more important than the number of compounds." There is a good reason for this, according to Vaisberg: "Compound libraries—like any library—are valuable primarily in the quality of the information that that they contain." The factors that influence the quality of the information content include: relevance (target focus), latitude (diversity), fidelity (purity), and synthetic feasibility (scalability).

Vaisberg and his colleagues help customers design the best libraries. He says, "We suggest ideas or work with their ideas. We often work with committees to come up with the best ideas, and then we take these all the way through chemistry feasibility studies and rapid process development."

Another company, ComGenex, offers 260,000 discrete structures for multitarget screening purposes. This primary discovery compound collection is composed of about 150 core structures (or chemical themes), and the analogue sublibrary's size is 1,000-4,000 compounds per scaffold as an average.

Speeding Up Screening

Once a company establishes a library of compounds, it must be screened quickly and efficiently, which drives the development of high throughput screening (HTS). For example, **PerkinElmer** developed the LumiLux Cellular Screening Platform. Claire Hooper, research director at PerkinElmer, says, "We developed this as a next generation screening platform for drug discovery. It is designed to run functional cell-based assays."

This system detects low levels of light with CCD imaging coupled with integrated sample handling and data analysis. Hooper explains that the optics in this system arose through a spinoff from high energy physics. She says, "To develop next generation platforms we need smarter optics that bring this technology to drug discovery to improve assay performance and the quality of data throughput, which is the big need today."

In the past, cell-based assays demanded several steps: grow and harvest cells overnight in plates and then screen them the next day. The LumiLux, on the other hand, can run homogeneous assays using cells in suspension, which are loaded into the instrument with test

compounds and analyzed in the same place. According to Joann Calve, marketing communications manager at PerkinElmer, "This is a walk-away system: Add your cells and chemistry and walk away."

Hooper and her colleagues designed the LumiLux to work primarily with G protein-coupled receptor (GPCR) screening, which she says accounts for about 25 percent of today's screens. Hooper adds, "This is used to search for leads from a screening campaign. Then, chemists distill the library into lead candidates." She adds, "Our customers tell us that the LumiLux lets them screen libraries in weeks or even days rather than months."

Several companies—including **BD Biosciences**, **Promega**, and **Upstate**—also offer so-called homogeneous assays, which eliminate error-prone washing and transferring steps. Several homogeneous assay techniques have been developed for radioactive, fluorescent, and luminescent assay formats.

Computational Chemistry

With the best candidate compounds screened, scientists can use computational chemistry to enhance the leads. Uli Heigl, principal scientist in the chemistry, workflow business group at **Elsevier MDL**, says, "Computational chemistry to me is using the computer to answer relevant chemistry questions and finding possible solutions or searching for better ideas or even asking new provocative questions. This may include docking, ab initio calculations, in silico screening, QSAR [quantitative structure activity relationships], or even searching for possible transformations in a reaction database to find better synthesis methods, et cetera."

One of the real keys to modern drug discovery, though, arises from the interaction of combinatorial and computational chemistry. To emphasize this point, Mensler of Tripos tells of a recent talk with Richard D. Cramer, vice president of science at Tripos. Cramer explained that drug discovery is like playing the lottery, and each compound made and tested is like a lottery ticket, and the potential payoff is developing a blockbuster. Combinatorial chemistry reduces the cost of each lottery ticket; computational technology helps companies pick lottery tickets that are most likely to win. Mensler says, "It's good if you can buy more lottery tickets, but a system for increasing your proportion of winning tickets is of immense value."

Tripos provides tools that improve the odds in the therapeutic lottery. For example, the SYBL suite of molecular modeling applications helps scientists choose the best compounds to synthesize. Mensler says, "It also provides capabilities to make predictions of pharmaceutically important molecular properties such as activity, selectivity or ADME [absorption, distribution, metabolism, and excretion] based on the properties of previously tested molecules or the biological target structure." This suite also uses CoMFA, or comparative molecular field analysis, a unique statistical method to predict the activity of new compounds.

Recently, Tripos developed its Galahad, which Mensler calls a hypothesis generator. She says, "It takes compounds that you know have relevant activity, aligns the structures, and then compares them to detect structural similarities; maybe, for example, there's an electron-donating group at one end. In that way, Galahad develops hypotheses about what makes compounds active, and that is used for the design of new compounds and libraries or data mining of chemical collections."

Dialing In the Data

A number of companies market software tools that support projects in computational chemistry efforts, especially in the area of drug discovery. These companies include **Accelrys**, **CeuticalSoft**, **InforSense**, and Elsevier MDL.

For example, Heigl of Elsevier MDL, describes this company's xPharm database as "a fully interactive database that covers pharmacological information: sets of records, targets, agents, information on disorders, principles that govern drug-target interactions, and so on." He adds, "All of the records are indexed and interlinked. Any information is just a mouse click away." In addition, this database adds references to the data and hyperlinks to full text of related journal articles. "This database can be used to see what kinds of targets are linked to specific diseases, what disorders are related to specific targets," says Heigl.

MDL's DiscoveryGate also provides information related to drug discovery. "Say you start from a chemical reaction library to synthesize a compound," Heigl explains, "while browsing a reaction library, you may get metabolite information and commercial availability and probably information on bioactivity, physicochemical data." He adds, "DiscoveryGate really gives you access to all of the different data—including patents, journal articles, and synthetic methodologies."

This company also offers a new integration platform, Isentris, which can be used in pharmaceutical research and development. Heigl says, "This is a new solution that we provide to drug discovery and development as well as to all other customers dealing with science. Isentris is a new way to manage and integrate all your research data to make faster, better decisions." He adds, "It integrates all of your different applications, as well as data sources at continued ›

Look for these upcoming Life Science Technology articles

Cell Signaling in Cancer Research	24 March
Proteomics	14 April
Biochips and Lab-on-a-Chip Devices	5 May
Pharmacogenomics	28 July
Mass Spectrometry	1 September
Functional Genomics	29 September
Aging and Neuroscience	6 October
Nanobiotechnology	3 November

Or, access recent articles at http://www.sciencemag.org/products/articles.dtl

Laboratory Automation	13 January

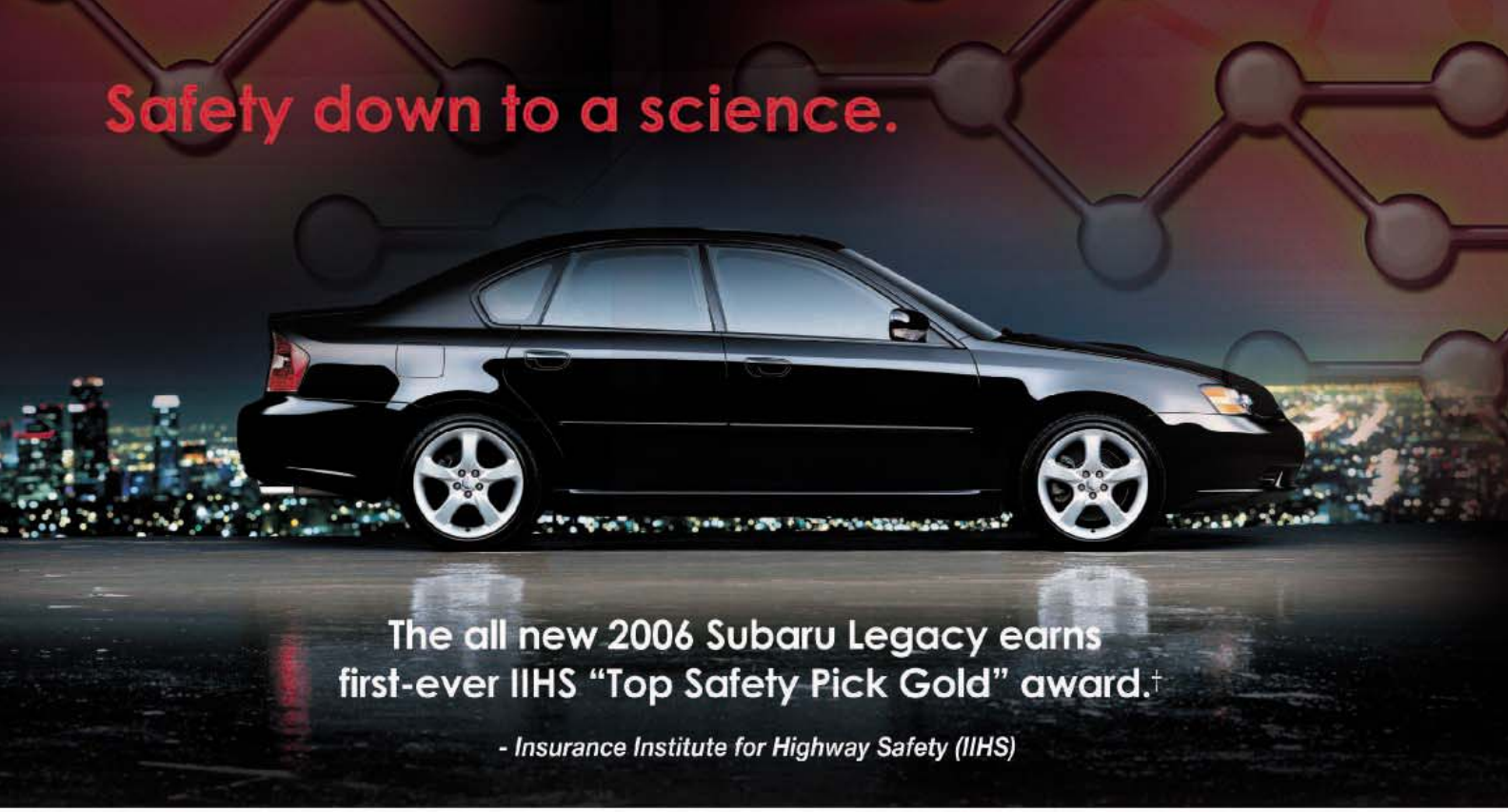

Subaru's sponsorship of the American Association for the Advancement of Science (AAAS) highlights our advanced design of symmetrical all-wheel drive technology to our target markets and underscores Subaru's commitment to further science, engineering and technology education both at the annual meeting and programs throughout the year. Subaru is proud to be the Premier Automotive Sponsor of the AAAS.

In a continuing effort to offer our partners unique and valuable benefits, we provide special offers for AAAS Members, the Subaru VIP Partners Program. AAAS Members can **save up to $3,000*** off the manufacturer's suggested retail price (depending on model and accessories) on the purchase or lease of a new Subaru from participating dealers. To qualify, you must be a AAAS member in good standing for at least six consecutive months prior to participation in this program. Please contact AAAS Member Services at 202.326.6417 or e-mail membership@aaas.org **BEFORE** visiting your local Subaru dealer. Access subaru.com to find a nearby dealer or learn more about Subaru vehicles.

Science AAAS

Think. Feel. Drive.™

SUBARU

*From MSRP to dealer invoice. MSRP does not include tax, title, and registration fees. Limited time offer subject to change without notice. Terms and conditions apply. This offer replaces all other existing offers, cannot be redeemed for cash and is not applicable in Canada and Hawaii. † Based on Insurance Institute for Highway Safety 40 mph offset frontal crash test, 31 mph side impact test, and 20 mph rear impact test.

one desktop. All scientists in a company are able to share their data worldwide and make decisions no matter whether they are using internal data or external data sources."

From Research to Rewards

Scientists apply combinatorial and computational chemistry in many ways. Besides biotech and pharma companies adopting these technologies, other fields of application include diagnostics and basic research on families of related molecules. **Celera Genomics**, for example, now uses its human genome knowledge to unravel associations between genetics and diseases on a genomewide scale, and to identify therapeutic targets through docking algorithms to predict the likelihood of binding between potential drugs and proteins that are targeted by a drug.

And at **Bayer Healthcare**, chemistry contributes to every drug discovery initiative. Although rooted in synthetic organic chemistry, this company uses combinatorial chemistry, high-speed analoging, computational chemistry, and automated synthesis and scale-up to discover what the industry calls new molecular entities. Hanno Wild, head of discovery Europe for Bayer Healthcare, says, "Chemistry plays a major role in finding novel lead structures. And pharma is in need of lead structures to design novel drugs for specific targets."

At Bayer Healthcare, like other big pharmaceutical companies, libraries make up a crucial part of the work. "There is still value in larger libraries if you're talking about lead finding—building up compound libraries and then applying high throughput screening," Wild says. "What is really new is combinatorial chemistry and automated synthesis integrated completely in the work flow in chemistry—whether you are making a few compounds, a small library, or a large library. That's the difference we see now."

To show just how effective chemistry can be in creating new therapeutics, Wild tells the story of Nexavar (sorafenib), which he calls "a nice example of combinatorial chemistry used in drug optimization." He begins, "This compound started off as a very weak lead structure, but we took it through several rounds of combinatorial chemistry and libraries used for stepwise optimization." A breakthrough in this compound's structure-activity relationship, says Wild, "was generated by combining two almost inactive fragments into a compound that is active. This would never have been done without using combinatorial chemistry methods."

In late December 2005, the U.S. Food and Drug Administration approved Nexavar for treating advanced renal carcinoma, or kidney cancer. This compound acts as a multikinase inhibitor, which targets serine/threonine and receptor tyrosine kinases in tumor cells as well as in the vascularization of the tumors. In thinking back over this work, Wild says, "This is a very important example of chemistry's power."

More Combinations Ahead

The application of combinatorial and computational chemistry—along with new data as well as new informatics tools—remains relatively young in the world of pharmaceuticals. As a result, many new discoveries surely lie ahead. "There are some targets around where the industry has been looking for novel chemical molecules," says Wild. In particular, he points to proteases as potentially fruitful targets. He adds, "Targets that were difficult to handle in the past might not be so difficult in the future, because of combining combinatorial and computational efforts."

Mike May (mikemay@mindspring.com) is a publishing consultant for science and technology based in Minnesota. Gary Heebner (gheebner@cell-associates.com) is a marketing consultant with Cell Associates in St. Louis, Missouri, U.S.A.

Featured Companies

Accelrys – a subsidiary of Pharmacopeia
scientific software, http://www.accelrys.com

Applied Biosystems
mass spectrometry systems, http://appliedbiosystems.com

Bayer Healthcare
pharmaceutical company, http://www.bayer.com

BD Biosciences
high throughput screening assay kits, http://www.bd.com

Bruker Daltonics, Inc.
mass spectrometry systems, http://www.bdal.com

Büchi Labortechnik AG
automated systems for chemical synthesis, http://www.buchi/com

Celera Genomics
drug discovery company, http://www.celera.com

CEM Corporation
automated systems for chemical synthesis, http://www.cem.com

CeuticalSoft
scientific software, http://www.ceuticalsoft.com

ChemBridge Corporation
contract research organization, http://www.chembridge.com

ChemBridge Research Laboratories
drug discovery company, http://www.chembridgeresearch.com

ComGenex, Inc.
chemical compound libraries, http://www.comgenex.com

Elsevier MDL
scientific software, http://www.mdl.com

Genevac
automated systems for chemical synthesis, http://www.genevac.com

InforSense, Ltd.
scientific software, http://www.inforsense.com

PerkinElmer Life and Analytical Sciences
high throughput screening systems, http://las.perkinelmer.com

Promega Corporation
high throughput screening assay kits, http://www.promega.com

Sigma-Aldrich Corporation
chemical compound libraries, http://www.sigmaaldrich.com

Thermo Electron Corporation
mass spectrometry systems, http://www.thermo.com

Tripos, Inc.
drug design software and services, http://www.tripos.com

Upstate
high throughput screening assay kits, http://www.upstate.com

Waters Corporation
mass spectrometry systems, http://www.waters.com

Wyatt Technology Corporation
light scattering systems, http://www.wyatt.com

Zinsser Analytic GmbH
automated systems for chemical synthesis, http://www.zinsser-analytic.com

ScienceCareers.org

Classified Advertising

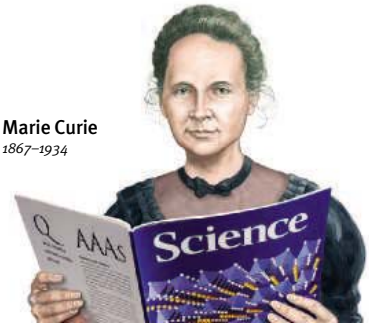

Marie Curie
1867–1934

For full advertising details, go to **www.sciencecareers.org** and click on **How to Advertise,** or call one of our representatives.

United States & Canada

E-mail: advertise@sciencecareers.org
Fax: 202-289-6742

JILL DOWNING
(CT, DE, DC, FL, GA, MD, ME, MA, NH, NJ, NY, NC, PA, RI, SC, VT, VA)
Phone: 631-580-2445

KRISTINE VON ZEDLITZ
(AK, AZ, CA, CO, HI, ID, IA, KS, MT, NE, NV, NM, ND, OR, SD, TX, UT, WA, WY)
Phone: 415-956-2531

KATHLEEN CLARK
Employment: AR, IL, LA, MN, MO, OK, WI, Canada; Graduate Programs; Meetings & Announcements (U.S., Canada, Caribbean, Central and South America)
Phone: 510-271-8349

EMNET TESFAYE
(Display Ads: AL, IN, KY, MI, MS, OH, TN, WV; Line Ads)
Phone: 202-326-6740

GABRIELLE BOGUSLAWSKI
(U.S. Recruitment Advertising Sales Director)
Phone: 718-491-1607

Europe & International

E-mail: ads@science-int.co.uk
Fax: +44 (0) 1223-326-532

TRACY HOLMES
Phone: +44 (0) 1223-326-525

HELEN MORONEY
Phone: +44 (0) 1223-326-528

CHRISTINA HARRISON
Phone: +44 (0) 1223-326-510

SVITLANA BARNES
Phone: +44 (0) 1223-326-527

JASON HANNAFORD
Phone: +81 (0) 52-789-1860

To subscribe to *Science*:
In U.S./Canada call 202-326-6417 or 1-800-731-4939
In the rest of the world call +44 (0) 1223-326-515

Science makes every effort to screen its ads for offensive and/or discriminatory language in accordance with U.S. and non-U.S. law. Since we are an international journal, you may see ads from non-U.S. countries that request applications from specific demographic groups. Since U.S. law does not apply to other countries we try to accommodate recruiting practices of other countries. However, we encourage our readers to alert us to any ads that they feel are discriminatory or offensive.

POSITIONS OPEN

The Idaho National Laboratory (INL), is one of the U.S. Department of Energy's premier research and development laboratories. We are seeking the following: **SENIOR MICROBIOLOGIST.**

As a senior-level scientist and molecular research Team Leader within the Biological Sciences Department, the selected individual will be expected to independently identify new research opportunities supporting the goals of a new research initiative in systems microbiology, direct technical teams to respond to those opportunities, generate proposals, and secure funding for the conduct of that research. This person will identify and develop program areas and establish research plans and experimental design for several research projects/programs. Will be responsible for the direction and oversight of junior- and mid-level scientific staff, and will provide assistance and guidance to other principal investigators. Will assimilate and interpret laboratory data, and serve as a technical resource to others as well as a liaison to other departments and external collaborators. Will serve as a major or sole contributor to the generation of reports, publications, and proposals. Also responsible for representing the Department to sponsors and peers through programmatic and technical presentations, and providing a lead role in Departmental business planning and marketing efforts. In addition, this individual will be responsible for leading the efforts to build and sustain new capabilities in systems microbiology associated with a new scientific thrust area within the Laboratory. This will require directing research so that these capabilities are enhanced, and serving as an advisor to mid-level management regarding investment planning and strategic decisions.

Ph.D. required. Must have a reputation for world-class research in microbial physiology and/or biochemistry of prokaryotic metabolic pathways, and be currently active in bacterial systems research. A strong familiarity with the modern research and analytical tools associated with metabolic profiling linked with genomic and proteomic analyses is desired. An established track record of preparing and winning peer-reviewed proposals from a variety of funding agencies is also required. Must have a demonstrated ability to successfully lead diverse research teams, and have an extensive network of collaborators and partners.

The INL is operated by Battelle Energy Alliance (BEA) and is located in scenic southeastern Idaho, close to Yellowstone and Grand Teton National Parks. Southeastern Idaho is known for some of the world's best recreational areas including top ranked ski resorts, world-class fly-fishing, and white water rafting.

Please apply for this position at **website: http://www.inl.gov.** Posting 2263.

The INL is a federal facility and performs work involving national security; therefore, *many of the jobs require U.S. citizenship. BEA is an Equal Opportunity Employer Minorities/Females/Persons with Disabilities/Veterans.*

Gene Therapy for Sickle Cell Disease

A **POSTDOCTORAL POSITION** (Ph.D. and/or M.D.) in the laboratory of **Dr. J. Victor Garcia** to study in vivo gene transfer for sickle cell disease as part of the NIH grant entitled Southwestern Comprehensive Sickle Cell Center. Red blood cell biology/hematology experience and/or molecular biology of globin expression experience is essential for these positions. Flow cytometry experience or experience with lentivirus vectors for globin expression is highly desirable. Strong written and verbal communication skills in English required.

Send letter of interest, curriculum vitae, and names of three references to: **Ms. Deborah Solomon, e-mail: deborah.solomon@utsouthwestern.edu, University of Texas Southwestern, Division of Infectious Diseases, 5323 Harry Hines Boulevard, Dallas, TX 75390-9113.** *The University of Texas Southwestern Medical Center at Dallas is an Equal Opportunity, Affirmative Action Employer.*

POSITIONS OPEN

PLANT BIOCHEMICAL GENETICIST

A joint, tenure-track **ASSISTANT PROFESSOR** position is currently available in the Plant Science Initiative **(website: http://psiweb.unl.edu)** at the University of Nebraska, Lincoln (UNL). The position is 80 percent research, 20 percent teaching and potential academic homes would include Department of Biochemistry or Department of Agronomy and Horticulture. As part of a newly emerging Nutritional Genomics Center, the successful candidate is expected to maintain a vigorous, externally funded research program focused onbiochemical genetics of plants. Strong preference will be given to research programs that focus on plant secondary metabolism, metabolic profiling and/or genetic regulation of plant metabolism. Teaching responsibilities include teaching one graduate or undergraduate level course annually in a relevant area, and mentoring students. A Ph.D. and postdoctoral experience in plant genetics, biochemistry, or related field is required. Salary is commensurate with qualifications and experience.

Review of applications will begin April 21, 2006, and continue until the position is filled or the search is closed. Applicants should go to **website: http://employment.unl.edu/** (requisition 051034) and complete the Faculty/Administrative Information form and then send a complete application file, consisting of a statement of research interests and curriculum vitae, and arrange for three letters of recommendation be sent to:

Search Committee Chair
Assistant Professor Plant Biochemical Genetics
N300 Beadle Centerfor Genetics Research
University of Nebraska, Lincoln
Lincoln, NE 68588-0660 USA

UNL is committed to a pluralistic campus community through Affirmative Action and Equal Opportunity and is responsive to the needs of dual career couples. We assure reasonable accommodation under the Americans with Disabilities Act. Contact ***Barbara Gnirk*** *at* ***telephone: 402-472-7867*** *or* ***e-mail: bgnirk1@unl.edu*** *for assistance.*

VISITING ASSISTANT PROFESSORS
Biology
Claremont McKenna, Pitzer, and Scripps Colleges

The Joint Science Department of Claremont McKenna, Pitzer, and Scripps, three liberal arts colleges in the Claremont Colleges Consortium in Southern California, seeks to fill two positions with visiting Assistant Professors: (i) a one year position for the 2006-2007 academic year, beginning August, 2006, to teach cell biology with laboratory both semesters and a genetics course in the spring, and (ii) a one semester position, beginning January 2007, to teach introductory biology (organismic/population). A Ph.D. in biology or related subject is required, and prior teaching experience is desirable.

Please submit curriculum vitae and a statement of interest, specifying which position is of interest to you, and arrange to have three letters of reference sent to: **Biology Search, W.M. Keck Science Center, 925 N. Mills Avenue, Claremont, CA 91711-5916** or to **Newton Copp** at **e-mail: ncopp@jsd.claremont.edu. Telephone: 909-621-8298.** Review of applications begins April 3, 2006, and the positions will remain open until filled.

In a continuing effort to enrich its academic environment and provide Equal Educational Employment Opportunities, the Claremont Colleges actively encourage applications from women and members of historically under-represented groups in higher education.

POSTDOCTORAL/SCIENTIST POSITIONS immediately available at Tufts Cummings School of Veterinary Medicine, Division of Infectious Diseases, Grafton, Massachusetts. Interested candidates with a strong background in either: (1) microbiology and immunology; (2) bioinformatics, molecular biology, functional genomics; or (3) cell biology/biochemistry to help identify inhibitors against microbial toxins, should e-mail curriculum vitae and names of references to **e-mail: donna.akiyoshi@tufts.edu.** *Tufts University is an Equal Opportunity Employer.*

FOCUS ON CAREERS

Chemistry
First-Principles Calculations

Modeling the behavior of electrons unveils the fundamental reactions between compounds. Computational quantum chemists track these interactions for both theoretical and applied tasks, such as drug development and materials science. According to the experts interviewed here, this field provides growing opportunities in academics, government laboratories, and industry. BY MIKE MAY

Northwestern University
http://www.northwestern.edu/

Purdue University
http://www.purdue.edu/

University of California, Berkeley
http://www.berkeley.edu/

University of Texas at Austin
http://www.utexas.edu/

Since 1926, when the Austrian physicist Erwin Schrödinger developed the equation that bears his name and describes the behavior of electrons, chemists imagined modeling the interactions of complex compounds. That dream grows closer to reality with every improved algorithm and increase in computing power. Today, computational quantum chemists can model the properties of hundreds—thousands in some cases—of electrons to predict the behavior of interacting elements and compounds. This development can be applied to biology, engineering, materials science, molecular electronics, and many other fields.

"Computational quantum chemistry," says Martin Head-Gordon, professor of chemistry at the University of California, Berkeley, "is basically the field that develops theoretical algorithms and software based on quantum mechanics to predict properties of molecules from first principles." He adds, "The success of this field was recognized with the Nobel Prize in chemistry in 1998." That year, Walter Kohn and John A. Pople were awarded the Nobel Prize for work in computational quantum chemistry. Today, work in this area leads to a wide range of career options.


JAMES R. CHELIKOWSKY

Expanding the Scope

Improved computing and novel algorithms allow quantum chemistry to treat more complex interactions. "Most chemical and biochemical processes are on the level of valence electrons that interact with each other," says Jorge H. Rodriguez, assistant professor of physics at Purdue University. "This makes electrons of one atom bond with electrons of another." In the past, hand calculations could not handle many electrons, because of the complexity of the equations. "Now," says Rodriguez, "much faster computers allow us to solve the Schrödinger equation for many valence electrons. Still, we cannot do this exactly, so we use approximations."

As one example of such an approximation, Rodriquez explains, the scientist assumes that in many chemical processes only the electrons move, and the nucleus is modeled as motionless. "From that perspective, the nuclei are just positive charges that keep electrons bound." Still, the large number of electrons and complexity of the calculations demand lots of computer time.

Today's computing power lets scientists apply quantum chemistry to more areas. Tamar Seideman, professor of chemistry at Northwestern University, says, "One uses computational quantum chemistry to understand complex biological processes, to design molecules for various applications, and to make predictions in different fields of science and technology, ranging from engineering and materials research through molecular electronics and photonics to environmental research and pharmaceuticals."

The Scope of Skills

The computational complexity of this field demands a strong foundation in mathematics, computing, and quantum physics. Rodriguez adds, "This is a multidisciplinary field, and you need extra skills to contribute to specific applications, such as some knowledge of organic, inorganic, and biochemistry, as well as some skill in statistical physics."

Nonetheless, success in computational quantum chemistry goes beyond the basics. James R. Chelikowsky, the W.A. "Tex" Moncrief, Jr., Chair of Computational Materials in the depart- CONTINUED »

ments of physics, chemical engineering, and chemistry and biochemistry and director of the Center for Computational Materials at the University of Texas at Austin, says, "To be really good in this field, you need to know what the numbers mean, not just how to create them." He asks: If your calculations produce garbage, how do you know that? "That takes physical intuition."

So some of the skills can be hard to teach. For example, Chelikowsky adds that researchers in computational quantum chemistry need infinite patience. "You can change one line of code that makes mistakes in two others. You need the ability to find trouble spots."


MARTIN HEAD-GORDON

Today's Opportunities

The sources of jobs in computational quantum chemistry continually change. "In the mid-1970s," says Chelikowsky, "the 'center of gravity' was in industry—IBM and Bell Labs—but there were a number of workers in universities and national labs." Now, jobs tend to be more spread out in academics, industry, and national labs.

Also, computational quantum chemists can work on many topics. Seideman points out a long list: biological and medical research, catalysis and design of materials, data analysis, development of computer algorithms, molecular modeling, and pharmacological modeling. She adds, "The number and variety of applications in industry are growing. At the same time, emerging industries—for example, in the broad field of nanotechnology—pose new fundamental questions for research in academic environments."

Head-Gordon also sees students going to national laboratories. There, he says, a postdoctoral fellowship at a national laboratory can lead to being hired as a permanent member of the staff. He also points out that software companies often hire computational quantum chemists right out of graduate school.

In addition, this field offers the opportunity to change directions. One of Head-Gordon's former students completed a thesis involving the Schrödinger equation and then moved to solving Maxwell's equations to develop photonic devices for the telecommunications industry. "Some people make major changes," Head-Gordon says. "There are many, many directions one can go. Virtually all leading universities have a faculty member in quantum chemistry and nearly every national lab has a staff in computational quantum chemistry."

Chelikowsky has also seen his students go to new fields. One of his graduate students worked on atomic clusters, and then got a job modeling reservoirs for a major petrochemical company. He says that computational quantum chemists can also work in many areas of material physics, including carbon nanotubes, electronic materials, magnetic systems, and nanomaterials.

Visit **www.sciencecareers.org** and plan to attend upcoming meetings and job fairs that will help further your career.


JORGE H. RODRIGUEZ

Tomorrow's Growth

Rodriguez sees new possibilities, especially in three areas. First, he points to quantum biochemistry, like his lab's work on active sites in metaloenzymes or proteins. He adds that understanding the quantum side of biochemistry generates wide opportunities in industry. For example, his research team explores an enzyme that catalyzes the conversion of methane to methanol. He says, "This will be of interest to the energy industry."

Second, Rodriguez mentions nanoscience. As an example, he describes single-molecule magnets—synthetic, discrete molecules that contain 10 to 20 metal ions. "These metal clusters can be candidates for building blocks for memory storage at the molecular level," he says, "which potentially will allow the knowledge industry to store huge amounts of information in a very small space, at the nanoscale."

Rodriguez also sees lots of potential for computational quantum chemistry in the pharmaceutical industry. "Drug design," he says, "would be enhanced by using the laws of quantum mechanics to understand how drugs interact with binding sites."

Moreover, Seideman expects growth for computational quantum chemistry in medical research. She says, "There are good reasons to expect that we will make growing use of computational quantum chemistry to better understand and control function-structure relationships in systems of biomedical relevance." Seideman says, "In the future, one expects the understanding of complex processes—such as protein folding and enzyme reactions—to bring medical research beyond trial and error. Instead, it could be based on calculations."


TAMAR SEIDEMAN

Funding the Computations

It's never easy to gauge the financing available in any field. Chelikowsky says, "In general, the funding environment isn't great." But after being in the field since the mid 1970s, he adds, "I only remember once when people said the funding would be pretty good. For the most part, nobody ever says that."

Head-Gordon agrees that the money side is tolerable. He calls the funding environment "generally reasonable." Then he adds, "We never seem to have quite as much as we want or as little as we might fear." It looks about the same to Rodriguez, who says, "There is a moderate amount of funding at the present time. It's not bad but it could improve." But he adds, "As the applications gain notice, the level of funding will likely increase."

The applications of this field depend on a scientist's imagination. As Head-Gordon says, "A computational quantum chemist can do research that ranges from curiosity driven work on fundamental problems in a university setting to software development and commercialization." He adds, "You can also make logical leaps to adjoining fields." Such leaps can carry a computational quantum chemist to areas limited only by creativity and inspiration.

Mike May (mikemay@mindspring.com) is a publishing consultant for science and technology based in Minnesota.

Invitation

BASF Symposium

on Bioinspired Materials for the Chemical Industry

ISIS, Strasbourg, France
August 7th – 9th 2006

Confirmed speakers:

Jean-Marie Lehn (Strasbourg)
Stefan Marcinowski (Ludwigshafen)
Joanna Aizenberg (Murray Hill)
George Chen (Bejing)
Lei Chiang (Bejing)
Peter Fratzl (Golm)
Andreas Greiner (Marburg)
Stephen Mann (Bristol)
Daniel Morse (Santa Barbara)
Thomas Scheibel (Munich)
Joachim Spatz (Heidelberg)

Nature provides an inexhaustable source of inspiration for chemists and engineers to create highly sophisticated functional materials. Many natural systems with complex structures show an unequalled level of adaptability, resistance and eco-efficiency. This spurs the creativity of the chemical industries to design improved and fundamentally new materials, interconnecting the multidisciplinary worlds of synthetic chemistry, material science and biology.

Invitation procedure
The Symposium is open to every young researcher at the PhD, post-doctoral or junior professor level, working in the fields mentioned above. Scholarships for participation are available – please send your CV and an abstract for a poster by April 15th 2006 to **mfricke@isis.u-strasbg.fr**

We are looking forward to meeting you at ISIS, Strasbourg, France.

ISIS, groupe BASF, ULP, 8 allée Gaspard Monge, 67083 Strasbourg Cedex, France, www-isis.u-strasbg.fr/BASF/

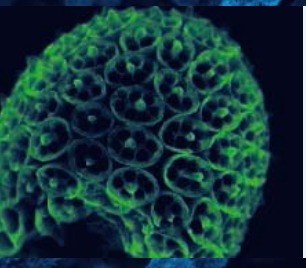

BASF
The Chemical Company

Career matters. Life matters. Health matters.

Sanofi-aventis is dedicated to maintaining our position as one of the world's best Science and Medical Affairs divisions. Employing 17,000 scientific personnel in 20 research centers on three continents, our US Science and Medical Affairs team ranks among the world's best. We are fully invested in continuing our research and development of life-enhancing medicines through the most advanced technology and state-of-the-art facilities.

One such facility is our Combinatorial Technologies Center in Tucson, AZ. The center, nestled in the Catalina Mountains in Northwest Tucson, serves as our discovery engine and is responsible for delivering novel lead compounds and enriching the company's chemical repository. This expanding Combinatorial Technologies Center has more than 70 professionals with high level expertise in biology, chemistry, and IS and is responsible for our Lead Discovery activities by applying High-Throughput Screening, Combinatorial and Medicinal Chemistry.

As one of the fastest growing communities, Tucson has one of the highest rates of population and job growth in the country. Amazing sunsets, majestic mountain ranges, hiking, golfing, a mild dry climate, and year-round sun are just some of the reasons why Tucson is a great place to visit. Its residents enjoy this excellent active lifestyle every day of the year. In addition, Tucson offers other exciting recreational, entertainment, and cultural opportunities.

In addition to our Tucson, AZ facility, we currently seek BS/MS and PhD level scientists for the Bridgewater, NJ and Cambridge, MA campuses in the following areas:

- **Analytical Chemistry**
- **Organic Chemistry**
- **Biochemistry**
- **Chemical Development**
- **Combinatorial Chemistry**
- **Pharmacology**
- **Medicinal Chemistry**
- **Biology**

Your expertise in your field and your passion for science and discovery will ensure we continue to improve the health of millions...because health matters.

Discover your future with sanofi-aventis. Apply online today to keyword search:

CTCAZ (for opportunities in AZ)
RDNJ (for opportunities in NJ)
CGCMA (for opportunities in MA)

www.careers.sanofi-aventis.us

Sanofi-aventis is an **equal opportunity employer** that embraces diversity to foster positive, innovative thinking that will benefit people worldwide. Sanofi-aventis is also committed to employing qualified individuals with disabilities and, where warranted, will provide reasonable accommodation to applicants, as well as its employees.

sanofi aventis
Because health matters

Positions @ NIH
THE NATIONAL INSTITUTES OF HEALTH

Director, Division of Extramural Activities
National Institute of Dental and Craniofacial Research

The National Institute of Dental and Craniofacial Research (NIDCR), a major research component of the National Institutes of Health (NIH) and the Department of Health and Human Services, seeks an outstanding scientist to lead its Division of Extramural Activities (DEA) located at the National Institutes of Health in Bethesda, Maryland.

The Director, DEA, provides leadership and advice in developing, implementing, and coordinating the Institute's extramural programs and policies. S/he serves as a senior advisor to the Director and other Institute officials on issues related to policies and procedures for extramural affairs, and represents the Institute on extramural program and policy issues within the NIH, the Department and with outside organizations. The Director oversees the initial scientific review of applications assigned to the Institute, including program projects, research grants in response to RFAs, training grants, cooperative agreements, and R&D contracts, and ensures effective and proper grants management. S/he manages and monitors all business aspects of the Institute's grants, provides information and guidelines for grant applications, and oversees the closed session of the National Advisory Dental and Craniofacial Research Council. In addition, the Director undertakes program evaluation and planning activities in conjunction with the Institute's programmatic Centers and the Office of Science Policy and Analysis.
Applicants must possess a Ph.D., D.D.S./D.M.D., M.D., or equivalent degree, in a biomedical or related field and have in depth knowledge of NIH policies and procedures governing extramural research activities (research grants, cooperative agreements, and contracts). Applicants must be able to serve as a spokesperson for NIDCR with research institutions, science professionals, and the general public, and have proven experience in directing and managing NIH extramural activities, with the requisite administrative and interpersonal skills to meet the demands of program direction.

Interested applicants should send their curriculum vitae and bibliography, and the names and addresses of four references. Applications must be received by the closing date and should be sent to:

Ms. Carol M. Beasley, National Institute of Dental and Craniofacial Research, Building 31, Room 2C39, Bethesda, MD 20892-2290, E-mail: carol.Beasley@nih.gov., Fax: 301-402-4088.

The closing date for this position is: **April 7, 2006**.

POSTDOCTORAL POSITIONS at the NIH

Laboratory of Developmental Biology at the National Heart Lung and Blood Institute of the National Institutes of Health is recruiting postdoctoral fellows for multiple positions in three research groups headed by:

Dr. Cecilia Lo	Congenital Heart Disease
Dr. Kenneth Kramer	Developmental Glycobiology
Dr. Yosuke Mukoyama	Stem Cell and Neuro-Vascular Development and Patterning

The Laboratory provides a highly interactive and stimulating environment that promotes the use of genetically engineered and chemically mutagenized animal models to elucidate the regulation of embryonic development and patterning. These cutting edge research studies utilize mouse, zebrafish, and chick embryos, and are aided by state of the art real time cellular and whole animal imaging together with high throughput genomic, proteomic, and transcriptome analyses. In addition, well supported core facilities provide ready access to mass spectrometry, microarray and informatics support, cell sorting, mouse transgenesis and gene targeting, confocal and two-photon microscopy, and functional imaging with ultrasound, MRI, and microCT. More details available at http://dir.nhlbi.nih.gov/labs/ldb/index.asp

Successful applicants should have a record of research accomplishments and enthusiasm for developmental biology. To apply, send a letter of interest and curriculum vitae to: Ms. Yolanda Carter, Laboratory of Developmental Biology, NIH/NHLBI, 50 South Drive MSC 8019, Bldg 50/Rm 4537, Bethesda, MD 20892. Communications by email are encouraged (cartery2@nhlbi.nih.gov).

Director, Division of Adult Translational Research and Treatment Development (DATR)

The NIH is seeking exceptional candidates for the position of Director, DATR, NIMH, to provide leadership for a national research program aimed at understanding the pathophysiology of mental illness and hastening the translation of behavioral science and neuroscience advances into innovations in clinical care. The DATR supports a broad research portfolio, which includes studies of the phenotypic characterization and risk factors for major psychiatric disorders; clinical neuroscience to elucidate etiology and pathophysiology of these disorders; psychosocial, psychopharmacologic, and somatic treatment development, and research training, and resource development on: novel pharmacological approaches to the treatment of mental disorders. In addition, the Division supports an integrated program to clarify the psychopathology and underlying pathophysiology of psychiatric disorders of late life and to develop new treatments for these disorders. This position offers a unique opportunity for the right individual to provide strong and visionary leadership to an organization dedicated to uncovering new knowledge and technologies, both basic and clinical, as well as ensuring that rigorous science guides the appropriate use of more conventional treatments. Applicants must possess an M.D. or equivalent degree and senior-level research experience and knowledge of research programs in one or more scientific areas related to mental health. Applicants should be known and respected within their profession, both nationally and internationally as distinguished individuals of outstanding scientific competence. Salary is commensurate with experience and accomplishments. A full package of Civil Service benefits is available including retirement, health and life insurance, and long-term care insurance). The position opens for receipt of applications March 20, 2006 and closes April 21, 2006. Applicants should send a complete application package as outlined in vacancy announcement number NIMH-06-04SES at: http://www.jobs.nih.gov (under Executive Jobs section). Questions may be addressed to Ms. Susan Corey at seniorre@od.nih.gov. Application packages, CV and bibliography must be received by the closing date of the announcement.

With nationwide responsibility for improving the health and well being of all Americans, the Department of Health and Human Services oversees the biomedical research programs of the NIH.

WWW.NIH.GOV

Health Research in a Changing World

Fighting Diseases and Improving Lives

DEPARTMENT OF HEALTH AND HUMAN SERVICES
NATIONAL INSTITUTES OF HEALTH
NATIONAL INSTITUTE OF ALLERGY AND INFECTIOUS DISEASES

Are you ready for an exciting career that could help improve millions of lives around the world?
Then consider joining the scientific and medical forces at NIAID. As part of the Division of Allergy, Immunology, and Transplantation (DAIT) at NIAID, the Asthma, Allergy, and Inflammation Branch (AAIB) is responsible for planning and conducting programs of extramural basic and clinical research aimed at understanding the biology of asthma and allergic diseases. AAIB/DAIT has the following scientific opportunities available:

Program Officer/Medical Officer

As a Program/Medical Officer, the selected candidate will provide leadership and scientific/medical expertise and guidance in the planning, development, implementation and evaluation of basic and clinical research concepts, projects and initiatives to appropriate advisory groups; identify opportunities and problem areas, research gaps and relevant program needs and make recommendations for and facilitate new research efforts, clinical studies, clinical trials or other initiatives; and communicate with grantees/contractors, cooperative group members/representatives and others on policy interpretation, merit review and evaluation processes and procedures, and on decisions, concerns or other issues/matters of a medical/scientific nature. The selected candidate will also oversee and advise on development of clinical trial protocols.

In order to be considered for this position, applicants should have experience in basic and/or clinical research to examine the causes, diagnosis, treatment and prevention of allergic diseases; research on bacteriology, mycology, virology, or research on parasitic and other tropical diseases, or vector biology is required; and the successful candidate must posses a Bachelor's degree, M.D., D.O., or Ph.D. and relevant laboratory research on asthma, allergy, inflammation, or immunology. Experience in clinical trial and/or project management is highly desirable. Only candidates with an M.D. or D.O. degree and current medical licensure are eligible to serve as Medical Officers.

For a complete job announcement and to apply for this position, visit http://usajobs.opm.gov:

Interdisciplinary Vacancy number: NIAID-06-110230
Open: 3/1/06 – 4/28/06
GS-401, 601-13/14 Salary: $77,353 - $118,828
Applications must be submitted to Nolan Jones, Human Resource Specialist, 301-402-0957

Section Chief

As Chief of the Asthma and Inflammation Section of AAIB, the selected candidate will lead an extramural research program with a diverse portfolio of grants and contracts focusing on the immunologic basis, etiology, pathogenesis, and treatment of asthma and inflammatory diseases. The Chief of the section leads a staff of physicians, scientists, and project managers responsible for development and implementation of new initiatives in these areas and the direction and oversight of ongoing research programs through site visits and frequent contact with principal investigators. The selected candidate will also oversee and advise on development of clinical trial protocols.

In order to be considered for this position, applicants should have experience in basic and/or clinical research to examine the causes, diagnosis, treatment and prevention of allergic diseases. Candidates must also have experience in managing complex biomedical research programs, including the development of pre-clinical animal models, human subjects, and/or clinical trials. Experience in the preparation and review of research project grant applications is also necessary. The selected candidate must posses an M.D. or D.O. to be considered for this position.

Salary is commensurate with research experience and accomplishments, and a full package of benefits (including retirement, health, life and long term care insurance, Thrift Savings Plan participation, etc.) is available for this position.

CV, bibliography, and a list of 3 references must be received by April 30, 2006. Application package should be sent to:

Jeryl Wilson
4900 Seminary Road, Suite 1100
Alexandria, VA 22311
1-888-798-4991 ext. 252
For further information, please contact Ms. Wilson by email:
sectionchief@stginternational.com

We are happy to respond to your questions, and you may contact us toll free at 1-888-798-4991 or visit online at: http://healthresearch.niaid.nih.gov/science

6 April 2006
San Francisco, CA

UCSF Mission Bay
Community Center
Fisher Banquet Hall
1675 Owen Street
1:00 - 4:30 pm

Science Careers has teamed up with UCSF to deliver an exciting career fair on the new Mission Bay campus of UCSF.

Scientists: Meet with HR representatives of biotech, pharmaceutical, and research organizations who will be exhibiting. Visit ScienceCareers.org and click on Career Fairs on the left side for complete details.

Exhibitors: This fair typically attracts over 800 attendees. To be among the recruiters call Daryl Anderson at 202-326-6543 or visit ScienceCareers.org and click on Exhibit at a Career Fair.

We hope to see you there.

ScienceCareers.org
We know science AAAS

UNIVERSITY OF NEW MEXICO SCHOOL OF MEDICINE

Faculty Position, Biocomputing

The Division of Biocomputing invites applications for a tenure-track faculty position rank and salary open depending on experience.

Minimum Requirements

- **Training:**
  - Ph.D., and/or M.D., or equivalent degree in Computational Biology and Bioinformatics or a closely related discipline
  - 2 years of postdoctoral experience in Medical and Biological Image Processing and Medical Informatics
- **Research Area:** Medical/Biological Image processing, Computational Biology, Med/Bio/Cheminformatics
- **Publications:** Recent publications in peer reviewed journals
- **Teaching:** Experience teaching
- **Applicant must be eligible to work in the U.S.A.**

Desirable Qualifications: Preference will be given to applicants with (1) Proven skills in pattern recognition and machine learning. (2) Demonstrated record of excellence in research as evidenced by sustained extramural research funding. (3) Evidence of mentoring trainees as evidenced by successfully published student research.

New faculty will be expected to develop research activities supported by independent extramural funding, develop a computational biology curriculum for graduate students, and participate in the continuing development and improvement of Health Sciences widely recognized record in cancer research, environmental health, computational biology and complex systems, and biomolecular screening. Appointee will have the opportunity to participate in several NIH funded interdisciplinary programs such as the NCI designated Comprehensive Cancer Center, the New Mexico NIEHS Center, and the New Mexico Molecular Libraries Screening Center.

Applicants should submit the following materials: a signed letter of interest, curriculum vitae, a two page description of research interests and goals emphasizing interdisciplinary expertise, three representative reprints, a statement of teaching experience and description of teaching philosophy, names and e-mail addresses of three references to: **Chair, Faculty Committee, c/o Sheryl Cohn, Division of Biocomputing, MSC08-4670, 1 University of New Mexico, Albuquerque, NM 87131-0001**.

For best consideration, materials must be submitted by **April 17, 2006**. The position will remain open until filled. This position may be subjected to criminal records screening in accordance with New Mexico law. Members of underrepresented groups are strongly encouraged to apply. For complete job description, please visit our website at **http://hsc.unm.edu/som/biocomputing/**.

The University of New Mexico is an Equal Opportunity/Affirmative Action Employer and Educator.

The University of Edinburgh

The University of Edinburgh is a world-leading centre for research in mammalian stem cell biology. Its mission is to acquire the knowledge and understanding of stem cells required for the development of regenerative and cell replacement therapies to treat human disease and injury.

Chair of Stem Cell Biology

Associate Director of the Centre for Regenerative Medicine

Applications are invited for the newly established Chair of Stem Cell Biology in the Centre for Regenerative Medicine (CRM). You will be an outstanding investigator with an international reputation in stem cell biology and will provide scientific leadership in basic and pre-clinical research.

The mission of this rapidly expanding Centre is to develop new treatments for human disease through innovative research with stem cells. The Centre is being formed by merging the Institute for Stem Cell Research with research groups within the College of Medicine and Veterinary Medicine. The Institute (www.iscr.ed.ac.uk) has a world-leading integrated programme of research in the molecular, cellular, developmental and translational biology of mammalian stem cells. You will work closely with the current Director of CRM, Professor Ian Wilmut FRS, to shape the long-term research strategy of this exciting development.

Informal enquiries to Professor Ian Wilmut (tel: 0131 242 6630 or e-mail: Ian.Wilmut@ed.ac.uk) or Professor Andrew Illius, Head of the School of Biological Sciences (tel: 0131 650 5525 or e-mail: a.illius@ed.ac.uk).

Apply online, view further particulars or browse more jobs at our website. Alternatively, telephone the recruitment line on 0131 650 2511. Ref: 3005587SI. Closing date: 10 April 2006.

Committed to Equality of Opportunity

www.jobs.ed.ac.uk

Max Planck Institute for Dynamics and Self-Organization

MAX-PLANCK-GESELLSCHAFT

The Max Planck Institute for Dynamics and Self-Organization invites applications for an

Independent Junior Research Group
(Selbstständige Nachwuchsgruppe der Max-Planck-Gesellschaft)

The Max Planck Institute for Dynamics and Self-Organization (MPIDS) is establishing an independent research group to pursue cutting edge research in

"Nonlinear Dynamics and Arrhythmias of the Heart"

The group will perform interdisciplinary research on the dynamics of the heart with the aim of understanding the self-organizing, electrophysiological excitations that lead to cardiac arrhythmia and sudden death. The experimental investigations should cover all scales from organ to cells and should be supported by numerical simulations (ionic full heart models, coupled maps, etc.). The investigations will be conducted in close collaboration with the Heart Center at the University of Göttingen.

The position includes a five-year grant (research positions, budget, investments) and a guaranteed access to the institute´s infrastructure.

Successful candidates will have demonstrated the ability to perform top international research in the field of cardiac arrhythmia.

The position has the nominal starting date of July 2006, but an earlier starting date could be arranged. Applications, including curriculum vitae, a two page statement of research plans, copies of three publications and three letters of recommendation should be sent before May 1, 2006 by email or regular mail to:

Max Planck Institute for
Dynamics and Self-Organization
Prof. Eberhard Bodenschatz
Am Fassberg 11 / Turm 2, D-37077 Göttingen
eberhard.bodenschatz@ds.mpg.de

The Max Planck Society is an equal opportunity employer.

Looking for a great science career?

Get the experts behind you.
Visit www.ScienceCareers.org

Your career is too important to leave to chance. So to find the right job or get career advice, turn to the experts. At ScienceCareers.org we know science. And we are committed to helping take your career forward. Our knowledge is firmly founded on the expertise of *Science*, the premier scientific journal, and the long experience of AAAS in advancing science around the world. Put yourself in the picture with the experts in science. Visit www.ScienceCareers.org.

Associate Chief of Staff (ACOS) for Research and Development

The Veterans Affairs Medical Center (VAMC), Albany, New York seeks an established scientist with a competitively-funded research program to serve as ACOS for Research & Development. The VAMC is a major teaching hospital in the University Heights health care research community and is affiliated with Albany Medical College. Other research partners of the VAMC are Albany College of Pharmacy, Ordway Research Institute and the Wadsworth Center of the New York State Department of Health. The ACOS will have a joint appointment at one or more of these institutions. The University Heights research community includes 600 inpatient beds and an 18 county catchment area that extend from the Canadian Border to the mid-Hudson Valley. The electronic medical record system maintained by the Veterans Health Administration (VHA) is an important asset in VAMC clinical research.

The ACOS must have administrative experience and a commitment to expanding inter-institutional, thematic research relationships. The Albany VAMC has a history of infectious disease, cancer and neurology research and hopes to build on these strengths, but will consider strong applicants in any field of biomedicine. The facility has a fully AALAC-accredited animal facility and remodeled bench laboratory space. Two 0.5 FTEE salary lines may also be available for recruitment of additional scientists with partner institutions. VHA makes Merit Review research grant awards and has other funding mechanisms.

Albany, the capital of New York State, is less than three hours by automobile from New York City and Boston. Over 30 post-secondary institutions are located within 60 miles and include Rensselaer Polytechnic Institute, Union College and the State University of New York at Albany. An array of cultural and outdoor activities are available locally including orchestras, theatre, opera and the largest collection of ski resorts in the country.

Applicants must have a doctoral degree (MD and/or PhD) and qualify for a senior academic appointment at Albany Medical College. American citizenship or resident alien status is required. Interested candidates should send a cover letter and a current CV to: **Paul Davis, MD, Chair, ACOS Search Committee, c/o Mary Ann Witt, Room B105, Albany VAMC, 113 Holland Avenue, Albany, NY 12208**. (**maryann.witt@med.va.gov**; Fax **518-626-6735**) Questions regarding the position should be directed to **Dr. Davis** at **518-641-6410** or **pdavis@ordwayresearch.org**. Information on Upstate New York VISN 2 VA Healthcare Network can be found at **www.va.gov/visns/visn02**. Position incumbent is subject to random drug-testing.

The VAMC is an Equal Opportunity Employer.

THE UNIVERSITY OF TEXAS
MD ANDERSON
CANCER CENTER
Making Cancer History™

Postdoctoral positions are available at The University of Texas M.D. Anderson Cancer Center for motivated and creative individuals to study the roles of MTA chromatin modifiers and PAK signaling in the action of estrogen receptor and in cytoskeleton remodeling. Lab is interested in the developmental and tumorigenesis issues using transgenic and knockout mouse models of MTA family members. Scientists with prior experience and track record in mouse genetics and cell biology are encouraged to apply. For immediate consideration, apply with referee list to: **Rakesh Kumar, John G. and Marie Stella Kenedy Memorial Foundation Chair, MD. Anderson Cancer Center, 1515 Holcombe Boulevard, Houston, Texas 77030**. E-mail: **jdagostino@mdanderson.org**.

M.D. Anderson Cancer Center is an Equal Opportunity Employer and does not discriminate on the basis of race, color, national origin, gender, sexual orientation, age, religion disability or veteran status, except where law requires such distinction. All positions at The University of Texas M. D. Anderson are considered security sensitive and subject to examination of criminal history record information. Smoke-free and drug-free.

University of South Carolina Biomedical Engineering and Biomedical Sciences Faculty Positions

The University of South Carolina seeks to fill a cluster of junior faculty positions in the area of Biomedical Engineering and Biomedical Sciences for a new multidisciplinary research and teaching initiative. Candidates for this cluster are expected to be at the forefront of research, and to support graduate and undergraduate education programs in Biomedical Engineering. Candidates with research interests that complement current expertise at the University of South Carolina in cardiovascular development, wound healing, and regenerative medicine are especially encouraged to apply. Candidates are expected to develop a nationally recognized externally funded research program. Candidates will have tenure-track appointments in the Department of Chemical Engineering, Department of Mechanical Engineering, or in the Department of Cell and Developmental Biology and Anatomy in the USC School of Medicine. For more information on the specific focus of this initiative, see **www.engr.sc.edu**. Applicants are requested to submit with their letter of application, a professional vitae, transcripts of undergraduate work, names of three references, and statements of their research plans and teaching interests. All materials should be addressed to the **Biomedical Faculty Search Committee, Office of the Dean, College of Engineering and Information Technology, Columbia, SC 29208**. Candidates may submit materials via electronic mail to **biomedfaculty@engr.sc.edu**. Review of applications will begin immediately and will continue until the positions are filled. *The University of South Carolina is an Affirmative Action/Equal Opportunity Employer.*

esf — State University of New York

Assistant/Associate Professor

WILDLIFE ECOLOGIST

The State University of New York College of Environmental Science and Forestry (SUNY-ESF) in Syracuse, NY, invites applications for an academic-year, tenure-track position as Assistant or Associate Professor in Wildlife Ecology. A Ph.D. in Wildlife Ecology or a related discipline is required. Qualified candidates must demonstrate a primary interest in wildlife ecology and management. Preference will be given to candidates with a record excellence in teaching, research, and outreach, commensurate with time since degree. Strong quantitative skills including population analysis, biometry and spatial analysis, and ability to mentor graduate and undergraduate students are also preferred. Application review begins April 17, 2006. For more information and application procedures, see *www.esf.edu/hr/search* or contact Dr. William Porter at *wfporter@esf.edu*.

SUNY-ESF is an Equal Opportunity/Affirmative Action employer.

THE UNIVERSITY OF HONG KONG

香 港 大 學

The University of Hong Kong is at the international forefront of higher learning and research, with more than 100 teaching departments and sub-divisions of studies, and more than 60 research institutes and centres. It has over 20,000 undergraduate and postgraduate students from 48 countries. English is the medium of instruction. The University is committed to international standards for excellence in scholarship and research.

Research Assistant Professorships and Post-doctoral Fellowships

Applications are invited for a number of positions as Research Assistant Professor (RAP) (Ref: RF-2005/2006-400) and Post-doctoral Fellow (PDF) (Ref: RF-2005/2006-401), tenable on or before January 31, 2007. Appointments will be made for a period of 2 to 3 years.

RAP and PDF posts are created by the University with the aim of injecting fresh impetus and vigour to the University's research enterprise, in order to complement and broaden its existing research expertise. Appointees are expected to bring in new research ideas and cutting-edge technologies.

Research Assistant Professors
The main focus of an RAP's duty is research. RAPs can however be assigned some teaching duties, up to 50% of the normal teaching load. Applicants should be research active and have a proven publication record. A highly competitive salary commensurate with qualifications and experience will be offered, with a contract-end gratuity and University contribution to a retirement benefits scheme (totalling up to 15% of basic salary). Annual leave, and medical/dental benefits will also be offered.

Post-doctoral Fellows
PDFs are expected to focus on research. Applicants should be Ph.D. degree holders. A highly competitive salary commensurate with qualifications and experience will be offered. Annual leave, and medical/dental benefits will be provided.

A full list of the research areas and the departments or academic units in which the above posts are recruited will be shown on the webpage at https://extranet.hku.hk/apptunit/.

Procedures
Interested applicants are strongly advised to contact, in the first instance and prior to making an application, the Head of the appropriate department or academic unit to ascertain the posts available and to obtain information about current research initiatives and activities.

Applicants must submit a completed University application form, which should clearly state **which position** they are applying for; and in which **academic discipline**. They should also provide further information such as details of their research experience, publications, research proposals, etc.

Further particulars and application forms (272/302 amended) can be obtained at https://extranet.hku.hk/apptunit/; or from the Appointments Unit (Senior), Registry, The University of Hong Kong, Hong Kong (Fax (852) 2540 6735 or 2559 2058; E-mail: apptunit@hkucc.hku.hk). **Closes April 15, 2006**. Candidates who are not contacted within 3 months of the closing date may consider their applications unsuccessful.

The University is an equal opportunity employer and is committed to a No-Smoking Policy

ACADEMIA SINICA, TAIPEI, TAIWAN
POSITION ANNOUNCEMENT

POSITION: The Institute of BioAgricultural Sciences (IBS), at Academia Sinica, Taipei, Taiwan, invites applications for several tenured Assistant to Associate Research Fellow positions or non-tenured Research Specialist. Candidates must have a Ph.D. (or equivalent) and have an outstanding record of research achievement. The successful candidates are expected to develop state-of-the-art research programs in the areas of Herbal Medicine and Vaccine Research. For the Herbal Medicine program, preference will be given to candidates who are trained in studies related to immune-modulatory or chemo-preventive effects on cancer, and are interested in approaches that incorporate use of plant metabolites, phytochemistry or metabolomics for herbal medicine studies. For the Vaccine Research program, candidates with expertise in fundamental or applied research on cellular immune systems, pathogen infection or molecular virology will be given with high priorities. An important mission of the IBS is to engage in translational research and development of platform technologies.

LOCATION: Academia Sinica, the most prominent academic institution in Taiwan, is located in Taipei. The infrastructure for research in the Academy is excellent, and Research Fellows are afforded well-equipped laboratories and excellent research funding.

IBS: The Institute of BioAgricultural Sciences pursues basic and translational researches that have the potential to generate new platforms or novel products in biotechnology. Herbal medicine, plant stress biology and vaccine research are three major research areas within the IBS. For more information, please visit our website at **http://ibs.sinica.edu.tw/E_www/**.

TO APPLY: Applicants should submit the following materials, online, at **http://ibs.sinica.edu.tw/job2/**: (a) Cover letter; (b) Curriculum vitae, including publications; (c) Summary of research accomplishments; (d) Clearly focused description of future research plans; (e) PDF copies of major publications; (f) Names and contact information for four referees.

Closing date: Open until filled although to assure full consideration, applications should be received prior to May 1, 2006.

Candidates should arrange four letters of recommendation to be submitted by e-mail to: **hireibs@gate.sinica.edu.tw** or sent by regular mail to: **Ning-Sun Yang, Director, Institute of BioAgricultural Sciences, Academia Sinica, No. 128, Academia Rd. Sec. 2, Nankang, Taipei 11529, Taiwan, ROC**.

University of Alabama at Birmingham
Faculty Positions in Microbiology

The Department of Microbiology invites applications from outstanding scientists for tenure track positions at any academic rank and tenure status. Rank and tenure status will be commensurate with qualifications and experience. We seek candidates with strong research records, commitments to developing independent, innovative, funded research programs, and concerned interests in graduate and medical education. UAB ranks in the top 20 US institutions in research funding and offers an exceptionally interactive environment. Many multi-disciplinary research centers and an interdepartmental graduate program in Cell and Molecular Biology facilitate collaborations among the basic science disciplines and between basic science and clinical faculty. For more information, please visit **http://www.microbio.uab.edu/**. We are interested in applicants with expertise in new research areas not currently represented in our department, as well as applicants who enrich areas of existing strength. Candidates in the following areas are invited to apply:

Bacterial Pathogenesis and Genetics – Current research strengths include mechanisms of pathogenesis, genetics, gene regulation and vaccine targets. Pathogens under study include *S. pneumoniae, Salmonella, B. anthracis, E. coli, F. tularensis, M. tuberculosis* and Mycoplasmas. **Job Code B-1**.

Immunology – Current research strengths include mucosal immunology, lymphoid and myeloid cell development, signal transduction, innate immunity, vaccine development, and autoimmunity. Candidates with special interest in mucosal immunology and vaccinology are particularly encouraged to apply. **Job Code B-2**.

Virology – Current research strengths include virus structure, control of gene expression, mechanisms of replication, protein structure/function, trafficking and viral assembly, immune recognition, viral vectors, and development of vaccines and antiviral drugs. Candidates with special expertise in HIV, hepatitis viruses, influenza, and emerging pathogens are particularly encouraged to apply. **Job Code B-3**.

Review of applicants begins immediately and interviews will continue until positions are filled. Anticipated starting dates are flexible. Please submit (preferably electronically) C.V., a 2-4 page description of research accomplishments and plans, and names of 3 references to: **Dr. David Chaplin, c/o Brian Fernandes, UAB Dept. of Microbiology, 845 19th Street S., BBRB 276/11, Birmingham, AL 35294; Email: brianuab@uab.edu; Phone (205) 934-3049**.

UAB is an Affirmative Action/Equal Opportunity Employer.

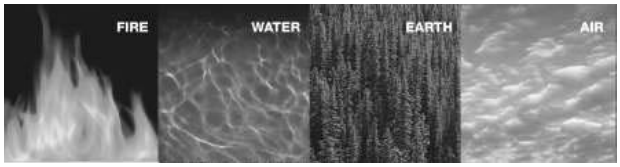

USDA Forest Service, Research & Development
Forest Management Science Staff, Arlington, VA

The Forest Service seeks expressions of interest for the position of Staff Director of the Forest Management Science Staff (formerly Vegetation Management and Protection Research). We are looking for a visionary and dynamic leader to manage a portfolio of science addressing issues from fire and fuels management to invasive species, forest productivity (silviculture and operations), and the Healthy Forest Restoration Act. The incumbent will also provide oversight of the Nation's network of experimental forests and long-term ecological research sites.

Forest Service Research & Development strives to be recognized as a world leader in innovative science for sustaining global forest resources for future generations. We have the flexibility to address today's issues as well as to respond to tomorrow's needs. The successful candidate will join a team of world research leaders to chart a vision and strategy for solutions to the sustainability of forests and grasslands. A key aspect of this position is collaboration and development of partnerships with other natural resource research organizations worldwide.

The position oversees a staff of 10 national science program leaders and a rotating cadre of top scientists from academia and other non-governmental organizations. Additional responsibilities include representing the agency before Congress, participating in national and international research efforts, and planning and oversight of a $100 million research program. The incumbent is the primary research contact for Agenda 2020 (public and private partnerships). Highly qualified candidates will demonstrate strong written and verbal communications skills, ability to work as a member of a team, and an extensive network of research colleagues at universities, NGOs, in industry, and across other federal agencies.

The salary range for the position is $109,808 to $165,200. The selected candidate will be eligible for a full benefits package including health insurance, life insurance, retirement benefits, and vacation and sick leave.

Expressions of interest, including a current CV, should be sent to Marty Longan (**mlongan@fs.fed.us**). For further information on the position, contact **Dr. Jim Reaves, Associate Deputy Chief for Research & Development (jreaves@fs.fed.us** or **(202) 205-1702**).

The Forest Service is an Equal Opportunity Employer.

THE HONG KONG UNIVERSITY OF SCIENCE AND TECHNOLOGY

DEPARTMENT OF BIOCHEMISTRY

Faculty Position

The Department of Biochemistry invites applications for a tenure-track faculty position at the Assistant/Associate Professor level. Applicants should have a PhD degree and relevant research experience.

The Department is interested in an appointment to strengthen existing research programs in molecular neuroscience and signal transduction (**www.ust.hk/bich/**). Preferences will be given to candidates who use model organisms to address fundamental questions in modern biology. Scientists prominent in other areas will also be considered. Teaching responsibilities include undergraduate and graduate courses.

Starting salary will be highly competitive and commensurate with qualifications and experience. Fringe benefits including medical/dental benefits, housing, etc. will be provided where applicable. The gratuity together with the University's total contributions made to the Mandatory Provident Fund Scheme will amount to 15% of the earned aggregate basic salary.

Applications/nominations should be sent with curriculum vitae, together with the names and addresses of three referees to **the Secretary of the Search Committee, Department of Biochemistry, The Hong Kong University of Science and Technology, Clear Water Bay, Kowloon, Hong Kong (Attn: Ms Amy Fong), Email: bcamy@ust.hk / Fax No: +852 2358 2765) before 30 April 2006 or until the position is filled.**

Massey University
NEW ZEALAND

Lecturer/Senior Lecturer in Zoology

Institute of Natural Resources

Palmerston North

You will lecture in vertebrate zoology and will be a member of a multi-disciplinary team teaching and researching zoological and ecological issues of national and international importance.

Te Kunenga ki Pūrehuroa

Closing date: 2 April 2006 Reference number: A607-05L

For further information and to apply online, visit:
http://jobs.massey.ac.nz

MAYO CLINIC

Faculty Positions in Developmental Biology and Disease

Rochester, Minnesota

The Mayo Clinic College of Medicine and Mayo Comprehensive Cancer Center in Rochester, MN, is conducting a search for highly competitive scientists at the Assistant, Associate, or Full Professor levels with a focus on organ development, cell migration/invasion, or apoptosis as it pertains to disease and/or neoplasia. Highly productive individuals who utilize genetic model systems to address human disease while interacting with other talented basic and clinician scientists are encouraged to apply.

Mayo Clinic in Rochester provides a unique research environment that combines state-of-the-art facilities and support with an exceptional academic medical center.

To learn more about Mayo Clinic and Rochester, MN, please visit **www.mayoclinic.org**.

Interested applicants should send a CV and a list of three or four references to:

Ms. Kristi Simmons
Mayo Clinic
200 First Street SW
Rochester, MN 55905

Mayo Foundation is an affirmative action and equal opportunity educator and employer. Post offer/pre-employment drug screening is required.

Director
The Black Family Stem Cell Institute
Mount Sinai School of Medicine

MOUNT SINAI SCHOOL OF MEDICINE

The Black Family Stem Cell Institute, funded by a $10M philanthropic gift, is seeking an outstanding Director with demonstrated scientific expertise and leadership to build a Program of Excellence in Stem Cells that has translational potential in regenerative medicine. This multi-departmental and interdisciplinary Institute currently has 18 faculty members who are actively conducting independent and integrative basic and translational research in various embryonic and adult stem cell studies. The Institute Director will have excellent space and financial resources to recruit a number of new faculty investigators in this important area of research, and will report directly to the Dean. Outstanding institutional shared resources to support stem cell research include, but are not limited to, a state-of-the-art cell sorting facility, live cell imaging with time-lapse photography, micro-array and bioinformatics, chemical biology for small molecule screening in target cells, transgenic and knock-out mouse services in a VAF barrier rodent facility with an irradiator and an optical imaging system for live laboratory animals. An excellent compensation package is also available to the Institute Director. The Mount Sinai School of Medicine, an equal opportunity employer, is situated along the Museum Mile on the Upper Eastside of Manhattan. Interested applicants should electronically submit their updated CV's and Bibliographies to **Savio L.C. Woo, PhD, Chairman of the Search Committee, at savio.woo@mssm.edu**

The University of Edinburgh

The University of Edinburgh is an exciting, vibrant, research-led academic community offering opportunities to work with leading international academics whose visions are shaping tomorrow's world.

Chair of Developmental Biology and Anatomy

Salary will be within the professorial range

This newly created post will be held in the School of Biomedical Sciences (SBMS). You will have a particular commitment to, and academic responsibility for, the discipline of Anatomy within the College. You will make a major contribution to the academic leadership of the School and will be encouraged to draw on excellent opportunities for collaboration within the School, College and University. You must have an established international reputation for excellence in research in Developmental Biology.

Informal enquiries to Professor John Savill, Head of College (headcmvm@ed.ac.uk) or Professor Tony Harmar, Head of School (head.SBMS@ed.ac.uk).

Apply online, view further particulars or browse more jobs at our website. Alternatively, telephone the recruitment line on 0131 650 2511. Ref: 3005586SI. Closing date: 14 April 2006.

Committed to Equality of Opportunity

www.jobs.ed.ac.uk

Positions Available
Division of Experimental Medicine
Immunology of Chronic Infectious Diseases

The Department of Medicine of the University of California San Francisco is establishing a Division of Experimental Medicine with its laboratory space based at San Francisco General Hospital, not far from the new Mission Bay campus. The Division welcomes applications from physician scientists and PhD scientists engaged in hypothesis-driven, patient- or disease-oriented research on the immunology of chronic infectious diseases in humans. Appointments will be made at the Assistant to Full Professor level in the In-Residence series, depending upon qualifications. Successful candidates will also become members of the UCSF Graduate Program in Biomedical Sciences. Particular attention will be devoted to those who could assume the role of Associate Director, with responsibilities to help the Director form the program, providing leadership and mentorship to the staff. Experience in management of large teams required. Favorable attention will also be devoted to those applicants who could serve as a faculty advisor and supervisor of the following core lab functions: Flow Cytometry Core – containing a high-speed multiparameter cell sorter and several multiparameter flow cytometers. Animal Model Core – providing animal models of chronic infectious diseases on site and collaborating with other animal model cores elsewhere. Core Immunology Lab – focused on the analysis of immune phenotype and function in humans.

Applicants must have an MD and/or a PhD and demonstrated potential to lead an independent research program. Nationally competitive start-up packages are available. If interested, please send CV and three letters of reference to: **J. M. (Mike) McCune, MD, PhD, Chief, Division of Experimental Medicine, Department of Medicine, University of California at San Francisco, Chair, Translational Research Search Committee, Bldg 3, Rm 601, San Francisco General Hospital, 1001 Potrero Ave., San Francisco, Ca. 94110; mmccune@gladstone.ucsf.edu.**

UCSF is an Affirmative Action/Equal Opportunity Employer. The University undertakes affirmative action to assure equal employment opportunity for underutilized minorities and women, for persons with disabilities and for covered veterans.

CHAIR
Department of Microbiology and Immunology
University of Maryland School of Medicine

Applications are invited from established, dynamic scientists with a creative vision, for the position of Chair of the Department of Microbiology and Immunology at the University of Maryland School of Medicine.

The department is ranked in the 30th percentile of all US Microbiology and Immunology Departments in NIH funding, with an outstanding tradition of research, training and service. Major strengths include bacterial pathogenesis, vaccine development, innate and adaptive immunity, cytokines and immune regulation, as well as retrovirology (**http://medschool.umaryland.edu/Microbiology/**). The highly regarded Graduate Program in Molecular Microbiology and Immunology, **http://microbiology.umaryland.edu/** is part of the interdisciplinary Graduate Program in Life Sciences (GPILS) in the School of Medicine.

The successful candidate is expected to have a distinguished record of scholarly activity, extramural funding and service, together with proven administrative leadership skills, a legacy of building interdisciplinary programs and resources and a commitment to further expand the high national and international visibility of the Department. Applicants should also have experience mentoring graduate and medical students, post-doctoral fellows and junior faculty. The successful candidate will be expected to form close and substantive ties with the other basic science departments as well as researchers in clinical disciplines.

Nominations and applications should be sent to **Dr. Michael T. Shipley**, Chair, Search Committee for Chair of Department of Microbiology and Immunology, at: (**misearch@umaryland.edu**). Applicants should submit, by email, a letter summarizing their qualifications and interest in the position, with an updated CV. The letter should describe research, teaching, service, administrative experience, previous mentoring, and achievements with interdisciplinary programs. All inquiries, nominations and applications will be treated confidentially. For more information, please visit the University of Maryland School of Medicine website at **http://medschool.umaryland.edu**. For questions or additional information please contact **Dr Shipley, mshipley@umaryland.edu**. Review of applications will begin **March 31, 2006**.

University of Maryland is an Equal Opportunity/Affirmative Action Employer.

POSITIONS OPEN

FACULTY POSITIONS
Human Molecular Genetics Program
Children's Memorial Research Center (CMRC)
Children's Memorial Hospital and
Northwestern University, Chicago, Illinois

The Human Molecular Genetics Program at CMRC is expanding and seeks applications for new Faculty positions. The aims of the program are to develop translational genetic medicine, particularly in areas directly related to pediatric disease. Ph.D and MD/Ph.D candidates with quality postdoctoral experience, a very strong publication record, and potential to attract nationally competitive research funds are encouraged to apply. New laboratory space and state-of-the-art equipment are in place. Startup packages will be generous and successful applicants will be eligible for tenure-track Faculty positions in the Department of Pediatrics, Feinberg Medical School, Northwestern University. Candidates with research interests in the areas of chromatin structure and the regulation of gene expression are particularly encouraged to apply, though research in all areas of human genetic disease will be considered.

For further details of the program see **website: http://www.childrensmrc.org/human_molecular_genetics.**

Please send applications/letters of interest including full curriculum vitae, an outline of research interests, the names and contact details of three references and PDF files of three recent publications to: **Chris Pomeroy, Program Assistant, Human Molecular Genetics Program, CMRC, 2430 N. Halsted Street (211), Chicago, IL 60614-4314 U.S.A. E-mail: c-pomeroy@northwestern.edu.** Review of applications will start on March 18, 2006, and continue until the positions are filled.

An Equal Opportunity/Affirmative Action Employer. Women and minority candidates are strongly encouraged to apply.

Department of Pharmacology, Temple University School of Medicine invites applications for a **TENURE-TRACK FACULTY POSITION**. The ranks are open; however, Assistant or Associate Professors are preferred. Applicants must have a Ph.D. and/or M.D. with at least two years of postdoctoral experience. Preference will be given to candidates in the area of signal transduction and molecular pharmacology with extramural funding. The successful candidates will be expected to develop and maintain, extramurally funded research programs and to contribute to the teaching mission. Candidates should submit curriculum vitae and statement of research plan to: **Dr. L.-Y. Liu-Chen, Chair, Faculty Search Committee, Department of Pharmacology, Temple University School of Medicine, 3420 N. Broad Street, Philadelphia, PA 19140,** or submitted via **e-mail: lliuche@temple.edu.** *Temple University is an Equal Opportunity/Affirmative Action Employer.*

PHYSIOLOGIST: TENURE-TRACK, ASSISTANT PROFESSOR, fall 2006. Ph.D. required, teaching experience and postdoctoral research preferred. Responsibilities include teaching human anatomy and physiology, upper-level animal physiology and a course of candidate's choice, as well as supervising undergraduate research/internships. Submit letter of application, curriculum vitae, undergraduate and graduate transcripts, statements of teaching philosophy and research interests, and three letters of recommendation to: **Dr. Dessie Severson, Search Committee Chair, University of Pittsburgh at Bradford, 300 Campus Drive, Bradford, PA 16701 (website: http://www.upb.pitt.edu).** Review of completed applications will begin immediately and will continue until the position is filled. Women and minorities are encouraged to apply. *Affirmative Action/Equal Opportunity Employer.*

A groundbreaking, international conference and exhibition for attendees from USA, Europe, Japan and Asia-Pacific to discuss global partnerships, emerging Asian markets and innovative R&D strategies…….

In Association with: SCRIP

Drug Discovery and Development Summit

JAPAN

April 24-26, 2006 • Tower Hall Funabori • Tokyo, Japan

Features

- **59** international speakers and panelists...over 50% from outside Japan to network with
- **30** technology and service providers showcasing tools to increase your R&D productivity
- **19** biotech company presentations in three showcases from Japan, India and China to help you find potential partners
- **12** sessions and case studies of global partnerships and East-West alliances
- **"Partnering Zone"**…a free pre-event partnering service for attendees

Silver Sponsors: GENE LOGIC, GNI

Bronze Sponsor: ELSEVIER, MDL

In Association with: Science AAAS, BioJapan 2006 World Business Forum

Endorsed by: U.S. Commercial Service Japan, Embassy of the United States of America
アメリカ大使館 商務部

4 Inspiring Keynote Speakers

Akira Miyajima, *Chief Executive,* **Pharmaceuticals and Medical Devices Agency**

Peter Corr, Ph.D., *Senior Vice President, Science and Technology,* **Pfizer Inc.**

Tadao Suzuki, Ph.D., *Head of R&D Division, Senior Managing Director,* **Daiichi Pharmaceutical Co., Ltd.**

Mitsuru Miyata, *Director, Biotechnology Center,* **Nikkei Business Publications, Inc.**

Produced by the Organizers of: Drug Discovery Technology & Development

www.drugdisc.com/Japan

NEW

Save money and promote your event easily!

Go to www.ScienceMeetings.org

Post your meeting or announcement ad directly to our website. It is quick, easy, and economical.

Rate: $299 per posting (commissionable to approved ad agencies). Credit card orders only.

Duration: Your ad will remain up until the end date of the meeting or one year, whichever comes first. It will be included in our searchable database within one business day of posting.

Specs: You can also include a hyperlink back to your website or your event information.

Visit: www.ScienceMeetings.org and click on Post your Meeting or Announcement or contact your sales representative.

U.S. Kathleen Clark
phone: 510-271-8349
e-mail: kclark@aaas.org

Europe and International
Tracy Holmes
phone: +44 (0) 1223 326 500
e-mail: ads@science-int.co.uk

Science AAAS

YYePG Proudly Presents,Thx for Support

POSITIONS OPEN

ASSISTANT PROFESSOR OF ENVIRONMENTAL SCIENCE
Temporary, Commencing Fall 2006

Description: Will teach 100 level general education science (introduction to environmental science) and upper level electives in appropriate technology, ecological agriculture, or in area of expertise. Responsibilities include teaching day and evening courses, advising students, engaging in scholarship/professional development, and participation in faculty governance.

Requirements: Ph.D. in environmental science, physics or related field preferred. All but dissertation with imminent completion date will be considered. Strong background in energy and energy technologies preferred. The applicant must demonstrate excellence in teaching at the college level and have a commitment to interdisciplinary learning.

Faculty members are expected to maintain active participation in research, scholarship, college governance, service, academic advisement, and professional development activities.

All applications must be completed online at **website: http://www.ramapojobs.com.** Attach resume, cover letter, statement of teaching philosophy, research interests, and a list of three references to your completed application. Since its beginning, Ramapo College has had an intercultural/international mission. Please tell us how your background, interest, and experience can contribute to this mission, as well as to the specific position for which you are applying.

Review of applications will begin immediately and continue until the position is filled. Position offers excellent state benefits. To request accommodations, call **telephone: 201-684-7734.** Contact:

Dr. Eric Karlin, Search Committee Chair
Ramapo College of New Jersey
Department 25, 505 Ramapo Valley Road
Mahwah, NJ 07430

"New Jersey's Public Liberal Arts College," Ramapo College is a member of the Council of Public Liberal Arts Colleges (COPLAC), a national alliance of leading liberal arts colleges in the public sector.

Ramapo College of New Jersey is located in the beautiful foothills of the Ramapo Valley Mountains approximately 25 miles northwest of New York City. Accredited by the Middle States Commission on Higher Education, Ramapo College is a comprehensive institution of higher education dedicated to the promotion of teaching and learning within strong liberal arts based curriculum, thus earning the designation "New Jersey's Public Liberal Arts College." Its curricular emphasis includes the liberal arts and sciences, social sciences, fine and performing arts, and the professional programs within a residential and sustainable living and learning environment. Organized into thematic learning communities, Ramapo College provides academic excellence through its interdisciplinary curriculum, international education, intercultural understanding and experiential learning opportunities.

Equal Employment Opportunity/Affirmative Action.

NATIONAL UNIVERSITY OF SINGAPORE
Department of Chemical and Biomolecular Engineering

The Department of Chemical and Biomolecular Engineering at National University of Singapore invites applications for **TENURE-TRACK FACULTY** positions at all levels. The Department is one of the largest internationally with excellent in-house infrastructure for experimental and computational research. A Ph.D. in chemical engineering or related areas and a strong research record with excellent publications are required. Please refer to **website: http://www.chbe.nus.edu.sg/** for more information on the areas of interest and for application details. Applicants should send full curriculum vitae (including key publications), a detailed research plan, a statement of teaching interest, and a list of names of at least three references to: **Professor Raj Rajagopalan, Head of Department (Attention: Ms. Nancy Chia, e-mail: nancychia@nus.edu.sg).**

INSTITUT PASTEUR
DE MONTEVIDEO

YOUNG GROUP LEADER POSITIONS
Basic Biomedical Research

The Institut Pasteur (IP) Montevideo is an international scientific institution recently founded in Montevideo, Uruguay, whose mission is to contribute to the development of biomedical research in the Mercosur region, by strengthening research and education in post-genomics biomedicine and biotechnology.

The IP Montevideo will bring together in 2007, three research groups lead by young researchers, supported by outstanding core facilities in genomics, protein biochemistry, proteomics, structural biology, cellular and molecular biology, and bioinformatics. Applications focused on post-genomic medicine, fully exploiting these facilities and having scientific excellence will be privileged.

The IP Montevideo invites young group leaders (Ph.D. degree obtained within the last seven years) to apply for a five-year research award (basic internal funding US$100,000 per year).

Deadline for applications: April 21, 2006.

Complete details to apply for this position at **website: http://www.pasteur.edu.uy.** Enquiries, **e-mail: llamados@pasteur.edu.uy.**

ASSISTANT/ASSOCIATE PROFESSORS
Department of Physiology

The Department of Physiology invites applications for two tenure-track Assistant/Associate Professorships. We seek well-trained researchers using state of-the-art approaches in endocrinology, cardiovascular, kidney, neurophysiology, and cell and molecular physiology to complement ongoing programs. For additional details see **website: http://www.med.wayne.edu/physiology/index.htm.** Wayne State University (WSU) is an exciting, dynamic, urban research environment with excellent facilities and is rated in the top third of all U.S. research institutions.

Highly competitive startup packages and salaries will be offered. Candidates will be expected to establish extramurally funded research programs and to be active in teaching. Formal review of candidates will begin April 15, 2006.

Applicants should attach curriculum vitae, research plan, and three letters of recommendation as PDF files to **e-mail: dyingst@med.wayne.edu.**

Wayne State University is a premier institution of higher education offering more than 350 academic programs through 14 schools and colleges to more than 34,000 students in metropolitan Detroit.

WSU is an Equal Opportunity/Affirmative Action Employer.

ASSISTANT PROFESSOR
Molecular Plant-Fungal Interactions

Division of Plant Sciences **(website: plantsci.missouri.edu)**, University of Missouri, Columbia (UMC) invites applications for a tenure-track position in molecular plant-fungal interactions. Ph.D. in plant pathology, microbiology, plant molecular biology, or related field and postdoctoral experience is required. This position is expected to establish an active, extramurally funded research program in the area of plant-fungal interactions using modern molecular approaches and to participate in the teaching (undergraduate and graduate) and service missions of the Division. UMC has a history of excellence in plant science and provides a rich environment for research collaboration. Electronically submit, by April 15, 2006, a letter describing qualifications and career goals and curriculum vitae to **e-mail: plantsci@missouri.edu.** Arrange to have selected reprints and three letters of reference sent to: **Division of Plant Sciences, Attn: Margie, 1-41 Agriculture Building, University of Missouri, Columbia, MO 65211.** Direct questions to: **Dr. Gary Stacey, Chair, Search Committee, telephone: 573-884-4752** or **e-mail: staceyg@missouri.edu.** JD 1506188; File 050700. *Affirmative Action/Equal Opportunity Employer.*

FACULTY POSITIONS
Beth Israel Deaconess Medical Center
Harvard Medical School

The Cardiovascular Division of the Beth Israel Deaconess Medical Center seeks outstanding investigators for positions at the **ASSISTANT/ASSOCIATE PROFESSOR** level. The successful candidate will have a doctoral degree and postdoctoral research experience, and is expected to develop a strong research program with extramural funding that complements and expands existing Departmental strengths. Areas of interest include but are not limited to signal transduction, heart failure, cardiac metabolism, cardiovascular progenitor cells, human genetics, and animal models of cardiovascular disease. Applicants should send curriculum vitae, a statement of current and future research interests, and three letters of recommendation to:

Anthony Rosenzweig, M.D.
Director, Cardiovascular Research
Beth Israel Deaconess Medical Center
330 Brookline Avenue, E/RW-453
Boston, MA 02215
E-mail: arosenzw@bidmc.harvard.edu

Harvard Medical School and the Beth Israel Deaconess Medical Center are Equal Opportunity/Affirmative Action Employers.

CHIEF, Environmental Processes Branch, Environmental Laboratory, U.S. Army Engineer Research and Development Center. The successful candidate will be responsible for developing, planning, and executing a broad program of multidisciplinary environmental research. Work is conducted in order to understand, predict, and to the degree possible, control changes in the environment attributable to all types of civil works and military activities. Research is conducted in the areas of geochemistry of soil and sediments, water quality of rivers and reservoirs, microbiological processes, genetics and molecular markers for contaminant fate and effects and chemical control processes for invasive species. Incumbent has responsibility for planning, direction, and management of the research, supervision of personnel, operation of facilities assigned to the branch, and communicating technical accomplishments to sponsors and stakeholders. Official announcement can be found at **website: http://acpol.army.mil** under Employment, Search for Jobs. The position is expected to be announced during the period March 8 through April 21, 2006. Vacancy announcement SWGR06178478 contains information on how to apply. For additional information on applying contact: **Ms. Patsy Abbott, Human Resources, patsy.i.abbott@us.army.mil, telephone 601-631-5857.**

POSTDOCTORAL POSITION
Quantitative Toxicology/Pharmacology

The U.S. Environmental Protection Agency (EPA), National Center for Environmental Assessment in Cincinnati, Ohio seeks Postdoctoral candidates in computational toxicology and biological modeling for human health risk assessments. Successful candidates will have experience in some of the following areas: toxicology, biochemistry, physiology, pharmacology, statistics, and computer modeling. Specialized education training and/or experience preferred include quantitative structure-activity (e.g., QSAR, SAR) modeling, pharmaco- or toxicokinetic modeling, or physiological or biologically-based dose response modeling. Salary ranges from $50,000 up to $70,000, commensurate with qualification plus benefits. Information on federal positions can be found at **website: http://cfpub.epa.gov/ncea/cfm/recordisplay.cfm?deid=134123 (CINC-SAST-010406-01).** For additional information contact **Dorothy Carr** at **telephone: 919-541-4356.** Information on nonfederal positions can be found at **website: http://www.orau.gov/orise/edu/needs/EPA-NCEA-2006-01.pdf.** For additional information please contact **Karen Proffitt** at **telephone: 513-569-7099.**

US EPA is an Equal Opportunity Employer.

Kuwait Foundation
For the Advancement of Sciences

مؤسسة الكويت للتقدم العلمي

KUWAIT PRIZE 2006
Invitation for Nominations

The **Kuwait Foundation for the Advancement of Sciences** (**KFAS**) institutionalized the **KUWAIT Prize** to recognize distinguished accomplishments in the arts, humanities and sciences. The Prizes are awarded annually in the following categories:

A. Basic Sciences
B. Applied Sciences
C. Economics and Social Sciences
D. Arts and Literature
E. Arabic and Islamic Scientific Heritage

The Prizes for **2006** will be awarded in the following fields:

1. **Basic Sciences :** Optical Science
2. **Applied Sciences :** Corrosion
3. **Economic and Social Sciences :** Future of Arabic Economy in light of the New World Order
4. **Arts and Literature :** Contemporary Voyages Literature
5. **Arabic and Islamic Scientific Heritage :** Botany, Agriculture and Irrigation of the Arab

Foreground and **Conditions** of the Prize:

1. Two prizes are awarded in each category:
   * A Prize to recognize the distinguished scientific research of a Kuwaiti citizen, and,
   * A Prize to recognize the distinguished scientific research of an Arab citizen.
2. The candidate should not have been awarded a Prize for the submitted work by any other institution.
3. Nominations for these Prizes are accepted from individuals, academic and scientific centers, learned societies, past recipients of the Prize, and peers of the nominees. No nominations are accepted from political entities.
4. The scientific research submitted must have been published during the last ten years.
5. Each Prize consists of a cash sum of K.D. 30,000/- (approx. U.S.$100,000/-), a Gold medal, a KFAS Shield and a Certificate of Recognition.
6. Nominators must clearly indicate the distinguished work that qualifies their candidate for consideration.
7. The results of KFAS decision regarding selection of winners are final.
8. The documents submitted for nominations will not be returned regardless of the outcome of the decision.
9. Each winner is expected to deliver a lecture concerning the contribution for which he was awarded the Prize.

Inquiries concerning the **KUWAIT PRIZE** and nominations including complete curriculum vitae and updated lists of publications by the candidate with **four copies** of each of the published papers should be received before **31/10/2006** and addressed to:

The Director General

The Kuwait Foundation for the Advancement of Sciences -
P.O. Box: 25263, Safat - 13113, Kuwait.
Tel: (+965) 2429780 / Fax: 2403891
E-Mail: **prize@kfas.org.kw**

POSITIONS OPEN

CYCLOTRON SPECIALIST 06-192

Requires a Bachelor's degree in physics or chemistry and two years of directly related experience in a specialized field. Knowledge of advanced electronic theory and its practical application, physics, and various mechanical disciplines needed. Demonstrated expertise on radio frequency and magnet systems associated with cyclotrons. Ability to fabricate, assemble, and install electronic components and assemblies following prints, diagrams, rough sketches, or verbal instructions needed. Must have demonstrated knowledge of radioactive procedures and protocols. Requires experience in monitoring electronic operating systems to prevent and detect equipment malfunction. Must obtain authorization from the North Dakota State Department of Health to operate cyclotron. Must have excellent interpersonal skills. Complete job description and application are available at **website: http://www.humanresources.und.edu.**

To apply, refer to position name and number, send letter of application, and resume to: **Human Resources, University of North Dakota, P.O. Box 8010, Grand Forks, ND 58202.** Salary: $50,000 to $65,000. Application deadline: March 24, 2006. *Equal Opportunity Employer/Affirmative Action.*

POSTDOCTORAL RESEARCH POSITION
Harvard Medical School
MassGeneral Institute for Neurodegenrative Disease
Boston, Massachusetts

A Postdoctoral position is available to study mechanisms of neurodegeneration, focusing on the role of transcriptional deregulation in polyglutamine diseases (**Dunah et al,** *Science* **296:**2238, 2002; **Zhai et al.,** *Cell* **123(7):**1241-53, 2005). Candidates should have a Ph.D. and/or M.D. degree and must have significant background in molecular biology and/or protein biochemistry. Interested applicants please send curriculum vitae to **Dr. Krainc** at **e-mail: krainc@helix.mgh.harvard.edu.**

POSITIONS OPEN

LEAD SCIENTIST
Division of Surgical Research
Sinai Hospital of Baltimore

A Lead Scientist position is available in a surgical research laboratory dedicated to studying immune and nutritional regulation of wound healing, biology of nitric oxide in healing processes, surgical nutrition and healing in the gastrointestinal tract. A Ph.D. or M.D. is required with a background in a broad range of molecular and cellular biology. Should have experience with both in vivo small animal and in vitro techniques. Responsibilities include day to day running of the surgical research laboratory, overseeing research fellows and technicians, ability to communicate results in a clear manner, both verbally and in writing, and ability to obtain peer-reviewed extramural funding. Financial support for three years is available. Interested candidates should send curriculum vitae and summary of research interests along with names of three references to: **Adrian Barbul, M.D., Chairman, Department of Surgery, Sinai Hospital of Baltimore, 2401 West Belvedere Avenue, Baltimore, MD 21215. Telephone: 410-601-5547; e-mail: abarbul@jhmi.edu.**

Sinai Hospital is an Equal Opportunity/Affirmative Action Employer.

Two **POSTDOCTORAL POSITIONS** are available, Albert Einstein College of Medicine (AECOM), Bronx, New York. Postdoctoral positions for research on function and regulation of guidance proteins that control branching morphogenesis and patterning during kidney development are available immediately. Applicants are required to hold M.S., Ph.D. or M.D./Ph.D. degrees and have experience in cell and molecular research. Send resume, a statement of research interests, and names of three references by **e-mail: atufro@aecom.yu.edu** or mail to: **Alda Tufro, Departments of Pediatrics and Developmental and Molecular Biology, 1300 Morris Park Avenue, Forchheimer 708, Bronx, NY, 10461.** *AECOM is an Equal Opportunity Employer.*

POSITIONS OPEN

Five **POSTDOCTORAL POSITIONS** available at the Hormel Institute, University of Minnesota, Austin, Minnesota, to study the signal transduction in tumor promotion, chemoprevention, and early development (see our review articles: *Science STKE* re2, 2003; *Nature Reviews Cancer* **4:**793-805, 2004; *Mutat. Res.* **555:**33-51, 2004; *Nutrition* **20:**89-94, 2004; *Mol Interv.* **3:**306-308, 2003; *Mutat. Res.* **523-524:**145-150, 2003; *Crit. Rev. Oncol. Hematol.* **42:**5-24, 2002; *Lancet Oncol.* **1:**181-188, 2000). We are seeking self-motivated Ph.D.s with experience in biochemistry, molecular and cellular biology. Experience in signal transduction, functional genomics, models such as Xenopus, fish development, mouse transgenics and knockouts are a plus. Please send your curriculum vitae, the names and telephone numbers of three references to: **Dr. Zigang Dong, The Hormel Institute, University of Minnesota, 801 16th Avenue NE, Austin, MN 55912; fax: 507-437-9606; e-mail: zigangdong@hi.umn.edu.** These positions will remain open until qualified candidates are found. *The University of Minnesota is committed to the policy that all persons shall have equal access to its programs, facilities and employment without regard to race, color, creed, religion, national origin, sex, age, marital status, disability, public assistance status, veteran status, or sexual orientation.*

POSTDOCTORAL FELLOWS (Three)

A cardiovascular laboratory in Temple University, Department of Pharmacology is looking for **POSTDOCTORAL SCIENTISTS** to study the mechanisms of cardiovascular disease and neurondegenerative disease. (*Blood* **99:**939, 2002; *Blood* **101:**3901, 2003; *Arterioscler. Thromb. Vasc. Biol.* **25:**2515, 2005; *Cardiovascular Res.* **69:**253, 2006). The applicants should have a strong background in molecular biology, cardiovascular science, or neuroscience. Send curriculum vitae and name of three references to: **Dr. Hong Wang, 3420 North Broad Street, MRB-307, Philadelphia, PA 19140,** or **e-mail: hongw@temple.edu.**

MARKETPLACE

Enhanced RNA Amplification

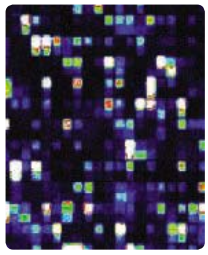

MessageAmp™ II-Biotin *Enhanced*

Single Round aRNA Amplification Kit

- **Enhanced Efficiency** – Single round of amplification from just 50 ng of RNA
- **Enhanced Yields** – Up to 10X greater yields than leading competitor
- **Enhanced Sensitivity** – Highest Present calls of any linear amplification kit
- **Enhanced Convenience** – Includes optimized NTP mix containing biotin-UTP

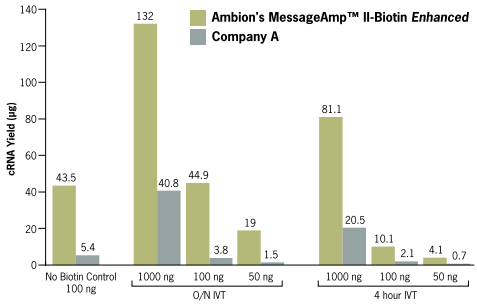

High Yields from Low Inputs. With just 50 ng of RNA input, a single round of amplification yields enough biotin labeled amplified RNA for Affymetrix® GeneChip® analysis.

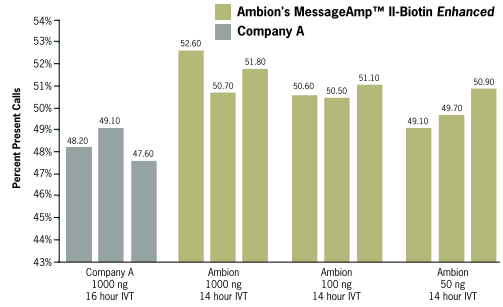

Detect More Genes. Ambion's new MessageAmp™ II-Biotin *Enhanced* kit consistently produces higher percent Present calls than the leading competitor, from 50 ng and just a single round of amplification.

Save up to 40% on Reaction Costs

MessageAmp II-Biotin *Enhanced* is a complete single round amplification and labeling kit validated for Affymetrix® GeneChip® analysis.

www.ambion.com/prod/ma2biotin

Ambion®
THE RNA COMPANY®

Ambion, Inc.
U.S. 800-888-8804 • Canada 800-445-1161
fax +1-512-651-0201

Ambion (Europe) Ltd
tel +44 (0)1480-373-020
fax +44 (0)1480-373-010

Ambion K.K. (Japan)
tel +81 (0)3-5638-2181
fax +81 (0)3-5638-2182

For a list of Ambion direct free phone numbers and distributors in your country, go to www.ambion.com/contact